Economical and Crack-Free High-Performance Concrete for Pavement and Transportation Infrastructure Construction

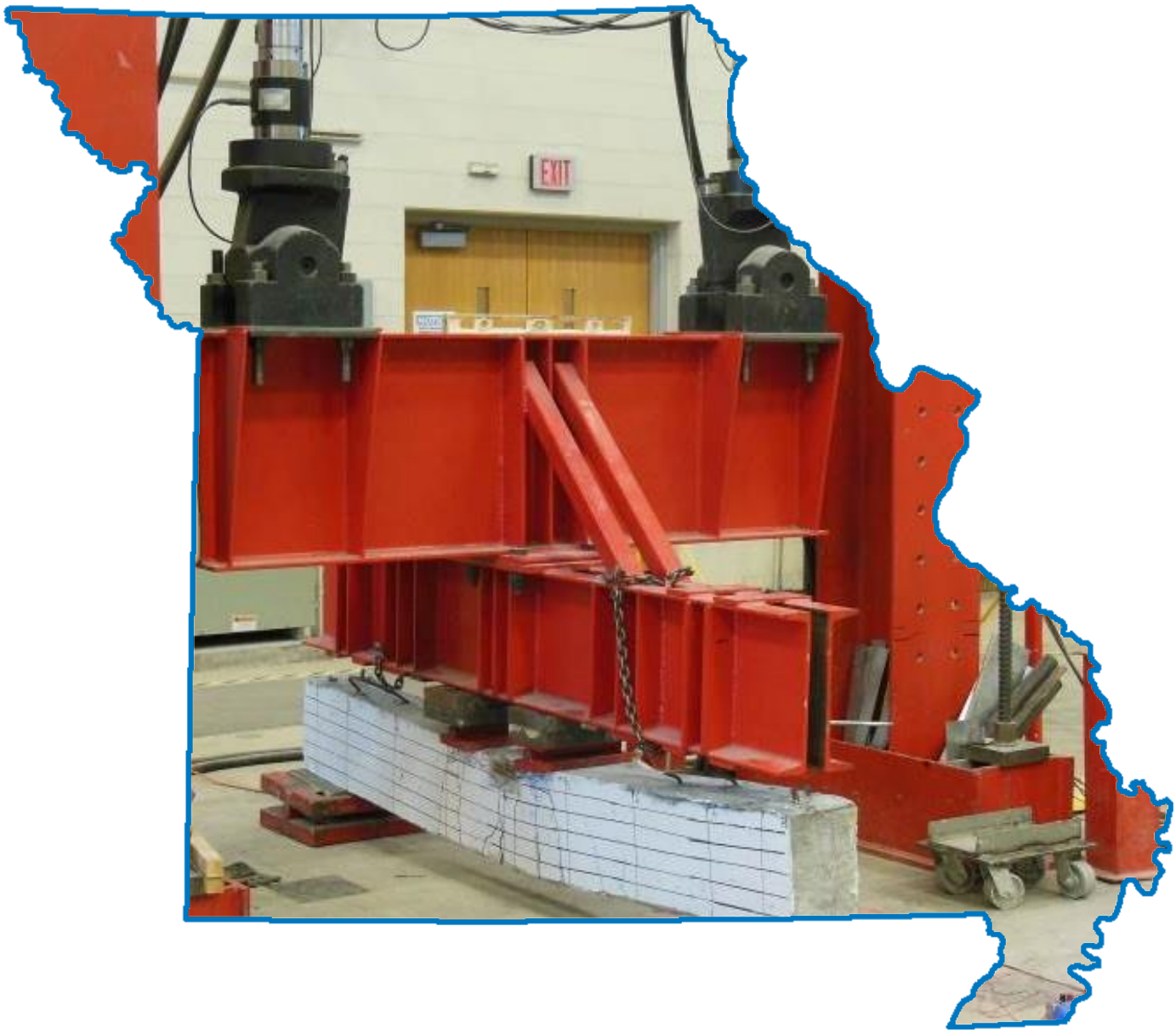

Prepared by:
Kamal H. Khayat, PhD, P.Eng. (principal investigator)
Iman Mehdipour, PhD Candidate (student)
Missouri University of Science and Technology

Final Report Prepared for Missouri Department of Transportation
May 2017 Project TR201503 Report cmr17-007

TECHNICAL REPORT DOCUMENTATION PAGE

1. Report No. cmr 17-007	**2. Government Accession No.**	**3. Recipient's Catalog No.**
4. Title and Subtitle Economical and Crack-Free High-Performance Concrete for Pavement and Transportation Infrastructure Construction		**5. Report Date** June 30, 2016 Published: May 2017 **6. Performing Organization Code**
7. Author(s) Kamal H. Khayat, PhD, P.Eng. http://orcid.org/0000-0003-1431-0715 Iman Mehdipour, PhD Candidate http://orcid.org/0000-0002-6841-3907		**8. Performing Organization Report No.** 00047062
9. Performing Organization Name and Address Center for Transportation Infrastructure and Safety/UTC program Missouri University of Science and Technology 220 Engineering Research Lab, Rolla, MO 65409		**10. Work Unit No.** **11. Contract or Grant No.** MoDOT project #TR2015-03
12. Sponsoring Agency Name and Address Missouri Department of Transportation (SPR) Construction and Materials Division P.O. Box 270, Jefferson City, MO 65102		**13. Type of Report and Period Covered** Final Report (June 23, 2014-June 30, 2016) **14. Sponsoring Agency Code**

15. Supplementary Notes
Conducted in cooperation with the U.S. Department of Transportation, Federal Highway Administration. MoDOT research reports are available in the Innovation Library at http://www.modot.org/services/or/byDate.htm. This report is available at https://library.modot.mo.gov/RDT/reports/TR201503/cmr17-007.pdf

16. Abstract
The main objective of this research is to develop and validate the behavior of a new class of environmentally friendly and cost-effective high-performance concrete (HPC) referred to herein as Eco-HPC. The proposed project aimed at developing two classes of Eco-HPC for the following applications: (i) HPC for pavement construction (Eco-Pave-Crete); and (ii) HPC for bridge infrastructure construction (Eco-Bridge-Crete). The binder contents for these construction materials were limited to 320 kg/m^3 (540 lb/yd^3) and 350 kg/m^3 (590 lb/yd^3), respectively, in order to reduce paste content, cost, CO_2 emissions, and shrinkage. Both Eco-HPC types were optimized to develop high resistance to shrinkage cracking as well as to secure high durability. Given the relatively low binder content, the binder composition and aggregate proportion were optimized based on the packing density approach to reduce the paste required to the fill the voids among aggregate particles. The optimized concrete mixtures exhibited low autogenous and drying shrinkage given the low paste content and use of various shrinkage mitigating strategies. Such strategies included the use of CaO-based expansive agent (EX), saturated lightweight sand (LWS), as well as synthetic or recycled steel fibers. Proper substitution of cement by supplementary cementitious materials (SCMs) resulted in greater packing density of solid particles, lower water/superplasticizer demand, and improved rheological and hardened properties of cement-based materials. A statistical mix design method was proposed and was shown to be effective in optimizing the aggregate proportioning to achieve maximum packing density. The synergistic effect between EX with LWS resulted in lower autogenous and drying shrinkage. For a given fiber content, the use of steel fibers recovered from waste tires had twice the flexural toughness of similar mixture with synthetic fibers. The optimized Eco-HPC mixtures had lower drying shrinkage of 300 μstrain after 250 days. The risk of restrained shrinkage cracking was found to be low for the optimized concrete mixtures (no cracking even after 55 days of testing). The results of structural performance of large-scale reinforced concrete beams indicated that the optimized Eco-Bridge-Crete containing ternary combination of 35% fly ash and 20% slag replacements and recycled steel fibers developed significantly higher flexural toughness compared to the MoDOT reference mixture used for bridge infrastructure applications.

17. Key Words Bridge decks; Bridge members; Bridge piers; Cast in place structures; Concrete; Girders; High performance concrete; Paving. Crack-free; Early-age cracking; Eco-Crete; Packing density; Shrinkage mitigating strategies, Supplementary cementitious materials	**18. Distribution Statement** No restrictions. This document is available through the National Technical Information Service, Springfield, VA 22161.

19. Security Classif. (of this report) Unclassified.	**20. Security Classif. (of this page)** Unclassified.	**21. No. of Pages** 218	**22. Price**

Economical and Crack-Free High-Performance Concrete for Pavement and Transportation Infrastructure Construction

Project Number: TR2015-03

Final Report

Kamal H. Khayat, PhD, P.Eng.

Iman Mehdipour, PhD Candidate

June 30, 2016

ABSTRACT

The main objective of this research is to develop and validate the behavior of a new class of environmentally friendly and cost-effective high-performance concrete (HPC) referred to herein as Eco-HPC. The proposed project aimed at developing two classes of Eco-HPC for the following applications: (i) HPC for pavement construction (Eco-Pave-Crete); and (ii) HPC for bridge infrastructure construction (Eco-Bridge-Crete). The binder contents for these construction materials were limited to 320 kg/m3 (540 lb/yd3) and 350 kg/m3 (590 lb/yd3), respectively, in order to reduce paste content, cost, CO2 emissions, and shrinkage. Both Eco-HPC types were optimized to develop high resistance to shrinkage cracking as well as to secure high durability. Given the relatively low binder content, the binder composition and aggregate proportion were optimized based on the packing density approach to reduce the paste required to the fill the voids among aggregate particles. The optimized concrete mixtures exhibited low autogenous and drying shrinkage given the low paste content and use of various shrinkage mitigating strategies. Such strategies included the use of CaO-based expansive agent (EX), saturated lightweight sand (LWS), as well as synthetic or recycled steel fibers. Proper substitution of cement by supplementary cementitious materials (SCMs) resulted in greater packing density of solid particles, lower water/superplasticizer demand, and improved rheological and hardened properties of cement-based materials. A statistical mix design method was proposed and was shown to be effective in optimizing the aggregate proportioning to achieve maximum packing density. The synergistic effect between EX with LWS resulted in lower autogenous and drying shrinkage. For a given fiber content, the use of steel fibers recovered from waste tires had twice the flexural toughness of similar mixture with synthetic fibers. The optimized Eco-HPC mixtures had lower drying shrinkage of 300 μstrain after 250 days. The risk of restrained shrinkage cracking was found to be low for the optimized concrete mixtures (no cracking even after 55 days of testing). The results of structural performance of large-scale reinforced concrete beams indicated that the optimized Eco-Bridge-Crete containing ternary combination of 35% fly ash and 20% slag replacements and recycled steel fibers developed significantly higher flexural toughness compared to the MoDOT reference mixture used for bridge infrastructure applications.

Keywords:

Bridge; Crack-free concrete; Early-age cracking; Eco-Crete; Expansive admixture; Packing density; Pavement; Shrinkage, Supplementary cementitious materials.

ACKNOWLEDGEMENT

The authors would like to acknowledge the many individuals and organizations that made this research project possible. First and foremost, the authors would like to acknowledge the financial support of Missouri Department of Transportation (MoDOT) as well as the RE-CAST (REsearch on Concrete Applications for Sustainable Transportation) Tier-1 University Transportation Center (UTC) at Missouri University of Science and Technology (Missouri S&T).

The authors would also like to thank the companies that provided materials required for the successful completion of this project, including LafargeHolcim, BASF, Euclid Chemical, Buildex, and Capital Sand Company, as well as Granuband Macon.

The cooperation and support from Abigayle Sherman and Gayle Spitzmiller of the Center for Infrastructure Engineering Studies (CIES) is greatly acknowledged, in particular the assistance of Dr. Soo-Duck Hwang, Lead Scientist, and Jason Cox, Senior Research Specialist is highly appreciated. Valuable technical support provided by technical staff of the Department of Civil, architectural, and Environmental Engineering at Missouri S&T is deeply appreciated, in particular Brian Smith, John Bullock, and Gary Abbott.

EXECUTIVE SUMMARY

This research project was undertaken to develop a new class of environmentally friendly, cost-effective, and crack-free high-performance concrete (HPC) for use in pavement (Eco-Pave-Crete) and bridge infrastructure (Eco-Bridge-Crete) applications. The binder content of these novel materials were limited to 320 kg/m^3 (540 lb/yd^3) and 350 kg/m^3 (590 lb/yd^3), respectively, in order to reduce paste content, cost, CO_2 emissions, and shrinkage. The rheological properties of the Eco-HPCs were adjusted to facilitate placement. Both Eco-HPC types were optimized to develop low shrinkage and high resistance to early-age cracking as well as to secure high durability. A number of parameters affecting concrete characteristics were investigated, including binder type and content, aggregate type and proportions, fiber type, and use of shrinkage mitigating materials. Based on the test results, performance-based specifications required for the design of such concrete mixtures are summarized in Table 1.

Table 1- Performance-based specifications for Eco-HPC

Eco-Pave-Crete (with different workability levels)	
Binder content	≤ 320 kg/m^3 (≤ 540 lb/yd^3)
Slump (without fibers)	50 ± 25 mm (2 ± 1 in.)
Slump (with fibers)	100 ± 25 mm (4 ± 1 in.)
Compressive strength at 56 days	≥ 35MPa (≥ 5100 psi)
Drying shrinkage after 120 days (7-d moist curing)	≤ 300 μm/m
Durability (frost and abrasion resistance)	High
Eco-Bridge-Crete (with different workability levels)	
Binder content	≤ 350 kg/m^3 (≤ 590 lb/yd^3)
Slump (without fibers)	100 ± 25 mm (4 ± 1 in.)
Slump (with fibers)	200 ± 25 mm (8 ± 1 in.)
Compressive strength at 56 days	40 to 50 MPa (5800-7250 psi)
Drying shrinkage after 120 days (7-d moist curing)	≤ 300 μm/m
Durability (frost, corrosion, and abrasion resistance)	High

Based on the obtained results, the optimized mixtures that meet the required characteristics are presented in Table 2.

Table 2- Recommended Eco-HPC mixtures for use in pavement and bridge applications

Concrete type	w/cm	Binder content		Binder type			Fiber type and content		Shrinkage reducing/compensating materials	
	0.40	320 kg/m^3 (540 lb/yd^3)	350 kg/m^3 (590 lb/yd^3)	60% OPC + 40% Class C FA	45% OPC + 20% SL + 35% Class C FA	35% OPC + 60% SL + 5% SF	TUF strand fibers (0.35%)	Steel fibers from tire (0.35%)	25% lightweight sand	7.5% Type G expansive agent
Eco-Pave-Crete	x	x		x					x	
	x	x			x				x	
	x	x			x		x			x
Eco-Bridge-Crete	x		x			x			x	
	x		x		x				x	
	x		x			x	x		x	x
	x		x		x			x		x
	x		x			x		x		x

Note: OPC: ordinary Portland cement, FA: fly ash, SL: slag, and SF: silica fume

Based on the results from binder compositions, aggregate characteristics, and shrinkage mitigating strategies, the mix design of Eco- and crack-free HPC were optimized for different construction applications (Eco-Pave-Crete and Eco-Bridge-Crete). Summary of test results of material performance for the recommended Eco-HPC mixtures are presented in Figure 1. The synergetic effect of the combination of shrinkage reducing materials, including LWS and EX coupled with fibers (synthetic fibers or recycled steel fibers) is quite effective to design low cracking potential concrete. The internal curing provided by the LWS can reduce the shrinkage and risk of early-age shrinkage cracking, especially for mixtures subjected to air drying without using any initial moist-curing. The incorporation of fibers (synthetic fibers or recycled steel fibers) in Eco-HPC mixtures containing high volume of SCMs was shown to have up to 35% greater splitting tensile and flexural strengths than MoDOT reference mixture with 25% fly ash.

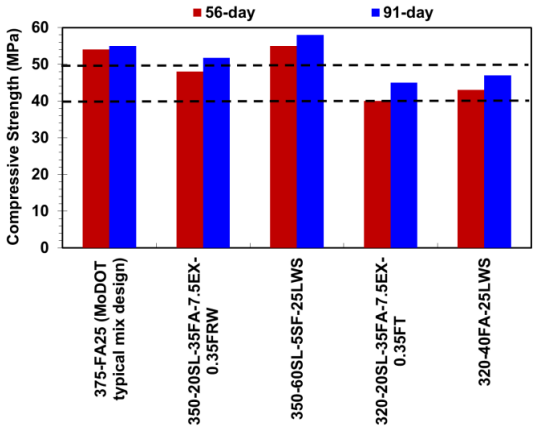

(a) Compressive strength

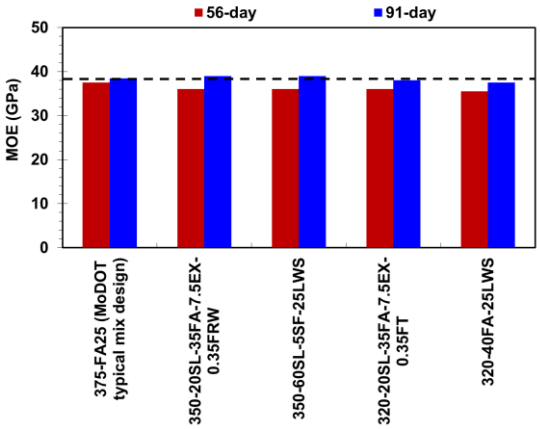

(b) Modulus of elasticity

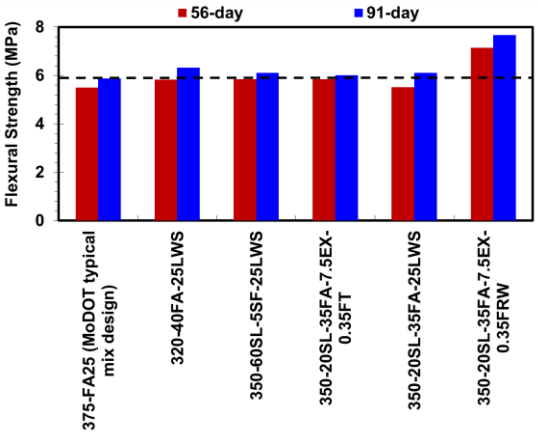

(c) Flexural strength

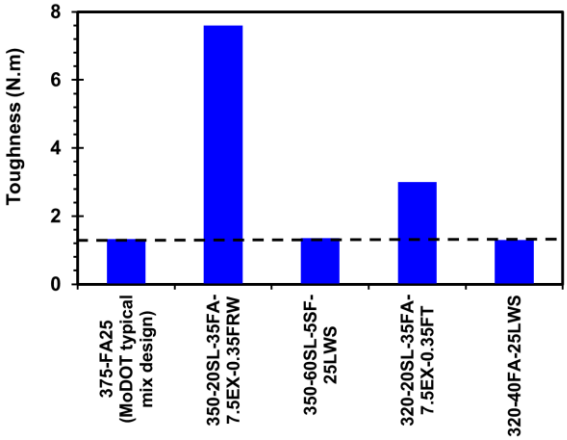

(d) Flexural toughness at 56 days

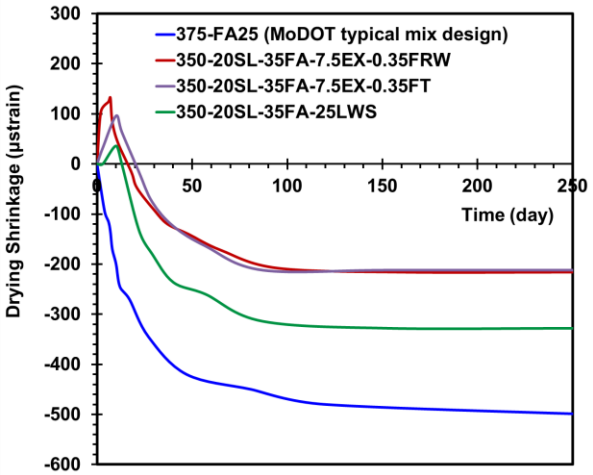

(e) Drying shrinkage

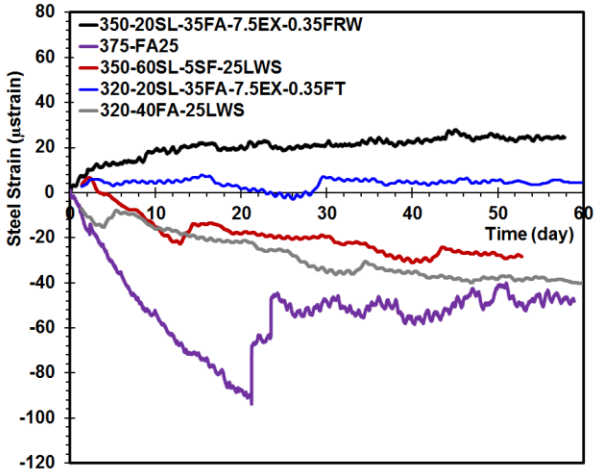

(f) Restrained shrinkage

Figure 1- Material performance evaluation of optimized Eco-HPC mixtures

(Note: 1 N.m = 8.85 lb.in, 1 kN = 0.245 kip)

The highest splitting tensile and flexural strengths were obtained for the mixture made with 35% recycled steel fibers containing 20% slag and 35% fly ash. For a given fiber content, the use of steel fibers recovered from waste tires had two times higher flexural toughness compared to the similar mixture made with synthetic fibers. The reference mixture (100% OPC) made without any fibers developed the lowest ductility behavior and residual strength among all mixtures. The optimized Eco-HPC mixtures had lower drying shrinkage of 300 μstrain after 250 days of drying compared to 500 μstrain for the MoDOT typical mix design (FA25). The incorporation of 7.5% Type G EX resulted in a significant early-age expansion of 100 μstrain that was followed by shrinkage of 200 μstrain after 250 days of drying. The MoDOT typical mix design (FA25) exhibited elapsed time to cracking of 29 days, that was tested under restrained shrinkage ring test. In case of mixtures made with shrinkage reducing materials no cracking was observed until 55 days of testing.

Shrinkage deformation of slab sections and flexural strength of reinforced concrete beams made with optimized Eco-Bridge-Crete were also evaluated. Three slabs measuring 1.8 × 1.8 m (6 × 6 ft) and 150 mm (6 in.) in depth were constructed to evaluate shrinkage deformation of different selected mixtures. The reference slab made with 25% FA replacement exhibited higher magnitude and rate of shrinkage compared to the optimized Eco-Bridge-Crete mixtures. This difference became more dominant for the top surface of concrete slab. In addition, eight reinforced concrete beams were cast to evaluate flexural strength of optimized Eco-Bridge-Crete mixtures. Each beam measured 2.40 m (8 ft.) in length with a cross section of 200 × 300 mm (8 ×12 in.). The results were compared with that of the control beam made with MoDOT reference mixture. The summary of structural performance evaluation for the recommended Eco-HPC mixtures is shown in Figure 2.

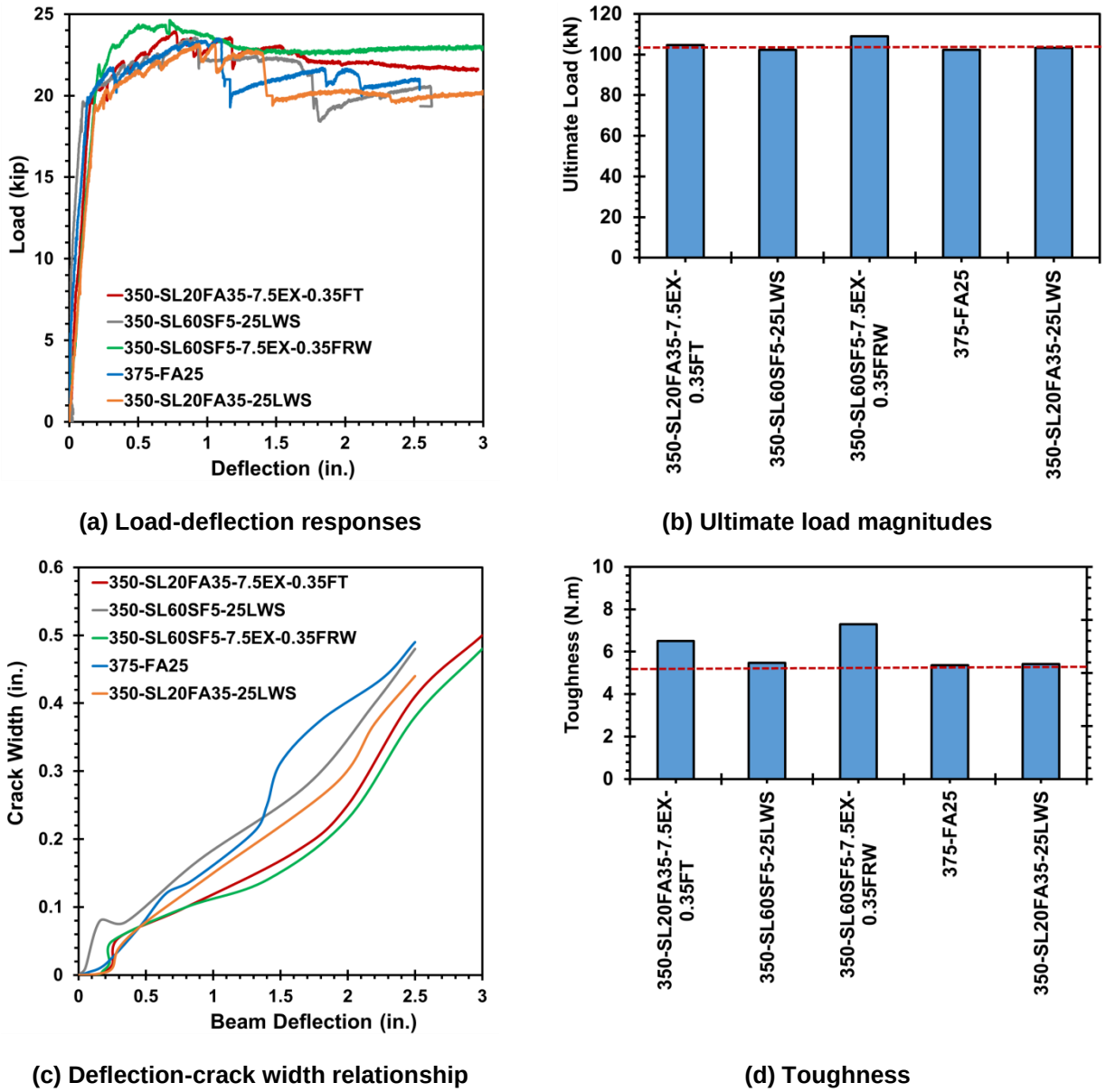

(a) Load-deflection responses

(b) Ultimate load magnitudes

(c) Deflection-crack width relationship

(d) Toughness

Figure 2- Structural performance of optimized reinforced Eco-HPC beams

(Note: 1 N.m = 8.85 lb.in, 1 kN = 0.245 kip)

All beams made with optimized concrete mixtures containing more than 50% SCM replacement had ultimate flexural load equivalent to that of the reference beam (FA25). The addition of either structural synthetic fibers or recycled steel fibers was shown to substantially enhance the post-cracking behavior of optimized Eco-HPC mixtures. The SL20FA35-7.5EX-0.35FT, SL60SF5-

7.5EX-0.35FRW, and SL20FA35-7.5EX-0.35FRW concrete beams developed 120%, 135%, and 130% higher flexural toughness, respectively, compared to the reference beam. The highest load carrying capacity of 64500 lb.in was obtained for concrete beam made with 60% slag and 5% SF replacements and having 0.35% recycled steel fibers.

CONTENTS

LIST OF FIGURES

LIST OF TABLES

1. INTRODUCTION

1.1. Problem statement

High-performance concrete (HPC) is typically characterized by high binder content. The binder is composed of cement and, in some cases, supplementary cementitious materials (SCMs) and/or fillers. High binder content is necessary to ensure high strength and durability. In the case of highly flowable HPC, such as self-consolidating concrete (SCC), relatively high cement paste volume is also required to increase flowability and segregation resistance. In the case of high-strength concrete and SCC, the binder content can range between 425 to 550 kg/m^3 (720 to 930 lb/yd^3). High binder contents can lead to higher cost and greater risk of cracking due to thermal, autogenous, and drying shrinkages, thus reducing service life of the structure. Early-age shrinkage cracking of concrete bridge decks is a common problem. When the induced tensile stress is larger than the tensile strength of the concrete, cracking can occur. The risk of early-age cracking in bridge decks increases the risk of freeze-thaw damage, corrosion of reinforcing steel, and ingress of various deleterious substances that can lead to premature deterioration and potential structural deficiencies of concrete infrastructure.

The aim of this project is to develop and validate the behavior of a new class of environmentally friendly and cost-effective high-performance concrete (HPC), which is referred to herein as Eco-HPC. The proposed project will develop two classes of Eco-HPC for the following applications: HPC for pavement construction (Eco-Pave-Crete) and HPC for bridge desk and transportation infrastructure construction (Eco-Bridge-Crete). Eco-Bridge-Crete can be used in cast-in-place girders, cast-in-place piers and piles, and other bridge elements. Both Eco-HPC types will also be designed to ensure high durability. The concrete should develop high resistance to early-age

cracking to limit the crack width of hairline cracks to 0.1 mm (0.004"). The rheological properties of these advanced materials were designed to facilitate construction operations and reduce labor and cost. Both Eco-HPC types will also be designed to ensure high durability. Table 1-1 summarizes some of the performance-based specifications that are required for these concrete types.

Table 1-1- Target properties of Eco-Pave-Crete and Eco-Bridge-Crete

Eco-Pave-Crete (with different workability levels)	
Binder content	≤ 320 kg/m^3 (≤ 540 lb/yd^3)
Slump (without fibers)	50 ± 25 mm (2 ± 1 in.)
Slump (with fibers)	100 ± 25 mm (4 ± 1 in.)
Compressive strength at 56 days	≥ 35MPa (≥ 5100 psi)
Drying shrinkage after 120 days (7-d moist curing)	≤ 300 μm/m
Durability (frost and abrasion resistance)	High
Eco-Bridge-Crete (with different workability levels)	
Binder content	≤ 350 kg/m^3 (≤ 590 lb/yd^3)
Slump (without fibers)	100 ± 25 mm (4 ± 1 in.)
Slump (with fibers)	200 ± 25 mm (8 ± 1 in.)
Compressive strength at 56 days	40 to 50 MPa (5800-7250 psi)
Drying shrinkage after 120 days (7-d moist curing)	≤ 300 μm/m
Durability (frost, corrosion, and abrasion resistance)	High

1.2. Research objectives

The project will establish new mix design methodology based on the maximum packing density with the aim of reducing cement content and high resistance to shrinkage cracking to enable the development of advanced materials for sustainable pavement and bridge infrastructure construction. It is expected that the results obtained in this work will provide a basis for the development and implementation of:

- New mix design methodology and guidelines for using Eco and crack-free HPC for various types of transportation infrastructure and pavement applications; and

- Performance-based design with substantial information regarding material characteristics and key engineering properties, structural behavior, and durability of concrete targeted for pavement and infrastructure applications.

The specific objectives of this project are described as follows:

- Optimization of binder composition (in binary and ternary systems) to reduce carbon foot print and cost, as well as shrinkage of concrete by replacing cement with high volume of supplementary cementitious materials (SCMs).
- Optimization of aggregate skeleton and proportioning based on packing density approach to reduce paste volume.
- Comparing the effectiveness of different shrinkage mitigating materials, including shrinkage reducing admixture (SRA), Type G and Type K expansive agents (EXs), lightweight sand (LWS) for internal curing, and synthetic and recycled steel fibers to reduce shrinkage and improve resistance to early-age cracking of concrete.
- Developing new classes of cost effective and crack-free environmentally friendly concrete materials with low binder content, high cracking resistance, and various slump consistencies targeted for pavement and transportation infrastructure applications.

1.3. Research methodology

The research project includes four tasks as presented below:

1. Literature review
2. Laboratory investigation
3. Deformation measurement and structural evaluation
4. Guidelines for using Eco-HPC in pavement and transportation infrastructure applications

Further details of the work tasks are described below.

Task 1: Literature review

The purpose of this task was to collect and review relevant literature, specifications, research findings, current practices, and other information relative to HPC and Eco-HPC. Literature review focuses on mix design methodology of HPC for different targeted applications. Furthermore, the effect of binder composition and aggregate characteristics on rheology, stability, mechanical properties, and durability of concrete is investigated. Particular emphasis is given to reducing shrinkage and early-age cracking of concrete. This includes binder composition, aggregate selection and volume, shrinkage mitigating materials, and fibers.

Task 2: Laboratory investigation

The information reviewed in Task 1 was analyzed to finalize the laboratory investigation program. A comprehensive investigation was undertaken to evaluate the influence of mixture proportioning and material characteristics on various properties, including workability, rheology, mechanical properties, shrinkage, and durability. This task consists of five subtasks that are presented below.

Subtask 2-1 Optimization of binder composition

The aim of this subtask is to optimize the binder composition based on packing density, minimum water and admixture demand, hydration heat, CO_2 emission, as well as rheological and mechanical properties of cement paste. Different replacement levels and types of binary and ternary binders were evaluated. The investigated SCMs include Class C fly ash, blast furnace slag, silica fume, and Portland limestone cement with 10% limestone substitution. At the end of this subtask, optimal binder compositions were selected based on the performance rank analysis.

Subtask 2-2 Optimization of aggregate characteristics

The effect of various physical characteristics of coarse and fine aggregates, including shape, particle-size distribution, fineness modulus, and sand-to-total aggregate ratio (S/A) on the packing density of the aggregate skeleton was evaluated. The packing density of aggregate blends was determined using the intensive compaction tester (ICT). The theoretical packing density models were also employed to estimate the packing density of various aggregate blends. The optimal aggregate proportion was selected for the mix design of Eco and crack-free HPC.

Subtask 2-3 Comparison of various shrinkage mitigating strategies

This subtask aimed at evaluating the effect of different shrinkage mitigating materials, including expansive agent (EX) [calcium sulfoaluminate-based and calcium oxide-based], crack reducing admixture (CRA), and different types of fibers, on autogenous and drying shrinkage, early-age cracking potential, and mechanical properties of concrete equivalent mortars. In this subtask, various types of fibers, including synthetic and recycled steel fibers from waste tires was used with the aim of enhancing both post-cracking behavior and early-age cracking resistance. In addition, the effect of the use of lightweight sand (LWS) on shrinkage and cracking potential was investigated. The effectiveness of shrinkage compensating materials on shrinkage and key engineering properties is affected by the initial moist curing duration of the material. Selected mixtures from this subtask were subjected to different moist curing durations to investigate the influence of initial moist curing period on the performance of various shrinkage mitigating materials.

Subtask 2-4 Optimization of concrete mixtures to develop Eco and crack-free HPC

The aim of this subtask was to develop and optimize Eco and crack-free HPC materials to meet the performance specification elaborated earlier in Table 1-1. Based on the obtained results from

Subtask II-1, II-2, and II-3, the effect of different binder compositions, aggregate characteristics, and shrinkage compensating materials was investigated to design Eco and crack-free HPC with various targeted applications (Eco-Pave-Crete and Eco-Bridge-Crete). The testing program included detailed evaluation of the workability, rheology, shrinkage, water absorption, electrical resistivity, and development of mechanical properties, as well as durability of selected concrete mixtures. The optimal concrete mixtures were used for large-scale shrinkage deformation and structural performance evaluation.

Task 3: Deformation measurement and structural performance evaluation

Large-scale specimens, including slab and reinforced beam elements were constructed to evaluate the shrinkage deformation and flexural performance of Eco-Pave-Crete and Eco-Bridge-Crete. Concrete mixtures were made in local concrete batching plants to confirm the ability of the proposed concrete to apply in the field. This task consists of two subtasks that are described below.

Subtask 3-1 Concrete slab section

The aim of this subtask was to evaluate the shrinkage deformation of concrete slabs made with the selected concrete mixtures from Task II. Three slabs were constructed to evaluate different concrete mix designs, including fibers and lightweight sand, and the results were compared with that of the MoDOT reference mixture. The investigated slabs were fully instrumented by using embedded concrete strain gauges, relative humidity sensors, and thermocouples to monitor the shrinkage behavior caused by concrete shrinkage, temperature and humidity variations over time.

Subtask 3-2 Concrete beam section

The aim of this subtask was to evaluate the flexural strength of reinforced concrete beams made with selected Eco-Bridge-Crete mixtures that were optimized in Task II. The results were

compared with the data obtained from beams prepared with MoDOT reference mixture. All beams were instrumented using strain gauges bonded on the reinforcing bars as well as the top and lateral side of the concrete surface at the mid-span. Due to incorporating high-volume SCMs in mixture proportioning of Eco-HPC, all beams were cured for 56 days using wet burlap and plastic sheet before testing. All investigated beams were tested under four-point bending over simply supported span.

Task 4: Anticipated guidelines for using Eco-HPC

Based on the literature survey, laboratory evaluation, and large-scale structural performance from Task 1 to Task 3, recommendations were established for the design of Eco- and crack-free HPC for pavement and bridge infrastructure applications. These recommendations include information on the selection of material constituents and mixture proportioning, performance-based specifications, and curing considerations.

The outline of the research project is presented in Figure 1-1.

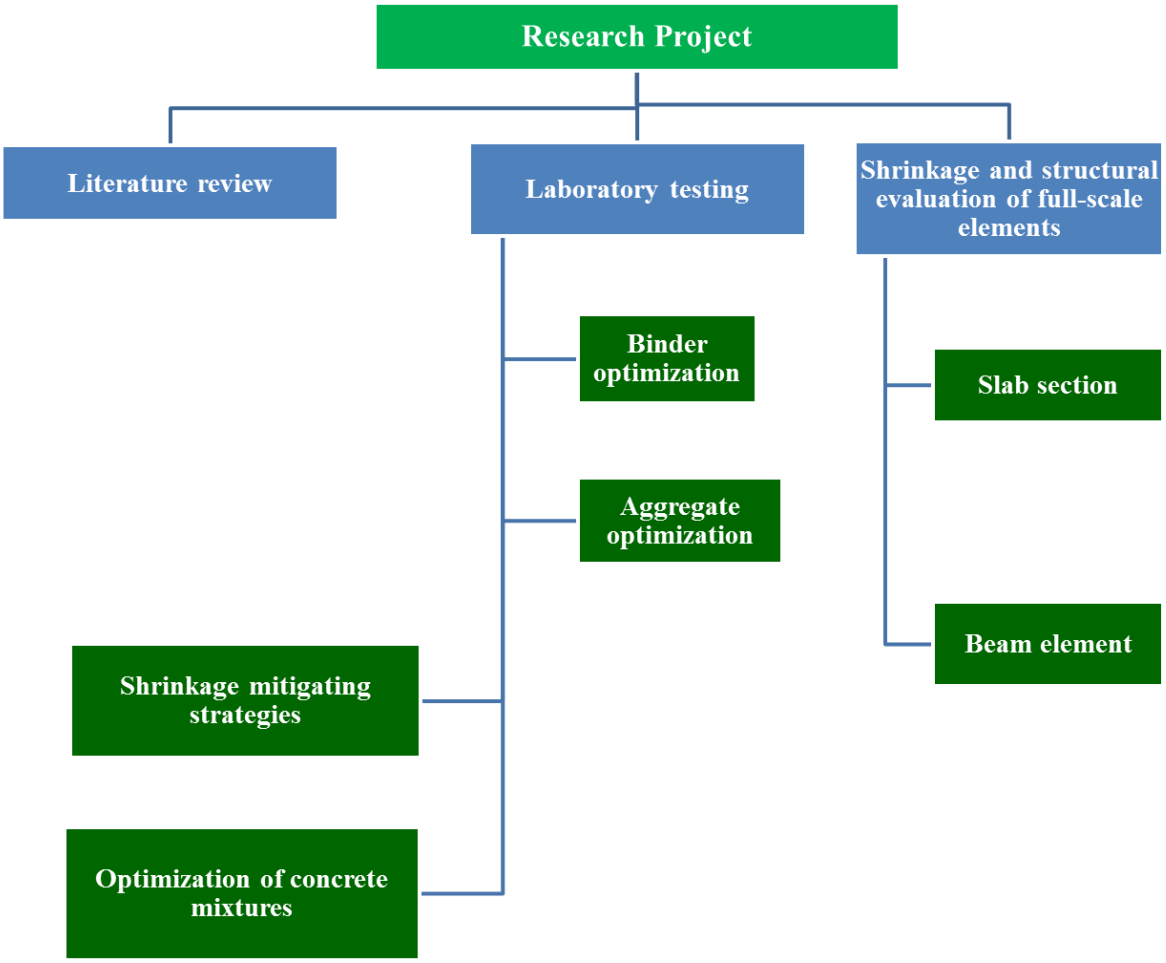

Figure 1-1- Outline of the research investigation

2. LITERATURE REVIEW

2.1. Introduction

Eco-Crete is an environmentally friendly and cost effective concrete in which the total binder content is substantially lower than that used for typical HPC. Given the lower amount of binders and higher water content needed to increase the paste volume to ensure proper flow, Eco-Crete can have higher risk of bleeding and segregation compared to typical HPC. Therefore, special attention is required to select material constituents and mix design to produce stable and robust Eco-Crete mixtures that can meet the targeted performance specifications.

The use of supplementary cementitious materials (SCMs) as partial replacement for cement plays a significant role in reducing cost and carbon footprint while maintaining the required rheology, mechanical properties, and durability characteristics of the concrete. Therefore, energy consumption and embodied CO_2 of concrete can be reduced when cement is replaced by secondary binder materials, such as industrial by-products, SCMs, and fillers. This strategy can indeed be used to reduce the carbon footprint of the construction materials as well as the life cycle cost for the structure. In additional to SCMs, recycled waste materials, including glass powder from recycled waste glass or rubber particles recovered from scrap tires can contribute to developing ecological concrete and reducing environmental impact. In 2010, 11.5 Megatons of waste glass was generated in the United States, mostly from containers and packaging, but only 27% of this valuable waste product was recycled (U.S. Environmental Protection Agency, 2011).

Packing density of aggregate can significantly help to optimize mixtures to lower the cement content in Eco-Crete without reducing its performance. Such low cement construction materials can be designed by optimizing the concrete composition in such a way that the highest packing

density is achieved. The packing density of coarse and fine aggregates plays a significant role for mixture optimization of concrete. In general, the increase in the aggregate packing density results in lower paste volume needed to fill voids in the aggregate skeleton.

Given its higher w/cm and lower coarse aggregate content, Eco-concrete may exhibit higher drying shrinkage. This can result in higher risk of shrinkage cracking, thus reducing durability and serviceability of concrete structures. The cracking potential of concrete depends on the mechanical properties and visco-elastic properties of the mixture. These characteristics are related to the mix design and constitutive materials. A number of parameters can influence the shrinkage cracking potential of concrete, including mix design, binder type and content, aggregate type and content, fiber type and volume, and the use of shrinkage reducing materials. Therefore, it is important to evaluate the effect of these material constituents and mixture proportioning on the resistance of cement-based material to shrinkage cracking.

Based on the above mentioned parameters, which can significantly affect the mix design and selection of material constituents of crack-free Eco-Crete, the literature review undertaken in this investigation consisted of:

1. Reviewing the effect of SCMs on packing density, workability, rheology, shrinkage, and mechanical properties, as well as durability.

2. Reviewing the effect of aggregate characteristics, including shape, texture, and particle size distribution on packing density, rheology, stability, and mechanical and transport properties of concrete.

3. Reviewing studies dealing with factors and materials influencing autogenous, drying, and restrained shrinkages, as well as shrinkage cracking tendency of cement-based materials.

2.2. Supplementary cementitious materials

Supplementary cementitious materials (SCMs), such as fly ash (FA), blast furnace slag (SL), silica fume (SF), and natural pozzolans, are commonly used as a replacement for a portion of Portland cement in concrete. The practice of using SCMs is increasing in the world, consequently the world average percent clinker in cement (or clinker factor) has been progressively reduced from 85% in 2003 to 77% in 2010, and it is projected to further decrease to 71% in the future (Mehta, 2002; Schneider et al., 2011). The use of SCMs as a partial replacement for Portland cement plays a significant role in reducing cost and carbon footprint of concrete, while enhancing rheological and mechanical properties, and durability.

Energy consumption and embodied CO_2 of concrete can be reduced when cement is replaced by secondary materials, such as co-products from other industries. This strategy can indeed be used to reduce the carbon footprint of the construction materials as well as the life cycle cost for the structure. Depending on their physical properties (particle gradation and shape) or chemical composition, SCMs will have either hydraulic activity and/or a pozzolanic activity. Recycled waste materials, including glass powder from recycled waste glass, can also contribute to developing ecological concrete and reducing environmental impact. The effect of SCMs, fillers, and recycled materials on fresh and hardened properties of concrete are reviewed in the next section.

2.2.1. Effect of SCMs on fresh properties

Workability and rheological properties

The effectiveness of incorporating SCMs to enhance workability and rheology is affected by the type and content of the SCM. The FA, SL, and SF are mostly used as a SCM in concrete. Given

the spherical shape and smooth surface characteristics of FA, the partial replacement of cement with FA can reduce the friction between particles, thus enhancing the rheology and flow characteristics. For a given cementitious material content, partial substitution of cement with FA, by mass, results in an increase in the paste volume due to the lower specific gravity of FA compared to Portland cement. The higher paste volume provides greater lubricant volume to the concrete, thus enhancing flow characteristics of concrete. Lee et al. (2003) reported that the fluidity of a cement paste made with 20% Class F FA (FFA) can increase by about 50% as the spread between the minimum and maximum size of particles becomes greater. Kwan and Chen (2013) reported that for a given w/cm, the flow-spread and flow rate of grout mixtures increase as the FA content increases up to 40%. Shi et al. (2002) pointed out that the addition of SF could have a beneficial or adverse effect on the rheology of concrete, depending on the replacement level of the SF. They found the use of 6% SF leads to a considerable reduction in plastic viscosity (40%) and yield stress (80%) of mortar mixtures. However, the substitution of cement with 12% SF resulted in a 30% and 20% increase in yield stress and plastic viscosity, respectively, compared to the control mortar made with 100% cement. Zhang et al. (2011 and 2012) pointed out that a ternary combination of 35% SL and 40% FFA can result in 10% higher packing density compared to the control mixture with 100% cement.

Hwang and Khayat (2006) found that regardless of the type of high-range water reducer (HRWR), concrete equivalent mortars (CEM) made with ternary blends of 25% SL and 5% SF is shown to require lower minimum water demand compared to the control mixture made with 100% ordinary Portland cement (OPC). The investigated mixtures had w/cm varying between 0.35 and 0.42 and binder content of 475 kg/m^3. This can be due to greater packing density and less water adsorption of such blended cement compared to Portland cement. Khayat et al. (2008)

investigated the effect of various types of SCMs on plastic viscosity and yield stress for grout mixtures made with w/cm of 0.40. Their results showed that the partial replacement of cement by FA, SF or SL increased the plastic viscosity, regardless of the dosage of HRWR. In the case of ternary systems, the combination of 20% FA with 40% SL resulted in the highest increase in viscosity (90%) among the tested mixtures. Assaad and Khayat (2004) evaluated the effect of binder type and binder content on degree of thixotropy of self-consolidating concrete (SCC). The investigated mixtures had 650 ± 15 mm (25.6 ± 0.60 in.) slump flow values, a w/cm of 0.46, and a binder content ranging between 400 and 550 kg/m^3 (675 to 930 lb/yd^3). The tested binder types included Type I and Type III cements along with three blended cements. The investigated blended binders included: a binary cement containing 8% SF and 92% Type I cement; a ternary cement made with 6% SF, 22% Class F FA, and 72% Type I cement; and a quaternary cement containing 6% SF, 28% FA, 16% SL, and 50% Type I cement. For a given binder content, the degree of thixotropy is shown to be significantly affected by the type of binder; mixtures made with Type III cement exhibit a greater degree of thixotropy compared to those prepared with binary or ternary cement. On the other hand, SCC made with a quaternary cement containing 50% SCM or those with Type I cement without any SCM exhibit a lower degree of thixotropy. For a given binder type, the degree of thixotropy is shown to increase with a decrease in the binder content. This is attributed to the relative increase in the coarse aggregate volume which can result in a higher level of internal friction between particles.

El-Chabib and Syed (2012) conducted an extensive experimental study to develop a high-performance SCC containing high volume of SCMs. In total, 20 SCC mixtures were prepared with 0.37 w/cm and a binder content of 450 kg/m^3 (760 lb/yd^3). Mixtures were designed to have up to 70% of Portland cement replaced by cementitious materials such as Class C and Class F

FA (30% to 70%), SL (30% to 70%), and SF (5% to 15%). The fresh characteristics, such as flowability, deformability, filling capacity, air content, and segregation resistance of SCC mixtures were evaluated. Mixtures containing 70% of FA and SL (70%) yielded 25% lower HRWR required for a given slump flow compared to the control mixture with 100% cement. Increasing the content of SF from 5% to 10% and 15% resulted in an increase in the dosage of HRWR from 1.31 to 1.37 L/m^3 and 1.43 L/m^3 (0.262 to 0.274 and 0.286 gal/yd^3), respectively. Given relatively high surface area of the SF, the mixture containing SF particles exhibited lower bleeding and aggregate segregation compared to other types of SCMs. Ahari et al. (2015) evaluated the rheological properties of SCC containing various amounts of SF (4%, 8%, and 12%), FA (18% and 36%), Metakaolin (MK) at 4%, 8%, 18%, and 36%, and SL (18%) as a partial replacement of cement with various w/cm ranging between 0.44 and 0.56. These SCMs were used in binary, ternary, and quaternary cementitious blends to investigate the variations of some properties, such as HRWR demand and rheological properties. For all w/cm, mixtures containing SF and MK had higher HRWR demand for a given slump flow compared to the other SCMs. Plastic viscosity of the mixtures containing FA and MK was higher than that of the control mixtures, regardless of the w/cm. The highest increase (90%) in plastic viscosity was observed in mixture containing 36% MK and w/cm of 0.50. Among the investigated SCMs, the incorporation of SF has a more significant influence on the viscosity compared to the MK at the same level of cement replacement.

Depending on the PSD of glass particles, waste glass can be used as a partial replacement for aggregate or cement in concrete. The pozzolanic reactivity of fine waste glass has been identified by an increase in C-S-H and decrease in $Ca(OH)_2$ (Sobolev and Arikan, 2002; Sobolev et al., 2007). There are contradictory reports about the effect of glass particles on workability. Some

studies reported a positive effect, whilst the others reported a negative effect. Wang et al. (2014) investigated the effect of replacement level of glass powder, varying between 10% and 50% as a cement replacement, on workability of mortar mixtures. For a given slump value, the water content of mortars decreases with an increase in the replacement level of glass powder. They also reported that the addition of glass powders leads to a decrease in the initial and final setting time of mortar mixtures compared to the control mixture made with 100% OPC. Malik et al. (2013) reported an increase in the workability of concrete mixtures by replacing natural sand with waste glass (size < 1.18 mm (0.05 in.)) at levels of 10%, 20%, 30%, and 40%, by mass. The workability increased as the replacement rate of glass sand increased. Ali and Al-Tersawy (2012) evaluated the workability of SCC mixtures containing recycled glass (size < 5 mm (0.2 in.)) at levels of 0, 10%, 20%, 30%, 40%, and 50%, by mass, as a partial replacement for natural sand. They reported that the inclusion of waste glass increased the slump flow of SCC made with a cement content of 400 kg/m^3 (675 lb/yd^3). The increase in the slump flow was 2%, 5%, 8%, 11%, and 12% with the addition of 10%, 20%, 30%, 40%, and 50% glass sand, respectively. On the contrary, Taha and Nounu (2009) reported a reduction in the workability with increasing glass sand content. The reduction in the slump value was 29% and 33% with the addition of 50% and 100% glass sand, respectively. The evaluated concrete had recycled glass (size <5 mm (0.2 in.)) as natural sand replacement at levels of 50% and 100%, by volume. Ling and Poon (2011) reported that concrete containing glass sand exhibits higher risk of bleeding and aggregate segregation compared to similar concrete without using glass sand. They found that the use of higher replacement of glass sand with large particle sizes (5–10 mm (0.2-0.4 in.)) results in higher bleeding and segregation. This is attributed to the smooth surface characteristics and

lower degree of water absorption for sand glass compared to the natural sand which can result in lower cohesion and bond between paste and aggregate.

Portland limestone cement (PLC) has recently been approved as a part of the ASTM C595 specifications. These cements are designed to enable more sustainable concrete production by replacing up to 15% of the clinker with interground limestone particles. The use of PLC enables a reduction in CO_2 embodied in the built infrastructure and extends the life of limestone quarries (Tennis et al., 2011). Based on the information provided in the literature, it appears that there are conflicting results on the role of PLC on workability (Tennis et al., 2011). In general, the degree of fineness of the limestone is the main factor affecting the workability of concrete. The results of literature review undertaken by Tennis et al. (2011) and Barrett et al. (2013) suggest that the use of limestone may alter the water demand, resulting in a slight increase or decrease when PLC is compared to conventional cement. Tsivilis et al. (1999, 2000) investigated the water demand of mortar and concrete containing various replacement levels of cement with limestone (0, 10%, 15%, and 20% limestone). They observed that the use of limestone cement increased the water demand necessary for a given slump value, especially in the case of higher limestone replacement. Ghezal and Khayat (2002) employed response surface method to optimize the mix design of SCC containing limestone filler. The investigated mixtures had various water-to-powder ratios (w/p) of 0.38 to 0.72, cement contents of 250 to 400 kg/m^3 (420 to 675 lb/yd^3), limestone filler additions of 0 to 120 kg/m^3 (0 to 202 lb/yd^3), and HRWR dosages of 0.12% to 0.75% by powder mass. The replacement of 100 kg/m^3 (170 lb/yd^3) of cement with finely ground limestone filler is shown to improve deformability and stability. The increase in limestone filler content was found to reduce the HRWR demand to secure a given deformability, thus leading to producing cost effective SCC. Mixtures containing approximately 300 kg/m^3 of Type I cement

and 100 kg/m^3 of limestone filler with Blain fineness of 565 m^2/kg were found to secure good overall performance. Based on the derived statistical models, concrete made with fine limestone filler as a cement replacement can exhibit up to 10% lower 28-day strength compared with similar concrete without filler.

In general, it has been reported that the influence of limestone on setting time is strongly related to the fineness of the limestone. As the limestone was ground finer, the setting time decreased (Hooton et al. 2007). Mounanga et al. (2010) reported that limestone filler could be used to reduce the setting time for concrete systems containing FA and SL. The partial substitution of cement by limestone can provide a synergistic effect on the rate of hydration and setting time of concrete made with relatively high SCM replacement. Ezziane et al. (2010) also reported that limestone additions to Portland cement in mortars provided nucleation sites which accelerated hydration according to the Vicat testing results.

Packing density of binders

Optimization of PSD in cement–SCM–filler systems is an approach that is used to design environmentally friendly concrete to optimize the granular skeleton of the powder phase and enhance the rheological properties. Given the higher specific surface area of binder materials compared to other material constituents of concrete, they have substantial influence on water and HRWR demands. The optimization of packing characteristics of binders can reduce the water demand, thus resulting in a reduction in binder content required for a given performance of concrete. For example, Bentz et al. (2012) measured rheological properties of cement–fly ash paste mixtures with different PSD of the FA. They found that yield stress of cement paste is related to particle density of cement and plastic viscosity is related to particle surface area and packing density of the binder. Vance et al. (2013) reported that the rheological properties of

paste mixtures containing various types and replacement levels of SCMs, such as limestone filler, MK, and FA depends on total particle specific surface area.

Lange et al. (1997) reported that improving the packing density of the cementitious materials by partially replacing cement with fine SL can significantly reduce the water demand and enhance the overall performance of concrete. Kwan and Wong (2008) concluded that there exists an optimum content of the SF replacement, beyond which the packing density of the binders decreases. The partial replacement of cement with 45% SF exhibited the packing density of 0.67 compared to 0.72 for similar binder containing 30% SF. Zhang et al. (2011 and 2012) reported that a ternary combination of 35% SL and 40% FFA is shown to have 10% higher packing density compared to the control mixture made with 100% cement, thus leading to higher flow characteristics. Kwan and Wong (2008) reported that the ternary blends of cement with FA and SF can significantly enhance the wet packing density of cement paste mixtures. The variation of the packing density with the mix proportions of the ternary cementitious materials is illustrated in Figure 2-1 (Kwan and Wong, 2008). Their results showed that, the ternary blends of 25% cement, 45% FA, and 30% SF exhibited the highest packing density of 0.75 among all investigated binary and ternary systems. The improvement in packing density of the binder can be attributed to the spherical shape effect of the FA and filling and shape effects of SF which can result in a decrease in the friction between particles and filling the voids between cement grains. Similarly, Amini et al. (2016) pointed out that the partial substitution of cement by FA or MK significantly improved the packing density of the binder system. Knop et al. (2014) investigated the influence of PSD and substitution of limestone powder as partial replacement for Portland cement on packing density and water demand for normal consistency of limestone cement. For a given replacement level of limestone, blended limestone cement with finer particles (3 μm

(0.0001 in.)) is shown to require higher water demand to achieve normal consistency compared to the larger particles (53 µm (0.002 in.)). Depending on the PSD of limestone powder from 3 µm (0.0001 in.) to 53 µm (0.002 in.), the increase in the replacement level of limestone from 0 to 20% resulted in 1% to 7% higher packing density compared to the mixture made with 100% OPC (Knop et al., 2014).

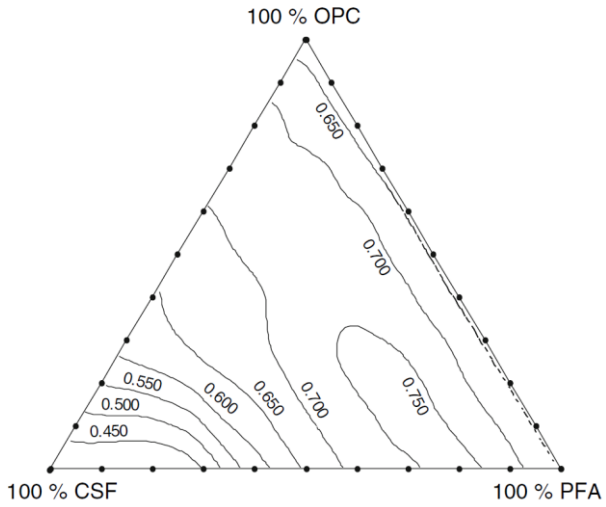

Figure 2-1- Effect of SCM substitutions on packing density of ternary binders (Kwan and Wong, 2008)

Mehdipour and Khayat (2016) investigated the effect of SCM types, replacement rates and degree of dispersion on packing density of the binder system. The authors reported that the effectiveness of incorporating high volume of SCM to enhance packing density is shown to increase with the increase of HRWR dosage resulting from greater degree of dispersion of the binder. The incorporation of a sufficient dosage of HRWR led to lower water demand needed to achieve maximum density and higher packing density. The coupled effect of these changes results in higher compressive strength. As shown in Figure 2-2, using ternary packing diagram, compared to the packing density of 0.58 for binder with 100% cement, the use of SCMs in a well-dispersed system is shown to secure packing density of 0.60 to 0.73

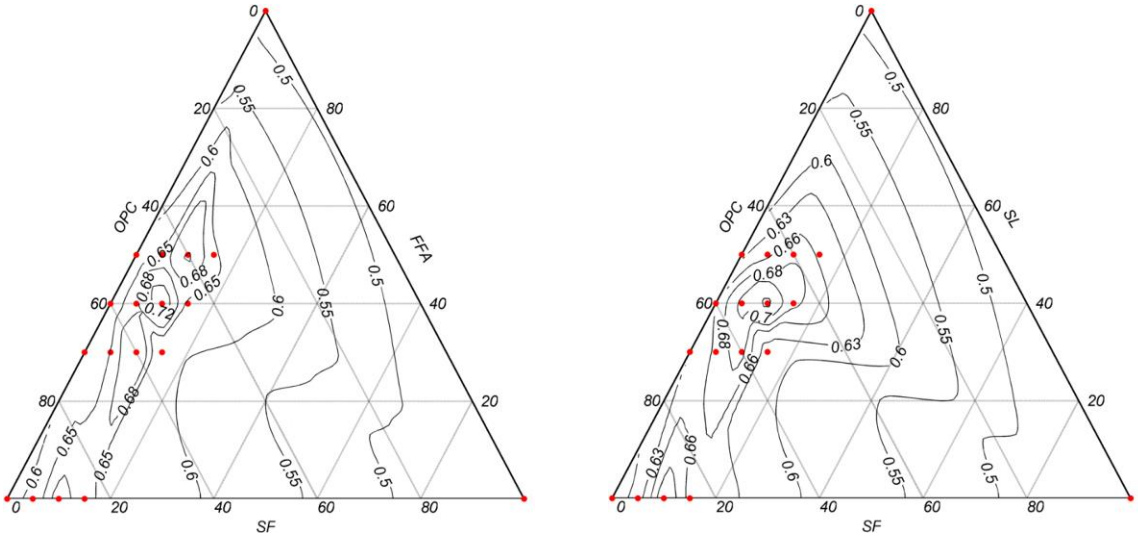

(a) Ternary system of OPC, SF, and FFA (b) Ternary system of OPC, SF, and SL

Figure 2-2- Effect of SCM substitutions on packing density of ternary systems made with 0.12% HRWR (Mehdipour and Khayat, 2016)

2.2.2. Effect of SCMs on hardened properties

Mechanical properties

In general, SCMs can contribute to long-term strength of concrete due to the pozzolanic reaction. Mixtures made with Class F FA exhibit slower strength development than similar mixtures prepared with only Portland cement. The 28-day mechanical properties may be lower for concrete containing FA, particularly Class F FA, however, pozzolanic reaction of FA continues over time, and the long-term strength of FA concrete can be the same as those of similar concrete mixtures made with 100% Portland cement (Lawler et al., 2007). Depending on the mixture proportions, chemical composition, and Blain fineness, some FAs may require up to 90 days to exceed a 28-day strength of control mixture containing 100% OPC. Jaturapitakkul et al. (2004) compared the compressive strength of concrete made with coarse FA particles (90-100 μm

(.0035-0.004 in.)) with those of concrete made with fine FA (3.8 μm (0.00015 in.)). Concrete mixtures prepared with 15% to 50% fine FA can achieve 10% to 30% higher compressive strength compared to concrete mixture containing coarse FA at the same replacement level. Concrete proportioned with Class C FA generally develops higher early-age strength than concrete with Class F FA (Kosmatka and Panarese, 2002, Uysal and Akyuncu, 2012). However, at later ages (beyond 28 days), concrete made with Class C FA may exhibit lower strength development compared to concrete containing Class F FA. El-Chabib and Syed (2012) reported that the partial replacement of cement by 60% Class C FA or by up to 70% of SL developed a 28-day compressive strength slightly lower than or comparable to the control SCC made with 100% OPC. Such mixtures exhibited a 1-day compressive strength of 5 MPa (725 psi) and 9.5 MPa (1380 psi), respectively, compared to 26 MPa (3770 psi) for the control mixture.

Ternary cementitious blends of SF or SL with FA can be used to enhance the rate of strength development at early-age. Khayat et al. (2008) reported that the combination of 3% SF with either 10% or 20% FA resulted in 5% to 30% higher 28-day strength compared to the reference grout made with 100% cement and w/cm of 0.40. Hwang and Khayat (2009) pointed out that for SCC mixtures made w/cm of 0.35 and 0.42, the use of 25% SL and 5% SF resulted in 15% to 22% higher compressive strength at 28 days compared to those prepared with 25% Class F FA and 5% SF. This can be due to the relatively high reactivity of the SL compared to the FA. The modulus of elasticity results of such mixtures made with various binder combinations had similar trends as those of compressive strength results for both of w/cm of 0.35 and 0.42. Kuder et al. (2012) investigated the binary and ternary blends of Class C FA and SL on compressive strength of SCC made with a binder content of 410 kg/m^3 (690 lb/yd^3). Ternary mixtures with 60% SCMs replacement, containing the combination of 25% FA and 75% SL or 50% FA and 50% SL

exhibited higher compressive strength than both FA and SL binary mixtures and developed similar strength to that of the control mixture made with 100% OPC. This is due to the synergetic effect of the combination of SL and FA in the ternary binder, which enhances engineering advantages over a simple binary system and produces more sustainable concrete mixtures.

Depending on the particle size and substitution rate of glass, the use of glass particles as replacement for sand or cement can result in an increase or reduction in mechanical properties. Corinaldesi et al. (2005) studied the compressive and flexural strengths, at age of 180 days, of mortars containing waste glass as fine aggregate. Natural sand was partially replaced with waste glass at levels of 0%, 30%, and 70% by weight with three different particle sizes of waste glass, including up to 36 µm (0.0015 in.), from 36 to 50 µm (0.0015-0.002 in.) and from 50 to 100 µm (0.002-0.004 in.). The results showed that the incorporation of 30% glass sand (36 µm (0.0015 in.)) exhibited the highest flexural strength followed by 70% (36 to 50 µm (0.0015-0.002 in.)) and 70% (36 µm (0.0015 in.)). Mixtures made with 30% (36 µm (0.0015 in.)) and 30% (36–50 µm (0.0015-0.002 in.)) exhibited comparable compressive strength to the control mortar. Lee et al. (2013) reported a reduction in the compressive strength at ages of 7 and 28 days by replacing natural sand in concrete blocks with waste glass (particle sizes < 2.36 mm (0.09 in.) and < 1.18 mm(0.046 in.)) at levels of 25%, 50%, 75%, and 100%. On the contrary, glass sand with particle size smaller than 600 µm (0.023 in.) increased the compressive strength by about 5% and 35% for replacement levels of 25% and 100%, respectively. Du and Tan (2014) investigated the compressive strength of concrete containing glass powder as cement replacement at levels of 15%, 30%, 45%, and 60% by weight of total binder. The evaluated concrete mixtures had a w/cm of 0.49 and slump values of 50 to 70 mm (2-2.75 in.). The results of 7-day compressive strength showed that the replacement of cement with glass powder led to a reduction in strength,

particularly the mixture with 60% glass powder replacement, which exhibited 35% lower compressive strength compared to the reference OPC mixture. Compared to the hydration of OPC, the pozzolanic reaction of fine glass powder is relatively slower and thus the early-age strength of concrete can be reduced. However, with a longer curing age, the benefits of pozzolanic reaction of glass powder can result in a significant enhancement in strength. At 91 days, the mixtures containing 30% and 60% glass powder replacements developed 25% greater and similar compressive strengths, respectively, compared to the control mixture with 100% OPC. They concluded that the 30% glass powder replacement can be suggested as the optimum substitution level of cement with glass powder.

The strength of concrete produced with PLC is significantly affected by several factors, including the quality and quantity of the limestone, the clinker and other cement ingredients, and the PSD of the blended cement (Tennis et al., 2011). Limestone contents up to 15% may increase early-age strength as a combined result of improving particle packing (Sprung and Siebel 1991), increasing the rate of cement hydration (Vuk et al. 2001; Bonavetti et al. 2003), and production of calcium carboaluminate (Voglis et al. 2005). Barrett et al. (2013) investigated the mechanical properties of concrete mixtures made with PLC and a w/cm varying between 0.38 and 0.46. In general, the PLC mixtures exhibited higher compressive strength at early age that diminished with time, thus resulting in similar 28-day compressive strength as that of the control mixture made with OPC. The flexural strength of the PLCs at 7 days of age was similar to the OPCs at all evaluated w/cm. The replacement of PLC with 20% FA resulted in 10% higher compressive strength at early-age compared to the similar mixture made with OPC and FA. This suggests that the relative high rate of hydration of PLC is able to overcome the slow early-age reaction of

mixtures containing FA, thus leading to higher compressive strength at early ages (Barrett et al., 2013).

Durability and transport properties

The use of proper type and content of SCMs can fill the voids among cement particles and enhance the density of the microstructure, thus leading to better durability. In general, SCMs can react with calcium hydroxide to form p hydration products which can reduce the connectivity of the capillary pores in the concrete, thus leading to pore refinement and enhancement in transport properties.

El-Chabib and Syed (2012) reported that SCC mixtures made with binary or ternary blends of SL and/or SF exhibited rapid chloride-ion permeability (RCP) values of 250 to 2100 Coulomb compared to 3700 Coulomb for the control mixture at 56 days. SCC containing 60% Class F FA also showed RCP value of 1510 Coulomb at 56 days. The greatest resistance to chloride ion penetration was observed for ternary blends of 30% Class F FA, 30% SL, and 10% SF with RCP value of 200 Coulomb at 56 days. Şahmaran et al. (2009) reported that regardless of FA type, SCC mixtures containing FA exhibited lower chloride-ion migration compared to similar mixtures made with 100% cement. Their results also indicated that sorptivity of the concretes containing Class C and Class F FAs decreased with the increase in FA content. Hwang and Khayat (2009) pointed out that for SCC mixtures made with a binder content of 475 kg/m^3 (800 lb/yd^3) and a w/cm of 0.35 and 0.42, the use of the quaternary blend of FA, SL, and SF resulted in substantial reduction in capillary porosity and critical pore diameter. This can be due to the greater synergistic effect of using three SCMs.

Yurdakul et al. (2013) investigated the influence of SCMs on electrical resistivity of concrete mixtures made with a binder content of 356 kg/m^3 (600 lb/yd^3) and w/cm of 0.40 and 0.45. For a

given w/cm, the increase in the replacement level of Class F FA in binary mixtures can lead to higher electrical resistivity, whereas binary mixtures with Class C FA exhibited similar results to control mixtures. They reported that binary mixtures with slag cement exhibited the greatest resistivity among all of the evaluated mixtures. Uysal et al. (2012) found that SCC mixtures with a w/cm of 0.33 and containing 35% FA or 60% SL are shown to have RCP values of 150 and 120 Coulomb compared to the 1250 Coulomb for the control mixture with 100% OPC. This reduction in chloride ion penetration can be due to the denser microstructure and higher amount of alumina (Al_2O_3) in mixtures containing SL and FA. As the alumina content increases the total charge decreases, which can lead to higher resistance to chloride ion penetration. Uysal and Akyuncu (2012) investigated the effect of Class C and F FAs at replacement levels of 10% and 17% on transport properties and frost durability of concrete mixtures made with various binder contents, varying between 260 and 400 kg/m^3 (440 and 675 lb/yd^3) . In general, given higher pozzolanic reaction of Class F FA, mixtures made with Class F FA exhibited higher resistance to chloride ion penetration and lower sorptivity compared to the similar mixture made with Class C FA at 91 days. The rate of weight loss of concrete after freezing and thawing increased when increasing the replacement level of Class C and Class F FAs. Hwang and Khayat (2009) reported that for SCC prepared with w/cm of 0.35 and 0.42 and a binder content of 475 kg/m^3 (800 lb/yd^3), the use of 25% SL and 5% SF led to 8% higher frost durability compared to those prepared with the 25% Class F FA and 5% SF.

In general, the incorporation of glass particles has been shown to enhance the transport properties of concrete. Chen et al. (2006) reported that the incorporation of waste glass in mortars as natural sand replacement at levels of 25%, 50%, 75%, and 100% by weight, led to higher resistance to chloride ion penetration. Du and Tan (2014) found that the use of glass sand

in concrete mixtures as natural sand replacement at levels of 25%, 50%, 75%, and 100% by weight, resulted in substantial enhancement in resistance to chloride ion penetration. This can be due to the improvement and densification of the microstructure at the interface between paste and aggregate, given pozzolanic reaction of fine glass particles. Du and Tan (2014) studied the transport properties of concrete containing glass powder as cement replacement at levels of 15%, 30%, 45%, and 60% by weight of total binder. The results of chloride content profiles showed that mixtures made with glass powder up to 60% replacement exhibited lower chloride diffusion coefficient compared to the control mixture with 100% OPC at both 28 and 91 days. The replacement of cement by up to 45% glass powder resulted in lower water penetration depth into concrete and greater resistance to water absorption compared with the mixture without any glass powder.

Barrett et al. (2013) studied the transport properties of concrete mixtures made with PLC and a w/cm varying between 0.38 and 0.46. The results from the migration cell testing showed that the chloride diffusion coefficients in mixtures containing PLC may range from 0 to 30% higher than the OPC. In the case of using FA, both OPC and PLC mixtures exhibited up to 90% lower chloride diffusion coefficients than those of the same systems without FA. The bulk resistivity of PLC mixtures were shown to range within ± 25% of their OPC references mixtures. This variation may be related to changes in pore solution conductivity due to the presence of limestone in these systems, however more research is required to determine these effects. Concrete produced with PLC up to 15% replacement can produce concrete with similar resistance to the penetration of fluids. However, an increase in chloride ion penetration can occur in PLC concrete mixtures when proportioning at the same w/cm as OPC mixture (Tennis et al., 2011).

Shrinkage and cracking resistance

The shrinkage of the concrete depends on several parameters, including the paste volume, water content, cement type and content, pore size distribution, and aggregate type and content. In general, the binder type has significant influence on shrinkage and cracking potential of concrete. Sounthararajan and Sivakumar (2013) reported that concrete made with binary blend of cement and FA had higher resistance to drying shrinkage. For a given workability, a mixture containing FA has lower water demand, which can contribute to lower drying shrinkage of concrete (Tangtermsirikul, 1995). Lee et al. (2006) reported that for the given w/cm, autogenous shrinkage of concrete made with SL increases with an increase in the replacement level of SL from 0 to 50%. On the other hand, partial substitution of cement by SL can result in lower drying shrinkage (the term "drying shrinkage" refers to "total shrinkage" which includes shrinkage induced by both autogenous and drying shrinkages) due to the denser microstructure and lower capillary porosity (Li and Yao, 2001). Li et al. (2010) investigated the autogenous shrinkage and the pore structure of the cement paste with ternary blends of FA and SF, or FA and SL. Their results indicated that the use of FA can reduce autogenous shrinkage, but using SF can increase autogenous shrinkage, which can be due to the higher surface tension in capillary pores. El-Chabib and Syed (2012) reported that replacing up to 70% of cement by SL decreased the free drying shrinkage of concrete by more than 45% compared to that of the control mixture. They found that the use of Class F FA is more effective than Class C FA in reducing drying shrinkage at the same replacement level. For example, SCC made with 60% Class F FA resulted in 20% lower free drying shrinkage compared to the similar mixture containing 60% Class C FA. This can be due to the relatively high pozzolanic reaction of Class F FA which can produce denser microstructure and reduce water evaporation. Güneyisi et al. (2010) studied the drying shrinkage of SCC incorporating various binary and ternary SCMs, including FA, SL, MK, and SF at a

w/cm of 0.32 and 0.44. In the case of a binary system, the replacement of cement with FA, SL or MK is shown to significantly reduce the free drying shrinkage of SCC at w/cm of 0.32. For example, the drying shrinkage of the concrete mixtures with 5% and 15% MK were 22% and 26% lower than that of the control concrete, respectively. The partial replacement of cement with either 60% FA or 60% SL resulted in 26% and 15% reduction in drying shrinkage, respectively. However, the binary use of SF from 10% to 15% increased the total shrinkage compared to the control mixture made with 100% OPC. The negative effect of SF on the shrinkage of SCCs was relatively eliminated with the ternary use of SCMs. The lowest shrinkage of 300 μstrain was observed for the mixture proportioned with 45% FA and 15% MK compared to the 480 μstrain for the control mixture.

Given the relatively low water absorption and impermeable properties of glass particles, the incorporation of glass particles in concrete can reduce the shrinkage (Rashad, 2014). Du and Tan (2014) reported that the use of glass sand in concrete specimens, as natural sand replacement at levels of 25%, 50%, 75%, and 100% by weight, resulted in 5% to 20% lower drying shrinkage compared to the control mixture.

The effect of SCMs on cracking resistance of concrete under restrained shrinkage is not well documented. A delay in the early-age hydration and rate of strength development of the concrete may lower cracking potential due to the increase in the early-age creep and higher stress relaxation. Replacement of cement with Class F FA is typically more effective in delaying the strength gain compared to Class C FA or SL replacement.

Hwang and Khayat (2010) evaluated the cracking potential of SCC made with two w/cm values of 0.35 and 0.42, and three blended binder types, including FA, SL, and SF. The type of binder is shown to have considerable influence on shrinkage cracking potential. For a given w/cm, SCC

made with the B1 binder (70% OPC + 25% Class F FA + 5% SF) exhibited 130% to 380% greater resistance to restrained shrinkage cracking than similar SCC made with the B2 (70% OPC + 25% SL + 5% SF) or B3 (quaternary blended cement containing Class F FA, SL, and SF) binders. Ray et al. (2012) investigated the effect of three different SCM combinations (B1: 30% SL + 5% SF, B2: 20% FA + 5% SF, and B3: 10% MK) and three different w/cm (0.4, 0.35, and 0.3) on shrinkage cracking potential of HPC targeted for bridge deck. The mixture made with 10% MK exhibited 10% lower drying shrinkage after 90 days of drying compared to mixtures made with other SCM combinations. In the case of w/cm of 0.40, the mixture with binder type of B1 developed elapsed time to cracking of 22 days compared to 20 days for mixtures made with B2 or B3 binder type. Li et al. (1999) indicated that the use of SF as a partial replacement of cement not only increases the cracking tendency, but also increases the crack width in the restrained shrinkage ring test.

Bucher et al. (2008) investigated the autogenous, free drying, and restrained shrinkages of mortars made with three cements containing 0%, 5%, and 10% limestone. The autogenous shrinkage during the first 3 days was highest for mortars without limestone (215 μstrain) and the lowest for mortars with 10% limestone (185 μstrain). The amount of drying shrinkage also decreased with increasing limestone content. Restrained mortar samples produced with cement without limestone exhibited elapsed time to cracking of 87 hours. The presence of limestone increased the time to cracking slightly, but all samples cracked after 96 hours. Based on the obtained results, mortars made with PLC exhibited slightly lower shrinkage and a lower tendency to shrinkage cracking compared with similar mortars produced with OPC.

Results presented in this chapter highlight the benefits and limitations of SCMs which can be employed to optimize the binder composition to achieve the required performance specification

for a variety of civil engineering applications. Based on the information provided in this literature, the effectiveness of incorporating SCMs to enhance rheological and mechanical properties, as well as durability is affected by the type and content of the SCM. Proper substitution of cement by SCMs can ensure greater packing density of solid particles, improve workability and mechanical properties, as well as enhance the transport properties of cement-based materials.

2.3. Aggregates

The volume of fine and coarse aggregates often represents more than 60% of total concrete volume. Therefore, the characteristics of aggregate, such as shape, angularity, texture, PSD, fine particle content, S/A, and packing density significantly affect fresh and hardened properties of concrete. In general, aggregate blends with well-graded, rounded, and smooth particles require less paste volume to yield a given workability compared to those with flat, elongated, angular, and rough particles. Concrete mixtures made with combined aggregate of continuous PSD can develop greater packing density, thus requiring less cement demand for a given workability. Therefore, the optimization of aggregate characteristics plays a major factor to produce Eco-Crete.

2.3.1. Particle packing and gradation

An essential step of producing Eco-Crete is to enhance the packing density of the aggregate skeleton. For a given paste volume, an increase in aggregate packing density can improve workability, given the increase in excess paste film thickness surrounding the aggregate particles. In other words, for a given workability, an increase in the packing density of aggregate can reduce the minimum paste volume needed to fill the voids between aggregate particles. The use

of packing density approach to optimize the aggregate skeleton is reported by several studies (de Larrard and Buil, 1987; de Larrard, 1999; Khayat et al. 2000; Chouicha, 2006; Kwan and Li, 2012; Nanthagopalan and Santhanam, 2012). Their results showed that the packing density of aggregate is an important parameter to optimize the mixture composition of concrete. Goltermann et al. (1997) used the packing density models to optimize the aggregate blends with the aim of maximum packing degree. Test results have shown that the modified Toufar model provides a good estimation of the packing density for aggregate combinations. The use of packing models is able to reduce a number of experimentally packing measurements, especially in the case of selection of two or three aggregates from a pool of different aggregates to reach a maximum packing density. Several studies (Andreasen and Anderson, 1929; de Larrard, 2000; Quiroga and Fowler, 2004) indicated that mixtures with good overall performance have packing densities close to the maximum packing density.

The PSD of aggregate significantly affects the fresh and hardened characteristics of concrete. The PSD can influence the packing density of the aggregate skeleton, which can determine the volume of voids to be filled with paste volume. In addition to the packing density, the PSD can affect the specific surface area (SSA) of the granular skeleton that needs to be coated with paste volume. A higher SSA of the granular skeleton can result in a reduction in paste film thickness surrounding the solid particles, thus leading to a lower workability or higher water/admixture demand for a given consistency (Li and Kwan, 2013). There have been many attempts to provide guidelines for an ideal grading curve of aggregate which ensures fresh and hardened performance requirements of concrete. Several theoretical and empirical grading models have been developed to optimize the aggregate combination, such as the Fuller, modified Andreasen

& Andersen (A&A), coarseness factor chart, and 8-18 distribution chart. These grading models are described below.

Fuller curve

Fuller and Thompson (1907) showed that a continuous gradation of aggregate in concrete can help to improve fresh and hardened properties of concrete. Based on the investigation of Fuller and Thompson (1907) and Andreasen and Andersen (1929), a minimal porosity can be theoretically achieved by using the ideal gradation curve shown in Eq. (2-1).

$$P(d) = \left(\frac{d}{d_{\max}} \right)^{q} \quad \textbf{(2-1)}$$

where $P(d)$ is a fraction of the particle size smaller than diameter d, and $d_{\max}$ and q are the maximum particle size diameter and distribution modulus, respectively. The Federal Highway Administration (FHWA) adopted the 0.45 power chart in the 1960 for use in the asphalt industry, and the chart was later adjusted for the concrete industry by reducing the optimum percentage of materials finer than the 2.36 mm (No. 8) sieve to account for the fine cementitious materials.

Funk and Dinger (1994) modified the Andreasen and Andersen (A&A) equation using the minimum particle size concept, as follows:

$$P(d) = \frac{d^{q} - d_{\min}^{q}}{d_{\max}^{q} - d_{\min}^{q}} \quad \textbf{(2-2)}$$

where $d_{\min}$ is the minimum particle size. The modified A&A packing model has been successfully employed to optimize the mix design of different types of concrete, such as conventional concrete (Hüsken, 2010), SCC (Brouwers and Radix, 2005; Mueller et al., 2014;

Khayat and Mehdipour, 2014), roller compacted concrete (Hüsken and Brouwers, 2008; Khayat and Libre, 2014), and lightweight concrete (Yu et al., 2013). A summary of research studies carried out to optimize the granular skeleton using the modified A&A model is provided in Table 2-1. Various types of concrete can be designed by applying different values of A&A distribution modulus, which varies the proportioning between fine and coarse particles in concrete. For example, flowable concrete mixtures necessitate applying a lower A&A distribution modulus, thus incorporating more fine particles to secure required deformability and stability.

Table 2-1- Summary of investigations carried out on granular optimization using A&A model

Reference	Concrete type	Cementitious materials (kg/m^3)	w/cm	Optimized granular materials	A&A distribution modulus
Brouwers and Radix (2005)	SCC	315	0.55	Aggregate and powder	0.25
Hüsken and Brouwers (2008)	Earth-moist concrete	250	0.49	Aggregate and powder	0.35
Yu et al. (2013)	Lightweight aggregate concrete	423	0.54	Aggregate and powder	0.25
Mueller et al. (2014)	SCC	317	0.6	Aggregate and powder	0.27
Yu et al. (2014)	Ultra-high performance fiber reinforced concrete	650	0.33	Aggregate and powder	0.23
Wang et al. (2014)	SCC	380–450	0.4	Aggregate and powder	0.23–0.29
Khayat and Mehdipour (2014)	SCC	315	0.45	Aggregate	0.29
Khayat and Libre (2014)	Roller compacted concrete	300	0.39	Aggregate	0.35

Note: 1 kg/m^3 = 1.69 lb/yd^3

Coarseness factor chart

The coarseness factor chart is another method to analyze the size distribution and uniformity of the combined aggregate gradation by determining the coarseness factor (CF) and workability factor (WF) for the aggregate (Shilstone, 1990). The CF and WF factors are calculated as:

$$CF = \frac{Q}{R}100 \quad \textbf{(2-3)}$$

$$WF = W + \frac{2.5(C-564)}{94} \quad \textbf{(2-4)}$$

where the Q and R values refer to the cumulative mass percent retained on 3/8" and No. 8 sieves, respectively. The W and C values are percent passing mass on the No. 8 sieve and the cementitious materials content (lb/yd^3), respectively. The coarseness factor chart is divided into five zones to identify the probability of satisfying the requirements of aggregate gradation as shown in Figure 2-3. Mixtures belonging to Zone I are gap-graded which require more paste volume to avoid segregation during placement and consolidation due to a lack of intermediate particles. Zone II is the optimum zone (well-graded zone) for maximum nominal coarse aggregate size between 19 and 37.5 mm (0.75 and 1.5 in.). Zone III is the well-graded zone for maximum nominal coarse aggregate size less than 12.5 mm (0.5 in.). Mixtures in Zone IV contain excessive fines which necessitate higher HRWR demand, and mixtures in Zone V are too coarse and harsh and may be difficult to place and consolidate. This chart is based on the assumption that as cementitious material is increased, the fine aggregate content should be reduced to maintain the same workability factor.

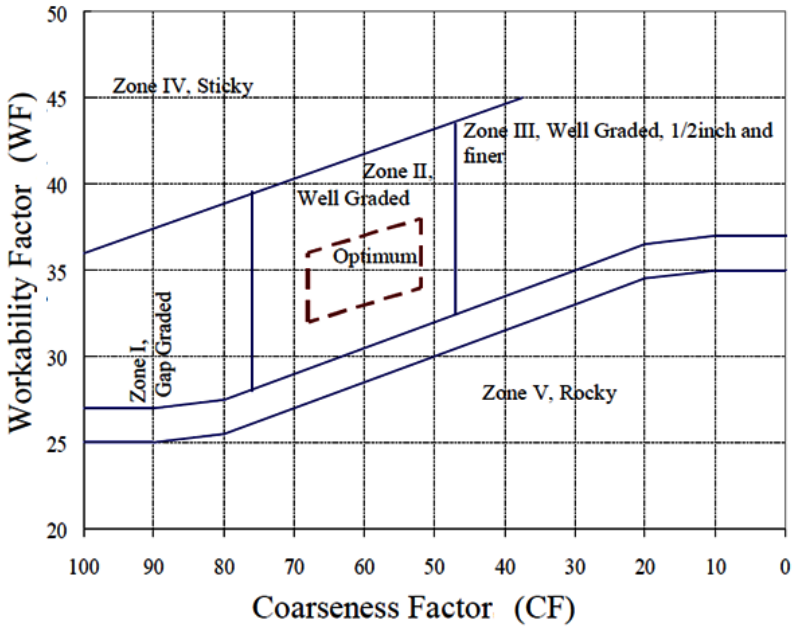

Figure 2-3-Coarseness factor chart

Percent retained chart

The third method that can be used to optimize aggregate gradation is the percent retained chart (referred to as 8-18 distribution chart) proposed by Holland (1990). The method specifies the limits corresponding to the 8% minimum and 18% maximum values of the total combined fine and coarse aggregates retained on each sieve. The aim of this method is to improve concrete performance, durability, and workability for critical structural elements, like high tolerance floor slabs. The results showed that concrete optimized with this method required less paste volume, thus leading to a lower shrinkage (Shilstone, 1990).

2.3.2. Effect of aggregate characteristics on concrete properties

Packing density and particle size distribution of aggregate

In general, the enhancement in the packing density of aggregate can improve the workability of concrete, given the increase in excess paste film thickness around the aggregate particles. Khayat et al. (2000) evaluated the effect of aggregate gradation on packing density and filling ability of

various SCC mixtures proportioned with 420, 480, and 550 kg/m^3 (710, 810, and 930 lb/yd^3) of a blended binder containing approximately 35% limestone filler. The incorporation of aggregate with 0.80 packing density compared to another aggregate combination with a packing density of 0.74 resulted in 40% lower HRWR demand and 10% higher filling capacity.

Nanthagopalan and Santhanam (2012) reported that the increase in packing density of combined aggregates from 0.64 to 0.68 resulted in an increase in slump flow from 420 to 615 mm (16.5 to 24 in.) for SCC made with 0.37 w/cm and a binder content of 495 kg/m^3. Mueller et al. (2014) pointed out that, an improved particle packing of granular materials can minimize the lubricant volume and HRWR demand and enhance the stability of the SCC made with a relatively low binder content of 315 kg/m^3 (530 lb/yd^3). Koehler (2007) reported that aggregate gradation, as well as shape and angularity of aggregate, can significantly affect SCC characteristics. In general, the 0.45 power curve of the combined aggregate gradation can result in an increase in packing density, thus leading to lower paste for a given workability. SCC made with coarser aggregate gradation may exhibit lower HRWR demand and plastic viscosity, but may be harsh and less cohesive due to a lack of fine particles. Finer gradations can contribute to higher HRWR demand and plastic viscosity, but reduce harshness of SCC mixtures.

Hüsken and Brouwers (2008) reported that a general relationship between the distribution modulus of the modified A&A model and the packing fraction of earth-moist concrete can be derived. Their results showed that the highest packing fractions of such concrete can be achieved for a distribution modulus of 0.35. Yu et al. (2014) reported that by enhancing packing density, it is possible to design ultra-high performance fiber reinforced concrete with relatively low binder content. Using the modified A&A model, it is possible to produce a dense skeleton of such concrete with a relatively low binder content of about 650 kg/m^3 (1100 lb/yd^3) to achieve

28-day compressive and flexural strengths of 150 MPa (21750 psi) and 30 MPa (4350 psi), respectively. Wang et al. (2014) employed the particle packing mix design method to design SCC and minimize the required paste volume for a given consistency. The use of A&A distribution modulus ranging from 0.23 to 0.28 is shown to reduce up to 20% binder content compared to the existing SCC mix proportioning methods and still maintain a good performance with moderate shrinkage cracking potential in accordance with ASTM C1581. Wang (2014) applied the concept of paste-to-void volume ratio to evaluate the performance of SCC mixtures made with different aggregate gradations and various binder contents ranging between 380 and 450 kg/m^3 (640 and 760 lb/yd^3). Given a higher packing density of aggregate and higher binder content, the SCC mixtures with higher paste-to-void volume ratio develop relatively higher compressive strength at 28 days.

Lindquist et al. (2015) developed a step-by-step concrete mixture design procedure to determine an ideal aggregate gradation for a given workability. This method uses both the coarseness factor and percent retained charts to establish an optimal blend of available aggregates used in the concrete mix design. The flowchart for the optimization procedure of aggregate gradation is summarized in Figure 2-4. The input data in this optimization procedure includes the gradation of available aggregates, content of cementitious materials, and maximum size aggregate.

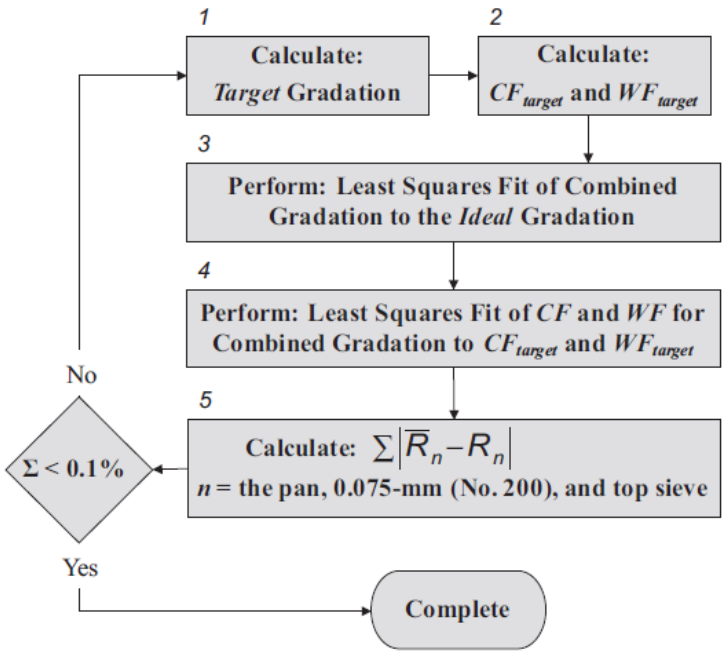

Figure 2-4- Flow chart for determining the optimum combination of aggregates (Lindquist et al., 2015)

Shape and volume of aggregate

The increase in aggregate volume fraction and sand-to-total aggregate ratio generally increase the water content required to reach a given workability. The use of higher fine aggregate proportion increases the surface area which necessitates a higher paste volume needed to coat the particles. The rounded aggregate typically has a lower degree of interlocking of particles than angular particles, thus enhancing the workability of concrete. In general, angular aggregate with rough surface texture has higher surface area, which can develop stronger interfacial transition zone between aggregate and paste, thus leading to greater mechanical properties. Westerholm et al. (2008) studied the effect of grading and particle shape of sand on rheology of mortars prepared with 0.57 w/c and a cement content of 635 kg/m^3 (1070 lb/yd^3). A total of 14 fine aggregates (0–2 mm (0- 0.08 in.) were used in this research, including 13 crushed sands and a natural sand. The results showed that the rheological properties and water demand of mortars

depend significantly on the properties of the fine aggregate. Depending on the shape of fine aggregate, mortars made with crushed sands were shown to have 33% to 133% higher plastic viscosity compared to the mortar prepared with natural sand. Mortar containing elongated sand particles exhibited three times more viscosity than mortar made with spherical sand particles.

Hu and Wang (2011) evaluated the effect of the volume of coarse aggregate on concrete rheology made with w/cm of 0.45. Seven coarse aggregate gradations (four single sizes at 19 mm (0.75 in.), 12.5 mm (0.05 in.), 9.5 mm (0.38 in.), and 4.75 mm (0.18 in.) and three gradations at G1, G2 and G3) were investigated. Results showed that for a given mortar content, the increase in coarse aggregate volume content from 35% to 41% resulted in 50% to 100% higher yield stress and 40% to 60% higher viscosity. Compared to the single-sized aggregate, continuous graded aggregate can exhibit higher packing density, thus leading to a lower yield stress and plastic viscosity.

Aïssoun et al. (2015) investigated the influence of physical characteristics of fine and coarse aggregates, such as fine particle content, shape, texture, and the quantity of elongated particles on the workability and rheological properties of superworkable concrete mixtures made with 0.41 w/cm and a binder content of 400 kg/m^3 (675 lb/yd^3). The results showed that an increase in the fine content (with diameter smaller than 315 μm (0.012 in.)) from 8% to 18% resulted in an increase in plastic viscosity from 15 to 40 Pa.s (0.0021 to 0.0058 psi.s) and reduction in surface settlement from 0.47% to 0.14%. For a given w/cm, the increase in the quantity of fine particles increase the cohesion of the paste, thus leading to an enhancement in static stability. For a given maximum size aggregate, mixtures with rounded aggregates are shown to have 22% to 42% higher surface settlement compared to the similar mixtures made with crushed aggregates. The

increase in the flat and elongated particle content of 22% to 31% led to a considerable increase in yield stress from 18 to 45 Pa (0.0026 to 0.0065 psi).

Based on the review of literature presented herein, a summary of research studies undertaken to optimize the combined aggregate blends is provided in Table 2-2.

Table 2-2- Summary of investigations on aggregate optimization

Reference	Methodology	Concluding remarks
Shilstone (1990)	Coarseness factor chart	water demand ↓ workability ↑ compressive strength ↑
Holland (1990)	Percent retained chart (8-18 distribution)	water demand ↓ cement demand ↓ shrinkage ↓ workability ↑ compressive strength ↑
Goltermann et al. (1997)	Packing model (modified Toufar)	Model effectively optimizes packing of binary and ternary aggregate blends
Jones et al. (2002)	Packing models (modified Toufar, Dewar, and De Larrard's Linear packing and compressible packing models)	All models effectively optimize packing of binary and ternary aggregate blends
Koehler (2007)	0.45 power curve	packing density ↑ cement demand ↓
Brouwers and Radix (2005); Hüsken and Brouwers (2008); Yu et al. (2013); Wang et al. (2014)	Modified A&A model	water demand ↓ cement demand ↓ shrinkage ↓
Khayat et al. (2000); Mueller et al. (2014)	Particle packing mix design for designing Eco-SCC	HRWR ↓ cement demand ↓ filling capacity ↑
Aïssoun, Hwang, and Khayat (2015)	Physical characteristics of aggregate on properties of super workable concrete	volume of granulates ↑ → water demand ↑ packing density ↑ → stability ↑ fine content ↑ → viscosity ↑ fine content ↑ → stability ↑ rounded aggregate ↑ → packing density ↑ rounded aggregate ↑ → stability ↓ flat and elongated particle ↑ → yield stress ↑

2.4. Shrinkage and cracking potential

The shrinkage cracking potential of concrete is influenced by the rate of development of mechanical properties and visco-elastic properties of the material. These properties vary with mixture proportioning and raw material characteristics, including binder type and content, aggregate content and type, fiber type and volume, and chemical admixtures. This section reviews the effect of material constituents and mixture proportions on the shrinkage and cracking potential of concrete.

2.4.1 Factors affecting shrinkage and cracking

Effect of cement type and w/cm content

The type of cement has a considerable effect on the shrinkage cracking potential of concrete. In general, Type II cement reduces cracking potential due to the lower thermal gradient during the early-stage of hydration. Type III cement, on the other hand, may considerably increase cracking potential due to the rapid setting and higher heat of hydration. Higher early-age stiffness results in lower stress relaxation, thus leading to a higher risk of shrinkage cracking (Mehta and Monteiro, 2006).

In the evaluation of 32 concrete bridge decks, Schmitt and Darwin (1999) found that concrete bridge decks containing a paste volume more than 27% exhibited relatively high potential of shrinkage cracking. The evaluated concrete bridge decks had a w/cm ranging between 0.36 to 0.44 and cement content varying from 350 to 390 kg/m^3. Yuan et al. (2011) investigated the effect of paste volume on restrained shrinkage using shrinkage ring test. In the case of 0.45 w/c, the mixture made with 28% paste volume exhibited 9 days longer elapsed time to shrinkage cracking compared to the similar mixture prepared with 33% paste volume. Brown et al. (2001)

show that concrete made with low w/cm tends to exhibit an increase in early-age shrinkage cracking. This is mainly due to the higher heat of hydration, autogenous shrinkage, and stiffness which result in higher magnitudes of stress development and lower stress relaxation.

Bentz et al. (2008) investigated the influence of cement fineness on early-age properties of cement-based materials. The finer cement had a mean particle diameter of 12 μm (0.004 in.) compared to 17 μm (0.006 in.) for coarser cement. In the case of w/c of 0.35 and fine cement, a peak residual stress of 2.45 MPa (355 psi) developed in the ring specimen at 87 h, and a visible crack appeared. On the other hand, for the mixture made with coarse cement, a peak tensile stress of 1.4 MPa (203 psi) developed at a specimen age of 165 h, and no cracking was observed in the coarse cement system during the restrained shrinkage ring test (ASTM C1581). This can be due to lower early-age compressive strength and autogenous shrinkage of mixture made with coarse cement compared to the similar mixture prepared with fine cement.

Hwang and Khayat (2010) evaluated the effect of various mix design approaches and binder types on restrained shrinkage cracking potential of SCC used in the repair applications. The first approach incorporated a low w/cm of 0.35, while the second one employed a viscosity-enhancing admixture (VEA) in SCC made with higher w/cm of 0.42. The mixture proportioning of SCC is shown to have significant influence on shrinkage cracking potential. Mixtures made with 0.42 w/cm exhibited approximately 25% to 35% longer time to cracking compared to similar SCC prepared with 0.35 w/cm. The former concrete had lower elastic modulus at 3 days which led to higher tensile creep coefficient, thus resulting in a greater stress relaxation. The SCC made with 0.42 w/cm exhibited slightly higher drying shrinkage after 56 days of drying (595 μstrain) compared to 565 μstrain for similar concrete prepared with 0.35 w/cm. In general, the tested SCC mixtures had higher cracking potential than the reference high-performance and

conventional concretes. This may be due to the higher paste volume and lower aggregate content of SCC that resulted in greater drying shrinkage.

Effect of internal curing

Shrinkage mitigation through internal curing has recently gained more attention. To implement this technique, several methods have been proposed, including the use of pre-saturated lightweight aggregate (LWA) and super-absorbent polymers. Pre-saturated LWA provides a source of additional water to maintain saturation of the capillary pores in the cementitious paste and avoid self-desiccation. Self-desiccation refers to the reduction in internal relative humidity of concrete stored in a sealed condition, that is, with no transfer of moisture into or out of the concrete. The process of self-desiccation is caused by the chemical shrinkage. As the cement hydrates, this extra water will be drawn from the relatively large pores in the LWA into the much smaller ones in the cement paste. There are many benefits associated with internal curing that include increased cement hydration, higher strength, less autogenous shrinkage and cracking, reduced permeability and higher durability (Bentz et al., 2005).

The efficiency of the LWA varies with the pore structure of aggregate. Generally, larger LWA has a larger pore structure, which results in more efficient internal curing (Hammer et al., 2004). However, it should be noted that well dispersed LWA provides efficient internal curing. This is similar case that properly dispersed air voids improve durability. Several studies proved that smaller LWA are better distributed than larger LWA (Bentz and Snyder, 1999, Bentz et al., 2005).

Henkensiefken et al. (2009) investigated the influence of replacement rates of saturated LWA on the performance of self-curing concrete. The inclusion of a sufficient volume of pre-wetted LWA can significantly reduce free drying shrinkage and delay the elapsed time to cracking. In the case

of 0.30 w/c and cement content of 700 kg/m^3 (1180 lb/yd^3), mortar mixture containing low volume of LWA of 7.3% by volume exhibited similar free drying shrinkage and cracking behavior to the control mixture without any LWA. This may be due to the fact that in the case of low replacement rate, the LWA particles are dispersed too far from each other to effectively supply internal curing water to the paste.

Şahmaran et al. (2009) studied the effect of replacement rate of saturated lightweight sand (LWS) as an internal curing agent on the shrinkage and mechanical behavior of engineered cementitious composites. The addition of saturated LWS was found to be very beneficial in controlling the development of autogenous shrinkage for mixtures made with w/cm of 0.27. A 67% reduction in autogenous shrinkage at 28 days compared to the control mixture can be attained with 20% substitution of normal sand by saturated LWS. In addition, the use of 20% LWS delivered 37% reduction in drying shrinkage after 90 days of drying compared to control specimens.

De la Varga et al. (2012) investigated the application of internal curing for mixtures containing low w/cm of 0.30 and high volumes of Class C FA (up to 60%) which are more susceptible to high shrinkage and cracking. They reported that the slower hydration reaction in the high volume FA mixtures results in less initial autogenous shrinkage deformations at early ages. However, due to the pozzolanic reaction and refining the porosity, the rate of autogenous shrinkage increases in the FA mixtures at later ages. This behavior can lead to higher risk of shrinkage cracking potential at later ages. Their results showed that the use of 15% LWA by volume can be a beneficial method to provide internal curing and reduce tensile stress development caused by restrained shrinkage.

Golias et al. (2012) studied the performance of LWA with different initial moisture content. Their results indicated that the oven-dried LWA is able to absorb water from the paste prior to setting, then absorbed water will be returned to the system as internal curing water. When mixture proportion adjustments are properly made to account for the water absorbed by the oven-dried LWA before setting, the mixture can provide internal curing benefits.

Hwang et al. (2013) conducted a factorial design approach to investigate the effect of initial moist curing duration (0 to 6 days) on HPC made with a cement content of 470 kg/m^3 (790 lb/yd^3) and different w/cm (0.30 to 0.40) and replacement rates of LWS (0 to 30% by volume). Concrete made with 30% LWS replacement with no moist-curing exhibited up to 45% lower shrinkage at 9 days compared to similar concrete without any LWS. Combined use of 30 % LWS and 7 days of moist curing can lead to greater decrease in total shrinkage compared to the incorporation of 30% LWS without moist curing or 7 days of moist curing without any LWS.

Effect of shrinkage reducing admixture

Shrinkage reducing admixtures (SRA) are used to reduce the rate and magnitude of both autogenous and drying shrinkage of concrete. Several studies have shown that the use of SRA in concrete reduced the shrinkage and cracking potential (Weiss and shah, 2002, Radlinska et al., 2008, Rajabipour et al., 2008). Weiss et al. (1998) showed that the use of SRA significantly reduced drying shrinkage and increased the elapsed time to cracking by reducing the rate and magnitude of the shrinkage. Shah et al. (1992) evaluated the effect of three different SRAs on the restrained shrinkage using the ring-type test. Restrained shrinkage was shown to decrease with the increase in SRA dosage, thus resulting in a delay in shrinkage cracking. The incorporation of SRA also resulted in a reduction in restrained shrinkage crack width.

Hwang and Khayat (2008) carried out an experimental program to investigate the influence of SRA on shrinkage cracking of SCC designated for repair applications. Two mixtures were proportioned with moderate and high dosage rates of SRA (4 and 8 L/m^3 (0.8 and 1.6 gal./yd^3)) and a w/cm of 0.42 to evaluate the effect of SRA addition on shrinkage cracking potential. The incorporation of SRA led to a substantial enhancement in the resistance to restrained shrinkage cracking. Mixtures made with moderate and high dosage rates of SRA developed longer elapsed time to cracking of 13.3 and 20.7 days, respectively, compared to 8.8 days for similar SCC made without any SRA. Depending on the dosage of SRA, mixtures containing SRA exhibited 25% to 37% lower drying shrinkage compared with the control mixture without SRA.

Lura et al. (2007) investigated the effect of SRA on the plastic shrinkage cracking of mortars in accordance with ASTM C1579 test. They found that mortars containing SRA exhibited fewer and narrower plastic shrinkage cracks compared to those made without any SRA. The lower surface tension of the capillary pores in the mortars containing SRA results in less evaporation, settlement, and capillary tension.

Effect of expansive cement

Expansive cements (EX) can lead to the early-age expansion which later counteracts the tensile stresses developed by drying shrinkage. Type K EX contains Portland cement and calcium sulfoaluminate (CSA-based system) cement, in which the expansion is achieved through formation of ettringite crystals. CSA-based cement also provides a sustainable alternative to Portland cement by reducing CO_2 emission during manufacturing. Type G EX (CaO-based system) is another type of EX in which the formation of calcium hydroxide ($Ca(OH)_2$) crystals results in an expansion. The third type of EX is magnesium oxide-based EX (MgO-based system) in which the hydration of MgO leads to the formation of magnesium hydroxide

($Mg(OH)_2$). $Mg(OH)_2$ has a larger volume than its constituents (MgO) which results in an expansion in concrete (Du, 2005). The efficiency of MgO on the concrete expansion depends on dosage rate and concrete temperature. The increase in concrete temperature can lead to higher and faster hydration of MgO, thus resulting in greater expansion in concrete (Du, 2005).

Chen et al. (2012) evaluated the effect of w/c for cement paste containing calcium sulfoaluminate cement. In the case of w/c of 0.30, there is less space for the formation of hydration products, including ettringite compared to similar mixture made with 0.45 w/c. The expansive pressure from ettringite growth increases when space is restricted, thus leading to a higher expansion. Also, since there is less water available for hydration reactions, fewer hydration products can form prior to self-desiccation, which could lead to expansion later when external water is supplied.

Chaunsali and Mondal (2014) evaluated the expansion characteristics of calcium sulfoaluminate cement in the presence of SCMs. The effect of incorporation of Class C FA (15%, by mass), Class F FA (15%, by mass), and SF (5%, by mass) on expansion of cement paste mixtures made with 15% CSA-based EX and different w/cm of 0.34 and 0.44 were investigated. Regardless of the w/cm, the incorporation of 15% Class F FA replacement led to higher expansion of cement paste compared to the control mixture without any SCMs. This can be due to the lower resistance of material to expansion due to the presence of Class F FA, given the lower compressive strength of such a mixture. On the other hand, the use of Class C FA or SF in CSA-based cement paste is shown to decrease the expansion value compared with the control mixture made with 85% cement and 15% CSA-based EX. The addition of SF resulted in incomplete hydration of CSA-based EX at both w/cm due to self-desiccation which led to lower expansion of CSA-based cement.

Effect of fiber

In general, the incorporation of fiber can enhance the resistance of concrete to restrained shrinkage cracking. This is attributed to the higher tensile strength and tensile creep coefficient of concrete containing fibers. Grzybowski and Shah (1990) evaluated the efficiency of different types and volumes of fibers on the reduction in the shrinkage cracking potential of concrete using ring-type specimens. Concrete mixtures were proportioned with steel fibers measuring 25 mm (1 in.) in length and 0.4 mm (0.016 in.) in diameter as well as 19 mm (0.75 in.) fibrillated polypropylene fibers. The dosage rates of the steel fibers were 0.25%, 0.5%, 1%, and 1.5%, by volume. These values were 0.1%, 0.25%, 0.5%, and 1% for the polypropylene fiber. Test results revealed that a steel fiber content of 0.25% can substantially reduce the crack width resulting from restrained shrinkage. For a given fiber dosage, the steel fiber was more effective in reducing cracking than polypropylene fiber.

Voigt et al. (2004) investigated the effect of different fiber types and geometries on shrinkage and early-age cracking potential. Their results indicated that, for a given fiber type, an increase in the number of fibers increases their effectiveness to reduce shrinkage cracking potential. The steel fiber with flat end and 30 mm (1.18 in.) length was the best-performing reinforcement in prolonging the age of the first crack and reducing the maximum crack width. Regardless of the fiber type, the incorporation of fiber (even at low fiber volume of 0.25) led to more than 50% reduction in crack width compared to the plain concrete without any fiber. They concluded that the correlation of the maximum crack width to the mortar thickness provides the best measure to characterize the shrinkage cracking behavior of the fiber-reinforced composites. For mortar thickness more than 0.522 mm (0.02 in.), the increase in mortar thickness led to higher crack width of restrained shrinkage using the ring test.

Hwang and Khayat (2008) compared the restrained shrinkage results of SCC mixtures made with various synthetic fiber volumes. Two types of polypropylene synthetic fibers were used: a monofilament fiber with a circular cross section measuring 50 mm (2 in.) in length and 0.67 mm (0.026 in.) in diameter (SyF1) and straight fiber with a rectangular cross section measuring 40 mm (1.6 in.) in length (SyF2). The increase in synthetic fiber volume from 0 to 0.5% resulted in a 40% increase in elapsed time before cracking. This is due to the increase in the tensile creep coefficient resulting from the use of synthetic fibers. The type of synthetic fiber is shown to have a considerable influence on the restrained shrinkage cracking potential. SCC made with 0.25% SyF2 fiber exhibited a longer time to cracking of 8.3 days compared to 5.2 days for the same SCC with 0.25% SyF1 fiber.

Effect of combined use of shrinkage reducing/compensating materials

In general, the combined use of shrinkage reducing and compensating materials can be more effective in reducing shrinkage and cracking tendency. Hwang and Khayat (2008) studied the effect of combined use of fiber and SRA on shrinkage cracking of high-performance SCC designated for repair applications. A ring-type test (ASTM C1581) was used to evaluate the potential for restrained shrinkage cracking and tensile creep behavior of the concrete. The elapsed time before cracking of SCC made with combined use of 0.5% synthetic fiber and 8 L/m^3 (1.6 $gal./yd^3$) SRA was approximately four times longer than that of the similar fiber-reinforced SCC prepared without SRA. This is mainly due to the synergistic effect of fiber and SRA that can increase the tensile creep coefficient and reduce the risk of cracking.

Passuello et al. (2009) evaluated the effect of combined use of PVA fiber and SRA on shrinkage and cracking potential of concrete mixtures made with a 0.50 w/c and a cement content of 400 kg/m^3 (675 lb/yd^3). The risk of cracking was evaluated in accordance with the standard ASTM

C1581, however, some geometry modifications were made. In their study, the thickness of the concrete ring was increased from 38 mm (1.5 in.) suggested by the ASTM C1581 to 50 mm (2 in.) to provide better situation for casting and vibration for the fiber reinforced concrete made with macro fibers. The incorporation of 4 kg/m^3 (6.75 lb/yd^3) SRA delays the time to cracking and reduces the crack width by 40% compared to the control mixture. The addition of fibers on the other hand, does not greatly increase elapsed time before cracking, but it can reduce the crack width by about 70% with the use of 0.5% fiber volume. The addition of SRA to the fiber-reinforced concrete produced a better cracking behavior, even at a lower fiber volume of 0.25%.

Kassimi and Khayat (2013) investigated the effect of combination of fiber, SRA, and EX on shrinkage cracking of SCC mixtures made with a w/cm of 0.42 designated for repair applications. Fiber used in this investigation included multifilament synthetic fibers and hooked-end steel fibers with lengths of 50 and 30 mm and aspect ratios of 74 and 55, respectively. The SRA and EA concentrations were set to 2% and 6%, by mass of cementituous materials. The highest resistance to restrained shrinkage cracking was observed for SCC made with 0.8% steel fiber and EX with an elapsed time to cracking of 36 days and a crack width of 85 μm (0.0033 in.).

Soliman and Nehdi (2014) evaluated the effect of SRA and wollastonite microfibers on the early-age shrinkage behavior and cracking potential of ultra HPC. Wollastonite microfibers were added at rates of 0, 4%, and 12%, by volume and SRA was used at 1% and 2%, by cement weight. The combined use of wollastonite microfibers and SRA in such concretes prolonged the time to cracking through the synergistic effect of reducing shrinkage strains and bridging micro cracks. For instance, the incorporation of 1% SRA and 4% wollastonite microfiber resulted in 84%, 33%, and 43% longer elapsed time before cracking compared to the control mixture

(without fiber and SRA), mixture made with 1% SRA, and mixture incorporating 4% wollastonite microfiber, respectively. They found that the use of wollastonite microfibers can promote pore discontinuity, thus leading to lower mass loss and less drying shrinkage.

Meddah et al. (2011) evaluated the induced stress development during autogenous shrinkage of HPC mixtures prepared with combined use of CaO-based EX and SRA. Concrete mixtures were proportioned with 6 kg/m^3 (10.1 lb/yd^3) SRA and different replacement rates of 15, 20, and 25 kg/m^3 (25.3, 33.7, and 42.1 lb/yd^3) of EX. Self-induced stress measurements were performed using a reinforcing bar embedded at the center of specimens measuring 100 × 100 × 1400 mm to provide partial restraint to the concrete specimen. The authors reported a substantial reduction of up to 50% of autogenous shrinkage and the induced self-tensile stress for concrete made with a combination of SRA and EX and w/cm of 0.15. Meddah and Sato (2010) investigated the effect of different shrinkage reducing materials, including a binary system of SRA and EX and ternary system of internal curing provided by the porous ceramic coarse aggregate, SRA, and EX on autogenous shrinkage and internal self-stress of HPC mixtures made with 0.15 w/c. Their results indicated that the ternary shrinkage reducing system containing 6 kg/m^3 (10.1 lb/yd^3) SRA, 15 kg/m^3 (25.3 lb/yd^3) CaO-based EX, and 20% of the porous aggregate significantly mitigated both autogenous shrinkage and induced tensile stress compared to the binary curing system of SRA and EX.

Based on the review of literature, the effect of mixture parameters and material constituent on the shrinkage and cracking potential of concrete is summarized in Table 2-4.

Table 2-3- Effect of mixture parameters and material constituents on shrinkage and early-age cracking

Parameter	Content	Autogenous shrinkage	Drying shrinkage	Cracking tendency
w/cm	Low	↑	↓	↑
	High	↓	↑	↑
Cement content	Low	↓	↓	↓
	High	↑	↑	↑
Aggregate content	Low		↑	↑
	High		↓	↓
SRA	↑	↓	↓	↓
Fiber	↑	↑↓	↑↓	↓
EA	↑	↓	↓	↓
LWA	↑	↓	↓	↓

2.4.2 Research on bridge deck shrinkage cracking by various DOTs

Texas Department of Transportation (TxDOT) evaluated the effectiveness of using alternative materials to control shrinkage cracking in concrete bridge deck (Folliard et al., 2003). The authors found that crack-free or highly crack-resistant concrete with a relatively low drying shrinkage and early-age modulus of elasticity, and high early-age tensile strength should exhibit no cracking when tested in the shrinkage ring test. The incorporation of shrinkage reducing materials, such as using high volume FA replacement, SRA, Type K EX (calcium sulfoaluminate based), and polypropylene fiber are shown to provide higher resistance to early-age shrinkage cracking.

Kansas DOT (KDOT) studied the effect of various factors on the drying shrinkage behavior of concrete mixtures (Deshpande et al., 2007). The results showed that drying shrinkage of concrete increases with a reduction in aggregate content and curing period. Darwin et al. (2010) proposed a new class of HPC with low shrinkage cracking designated for bridge construction. Some of the mix design specifications of such HPC include: optimization of aggregate gradation using

coarseness factor and percent retained chart, moderate w/cm (0.43-0.45), air volume of 8% ± 1.5%, low slump of 40 to 90 mm (1.6 to 3.5 in.), and low cementitious materials content (less than 320 kg/m^3 (540 lb/yd^3)).

New Jersey DOT (NJDOT) performed a research project to investigate the shrinkage cracking potential of the HPC mixtures for bridge decks in New Jersey State (Nassif et al., 2007). An extensive experimental program was conducted, including compressive strength, splitting tensile strength, modulus of elasticity, free drying shrinkage, and restrained shrinkage. The content cementitious materials, content of coarse aggregate, and coarse-to-fine aggregate volume ratio are shown to have a significant effect on both drying and restrained shrinkages. They reported that the use of high content of coarse aggregate (more than 1110 kg/m^3 (1870 lb/yd^3)) with high coarse-to-fine aggregate volume ratio (more than 1.5) and limitation of cementitious material to 415 kg/m^3 (700 lb/yd^3) could significantly reduce the risk of shrinkage cracking. The lower drying shrinkage of 450 μstrain at 56 days was recommended to ensure the high cracking resistance for bridge decks made with HPC.

New York DOT (NYDOT) investigated the effectiveness of ternary cement blends containing SF and Class F FA on shrinkage cracking reduction of HPC (Subramaniam and Agrawal, 2009). The combined use of FA and SF is shown to reduce the shrinkage cracking potential under restrained condition. This can be attributed to the lower magnitude of elastic modulus with a slower rate of strength development, which can lead to a relatively high stress relaxation compared to the control mixture made with 100% cement.

Colorado DOT (CDOT) focused on changes in material specifications and construction practices to reduce the concrete bridge deck cracking (Shing and Abu-Hejleh, 1999). The use of Type II cement and Class F FA was suggested to reduce heat of hydration and early-age strength

development. A maximum 6% SF by mass of the binder and well-graded aggregate blends were recommended to reduce shrinkage cracking of concrete bridge decks.

Ohio DOT (ODOT) investigated the bridge deck cracking issues through an in-state field survey (Crowl and Sutak, 2002), laboratory testing (Delatte et al., 2007), and a full-scale bridge deck study (Delatte and Crowl, 2012). The field survey included a total of 116 HPC bridge decks constructed between 1994 and 2001. The results of the survey showed that concrete bridge decks made with coarse aggregate with a relatively high absorption capacity (more than 1%) exhibited minimal or no cracking. Laboratory testing results indicated that the internal curing provided by fine lightweight aggregate reduced the shrinkage behavior of HPC mixtures, especially in the case of using high absorptive coarse aggregate (more than 1%).

Pennsylvania DOT (PennDOT) performed a comprehensive experimental investigation on the material properties of concrete mixtures typically used for PennDOT bridge deck projects to evaluate the early-age and long-term performance and the risk of cracking of concrete mixtures (Rajabipour et al., 2012). The risk of plastic shrinkage cracking should be eliminated by implementing water curing with adequate duration (minimum of 7 days) to minimize water evaporation from the surface of fresh concrete during construction and reduce the restrained shrinkage cracking.

Based on the review of literature presented herein, a summary of research recommendations provided by different DOTs for low shrinkage concrete bridge decks is presented in Table 2-4.

Table 2-4- Summary of recommendations provided by DOTs for low cracking concrete bridge decks

DOT	Reference	Recommendations
TxDOT	Folliard et al. (2003)	Optimized concrete mix design to develop low shrinkage, high tensile strength, and low elastic modulus using polypropylene fiber SRA Type K EX high volume FA
KDOT	Deshpande et al. (2007) Darwin et al. (2010)	Optimized aggregate gradation binder content less than 320 kg/m^3 (540 lb/yd^3) moderate w/cm of 0.43-0.45
NJDOT	Nassif et al. (2007)	Coarse-to-fine aggregate volume ratio of 1.5 cementitious material less than 415 kg/m^3 (700 lb/yd^3) lower drying shrinkage to 450 µstrain at 56 days
NYDOT	Subramaniam and Agrawal (2009)	Ternary blends of Class F FA and SF
CDOT	Shing and Abu-Hejleh (1999)	Type II cement and Class F FA well-graded aggregate blends SF less than 6%, by mass of binder
ODOT	Crowl and Sutak (2002) Delatte et al. (2007) Delatte and Crowl (2012)	Lightweight aggregate and high absorptive coarse aggregate (more than 1%) to provide internal curing.
PennDOT	Rajabipour et al. (2012)	Water curing with sufficient duration (minimum of 7 days) to reduce plastic shrinkage

Note: 1 kg/m^3 = 1.7 lb/yd^3

3. EXPERIMENTAL PROGRAM

3.1. Materials

Cementitious materials

Commercially available Type I/II ordinary Portland cement (OPC) was used in this study. Class C FA, SL, and SF were employed in the binary and ternary cementitious systems. Figure 3-1 shows the PSD of cementitious materials. The SEM images of the investigated cementitious materials are presented in Figure 3-2. A commercially available Type G expansive agent was used. Type G expansive agent (Type G EX) is CaO-based system in which the formation of calcium hydroxide ($Ca(OH)_2$) crystals causes expansion. The physical and chemical characteristics of the cementitious materials used in this investigation are presented in Table 3-1.

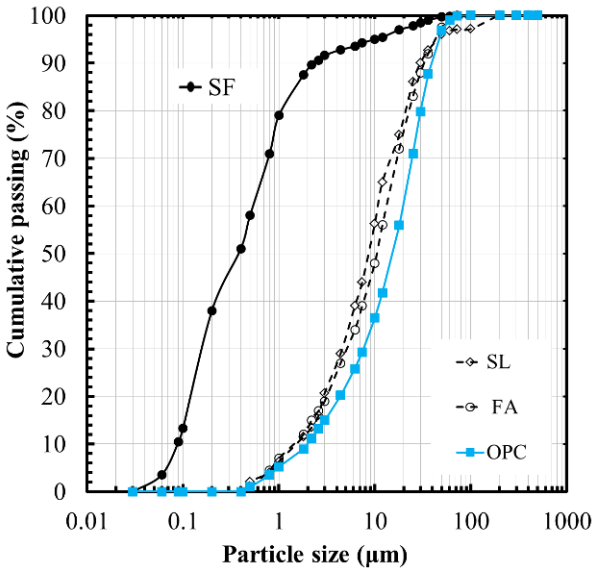

Figure 3-1- PSD of cementitious materials

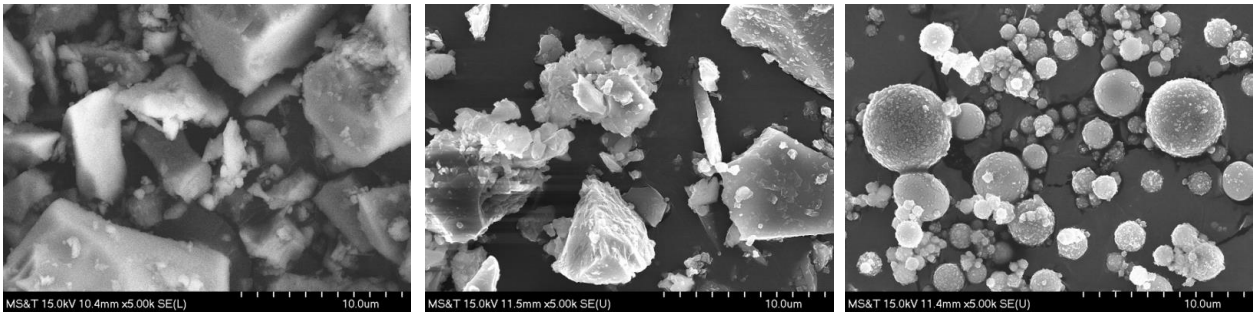

OPC **SL** **Class C FA**

Figure 3-2- SEM images of cementitious materials with magnification of 5000

Table 3-1- Physical and chemical characteristics of cementitious materials and expansive agents

	OPC	Class C FA	SL	SF	Type K EX	Type G EX
SiO_2, %	19.8	36.5	36.8	85	7.7	12.6
Al_2O_3, %	4.5	24.8	9.2	0.4	7	5.7
Fe_2O_3, %	3.2	5.2	0.8	0.5	1.2	1.9
CaO, %	64.2	28.1	37.1	–	50.1	82.6
MgO, %	2.7	5	9.5	–	0.1	0.1
SO_3	3.4	2.5	0.1	–	26	
Na_2O eq., %	–	–	0.3	–	0.6	0.9
$CaCO_3$, %	3.3	–	–	–	–	–
Blaine surface area, m^2/kg	390	498	570	16500	–	–
Density	3.14	2.71	2.86	2.3	2.9	3.1
LOI, %	1.5	0.5	–	2	2.1	–

Chemical admixtures

The chemical admixtures used in this study included a polycarboxylate-based HRWR, a liquid-based cellulose viscosity-enhancing admixture (VEA), and a synthetic-based air-entraining agent (AEA). A commercially available crack-reducing admixture (CRA) was also incorporated to reduce shrinkage. The CRA is a liquid chemical admixture based on a specialty alcohol alkoxylate, which is formulated to reduce drying shrinkage and minimize the potential for early-

age shrinkage cracking. Similar to conventional SRAs, the CRA reduces the surface tension of water, and it provides similar reduction in drying shrinkage at equal dosages. However, typical results for restrained shrinkage testing of untreated concrete, conventional SRA-treated concrete, and concrete treated with the CRA show that the CRA changes the mode of failure from a sudden release of all the compressive strain to a gradual reduction in strain in the inner steel ring, thereby providing a greater increase in time-to-cracking (Nmai et al., 2014)). This phenomenon may be attributed to the relaxation of tensile stress within the CRA-treated concrete specimens (Nmai et al., 2014).

The AEA dosage was adjusted to secure fresh an air volume of 5% ± 2%. The HRWR dosages varied to obtain various slump consistencies targeted for pavement (50-100 mm (2-4 in.)) and bridge deck (100-200 mm (4-8 in.)) applications. Table 3-2 presents the characteristics of the chemical admixtures in use.

Table 3-2- Characteristics of chemical admixtures

	Solid content (%)	Specific gravity
HRWRA	23	1.05
VEA	1.5	1
AEA	12.5	1.01
CRA	–	0.98

Fibers

Two types of fibers, including synthetic fibers and steel fibers recycled from waste tires were used, as shown in Figure 3-3. The synthetic fiber (structural fiber) is multi-filament with a length and diameter of 50 mm (2 in.) and 0.67 mm (0.027 in.), respectively. It has a specific gravity of 0.92 and tensile strength of 625 MPa (90 ksi). Recycled steel fibers are generally recovered by a shredding process of tires, followed by an electromagnetic procedure aiming at separating steel

fibers from the rubber. The fibers obtained are typically characterized by an irregular shape (wavy shape) and variable lengths and thicknesses, as shown in Figure 3-3. The geometry of recovered steel fibers was characterized using statistical distribution of around 100 steel fibers that were randomly selected. The statistical distributions of variation in lengths and thicknesses of recycled steel fibers are presented in Figure 3-4. The fiber thickness and length varied between 0.2–1.6 mm (0.008–0.063 in.) and 5–55 mm (0.2–2.15 in.), respectively. Based on the results, the majority of steel fibers had lengths varying between 10–30 mm (0.4–1.18 in.) and thicknesses of 0.2–0.4 mm (0.008–0.16 in.). Recently, in the context of a growing interest towards innovative materials recycling and sustainable buildings, some studies proposed the use of steel fibers recovered from waste tires, in concrete. However, more research is required to assess the performance of such fibers for the use in pavement and structural applications. In this research, the reinforcing efficiency of such fibers was compared with that of the synthetic structural fibers in terms of flexural strength, toughness, post-cracking behavior, and load-deflection of large-scale beam elements. It is important to note that the use of recycled steel fibers for pavement and structural applications

(a) Recycled steel fibers **(b) Synthetic fibers**

Figure 3-3- Fiber types used in this study

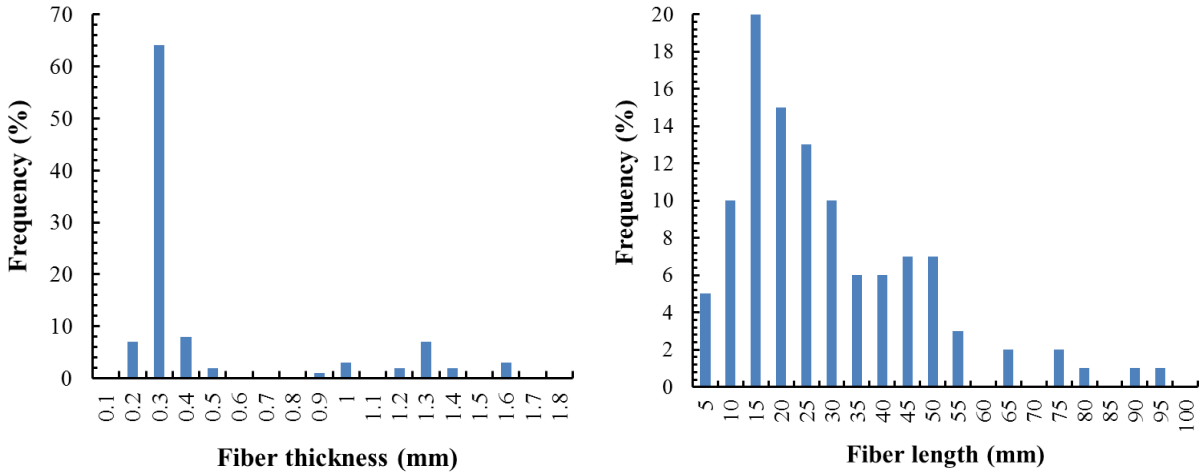

Figure 3-4- Variation in geometries of recovered steel fibers

Aggregates

The research team visited different aggregate quarries in Missouri to evaluate the performance of locally available aggregates. Figure 3-5 shows the locations of various aggregate quarries visited in this investigation to study the aggregate characteristics.

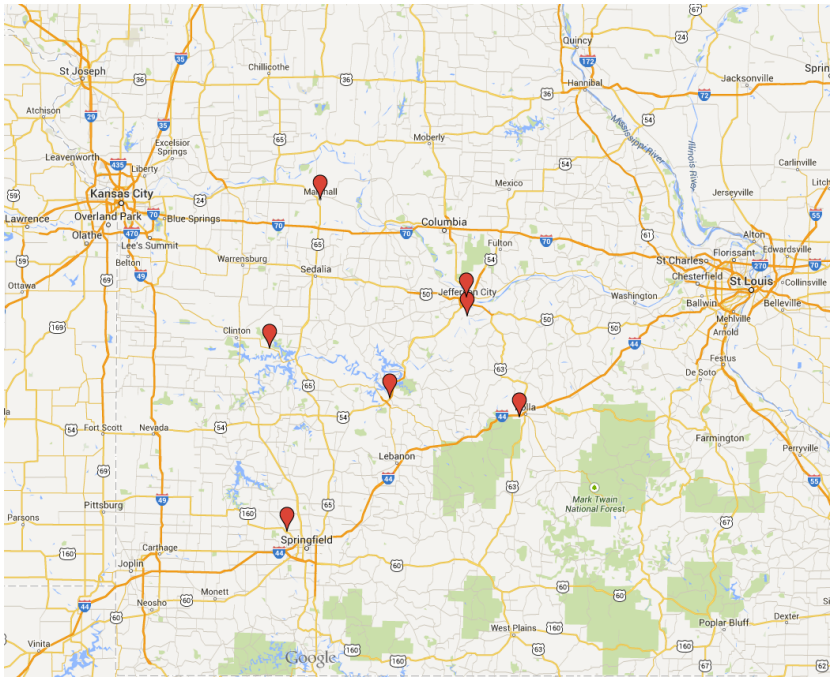

Figure 3-5- Location of aggregate quarries visited in this investigation

In total, 17 different aggregate samples with different shapes, textures, and PSDs were taken from various aggregate quarries for preliminary evaluation, as listed in Table 3-3. The physical characteristics of aggregates, including specific gravity and water absorption, were collected from aggregate producers. A photograph of selected aggregates employed for preliminary evaluation is shown in Figure 3-6.

Table 3-3- Selected aggregates from different quarries for preliminary evaluation

Name	Producer	Quarry	Size	Angularity
River sand	Rolla ready Mix	Jefferson City, Missouri River	Fine	Rounded
3/8" Clean CapitCoInc	Capital Sand Company, Inc.	Wardsville, Osage River	Intermediate*	Crushed
Gravel (5/16") CapitCoInc	Capital Sand Company, Inc.	Jefferson City, Missouri River	Intermediate	Rounded
Gravel (7/16") CapitCoInc	Capital Sand Company, Inc.	Jefferson City, Missouri River	Intermediate	Rounded
Sand (Osage riv.) CapitCoInc	Capital Sand Company, Inc.	Wardsville, Osage River	Fine	Crushed
3/8" Minus CapitCoInc	Capital Sand Company, Inc.	Wardsville, Osage River	Intermediate	Crushed
1/2" Clean CapitCoInc	Capital Sand Company, Inc.	Wardsville, Osage River	Intermediate	Crushed
Sand (Osage riv.) CapitCoInc	Capital Sand Company, Inc.	Wardsville, Osage River	Fine	Rounded
1" Clean CapitCoInc	Capital Sand Company, Inc.	Wardsville, Osage River	Coarse	Rounded
1/2" (Captial Quar)	Capital Quarries	Rolla	Intermediate	Crushed
3/8" (Captial Quar)	Capital Quarries	Rolla	Intermediate	Crushed
1" (Captial Quar)	Capital Quarries	Rolla	Coarse	Crushed
Crushed Dolo (1/2")	Capital Quarries	unknown	Intermediate	Crushed
APAC 1", LinCreek	APAC - Missouri, Inc	Linn Creek Quarry, Gasconade	Coarse	Crushed
APAC MFS, LinCreek	APAC - Missouri, Inc	Linn Creek Quarry, Gasconade	Fine	Crushed
1” Dolo	Riverstone Quarry Inc	Sullivan	Coarse	Crushed
APAC MFS, Tightwad	APAC - Missouri, Inc	Tightwad Quarry, Burlington	Fine	Crushed

* Intermediate aggregates have nominal maximum size varying from 12 mm to 6 mm.

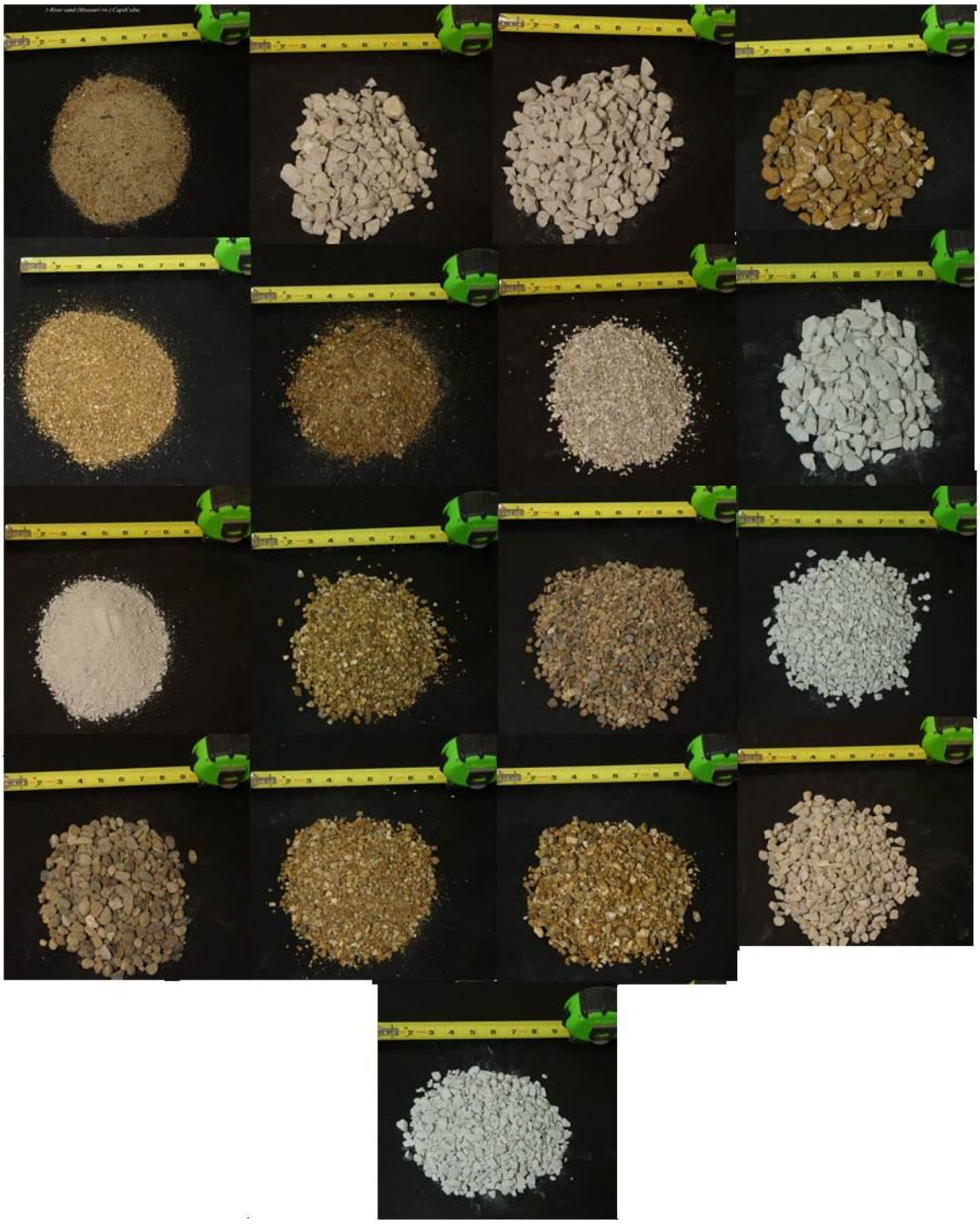

Figure 3-6- Photo of sampled aggregates

The PSDs of the fine, intermediate, and coarse aggregates are shown in Figure 3-7. The PSDs of sampled aggregates represent a wide range of aggregates located in Missouri. The fineness

modulus of fine aggregates varies from 2.56 to 4.2. The maximum nominal size of coarse aggregate was limited to 25 mm (1 in.), which is typically used for pavement and transportation infrastructure applications.

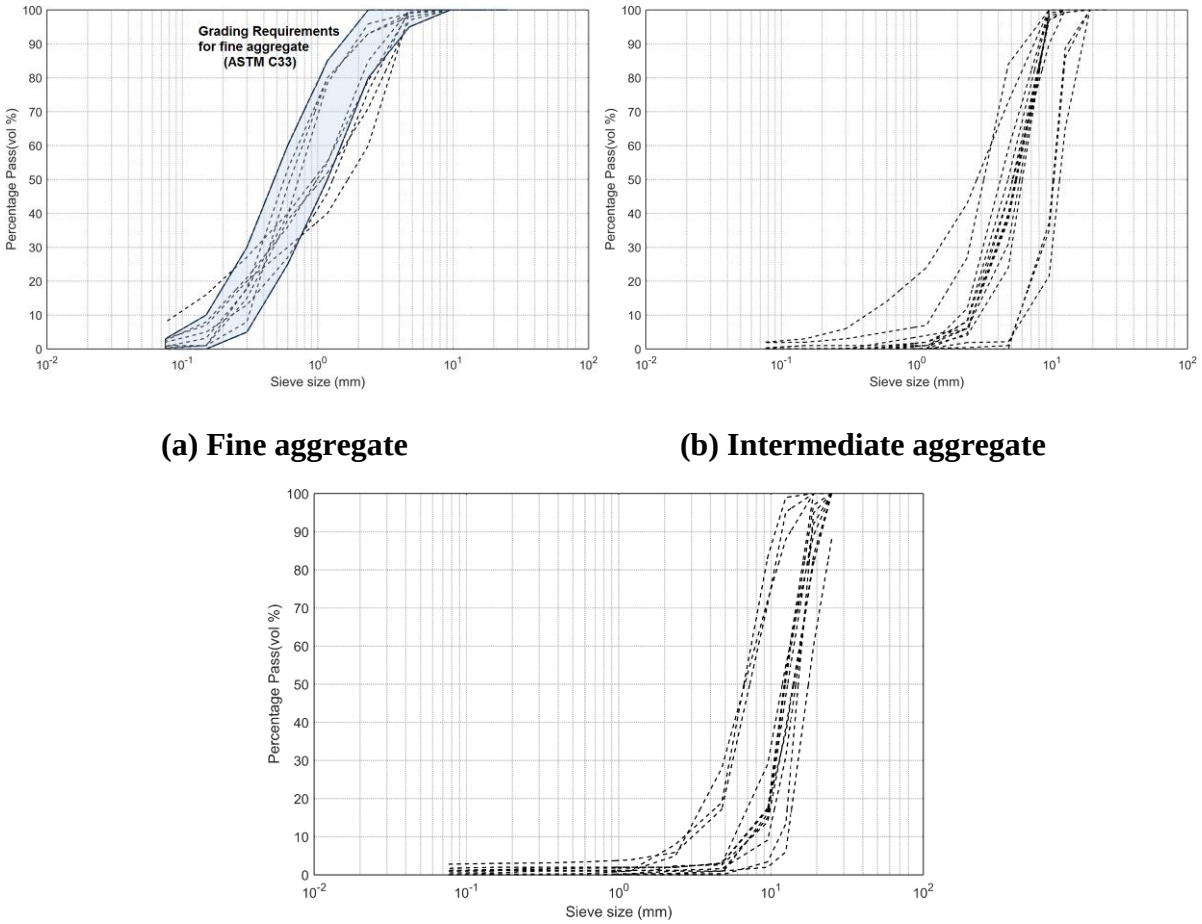

(a) Fine aggregate **(b) Intermediate aggregate**

(c) Coarse aggregate

Figure 3-7- PSDs of examined aggregates

(Hatched area refers to grading limits in accordance with ASTM C33)

The influence of physical characteristics of aggregates, including shape, texture, PSD, and fineness modulus on packing density was determined. The packing density of aggregate was measured using three different methods. This included the loose packing (ASTM C29), dense

packing using rodding procedure (ASTM C29), and dense packing using intensive compaction tester (ICT), as shown in Figure 3-8. ICT is generally used for compaction of granular materials, such as soil, as well as zero slump/stiff concrete such as roller compacted concrete. A constant vertical pressure is applied on a sample placed inside the cylinder mold that rotates at a gyratory angle for a maximum of 512 cycles. Due to the gyratory inclination, a shear body develops during the measurement. Shear movement under vertical pressure allows solid particles to get closer to each other, thus leading to achieving a higher packing density. The packing density of granular materials (ϕ) is calculated as follows:

$$\phi = \frac{\rho_d}{\rho_{d\max}} \quad \textbf{(3-1)}$$

$$\rho_{d\max} = \frac{1}{\frac{P_1}{\rho_1} + \frac{P_2}{\rho_2} + \frac{P_3}{\rho_3} + \ldots} \quad \textbf{(3-2)}$$

where P_1, P_2, and P_3 are mass percentages of the various materials used in the mixture, and ρ_1, ρ_2, and ρ_3 refer to specific gravity values of the different materials. The applied vertical pressure should be selected below a critical value that would lead to grinding or crushing of the particles. The critical pressure for tested granular material can be determined using the difference between its PSD before and after applying the various pressure values. After preliminary evaluation of various types of aggregates under different pressure values and consolidation cycles, the parameters of ICT were fixed, as presented in Table 3-4. The vertical pressure was adjusted to 2 bar (29 psi) to avoid aggregate crushing or grinding during the IC-testing.

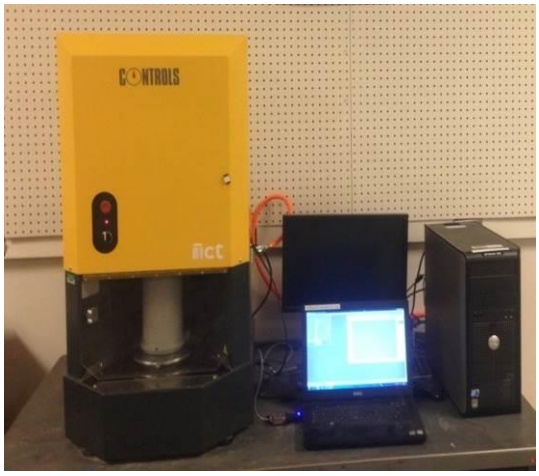

Figure 3-8- Gyratory intensive compaction tester

Table 3-4- Testing parameters selected for ICT

Parameter	Unit	Available range	Selected
Vertical pressure	bar	0.5-10	2
Number of cycles		2-512	256
Velocity	rpm	0-60	60
Gyratory angle	mrad	0-50	40

3.2. Experimental program

The methodology to develop and optimize the crack-free and Eco-HPC for a given performance-based specification was carried out through four phases, as described below:

Subtask 1- Optimization of binder composition

This subtask aims at optimizing the binder composition of Eco-Pave-Crete and Eco-Bridge-Crete based on the HRWR demand, packing density, flow characteristics, rheological properties, and development of compressive strength, as well as drying shrinkage and bulk resistivity. Extensive information reviewed from current literature was analyzed to finalize the laboratory testing program. This phase was conducted using concrete equivalent mortar (CEM) formulated from

environmentally friendly Eco-HPC mix design proportioned with various binder contents of 320 kg/m^3 (540 lb/yd^3) and 350 kg/m^3 (590 lb/yd^3) targeted for Eco-Pave-Crete and Eco-Bridge-Crete, respectively. The mix design parameters and material constituents targeted for different applications (Eco-Pave-Crete and Eco-Bridge-Crete) are summarized in Table 3-5.

Table 3-5- Testing program for binder optimization

Concrete type	Powder type	Content, by volume	w/cm	Cementitious materials content	Chemical admixture type	HRWRA content
Eco-Pave-Crete	Ordinary portland cement (OPC)		0.40	320 kg/m^3 (540 lb/yd^3)	High-range water reducer (HRWR)	Adjusted to secure the mini slump flow of 135 ± 10 mm (5.31 in.)
	Blast furnace slag (SL)	0-60%				
	Class C fly ash (CFA)	0-55%				
Eco-Bridge-Crete	Ordinary portland cement (OPC)		0.40	350 kg/m^3 (590 lb/yd^3)	High-range water reducer (HRWR)	Adjusted to secure the mini-slump flow of 190 ± 10 mm (7.5 in.)
	Blast furnace slag (SL)	0-60%				
	Class C fly ash (CFA)	0-55%				
	Silica fume (SF)	0-10%				

In total, 11 CEM mixtures were made with different types and replacement rates of binary and ternary cementitious materials. The mixture proportions of the evaluated mortar mixtures are listed in Table 3-6.

Table 3-6- Mixture proportions of the investigated CEM mixtures (volume-basis)

Type	Mixture no.	Codification	OPC	SL	CFA	SF
Eco-Pave-Crete	1-1	1-OPC	100	0	0	0
	1-2	1-FA55	45	0	55	0
	1-3	1-SL60	40	60	0	0
	1-4	1-SL20FA35	45	20	35	0
	1-5	1-SL20FA50	30	20	50	0
Eco-Bridge-Crete	2-1	2-OPC	100	0	0	0
	2-2	2-FA40	60	0	40	0
	2-3	2-SL60	40	60	0	0
	2-4	2-FA40SF5	55	0	40	5
	2-5	2-SL60SF5	35	60	0	5
	2-6	2-SL20FA35	45	20	35	0

Note: CFA: Class C fly ash, SL: slag, and SF: silica fume

Subtask 2- Optimization of aggregate characteristics

The goal of this subtask was to optimize the aggregate proportions to achieve the maximum possible packing density that was evaluated on blends of fine, intermediate, and coarse aggregates. Given various aggregate combinations and blends, the preliminary selection of optimum aggregate combination was carried out using existing theoretical packing density models to determine the optimal aggregate combinations and blends. The selected aggregate combinations (sand, intermediate, and coarse aggregates) with relatively high packing density were experimentally validated. In this phase, the results of experimentally measured packing densities were compared with those estimated from theoretical packing density models. The selected aggregate combinations were proportioned with various sand-to-total aggregate ratios to optimize the proportioning for a given aggregate combination. In order to determine the optimum proportioning of aggregate blend, the statistical mixture design (SMD) method was utilized. SMD method provides an efficient tool for determining the predicted model as well as for optimizing the mixture proportion. In this method, the main principle is that the sum of all

constituents for a given mixture is equal to 1. In general, assuming that the mixture consists of n constituents at which x represents the proportion of the i*th* constituent in the mixture, the sum of the material constituents is expressed as follows:

$$0 \le x_i \le 1 \qquad i = 1, 2, ..., n \qquad \sum_{i=1}^{n} x_i = 1 \qquad \textbf{(3-3)}$$

This method can be effectively employed to determine the optimum proportions of blended aggregates to achieve the maximum possible packing density. An example of various aggregate proportions used for SMD is given in Table 3-7. The results of packing density of blended aggregates are used as input to derive the prediction model for packing density response. The derivation of numerical model enables the determination of optimal aggregate proportion corresponding to the maximum achievable packing density.

Finally, the selected aggregate blends were ranked based on the residual error defined as the minimum deviation of aggregate blends from the target grading. The target grading was considered to be the modified Andreasen grading with the maximum and minimum particle size varying between 20 micron and 19 mm (0.75 in.), respectively.

Table 3-7- Random proportions of aggregate blends used for SMD

Run	Fine Agg.	Intermediate Agg.	Coarse Agg.
1	45	30	25
2	30	0	70
3	55	0	45
4	20	30	50
5	70	10	20
6	35	30	35
7	40	20	40
8	55	15	30
9	25	45	30
10	30	15	55
11	40	5	55
12	20	60	20
13	100	0	0
14	0	100	0
15	0	0	100

Subtask 3- Evaluation of shrinkage mitigating strategies

This subtask focused on evaluating the effect of different shrinkage mitigating materials on autogenous and drying shrinkage, and compressive strength development of CEM mixtures. Depending on the binder composition, the effectiveness of incorporating shrinkage mitigating materials can be different. Therefore, in this phase the effect of shrinkage mitigating materials on shrinkage properties of mortars proportioned with optimized binder compositions from phase 1 of this investigation was examined. The investigated materials included expansive agents (CaO-based and MgO-based), crack reducing admixture (CRA), and lightweight sand (LWS). In total, 20 mortars made with different binder compositions and shrinkage mitigating materials were evaluated, as given in Table 3-8. The experimental program, including workability, shrinkage, mechanical properties, and durability is presented in Table 3-9.

Table 3-8- Testing parameters to evaluate various shrinkage mitigating materials

Series	Description	Binder type				Lightweight sand (LWS)	Expansive agent (EX)		No. of mixtures
		Ref	Pavement	Bridge deck					
		100% OPC	Selected binder 1	Selected binder 1	Selected binder 2	25% replacement	7.5% CaO-based system	5% MgO-based system	
1	Effect of binder type	x	x	x	x				4
2	CaO-based EX	x	x	x	x		x		4
3	MgO-based EX	x	x	x	x			x	4
5	Effect of LWS 1 combined with EX	x	x	x	x	x	x		4
6	Effect of LWS 2 combined with EX	x			x	x	x		2
7	Crack-reducing admixture	x			x				2

Table 3-9- Experimental program used for phase 3

Property	Test
Flow characteristics	Admixture demand for a given fluidity
Kinetics of cement hydration	Calorimetry
Setting time	Penetration resistance for autogenous shrinkage measurement
Mechanical properties	Compressive strength at 7, 28, and 56 days for different curing regime
Durability	Surface resistivity (AASHTO T95) at 28, 56, and 91 days Bulk electrical conductivity (ASTM C1760) at 28, 56, and 91 days
Shrinkage properties	Autogenous shrinkage (ASTM C1698) Drying shrinkage (ASTM C157)

The investigated mixtures from this subtask were also subjected to different durations of initial moist curing to evaluate the influence of curing regime on the performance of various shrinkage mitigating materials. Table 3-10 presents the proposed initial moist curing duration of the investigated mixtures.

Table 3-10- Proposed initial moist curing period

Moist curing duration	Detail
Air curing	1 day in mold, then air drying at 23 °C and 50% RH
Moist-curing of 3 d	1 day in mold, then 2 days moist-curing, then air drying at 23 °C and 50% RH
Moist-curing of 7 d	1 day in mold, then 6 days moist-curing, then air drying at 23 °C and 50% RH
Continuous moist curing	1 day in mold, then continuous moist-curing until the age of testing

Subtask 4- Development of crack-free Eco-Crete

This subtask was carried out to evaluate and optimize Eco- and crack-free HPC. Based on the obtained results from previous phases, the effect of different binder compositions, aggregate characteristics, and shrinkage mitigating materials were evaluated and the results were analyzed to design Eco- and crack-free HPC with different targeted applications (Eco-Pave-Crete and Eco-Bridge-Crete). The investigated mix design parameters for the design of Eco-HPC are summarized in Table 3-11.

Table 3-11- Mix design parameters for design of Eco-HPC

Mix	Description	Binder content		Binder type				Fiber type and content			Shrinkage reducing/compensating materials	
		320 (kg/m^3)	350 (kg/m^3)	100% OPC	Selected binder 1	Selected binder 2	Selected binder 3	TUF strand fiber (0.35%)	STRUX® 90/40 synthetic fiber (0.35%)	Steel fiber from tire (0.35%)	25% LWS	7.5% Type G EX
R	Reference		x	x								
B1	Effect of binder type	x				x						
B2			x			x						
B3		x			x							
B4			x				x					
B1	Effect of LWS		x			x					x	
B2		x			x						x	
B3			x				x				x	
F1	Effect of fiber type		x			x		x				
F2			x			x			x			
F3			x			x				x		
E1	Effect of EX		x			x						x
EF1	Combined effect of fiber and EX		x			x		x				x
EF3			x			x				x		x

3.3. Mixing and test methods

3.3.1. Mixing procedure

The mixing sequence for the mortar mixtures consisted of homogenizing the sand for 60 sec, before introducing half of the mixing water. The cementitious materials were then added and mixed for 30 sec followed by the HRWR diluted in the remaining water. The mortar was mixed

for 3 min and remained at rest for 2 min for fluidity adjustment before remixing for 3 additional min.

The mixing procedure for the concrete mixtures that were prepared using a drum mixer with 150 L capacity is as follows:

1. Homogenize sand and pre-wetted lightweight sand (if used) for 60 sec.
2. Incorporate coarse aggregate, fibers (if used), half of the mixing water, and AEA and mix for 1 min.
3. Add the powder materials (and EX if used) and mix for 30 sec.
4. Add half of remaining water, and mix for 1 min.
5. Add the remaining water and HRWR, and mix for 3 min (and SRA if used).
6. Keep the concrete at rest for 2 min followed by remixing for additional 2 min.

3.3.2. Test methods for mortar mixtures

Concrete equivalent mortar (CEM) mixtures were made to evaluate the performance of different SCM types and replacement rates on fresh and hardened properties as well as assess the effect of various shrinkage mitigating materials on autogenous shrinkage, drying shrinkage, and compressive strength development. The laboratory investigations used for CEM are presented below.

Hydration kinetics

The heat flow evolution during hydration of the investigated CEMs was determined using isothermal calorimetry (Figure 3-9) at a constant temperature of 20°C for 3 days. The thermal power and energy measured to maintain the temperature at 20°C were then used to evaluate the

influence of SCM replacements on reaction kinetics and cumulative heat released of the mortar mixtures.

Figure 3-9- Isothermal calorimetry used for hydration kinetics of mortar

Rheological properties

The coaxial cylinders rheometer with inner and outer radii of 50 and 62 mm, respectively, was employed to determine the rheological properties of mortar, as shown in Figure 3-10. The testing procedure consisted of pre-shearing the sample at the maximum rotational velocity applied during the test for 30 s, followed by a time step decrease of the rotational velocity from 0.5 rps (10 steps) to 0.025 rps. The rheological properties were obtained by taking the average of the torque and rotational velocity during the last four seconds of each step, ensuring the fact that the torque was in equilibrium. The Reiner–Riwlin transformation was applied to calculate yield stress and plastic viscosity. Special attention was provided during the measurements and analysis to identify and eliminate artefacts, such as thixotropy, segregation, and plug flow. In the case of potential plug flow, the correction was applied by means of an iterative procedure (Feys et al., 2015). In parallel to the rheological properties, the mini-slump flow test was used to evaluate the fluidity retention of the mortar mixtures at 10 and 70 min following the first contact of cementitious materials with water.

Figure 3-10- Coaxial cylinders rheometer used to determine rheological properties of mortar

Packing density

The packing density of solid particles in mortar was determined based on the "wet packing approach" proposed by Wong and Kwan (2008). The test procedure for mortar made with a 350 kg/m^3 binder content (100% OPC) and 0.10% HRWR is presented in Figure 3-11. The method involves the preparation of mixtures with various volume-based water-to-binder ratio $(w/b)_V$ and measuring the wet density of the mixture. The wet density was determined using a cylindrical mold of 400 ml in volume, filled with mortar and consolidated using a vibrating table for 30 sec before measuring the packing density, as shown in Figure 3-12. This can enable any large air bubbles entrapped during mixing to rise to the surface. The wet density is calculated as follows:

$$\rho_i = \frac{M_i}{V} \quad \textbf{(3-4)}$$

where V refers to the volume of mold (400 ml). ρ_i, and M_i are wet density and mass of the sample, respectively.

As indicated in Figure 3-11, the wet density of the mortar increases with increasing water content until reaching a threshold value (point A), beyond which the wet density decreases with further

water addition. The water content corresponding to the maximum wet density is considered as the optimum water demand (OWD) for a given mixture (point A in Figure 3-11). It is important to note that at point A, corresponding to the peak wet density, the mixture does not have flow value measured using a mini-slump flow test. In the case of a mixture with low water content (before point A), the mixture looks like a wet powder composed of agglomerated grains at which water is not sufficient to lubricate the matrix, thus leading to a lower density. On the other hand, with further water addition (beyond point A) the mass of sample decreases, thus resulting in lower wet density.

The measurement of the mass corresponding to the maximum wet density enables the calculation of the packing density of solid phase (cementitious grains and sand particles) in the mortar as follows:

$$\phi = \frac{V_s}{V} \quad \textbf{(3-5)}$$

where ϕ is the packing density of solid phase and V_s refers to the total volume of solid phase in the mold, which is calculated as follows:

$$V_s = \sum_i^n V_{si} = \frac{M_{\max}}{\rho_w (V_w / V_s) + \sum_i^n \rho_{si} R_{si}} \quad \textbf{(3-6)}$$

where $\sum_i^n V_{si}$ represents to the sum of volumes of solids and M_{max} is the mass of sample corresponding to the maximum wet density (point A in Figure 3-11). ρ_w and ρ_{si} are the density of water and specific gravities of solids (cementitious grains and sand particles), respectively. R_{si} refers to the volumetric ratio of solids.

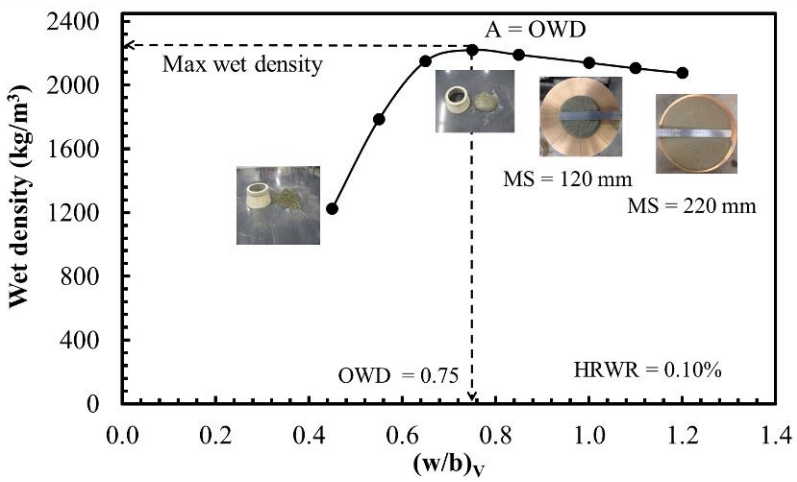

Figure 3-11- Variation in wet density with water addition for mortar made with 100% OPC and 0.10% HRWR (MS refers to mini-slump flow)

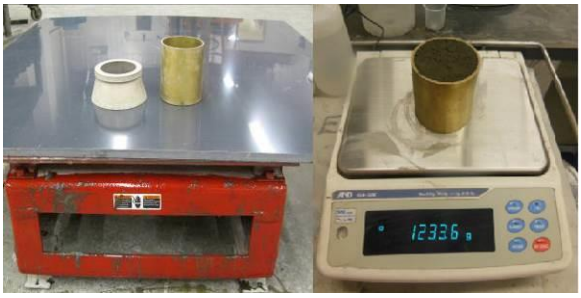

Figure 3-12- Packing density test setup

Autogenous shrinkage

Autogenous shrinkage of mortars made with different shrinkage reducing strategies was determined according to ASTM C1698, as seen in Figure 3-13. For each mixture, two corrugated cylindrical samples were prepared using polyethylene tubes. According to ASTM C1698, the initial reading for the autogenous shrinkage of a mortar sample should be carried out at the final setting time of the mortar. Therefore, the final setting time of mortar mixtures were determined according to ASTM C403, as indicated in Figure 3-14.

Figure 3-13- Autogenous shrinkage measurement device

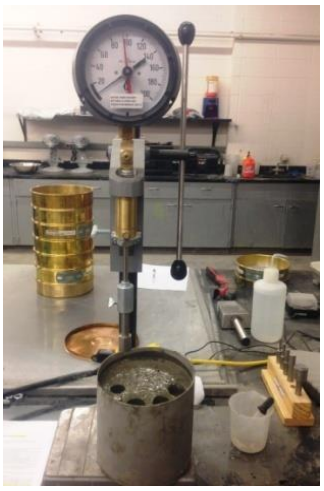

Figure 3-14- Setting time test setup

Drying shrinkage

Drying shrinkage of the mortar (ASTM C596) was determined using a digital type extensometer to measure changes in length of prismatic specimens measuring 25 × 25 × 285 mm (1 × 1 × 11.25 in.), as shown in Figure 3-15. After demolding at 24 h, the beam specimens were immersed in water for 6 days, then the samples were transferred to a temperature and humidity controlled room set at 23 ± 1°C and 50% ± 3% RH, and the shrinkage was monitored until the age of 56 days.

Figure 3-15- Drying shrinkage measurement of mortar

Compressive strength

The 1-, 3-, 7-, 28-, 56-, and 91-day compressive strengths of mortars were determined using 50-mm cube specimens according to ASTM C109. The cubes were demolded after one day and stored in lime-saturated water at 21 ± 2°C until testing age. The results of compressive strength represent the average values of three specimens. The values of coefficient of variation (COV) of compressive strength results were lower than 5%.

3.3.3. Test methods for concrete mixtures

The experimental matrix carried out on the concrete phase is summarized in Table 3-12.

Mechanical properties

Cylindrical specimens measuring 100 × 200 mm (4 × 8 in.) were cast to determine compressive strength (ASTM C39), modulus of elasticity (ASTM C469), and splitting tensile strength (ASTM C496) at 3, 28, 56, and 91 days. Prismatic specimens measuring 75 × 75 × 400 mm (3 × 3 × 16 in.) were cast to determine the flexural strength and toughness of fiber-reinforced concrete (FRC) according to ASTM C1609 (Figure 3-16). The toughness of the FRC was calculated from the load-deflection curve under displacement control.

Table 3-12- Experimental matrix for concrete phase

Concrete property	Concrete type		Test
	Eco-Pave-Crete	Eco-Bridge-Crete	
Workability	*	*	Unit weight (ASTM C138), air content (ASTM C 231), slump
Mechanical properties	*	*	Compressive strength (ASTM C39) at 3, 7, 28, 56, and 91 days
	*	*	Modulus of elasticity (ASTM C469), splitting tensile strength (ASTM C496) at 56 days
	*	*	Flexural strength (ASTM C78) at 56 and 91 days
	*	*	Flexural performance of fiber reinforced concrete (ASTM C1609) at 56 and 91 days
Durability	*	*	Resistance to freezing and thawing (ASTM C666, Proc. A)
	*	*	De-icing salt scaling resistance (ASTM C672)
	*	*	Water absorption (ASTM C642) at 56 and 91 days
	*	*	Sorptivity (ASTM C1585) at 56 and 91 days
		*	Surface resistivity (AASHTO T95) at 56 and 91 days
		*	Bulk electrical conductivity (ASTM C1760) at 56 and 91 days
	*	*	Abrasion resistance (ASTM C944) at 56 days
Shrinkage properties	*	*	Autogenous shrinkage (ASTM C1698) and drying shrinkage (ASTM C157)
	*	*	Restrained shrinkage ring test (ASTM C1581)

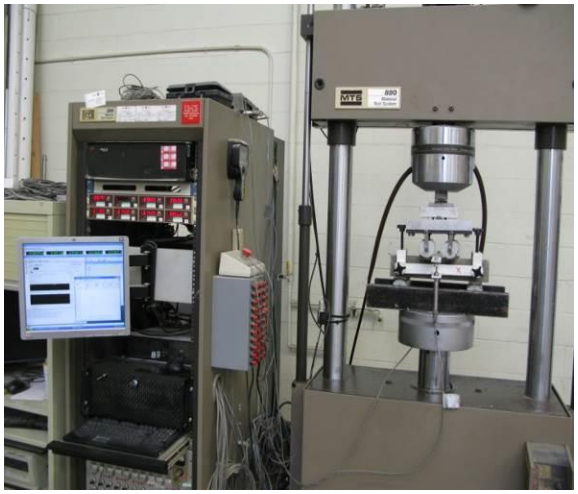

Figure 3-16- Test setup for flexural toughness measurement of FRC beams

Durability

The abrasion resistance of concrete mixtures was evaluated in accordance with ASTM C944, as shown in Figure 3-17. The specimens were moist cured for 56 days before testing. The abrasion test consists of three abrasion cycles at which each cycle lasts two minutes. A double load of 197 N [44 lbf] was applied at a rate of 300 rpm using a drill press. After each cycle, mass loss was calculated by subtracting the initial from final mass.

Figure 3-17- Abrasion resistance test setup

Prisms measuring 75 × 75 × 400 mm (3 × 3 × 16 in.) were prepared to evaluate freeze-thaw resistance of concrete mixtures according to the ASTM C666, procedure A (Freezing and thawing in water). Given pozzolanic reactivity of SCMs, concrete made with a high replacement rate of SCMs requires higher curing time compared to concrete made with 100% OPC. In general, the use of longer period of moist curing for concrete containing high volume of SCMs can result in a denser microstructure and lower capillary porosity compared to the similar mixture subjected to lower moist curing period. Therefore, the specimens were moist cured for 56 days before freeze-thaw testing. Specimens were subjected to 300 freeze-thaw cycles, and after every 36 cycles, the mass loss and transverse frequency of concrete specimens were

monitored. The ultrasonic pulse velocity test was used to determine the dynamic modulus of elasticity of the specimens. Figure 3-18 shows the freeze-thaw chamber and ultrasonic pulse velocity instrument.

Figure 3-18- Freeze-thaw chamber (left) and ultrasonic velocity instrument (right)

The de-icing salt scaling was determined in accordance with ASTM C672. Slabs had a minimum surface area of 0.045 m^2 (72 in.) and 75 mm (3 in.) in depth. A dike was placed on the finished surface of the specimen. This dike was used for ponding the surface of the specimen with a solution of calcium chloride with a concentration of 4.0%. The specimens were subjected to 50 cycles of freezing and thawing. The top surface of the slab was washed, and the damage was qualitatively assessed after every five cycles. In this procedure, the surfaces of samples were rated based on a scale of 0 to 5, corresponding to no scaling to severe scaling, respectively. The mass of scaling residue of the tested mixtures was also measured.

The electrical resistivity measurement was used to classify the concrete according to the corrosion rate. The measurement of electrical resistivity was determined using two different methods; direct two-electrode method (ASTM C1760) and the four-point Wenner probe method (AASHTO TP 95-11), corresponding to bulk electrical conductivity and surface resistivity, respectively (Figure 3-19). The electrical resistivity was measured using cylindrical samples

measuring 100 mm (4 in.) in diameter and 200 mm (8 in.) in height and cured in saturated lime water until the age of testing. The electrical resistivity is calculated as follows:

$$\rho = R \times k \quad \textbf{(3-7)}$$

where ρ is the resistivity, and R and k refer to measured resistance and geometry correction factor, respectively. The geometry correction factor for surface resistivity and bulk electrical conductivity can be calculated as:

$$k(\textit{surface resistivity}) = \frac{2\pi a}{1.1 - \frac{0.73}{d/a} + \frac{7.82}{(d/a)^2}} \quad \textbf{(3-8)}$$

$$k(\textit{bulk electrical conductivity}) = \frac{A}{L} \quad \textbf{(3-9)}$$

where d, A, a, and L refer to diameter, cross section area, probe spacing, and length of the specimen, respectively.

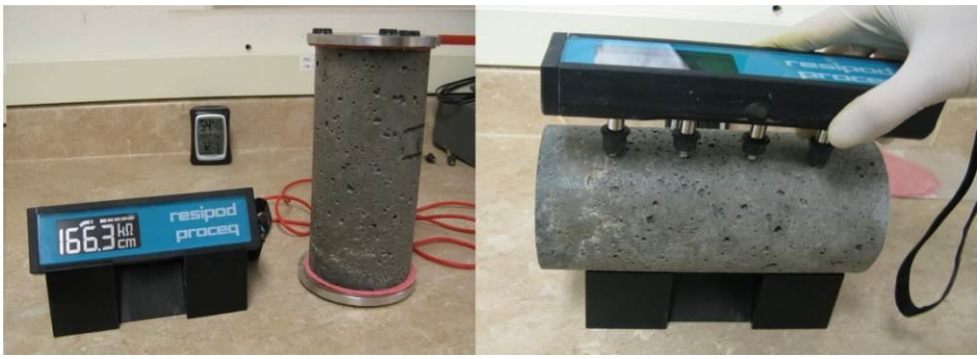

Figure 3-19- Bulk electrical conductivity (left) and surface resistivity (right)

Cylindrical specimens measuring 100 × 100 mm (4 × 4 in.) were sampled to determine the water absorption of concrete according to ASTM C642. This test method determines the water absorption after immersion in water (B). Samples were dried in an oven at a temperature of 110

± 5°C until the difference between any two consecutive mass values is less than 0.5% of the obtained lowest value (A). The water absorption of concrete specimens is calculated as follows:

Absorption after immersion = [(B-A)/A] ×100 **(3-10)**

The sorptivity of concrete mixtures was determined in compliance with ASTM C1585. The test consisted of measuring the increase in mass of a disc specimen at given intervals of time when permitted to absorb water by capillary suction. After 56 days moist curing, cylinder samples from each mixture were cut in three disc specimens measuring 50 mm (2 in.). The specimens were then placed in the environmental chamber at a temperature of 50°C and RH of 80% for 3 days. After the 3 days, each specimen was placed inside a sealable container and stored at a temperature of 23 ± 2°C for at least 15 days until the samples reached the equilibrium mass at which the moisture distribution is consistent within the test specimen. Prior to absorption testing, the side surface of the samples was sealed with aluminum tape and the top surface was covered with plastic wrap. This was to prevent drying of the sample from these surfaces. The test procedure is schematically illustrated in Figure 3-20. The amount of absorbed water is normalized by the cross-section area of the specimen exposed to the fluid as follows:

$$I = \frac{m_t}{a \times d} \quad \textbf{(3-11)}$$

where I is the absorption, m_t is the specimen mass at time t (gr); a is the exposed area of the specimen (mm^2), and d is the density of the water. The absorbed fluid volumes are then plotted as a function of the square root of time. The initial sorptivity is determined from the slope of the curve during the first 6 h according to ASTM C1585, while secondary sorptivity is determined

using the slope of the same measurements between 1 day and 7 days, as outlined in ASTM C1585.

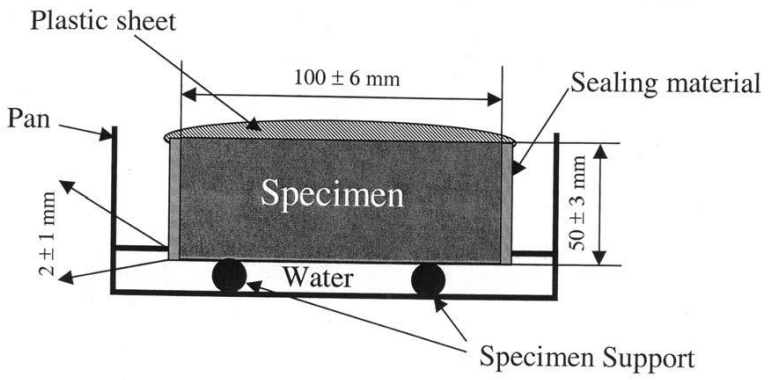

Figure 3-20- Schematic illustration of sorptivity test

Shrinkage and cracking resistance

Drying shrinkage of concrete mixtures (ASTM C157) was determined with a digital type extensometer using prismatic specimens measuring 75 × 75 × 285 mm (3 × 3 × 11.25 in.). After demolding at 24 h, the prismatic specimens were immersed in water for 6 days. The samples were then stored in a temperature and humidity controlled room at 23 ± 1°C and 50% ± 3% RH. Shrinkage was then measured until stabilization of shrinkage readings. Similarly, prismatic samples were cast and sealed after demolding at 24 h using adhesive aluminum tape to determine autogenous shrinkage. Figure 3-21 shows the shrinkage setup used for sealed and unsealed specimens.

A ring-type test (ASTM C1581) was used to evaluate the resistance of concrete to restrained shrinkage cracking (Figure 3-22). The test consists of casting concrete in an annular spacing with two concentric rings with an inner rigid steel ring instrumented with three electrical strain gauges. The gauges are used to monitor stress development induced by restrained shrinkage in the concrete. The steel strain is monitored starting immediately after casting with subsequent readings

taken every 20 min until the concrete shell element begins to crack. A sudden decrease in steel strain refers to shrinkage cracking of the concrete ring. Two concrete ring specimens were cast for each mixture. The concrete rings were moist cured for 24 h under wet burlap after casting. The specimens were demolded and moist cured for an additional two days before the initiation of the drying process. After the curing process, the top surface of the ring specimen was sealed with adhesive aluminum tape, thus restricting drying to the outer circumferential surface of the concrete ring. The ring specimens were stored at 23 ± 1°C and 50 ± 3% RH and the results were continuously recorded until the onset of restrained shrinkage cracking.

Figure 3-21- Shrinkage measurement of unsealed (left) and sealed specimens (right)

Figure 3-22- Restrained shrinkage ring test setup

4. TEST RESULTS AND DISCUSSION

4.1. Optimization of binder composition

In total, 11 CEM mixtures were made with different types and replacement rates of binary and ternary cementitious materials. The mixture proportions of the evaluated mortar mixtures are presented in Table 4-1. The binder contents of the mortars varied between 320 kg/m^3 (540 lb/yd^3) and 350 kg/m^3 (590 lb/yd^3) targeted for Eco-Pave-Crete and Eco-Bridge-Crete, respectively. As presented in Table 4-1, the partial substitution of cement by SCMs varied from 40% to 70%, by total volume of binder content. Given different target slump consistencies aimed for different applications, the HRWR dosage was adjusted to secure the mini-slump flow of 135 ± 10 mm (5.3 in.) and 190 ± 10 mm (7.5 in.) for Eco-Pave-Crete and Eco-Bridge-Crete, respectively. The water-to-cementitious material ratio (w/cm) was fixed at 0.4 for all mixtures.

Table 4-1- Mixture proportions of investigated CEM mixtures (volume-basis)

Type	Mixture no.	Codification	OPC	SL	CFA	SF	Binder content (kg/m^3)	HRWR, by mass of binder (%)
Eco-Pave-Crete having mini-slump flow of 135 ± 10 mm	1-1	1-OPC	100	0	0	0	320	0.34
	1-2	1-FA55	45	0	55	0	320	0.27
	1-3	1-SL60	40	60	0	0	320	0.28
	1-4	1-SL20FA35	45	20	35	0	320	0.26
	1-5	1-SL20FA50	30	20	50	0	320	0.29
Eco-Bridge-Crete having mini-slump flow of 190 ± 10 mm	2-1	2-OPC	100	0	0	0	350	0.42
	2-2	2-FA40	60	0	40	0	350	0.27
	2-3	2-SL60	40	60	0	0	350	0.28
	2-4	2-FA40SF5	55	0	40	5	350	0.38
	2-5	2-SL60SF5	35	60	0	5	350	0.38
	2-6	2-SL20FA35	45	20	35	0	350	0.27

Note: CFA: Class C fly ash, SL: slag, and SF: silica fume
1 mm = 0.0394 in., 1 kg/m^3 = 1.685 lb/yd^3

4.1.1. HRWR demand

The HRWR dosages necessary to achieve target fluidity of the investigated mixtures are compared in Figure 4-1. All mixtures made with SCM replacements exhibited lower HRWR demand compared to the control mixture containing 100% OPC. The lowest HRWR demand was observed for mixtures made with 20% SL combined with 35% FA. For a given fluidity, this mixture necessitated 24% lower HRWR dosage compared to the control mixture. Despite the relatively high surface area associated with SF replacement, the incorporation of 5% SF in combination with FA and SL resulted in no significant increase in HRWR demand. The spherical shape of FA particles can reduce the inter-particle friction between the cementitious grains, leading to higher flowability and lower admixture demand. The relatively low HRWR demand in the mixture containing SL can be possibly due to the morphology of glassy slag particles that can develop a relatively low degree of HRWR adsorption (Khayat et al., 2008; Mehdipour and Khayat, 2016). Therefore, the proper substitution of cement by SCMs enables the reduction in HRWR concentration required to achieve target fluidity, thus resulting in more cost effective concrete materials.

The effect of binder composition on packing density of mortar mixtures is shown in Figure 4-2. In general, the partial substitution of cement by FA, SL, or FA improved the packing density of mortar mixture. All of the investigated binary and ternary binders exhibited higher packing density compared to the reference mortar mixture. For instance, the mixture made with the combination of 20% SL and 35% FA replacements had a packing density of 0.775 compared to 0.73 for the control mixture. Given the spherical shape and smooth surface characteristics of FA particles, the partial replacement of cement with FA can lead to lower particle inter-locking and higher ball-bearing effect at the contact point. In addition, the FA and SL have higher mean diameter (D50) and greater SSA of 490 and 590 m^2/kg (2392 and 2880 ft^2/lb), respectively,

compared to 410 m^2/kg (2002 ft^2/lb) for the portland cement. This can lead to filling the voids between cement particles and increase the packing density of solid particles. The greatest packing density of 0.796 was observed for the ternary binder composition containing 60% SL and 5% SF. The use of 5% SF was shown to significantly enhance the packing density of the binder. This is due to both the filling effect and spherical shape of the SF particles that enhance the packing density of the binder. The SF employed in this study has a D50 of 0.4 μm (1.5×10^{-5} in.), which is approximately 40 times finer than that of the OPC. An increase in the packing density can generally reduce the water/admixture demand. Therefore, for a given workability, the increase in the packing density of cementitious materials can result in a decrease in the paste volume needed to fill the voids between particles, which is essential for the design of ecological and economical concrete.

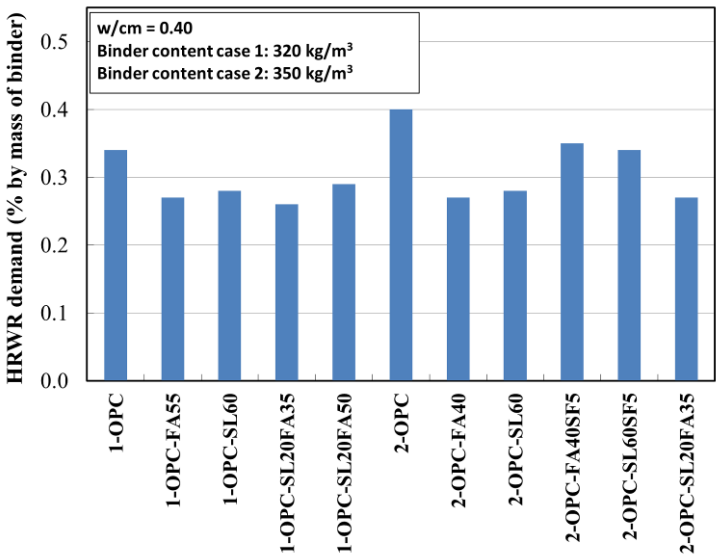

Figure 4-1- Comparison of HRWR demand for CEMs made with various SCM substitutions

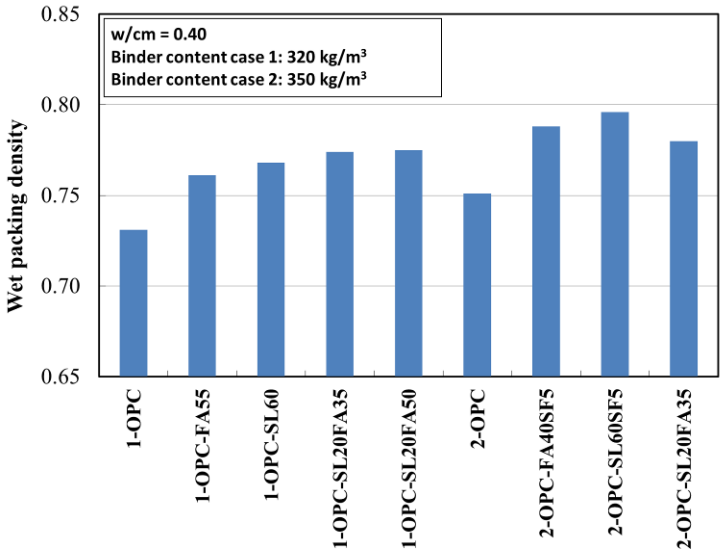

Figure 4-2- Effect of SCM substitutions on wet packing density of mortars

4.1.2. Time dependent rheological properties

The effect of SCM substitutions on time dependent rheological properties of the investigated binary and ternary binder compositions is presented in Figure 4-3. The retention of rheological properties was evaluated over 60 min following the initial contact of the cementitious material with water. The tested mixtures remained covered in the recipient of the viscometer at rest between the 10- and 60-min test durations. Regardless of the binder composition, all of mixtures exhibited similar yield stress values, which is due to the similar initial fluidity values. Except for binary mixture containing 60% slag replacement, all of the investigated binary and ternary mixtures had relatively lower yield stress and plastic viscosity values at 70 min of age compared to the reference mixture made with 100% OPC. In general, the high volume replacement of cement by slag was shown to increase the yield stress and plastic viscosity by 20% and 15%, respectively, after 70 min of age compared to the reference mixture. However, the ternary blends of 60% SL and 5% SF exhibited lower yield stress and plastic viscosity. This can be attributed to the lower inter-particle friction and higher packing density of such binder due to the use of SF

replacement, thus reflecting lower changes in rheological properties over time. The highest retention of rheological properties (lowest variations in results between 10- and 70-min of age) was observed for binary mixture containing 40% FA. This corresponds to the fact that the proper substitution of cement by SCMs can lead to longer retention of rheological properties and lower fluidity loss with respect to the mixture with 100% cement. Caufin and Papo (1986) reported that hydration resulting from portland cement increases the solid volume concentration through the production of a large number of very fine particles, thus increasing viscosity and yield stress. Therefore, when substituting cement by a quantity as high as 50% SCM, it can be expected that the magnitude of restructuring and strength of inter-particle links can be reduced due to the lower reactivity of such materials. This results in lower variation in rheological properties over time.

It is important to point out that all of the mixtures made with 350 kg/m^3 (590 lb/yd^3) and initial mini-slump flow value of 190 ± 10 mm (7.5 in.) had lower variation in rheological properties over time compared to the similar mixtures made with 320 kg/m^3 (540 lb/yd^3) and initial mini-slump flow of 135 ± 10 mm (5.3 in.). Lower degree of variation in rheological properties contributes to the ease of handling and casting operations of the mixture.

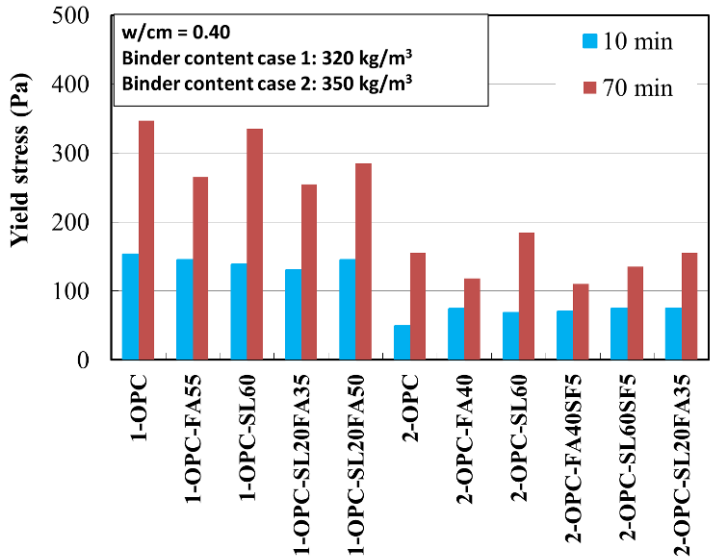

(a) Yield stress

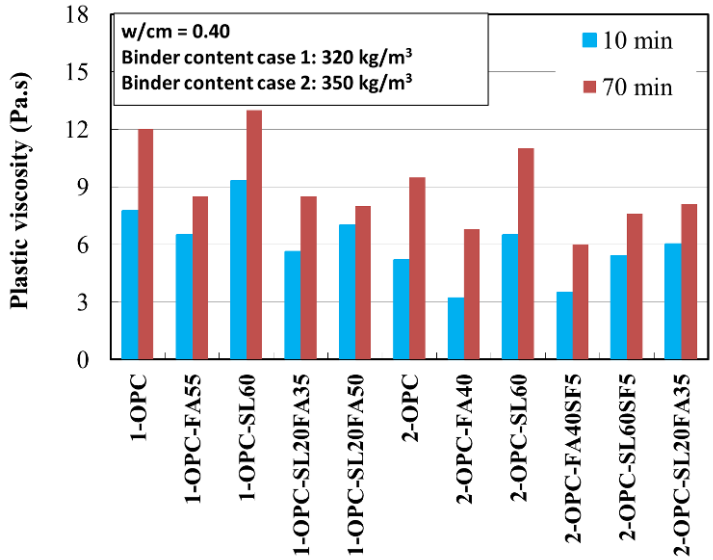

(b) Plastic viscosity

Figure 4-3- Effect of SCM substitutions on rheological properties of mortars

4.1.3. Heat of hydration

The heat flow evolution and cumulative heat release (normalized per gr binder) of the investigated mixtures is shown in Figure 4-4. As expected, the partial substitution of cement by

FA and SL reduces the heat evolution of the matrix, given lower reactivity and dilution effect of the SCMs. Generally, the total amount of heat liberated depends on the pozzolanic activity and proportion of the added SCMs (Snelson et al., 2008). An increase in the FA replacement resulted in a longer induction period and lower heat flow at peak, while the incorporation of SL shifted the peak heat toward the left side, corresponding to a shorter induction period, and increased the slope of acceleration phase. This results in higher early-age mechanical properties compared to the mixtures containing FA mixtures. The incorporation of 5% SF was shown to significantly accelerate the heat of hydration and enhance the heat peak. This is attributed to the relatively fine surface area of SF, which can provide additional surface sites for hydration products as well as enhance the pozzolanic reactivity, thus shortening the induction period and enhancing the nucleation density of C-S-H. Therefore, the ternary combination of FA with either SL or SF can lead to an acceleration of hydration reaction, thus enhancing the rate of mechanical properties development compared to the similar mixtures containing binary mixture of FA replacement.

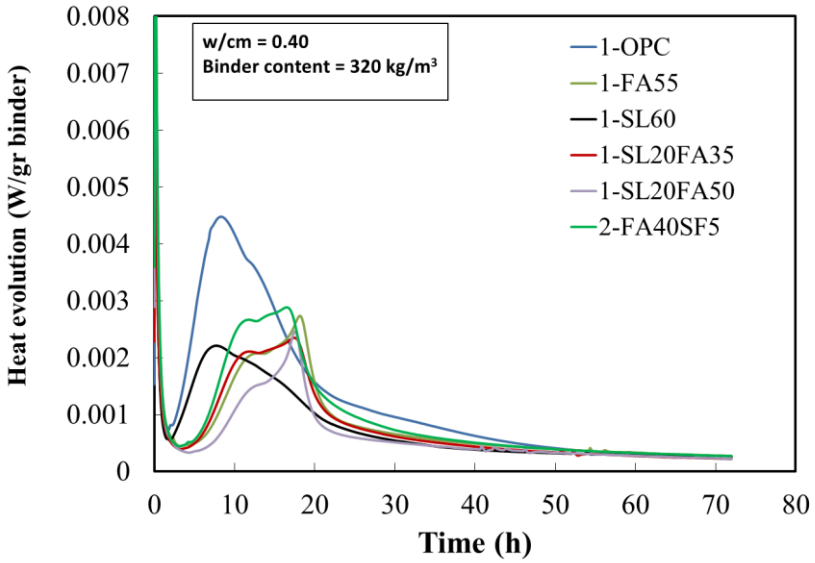

(a) Heat flow evolution

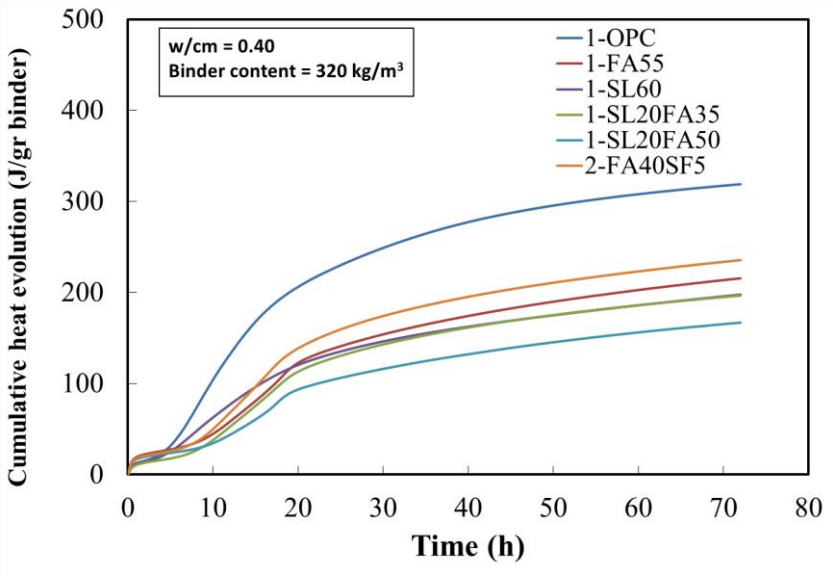

(b) Cumulative heat release

Figure 4-4- Effect of SCM substitutions on hydration heat evolution

4.1.4. Hardened characteristics

Figure 4-5 indicates the compressive strength development of the evaluated CEM mixtures made with different binder compositions. The compressive strengths at 3 and 91 days of the evaluated CEM mixtures ranged from 14 to 40 MPa (2.03 to 5.8 ksi) and 40 to 71 MPa (5.8 to 10.3 ksi), respectively. As expected, the greatest early-age compressive strength of 40 MPa (5.8 ksi) at 3 days was observed for mortar made with 100% OPC followed by 27.5 MPa (3.98 ksi) for ternary binder composition containing 20% SL and 35% FA replacements. On the other hand, regardless of the binder content, all of the evaluated binder compositions exhibited approximately comparable long-term compressive strength to that of the control mixture, with the exception of the mortar made with 20% SL and 50 FA. The SL20FA50 and FA40SF5 mixtures had the lowest and greatest strengths among the evaluated SCM combinations. Given higher reactivity, the incorporation of 5% SF combined with other cementitious materials was shown to be fully effective in developing compressive strength at both early and later ages. For example, the ternary mixture made with 40%

FA in combination with 5% SF resulted in 17% and 20% higher compressive strength values at 3 and 91 days, respectively, compared to the similar mixture made with only 40% FA replacement.

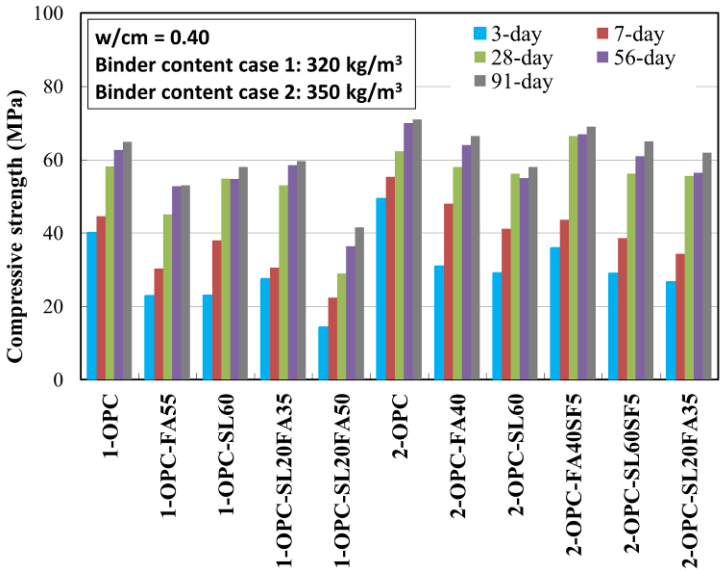

Figure 4-5- Effect of SCM substitutions on compressive strength development of mortars

The effect of binder composition on the electrical resistivity of the mortar mixtures is compared in Figure 4-6 as a function of time. All of the investigated binder compositions exhibited larger bulk resistivity, especially in the case of incorporating SL and SF. The ternary blends of 5% SF and 40% FA had 2.5 times higher electrical resistivity compared to the similar mixture made with 40% FA replacement. The highest electrical resistivity was observed for mixtures made with ternary blends of 60% SL and 5% SF replacements. This mixture exhibited 10 times higher bulk resistivity compared to 8 kΩ.cm for the reference mixture made with 100% OPC. This can be attributed to the higher density of the microstructure and lower capillary porosity of such mixtures, thus resulting in lower permeability and higher resistivity. Regardless of the binder compositions, good agreement was observed between the results of surface resistivity and bulk resistivity. Chini et al. (2003) investigated the correlation between surface resistivity and rapid chloride ion permeability. The

experimental program included a wide range of concrete mixtures made with various binder types, binder contents, and w/cm. Table 4-2 presents the relationship between the surface resistivity and the rapid chloride ion permeability which was proposed by proposed by Chini et al. (2003). According to the proposed criteria, mixtures containing either 60% SL, combinations of 40% FA and 5% SF, or 20% SL and 35% FA can be categorized as relatively low chloride ion permeability. Ternary blends of 5% SF combined with 60% SL can be considered as a very low chloride ion permeability. Other tested binder compositions can be classified with moderate chloride ion permeability.

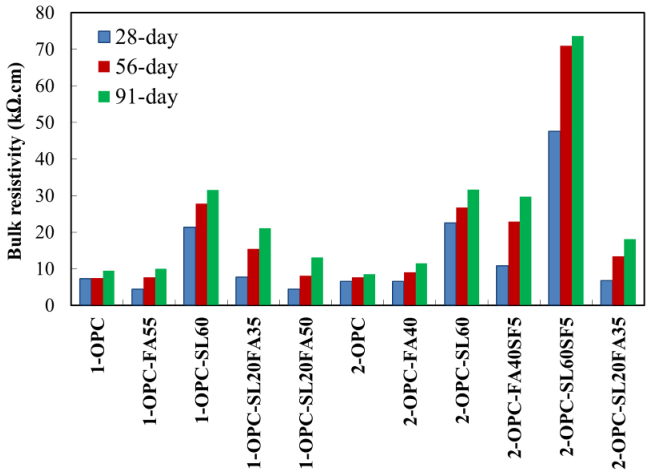

(b) Bulk resistivity

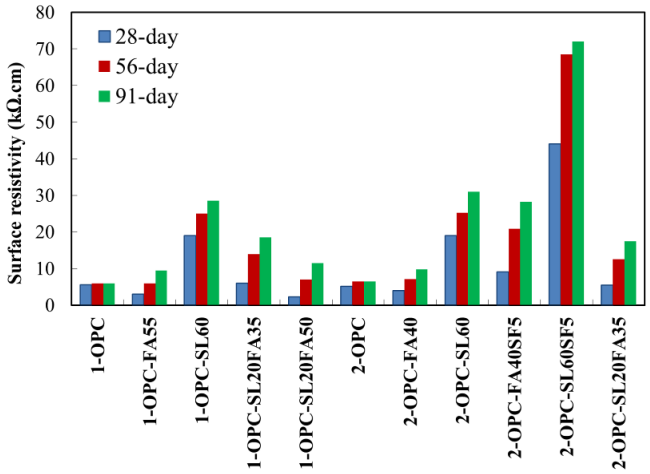

(b) Surface resistivity

Figure 4-6- Comparison of electrical resistivity for mortars made with various SCM substitutions

Table 4-2- Correlation between the surface resistivity and chloride ion permeability proposed by Chini et al. (2003)

Chloride ion permeability	RCP test	Surface resistivity
	Coulomb	(kΩ.cm)
High	>4000	<12
Moderate	2000-4000	12-21
Low	1000-2000	21-37
Very low	100-1000	37-254
Negligible	<100	>254

The effect of SCM substitution on drying shrinkage of the investigated mortar mixtures is presented in Figure 4-7. Regardless of the binder content, all binary and ternary blends of SCMs resulted in lower drying shrinkage compared to that of the control mixture made with 100% OPC. As expected, the increase in the binder content resulted in higher drying shrinkage, regardless of the binder compositions. The control mixtures with binder contents of 320 kg/m^3 (540 lb/yd^3) and 350 kg/m^3 (590 lb/yd^3) and containing 100% OPC exhibited the highest drying shrinkage values of 840 and 940 μstrain, respectively, after 150 days of drying, among the investigated binder compositions. Mixtures proportioned with SCMs exhibited drying shrinkage values ranging between 520-790 and 695-810 μstrain for binder contents of 320 kg/m^3 (540 lb/yd^3) and 350 kg/m^3 (590 lb/yd^3) after 150 days of drying. The mixture made with 320 kg/m^3 (540 lb/yd^3) containing 20% SL and 50% FA exhibited the lowest drying shrinkage value of 520 μstrain after 150 of drying. In addition, in the case of binder content of 350 kg/m^3 (590 lb/yd^3), the ternary blends of 40% FA and 5% SF was shown to have the lowest drying shrinkage of 695 μstrain after 150 of drying. Therefore, the incorporation of Class C FA was shown to be quite beneficial in mitigating drying shrinkage. This can be attributed to the slower reactivity at early-age and pozzolanic reactivity at later ages, which can lead to a denser microstructure and reduce the capillary porosity.

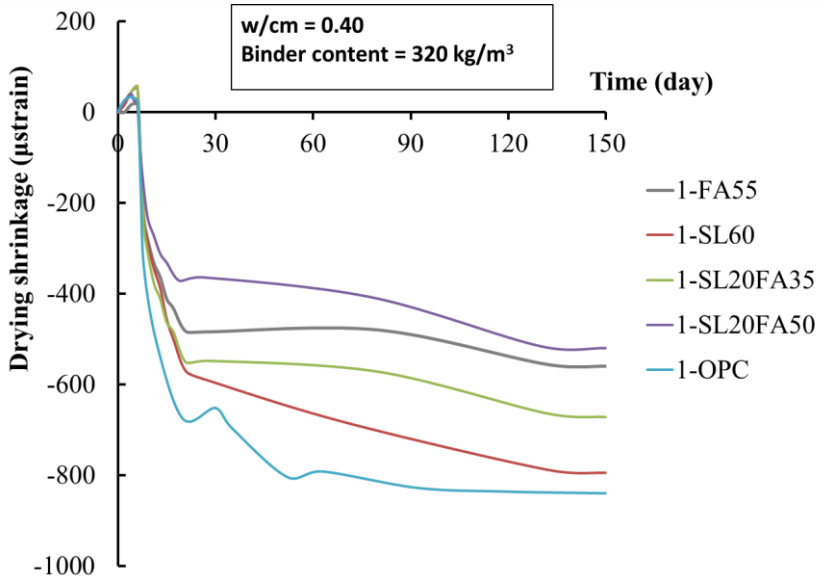

(a) Mortars made with binder content of 320 kg/m^3

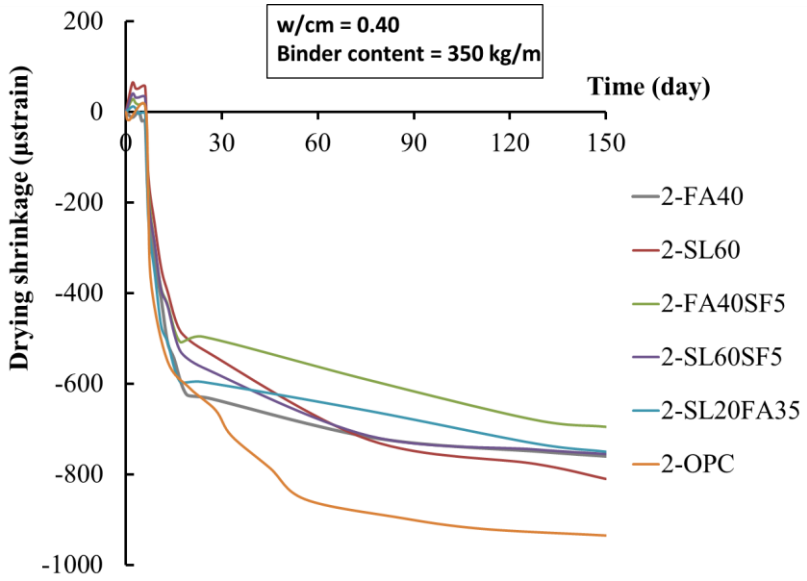

(b) Mortars made with binder content of 350 kg/m^3

Figure 4-7- Drying shrinkage of mortars made with different SCM substitutions

4.1.5. Selection of optimum binder composition

In order to select the optimum binder compositions for construction applications defined in this investigation, the performance rank analysis was carried out. The selected test properties for the

selection of optimum binder composition and the weighted factor assigned to each test property are presented in Table 4-3 and Table 4-4 for Eco-Pave-Crete and Eco-Bridge-Crete, respectively.

Table 4-3- Selected test properties to optimize binder composition for Eco-Pave-Crete

Fresh properties (weighted factor)	Hardened properties (weighted factor)
HRWR demand (2) Initial plastic viscosity (1) Variation in plastic viscosity (1) CO_2 emission (2)	Compressive strength at 3 days (1) Compressive strength at 91 days (1) Drying shrinkage at 3 days of moist-curing (1) Drying shrinkage at 120 days of drying (2)

Table 4-4- Selected test properties to optimize binder composition for Eco-Bridge-Crete

Fresh properties (weighted factor)	Hardened properties (weighted factor)
HRWR demand (2) Initial plastic viscosity (1) Variation in plastic viscosity (1) CO_2 emission (2)	Compressive strength at 3 days (1) Compressive strength at 91 days (1) Drying shrinkage at 3 days of moist-curing (1) Drying shrinkage at 120 days of drying (2) Electrical resistivity at 91 days (2)

Based on the obtained results from fresh and hardened characteristics of the investigated binders, all mixtures were ranked using performance rank analysis. The normalized response of the investigated mixtures for each property is calculated as follows:

$$Normalized\ property\,(\%) = \frac{R_{\max} - R_i}{R_{\max} - R_{\min}} \times 100 \qquad \textbf{(4-1)}$$

where R_i is the test response of the investigated mixture, for a given property; and R_{max} and R_{min} are the maximum and minimum test response among the investigated mixtures for any particular property. The normalized response ranges from 0 to 100%, corresponding to the least and best performing mixtures among the investigated systems. Figure 4-8 and Figure 4-9 indicate the normalized ranking analysis of the investigated binders targeted for Eco-Pave-Crete and Eco-Bridge-Crete, respectively. For both types of binder optimization, the lowest performance was

obtained for the control mixture made with 100% OPC. The ternary blend of 20% SL and 35% FA was shown to have desirable performance for both the pavement and transportation infrastructure applications. The ternary combination of 60% SL and 5% SF was considered to be the best binder among the investigated mixtures made with binder content of 350 kg/m^3 (590 lb/yd^3). Therefore, proper substitution of cement by SCMs can ensure greater packing density of solid particles, reduce water/admixture demand, and improve rheological and hardened properties of cement-based materials.

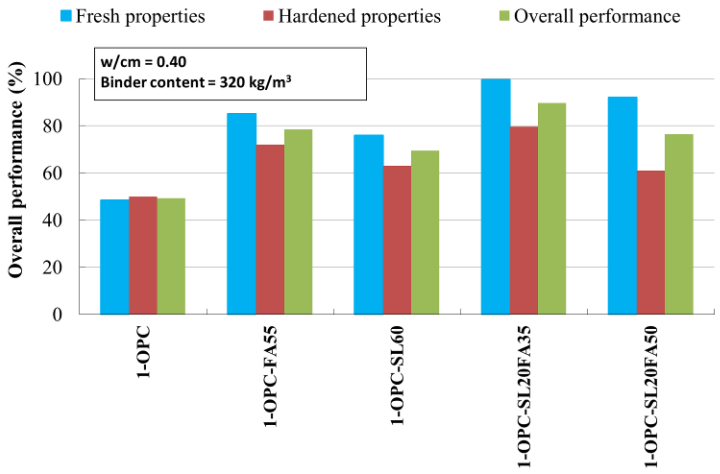

Figure 4-8- Overall performance of mortars made with 320 kg/m^3 binder content

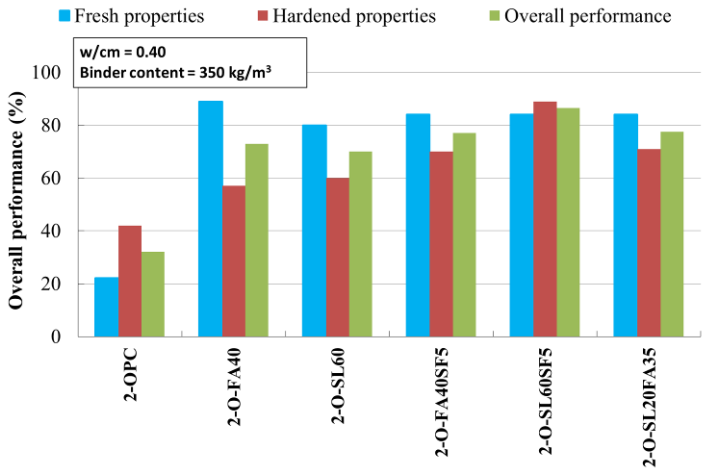

Figure 4-9- Overall performance of mortars made with 350 kg/m^3 binder content

Based on the obtained results from fresh and hardened characteristics of the investigated and ternary binders in Subtask I, the selected optimum binder compositions for the Eco-Pave-Crete and Eco-Bridge-Crete applications are summarized in

Table 4-5.

Table 4-5- Selected optimal binder compositions

Concrete type	Cementitious materials content	Codification	Replacement rate of cementitious materials (% by volume)			
			OPC	SL	CFA	SF
Reference		Ref	100	0	0	0
Eco-Pave-Crete	320 kg/m^3	1-FA40	60	0	40	0
		1-SL20FA35	45	20	35	0
Eco-Bridge-Crete	350 kg/m^3	2-SL60SF5	35	60	0	5
		2-SLA20FA35	45	20	35	0

OPC: Ordinary portland cement, SL: Blast furnace slag, CFA: Class C fly ash, and SF: silica fume

4.2. Optimization of aggregate characteristics

The aim of this phase is to optimize the aggregate proportions to achieve the maximum packing density. In total, 17 different aggregate types (fine, intermediate, and coarse aggregates) were sampled to evaluate the effect of aggregate characteristics on packing density of the granular skeleton. The packing density of aggregate was measured using three different methods, including loose packing (ASTM C29), dense packing using rodding procedure (ASTM C29), and dense packing using ICT (combination of shear and compression stresses). The results of packing density of individual aggregate samples are presented in

Table 4-6. The packing density of mono aggregate is required for numerical modelling of packing density for various aggregate blends.

Variations in packing density of mono aggregates are shown in Figure 4-10. The packing densities of aggregates are shown to vary with size, shape, surface texture, and angularity of aggregate. The packing densities of the investigated fine, intermediate, and coarse aggregates vary between 0.58-0.73, 0.6-0.73, and 0.57-0.61, respectively.

Table 4-6- Packing densities of investigated aggregates

	Name	Relative density	Bulk density (kg/m^3)			Packing density		
			ICT	loose	rodding	ICT	loose	rodding
Fine Aggregate	Sand (Osage riv.) CapitCoInc	2510	1834	1677	1799	0.730	0.668	0.717
	Sand (Osage riv.- Manufactured) CapitCoInc	2480	1616	1454	1549	0.652	0.586	0.624
	River Sand, Missouri River	2517	1816	1729	1793	0.721	0.687	0.712
	APAC MFS, LinCreek	2582	1535	1353	1493	0.594	0.524	0.578
	APAC MFS, Tightwad	2606	1891	1670	1760	0.726	0.641	0.675
Intermediate Aggregate	Gravel (7/16") CapitCoInc	2590	1660	1583	1652	0.641	0.611	0.638
	3/8" Clean CapitCoInc	2430	1485	1354	1471	0.611	0.557	0.605
	Gravel (5/16") CapitCoInc	2590	1698	1604	1695	0.645	0.619	0.654
	1/2" Clean CapitCoInc	2430	1537	1415	1505	0.655	0.582	0.619
	3/8" Minus CapitCoInc	2450	1651	1546	1653	0.674	0.631	0.675
	1/2" (Captial Quar)	2462	1613	1452	1570	0.640	0.590	0.637
	3/8" (Captial Quar)	2450	1518	1362	1473	0.620	0.560	0.600
	Crushed Dolo (1/2")	2730	1642	1502	1622	0.601	0.550	0.594
Coarse Aggregate	1" Clean CapitCoInc, Osage River	2450	1485	1426	1499	0.606	0.582	0.612
	1" (Captial Quar)	2572	1515	1464	1534	0.591	0.569	0.596
	1” Dolo Riverstone Quarry	2570	1500	1419	1531	0.583	0.552	0.596
	APAC 1", LinCreek	2689	1644	1471	1584	0.611	0.547	0.589

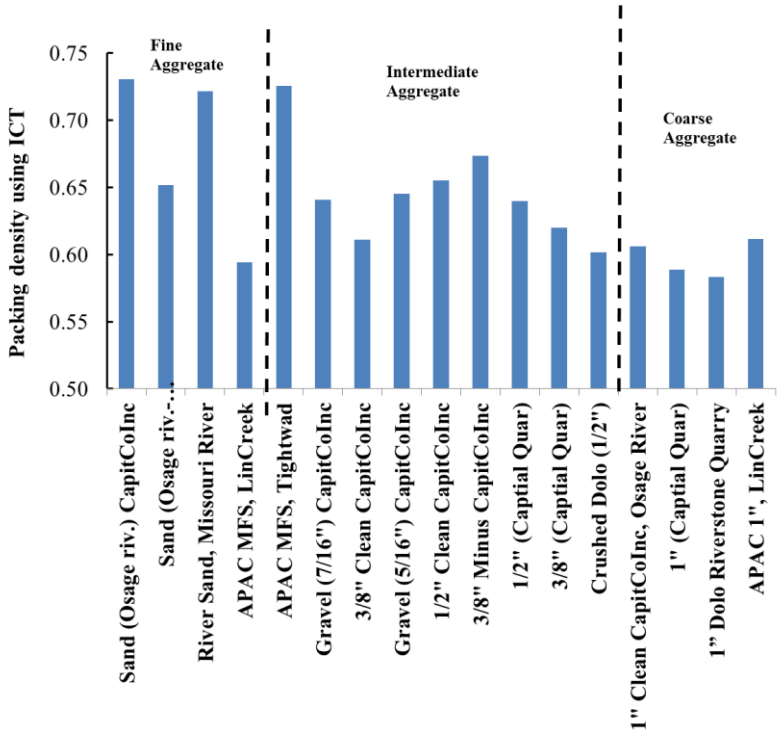

Figure 4-10- Variations in packing density of mono aggregates using ICT

4.2.1. Aggregate optimization using packing density approach

Packing density of binary aggregate blends

The experimental packing density study is initially focused on binary mixtures. As presented in Table 4-7, nine different binary mixtures were tested at different fine-to-total aggregate ratios (F/A) to determine the optimum combination of binary mixtures. For each set of aggregate blend, 7 to 12 different mixtures were tested to determine the packing density as a function of fine to coarse aggregate ratio.

Table 4-7- Packing density of binary aggregate blends

Blend	Aggregate 1	Aggregate 2	Φ_2/Φ_1	proportion corresponding to Φ_{max}	Φ_{max}
B1	River Sand, Missouri River	1" Clean CapitCoInc, Osage River	0.84	50% – 50%	0.79
B2	Gravel (5/16") CapitCoInc	1" Clean CapitCoInc, Osage River	0.93	80% – 20%	0.608
B3	River Sand, Missouri River	1" Dolo Riverstone Quarry	0.88	60% – 40%	0.783
B4	3/8" Clean CapitCoInc	1" (Capital Quarry)	0.96	50% – 50%	0.642
B5	Sand (Osage riv.) CapitCoInc	1" (Capital Quarry)	0.81	60% – 40%	0.774
B6	APAC MFS, LinCreek	APAC 3/4", Marshall	0.98	50% – 50%	0.685
B7	Sand (Osage riv.-Manufactured)	Gravel (5/16") CapitCoInc	1.00	50% – 50%	0.709
B8	Sand (Osage riv.-Manufactured)	APAC 3/4", Marshall	0.89	50% – 50%	0.740
B9	Sand (Osage riv.) CapitCoInc	3/8" Minus CapitCoInc	0.92	40% – 60%	0.714

Φ: packing density of aggregate

The variations of packing density for different aggregate types and proportions are shown in Figure 4-11. Regardless of aggregate type, the packing density of blended aggregate increases with the increase in F/A up to a certain threshold value, beyond which the maximum packing density decreases with further increase in fine aggregate replacement. This decrease in packing density can be due to the loosening and wall effects, which can push the large particles away, thus resulting in lower packing density. For instance, for B1 blend proportioned with rounded fine and coarse aggregates, the increase in F/A from 0 to 50% resulted in an increase in the packing density from 0.61 to 0.78, while the use of 80% F/A reduced the packing density to 0.76. Therefore, there exists an optimum F/A corresponding to the maximum achievable packing density, which varies with aggregate types and combinations. Blends made with rough and angular aggregate need more content of fine particles to reach similar packing density as those of

mixtures proportioned with smooth and rounded aggregate blends. This can be attributed to the higher internal friction between crushed particles which requires more fines to reduce the inter-particle friction and achieve maximum packing density. Among the investigated binary blends, the B1, B3, and B5 blends exhibited packing density higher than 0.75.

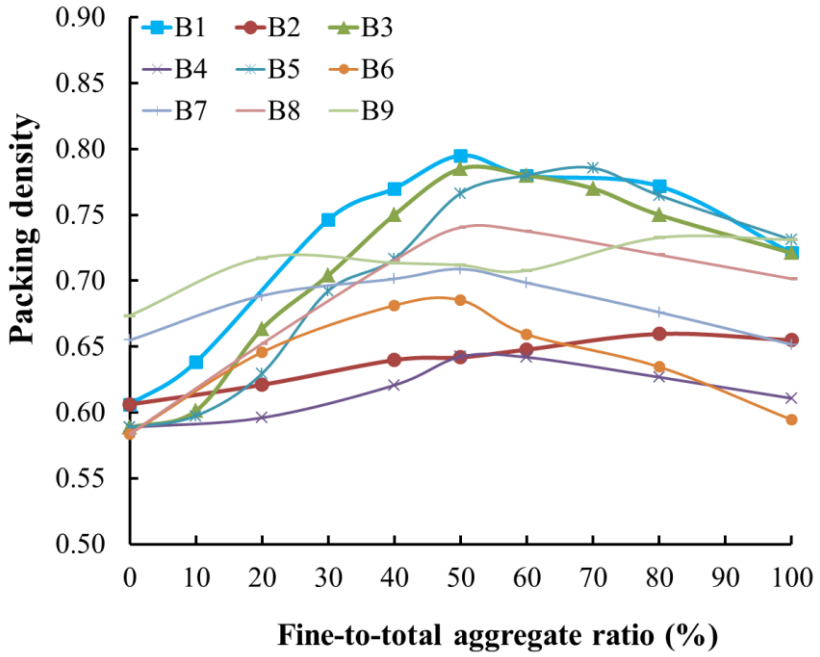

Figure 4-11- Variations in packing density for binary aggregate blends

Packing density of ternary aggregate blends

Based on the results of packing density determined for mono and binary aggregates, five ternary combinations of aggregate were selected. The investigated ternary aggregate blends are presented in Table 4-8. For each ternary combination, 15 to 25 different proportions were made by varying fine/intermediate/coarse aggregate proportions to cover a wide range of experimental domain.

Table 4-8- Packing density of ternary aggregate blends

Code	Type	Aggregate name	Packing density	Mix Proportion (at Φ_{max})	Φ_{max}
TM1	Fine	River Sand, Missouri River	0.721	55%	0.803
	Inter.	3/8" Clean CapitCoInc	0.611	6%	
	Coarse	1" (Capital Quarry)	0.589	39%	
TM2	Fine	River Sand, Missouri River	0.721	40%	0.815
	Inter.	Gravel (5/16") CapitCoInc	0.655	20%	
	Coarse	1" Clean CapitCoInc, Osage	0.606	40%	
TM3	Fine	River Sand, Missouri River	0.721	56%	0.787
	Inter.	1/2" Clean CapitCoInc	0.632	15%	
	Coarse	APAC 3/4", Marshall	0.583	29%	
TM4	Fine	River Sand, Missouri River	0.721	40%	0.808
	Inter.	3/8" Minus CapitCoInc	0.674	25%	
	Coarse	1” Dolo Riverstone Quarry	0.58	35%	
TM5	Fine	APAC MFS, Tightwad	0.674	56%	0.780
	Inter.	1/2" (Capital Quarry)	0.64	0%	
	Coarse	APAC 1", LinCreek	0.611	44%	

A ternary packing diagram (TPD) was developed based on the packing density of measured and interpolated data points, as shown in Figure 4-12. Given different aggregate blends and proportions, packing density varied from 0.63 to 0.82. The maximum packing density obtained for each ternary aggregate blend and its corresponding proportion are given in Table 4-8. The maximum packing density of rounded and crushed aggregates were 0.815 and 0.809, respectively. In general, smooth and rounded blends exhibited higher packing density compared to the crushed and rough aggregate combinations. In the case of rounded aggregates, the difference between minimum and maximum packing density is 0.21, which should be filled with the paste. Therefore, there exists an optimum value of aggregate proportions, corresponding to

maximum packing density, which can significantly reduce the void volume between particles, thus lowering the paste volume required to fill the voids between the granular skeleton. This is an essential step and key parameter in the design and mixture proportioning of Eco-Crete. The packing density contours in **Error! Reference source not found.** indicates that higher packing density of blended aggregate was obtained with low volume of medium aggregate, regardless of the aggregate types. In other words, coarse and fine aggregates play a more dominant role in the increase of packing density. The highest packing density (more than 0.80) values were obtained for the blends TM2 and TM4.

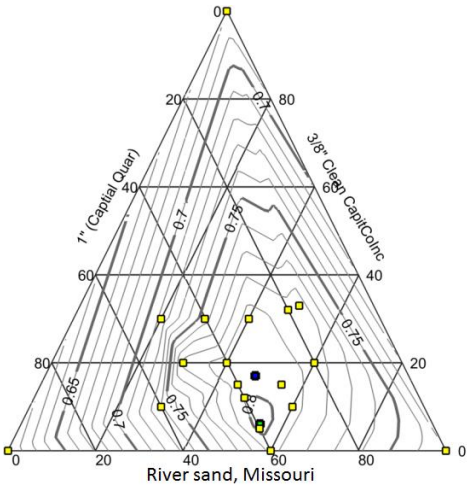

(a) Blend TM1

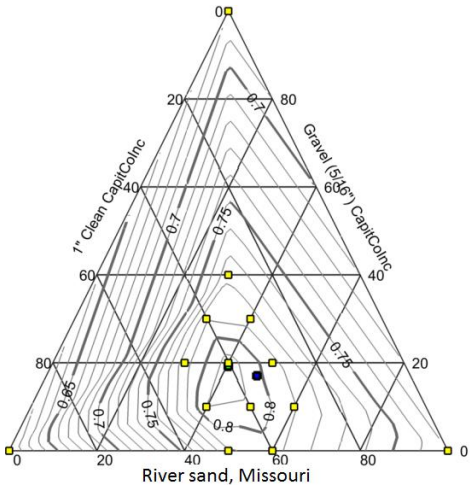

(b) Blend TM2

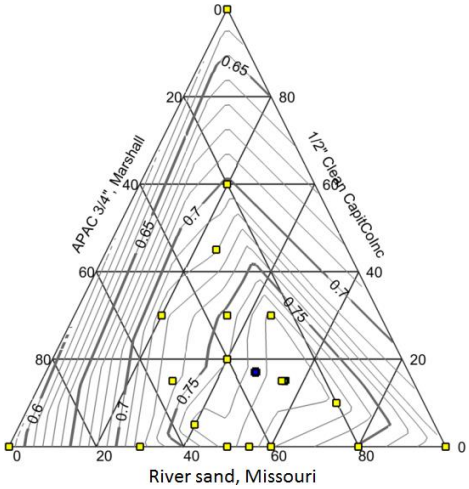

(c) Blend TM3

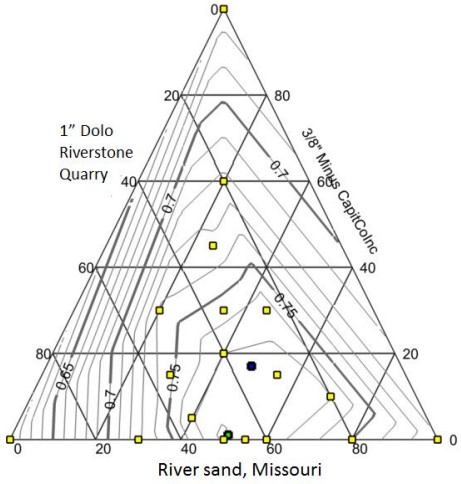

(d) Blend TM4

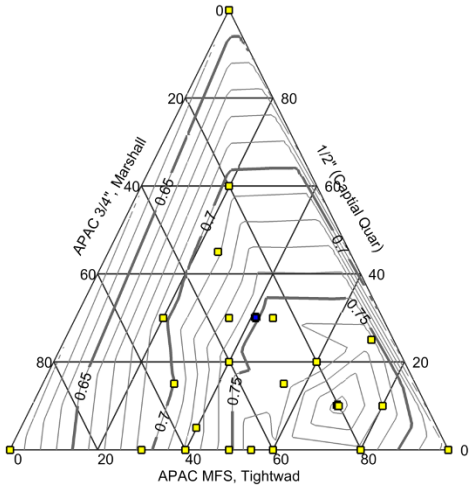

(e) Blend TM5

Figure 4-12- Ternary Packing diagram of various aggregate blends measured by ICT

4.2.2. Optimization of aggregate proportioning using SMD method

The aim of using SMD technique was to determine the optimum aggregate proportioning to achieve maximum possible packing density as well as derive the statistical model to estimate the packing density of the blended aggregate. This phase was carried out on the TM4 blend that was one of the optimal aggregate combinations among the investigated aggregate blends in the previous section. In order to cover a wide range of experimental domain, the packing density of 20 different aggregate proportions were experimentally measured using ICT. The red points in Figure 4-13 refer to experimentally measured data points. The significance of variables and their interactions was determined by the analysis of variance (ANOVA) using the least squares fitting technique. Statistical models presented in this study were established by multi-regression analysis, as follows:

$$Y = \beta_0 + \sum_{i=1}^{n} \beta_i X_i + \sum_{i<j}^{n} \sum_{j}^{n} \beta_{ij} X_i X_j \qquad \textbf{(4-2)}$$

where Y is the predicted response, X_i and X_j are the coded values of the modeled variables, β_i is linear coefficient, β_{ij} is the coefficient of the interaction, and n is the number of the modeled parameters.

The contour diagram and surface response of the packing density for the ternary aggregate blend are presented in Figure 4-13 and Figure 4-14, respectively. Depending on the aggregate proportions, the packing density values varied from 0.60 to 0.80. The packing density of blended aggregate is shown to increase with incorporating fine aggregate to a maximum possible packing

density, thereafter the packing density of blended aggregate decreased with further fine particles addition.

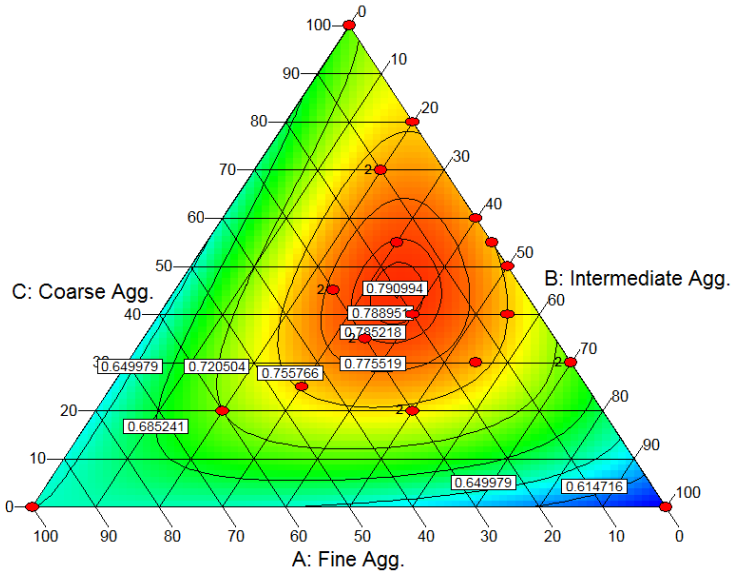

Figure 4-13- Contour diagram of packing density for ternary aggregate blend

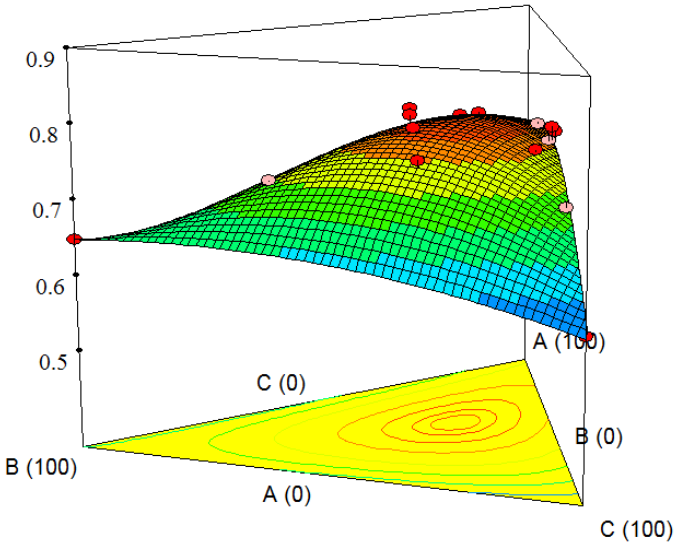

Figure 4-14- Surface response of packing density for ternary aggregate blend

The derived statistical model to estimate the packing density is expressed as follows:

$$
\begin{aligned}
&\textit{Packing density} = \\
&+ 0.71 * \textit{Fine Agg.} \\
&+ 0.45 * \textit{Intermediate Agg.} \\
&+ 0.62 * \textit{Coarse Agg.} \\
&- 0.14 * \textit{Fine Agg.} * \textit{Intermediate Agg.} \\
&+ 0.42 * \textit{Fine Agg.} * \textit{Coarse Agg.} \\
&+ 0.12 * \textit{Intermediate Agg.} * \textit{Coarse Agg.}
\end{aligned}
\qquad \textbf{(4-3)}
$$

The correlation coefficient (R^2) of the derived model is about 0.95. As indicated in Eq. (4-3), the fine aggregate has a higher significant effect on the packing density of the blended aggregated compared to other constituents.

A multi-objective optimization technique was carried out to determine the optimum combination of aggregate blends required to achieve maximum packing density. This technique involves satisfying the defined properties without compromising any of the requirements (Montgomery, 2005). For the targeted properties, the desirability functions (d_i) are obtained and these functions are simultaneously optimized to determine the best combination. The overall desirability function (D) proposed by Derringer and Suich (1980) is expressed as follows:

$$
D = (d_1^{r_1} \times d_2^{r_2} \times d_3^{r_3} \times \ldots \times d_n^{r_n})^{1/\sum r_i} = \left(\prod_{i=1}^{n} d_i^{r_i}\right)^{1/\sum r_i} \qquad \textbf{(4-4)}
$$

where n is the number of individual responses in the optimization, and r_i refers to the relative importance of each individual property. The r_i varies from 1 to 5, reflecting the least to most important, respectively. The d_i ranges between 0 (for a completely undesired response) and 1 (for a fully desired response). The D value close to 1 reflects that the optimal combination of variables is able to secure the target properties.

The contour diagram of overall desirability for target property (maximum possible packing density) is shown in Figure 4-15. The highest desirability value of 0.96 was achieved for the aggregate combination of 43% fine aggregate (River Sand, Missouri River), 22% intermediate aggregate (3/8" Minus CapitCoInc), and 35% coarse aggregate (1" Dolo Riverstone Quarry) that resulted in packing density of 0.801.

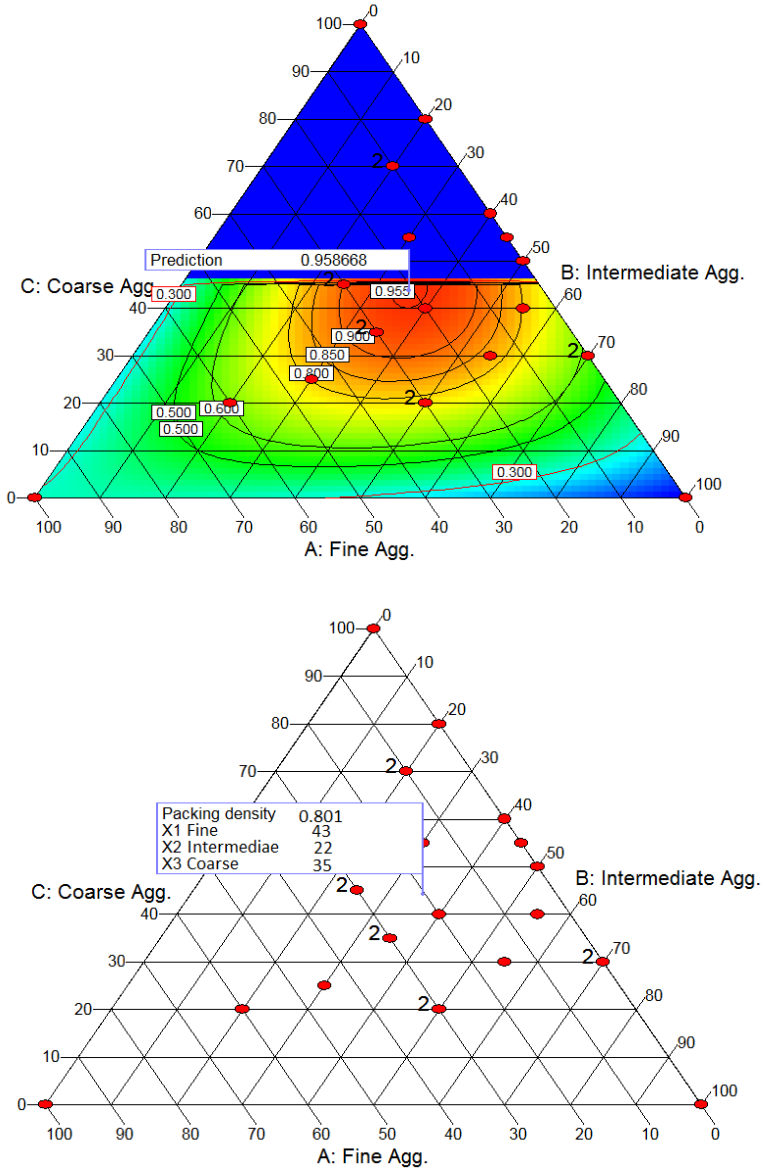

Figure 4-15- Contour diagram of desirability to achieve maximum packing density

Based on the derived statistical model, the optimum proportioning for the investigated aggregate blend, corresponding to maximum packing density, is presented in Table 4-9. The optimal aggregate proportioning determined from the SMD method is consistent with those determined from experimentally measured packing density.

Table 4-9- Optimum aggregate proportions using SMD method

Type	Aggregate name	Proportion	Max. packing density
Fine Agg.	River Sand, Missouri River	40%	0.808
Intermediate Agg.	3/8" Minus CapitCoInc	25%	
Coarse Agg.	1” Dolo Riverstone Quarry	35%	

4.2.3. Theoretical grading model for PSD optimization

The distribution modulus (q) of modified Andreasen packing model has significant influence on packing density of aggregate. The use of a lower q value results in a mixture with higher content of fine materials that can improve the packing density by reducing the inter-particle friction and reduces the risk of segregation. On the other hand, the PSD of the combined aggregate can influence the mean particle size and specific surface area of the aggregate. For a given lubricant volume, an increase in the specific surface area will result in a smaller paste film thickness around the aggregates, thus leading to a lower workability. Investigations on highly flowable mixtures showed that the Andreasen model with $0.22 < q < 0.30$ provides appropriate PSD for SCC mixtures. Mueller et al. (2014) reported that the modified Andreasen model with q of 0.27 can be effectively used for the design of Eco-SCC. Brouwers and Radix (2005), and Hunger and Brouwers (2006) also pointed out that the modified Andreasen packing model with q values

between 0.25 and 0.30 yield appropriate PSD to enhance flow characteristics and stability of SCC mixtures.

An optimization algorithm was developed to determine q value of modified Andreasen equation representing the PSD of the aggregate blend. This was done to determine the optimum q value corresponding to the maximum packing density experimentally measured from ICT. This optimization was carried out in the MATLAB program by minimizing the difference between combined gradation of blended aggregate and Andreasen particle packing model. Least squares technique was used to minimize the residual between the gradation of the densely packed mixture and the Andreasen model as follows:

$$RSS = \sum_{i=1}^{n} e_i^2 = \sum_{i=1}^{n} (P_{\text{modified A\&A}(q_i)}(d_i) - P_{\text{target mixture}}(d_i))^2 \rightarrow \min$$
$$P_{\text{modified A\&A}(q_i)}(d_i) = \frac{d_i^{q_i} - d_{\min}^{q_i}}{d_{\max}^{q_i} - d_{\min}^{q_i}} \quad \forall d_i \in [d_{\min}, d_{\max}] \text{ and } q_i \in [0.01, 0.5] \tag{4-5}$$

where RSS is sum of the squares of residuals. $P_{\text{modified A\&A}(q_i)}$ is the fraction of the particle size smaller than diameter d for the modified Andreasen with q_i, and $P_{\text{target mixture}}$ refers to the fraction of the particle size smaller than diameter d_i for the gradation of the target mixture, respectively. Based on the obtained results from different types and proportions of aggregate investigated in this study, the combination of river sand, river gravel 5/16", and river gravel 1" with the proportions of 42%, 20%, and 38%, respectively, was selected for the design of the Eco-crete. The PSD of the selected aggregate combination is plotted in Figure 4-16. The selected aggregate blend had a packing density of 0.808 and its PSD is close to Andreasen model with a q value of 0.275.

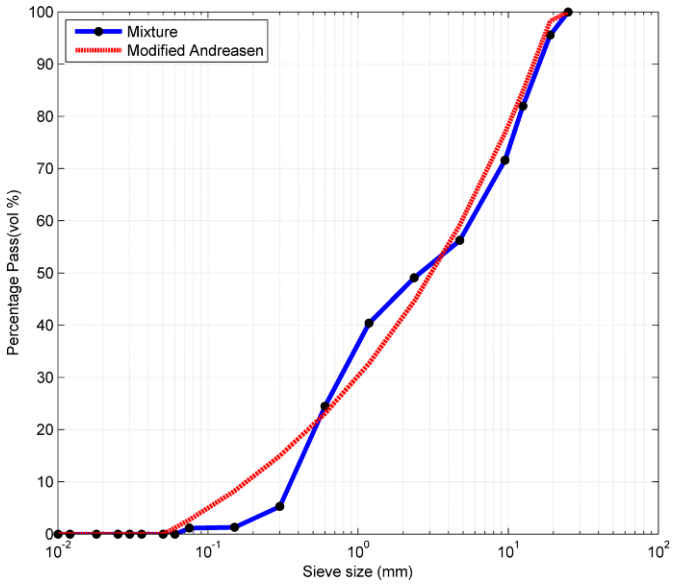

Figure 4-16- PSD of selected aggregate blend

4.3. Comparison of shrinkage mitigating strategies

This subtask focused on evaluating the effect of different shrinkage reducing/compensating materials on autogenous and drying shrinkage and mechanical properties of concrete equivalent mortars (CEMs) proportioned with optimized binder compositions determined from Subtask I. The investigated shrinkage mitigating materials included expansive agents (CaO-based and MgO-based), crack reducing admixture (CRA), and lightweight sand (LWS) with various particle size distributions. The use of lightweight aggregate has the significant benefit of providing internal curing and enhance cement hydration along with forming new hydration products via pozzolanic reaction of the SCMs.

Based on the obtained results from fresh and hardened properties of investigated binders in Subtask I, the selected binder compositions for Eco-Pave-Crete and Eco-Bridge-Crete applications are summarized in Table 4-10. In total, 18 CEMs made with different binder compositions and shrinkage reducing/compensating materials were evaluated, as given in Table 4-11. The w/cm of the investigated mixtures remained constant at 0.40. The EX and CRA

contents were considered as a part of cementitious materials and mixing water, respectively. Depending on the concrete type, the binder content of the evaluated mortars varied between 320 (540 lb/yd^3) and 350 kg/m^3 (590 lb/yd^3), as presented in Table 4-10. Given different target slump consistencies aimed for different construction applications, the HRWR concentrations were adjusted to secure the mini-slump flow of 135 ± 10 mm (5.3 in.) and 190 ± 10 mm (7.5 in.) for Eco-Pave-Crete and Eco-Bridge-Crete, respectively.

The investigated mixtures were subjected to different durations of initial moist curing of 0, 3, and 7 days to examine the influence of initial moist curing period (IMCP) on shrinkage and compressive strength development.

Table 4-10- Selected optimum binders targeted for Eco-Pave-Crete and Eco-Bridge-Crete

Concrete type	Cementitious materials content	Codification	Replacement rate of cementitious materials			
			OPC	SL	CFA	SF
Reference		Ref	100	0	0	0
Eco-Pave-Crete	320 kg/m^3	1-FA55	45	0	55	0
		1-SL20FA35	45	20	35	0
Eco-Bridge-Crete	350 kg/m^3	2-SL60SF5	35	60	0	5
		2-SLA20FA35	45	20	35	0

OPC: Ordinary portland cement, SL: Blast furnace slag, CFA: Class C fly ash, and SF: silica fume
1 kg/m^3 = 1.685 lb/yd^3

Table 4-11- Mix design parameters investigated for shrinkage mitigating strategies

Codification	Description	Binder type				Lightweight sand (LWS)	Expansive agent (EX)		Crack reducing admixture (CRA)
		Ref	Pavement	Bridge deck					
		100% OPC	45% OPC + 55% Class C FA	35% OPC + 60% SL + 5% SF	45% OPC + 20% SL + 35% Class C FA	25% replacement	7.5% CaO-based system	5% MgO-based system	2%
OPC	Effect of binder composition	x							
FA55			x						
SL60SF5				x					
SL20FA35					x				
E-OPC	Effect of CaO-based EX	x					x		
E-SL60SF5			x				x		
E-FA55				x			x		
E-SL20FA35					x		x		
P-OPC	Effect of MgO-based EX	x						x	
P-SL60SF5			x					x	
P-FA55				x				x	
P-SL20FA35					x			x	
E-L-OPC	Combined Effect of LWS 1 and EX	x				x	x		
E-L-SL60SF5			x			x	x		
E-L-SL20FA35				x		x	x		
E-L-FA55					x	x	x		
C-OPC	Effect of CRA	x							x
E-L2-OPC	Effect of LWS type	x				x	x		

Codification: E-L-OPC = 7.5% CaO-based EX + 25% lightweight sand type 1.

The quantity of LWS was theoretically estimated based on the internal curing water required to eliminate the self-desiccation proposed by Bentz et al. (2005). This can be expressed as follows:

$$M_{LWS} = \frac{C_f \times CS \times \alpha_{max}}{S \times W_{LWS}} \quad \textbf{(4-6)}$$

where M_{LWS} and C_f refer to the dry mass of LWS (kg/m^3) and binder content (kg/m^3), respectively. The CS is the chemical shrinkage of the binder (kg of water per kg of binder) and

α_{max} is the maximum potential degree of hydration of binder varying from 0 to 1. The S value represents the degree of saturation of the LWS, and W_{LWS} is the mass of internal curing water released by LWS. In this study, the CS and α_{max} values were considered to be 0.07 and 1, respectively (Bentz et al., 2005). The partial replacement of sand by 25% LWS, corresponding to M_{LWS} of 185 kg/m^3 (311.8 lb/yd^3), can provide internal curing water of 24 kg/m^3 (40.5 lb/yd^3).

In this investigation, the performance of two different LWSs made from expanded shale was evaluated. The PSD, time dependent water absorption, and desorption capacity of LWSs are shown in Figure 4-17. The results of time dependent water absorption of LWS indicate that the rate of water absorption is substantially higher during the 24 hours. Total water absorption increases over time; these values were stabilized after approximately 36 hours. The LWS-2 had finer grading and higher water absorption compared to the LWS-1. The LWS-1 reached 97% of its absorption capacity after 24 h, while this value was about 90% for LWS-2 after 24 h water immersion. Therefore, intention should be taken to ensure that the aggregates have reached their absorption capacity prior to using in mixture to provide internal curing.

The results of desorption capacity of the LWSs in Figure 4-17 (c) show that both aggregate are able to release more than 85% of their absorbed water when subjected to RH of 94%. One of the crucial properties of LWA that needs to be examined is the ability of LWS to release the absorbed water to the surrounding cementitious matrix to enhance hydration and fill capillary voids that are being depleted, especially at the early stages of hydration (Bentz et al., 2005). The desorption responses of the LWSs indicate that the LWSs used in this investigation readily release the absorbed water when the internal RH of the mixture drops due to hydration, as well as internal and external drying.

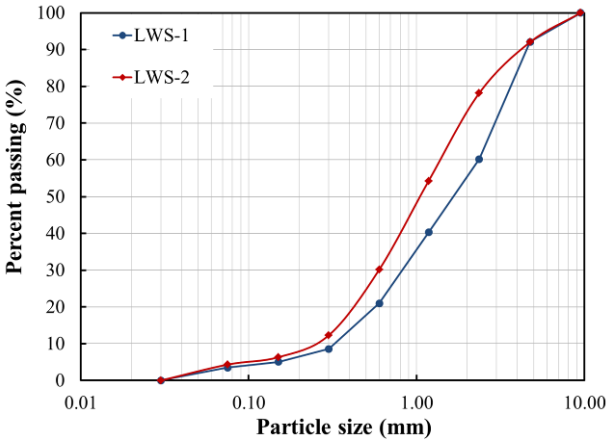

(a) PSD of different LWSs

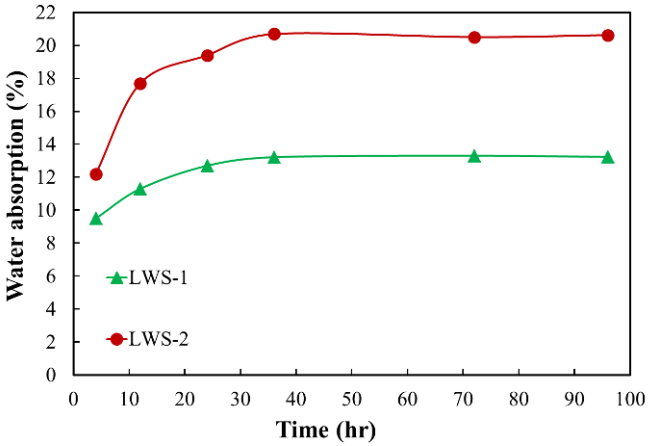

(b) Time dependent water absorption of different LWSs

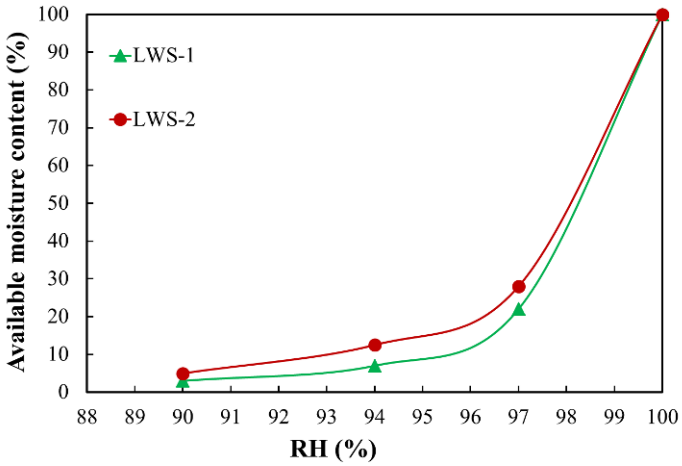

(c) Desorption response of different LWSs as a function of RH

Figure 4-17- Characteristics of LWSs used in this investigation

4.3.1. Fresh properties

The HRWR dosages required to reach the target fluidity is shown in Figure 4-18. The HRWR demand of the investigated CEMs varied between 0.3% and 0.48%. Mortars containing the MgO-based EX system necessitated higher HRWR content. Regardless of the binder composition, mixtures made with CaO-based EX system had similar HRWR demand to the similar mixtures made without any EX. Regardless of EX type, the combination of EX with LWS, resulted in approximately similar HRWR demand to those prepared with only EX. Given

finer particles and higher surface area, the mixture made with LWS-2 was shown to have higher HRWR demand compared to the similar mixture made with LWS-1. For a given type of shrinkage mitigating material, all optimum binder compositions selected from Subtask 1 exhibited lower HRWR demand than the control mixtures made with 100% OPC.

The variations in setting time of the investigated mortar mixtures are presented in Figure 4-19. The setting time values of the mortars ranged from 234 to 630 min and 312 to 810 min for the initial and final setting times, respectively. Based on the results, the effect of tested shrinkage mitigating materials on setting time can be classified into two groups. The CEMs incorporating LWS or CRA exhibited longer setting times compared to the control mixture. This can be due to the fact that the addition of CRA reduces the affinity and rate of dissolution of alkalis in the pore solution, which can delay the cement hydration (Rajabipour et al., 2008). On the other hand, the use of CaO-based EX was shown to accelerate the setting time. However, this trend was reversed for MgO-based EX. Regardless of the SCM types and replacement rates, mixtures containing MgO-based EX resulted in longer setting time values compared to the similar mixtures made without any MgO-based EX. Similar results was reported by Temiz et al. (2015), who noted that the incorporation of MgO-based EX retards the hydration of cement. This can be in part due to the fact that the production of $Mg(OH)_2$, which is formed by MgO hydration in a high alkali medium, precipitates with a tiny crystallite size on the cement grains and forms a "protective layer", which delays hydration of the cement (Zheng et al., 1992).

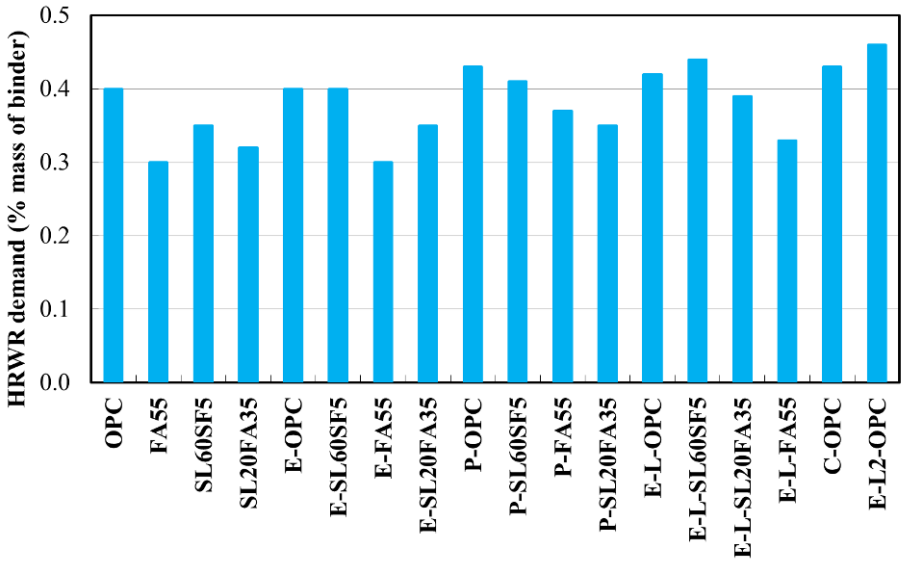

Figure 4-18- Comparison of HRWR demand for mortars made with various binder compositions and shrinkage mitigating materials

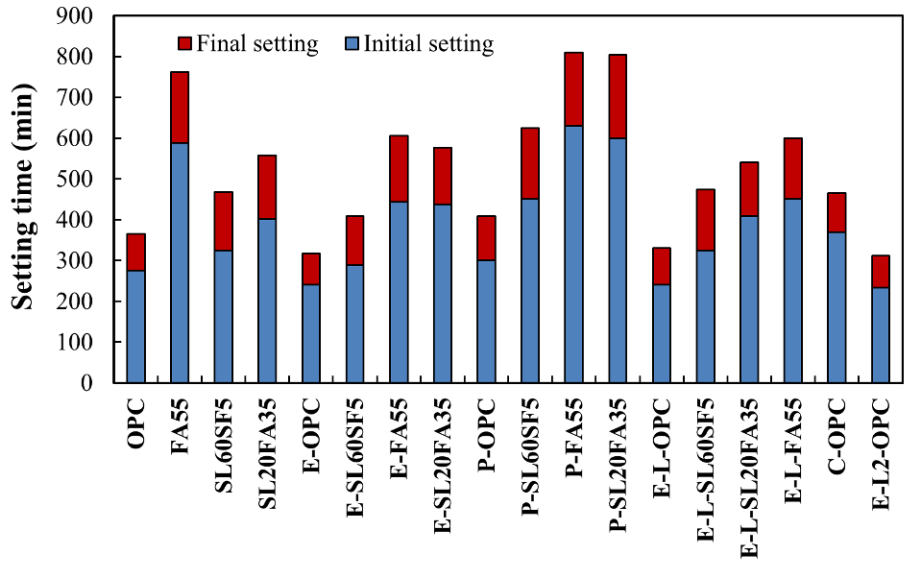

Figure 4-19- Variations in setting time for mortars made with various binder compositions and shrinkage mitigating materials

4.3.2. Compressive strength development

Figure 4-20 shows the effect of binder compositions and shrinkage mitigating materials on compressive strength development as a function of IMCP. Regardless of the shrinkage mitigating

materials, moist-cured mixtures developed higher compressive strength than similar mixtures exposed to air-drying at 23°C and 50% RH, especially at later ages for mixtures incorporating high volume SCMs. In the absence of IMCP, the CEM mixtures had 56-day compressive strength ranging between 28 (4060 psi) and 67 MPa (9718 psi). These values varied between 39 (5657 psi) and 76 MPa (11023 psi) for similar mixtures subjected to 7 days of IMCP.

For a given IMCP and binder composition, mortars made with 25% LWS replacement exhibited higher compressive strength. This is attributed to there being more hydration products surrounding the LWS particles due to internal curing as well as more uniform and dense interfacial transition zone (ITZ) between the LWS and cement paste (Elsharief et al., 2005; Bentz and Stutzman, 2008; Bentz, 2009). The combined use of 20% LWS and 7 days of IMCP led to a greater increase in mechanical properties compared to the use of 20% LWS without moist curing or 7 days of moist curing without LWS. Regardless of IMCP, the partial replacement of cementitious materials by CaO-based or MgO-based EX systems resulted in a reduction in compressive strength. In other words, mixtures containing EXs exhibited comparable compressive strength at early and later ages. The strength gain resulting from IMCP was found to be more critical for mixtures containing high volume SCMs, which caused the highest spread in compressive strength. The use of 25% LWS replacement was shown to compensate for the drop in compressive strength resulting from the absence of IMCP. Therefore, the internal curing provided by the use of LWS replacement is more crucial for mixtures containing high replacement rates of SCMs to enhance the cement hydration and promote the pozzolanic reactivity.

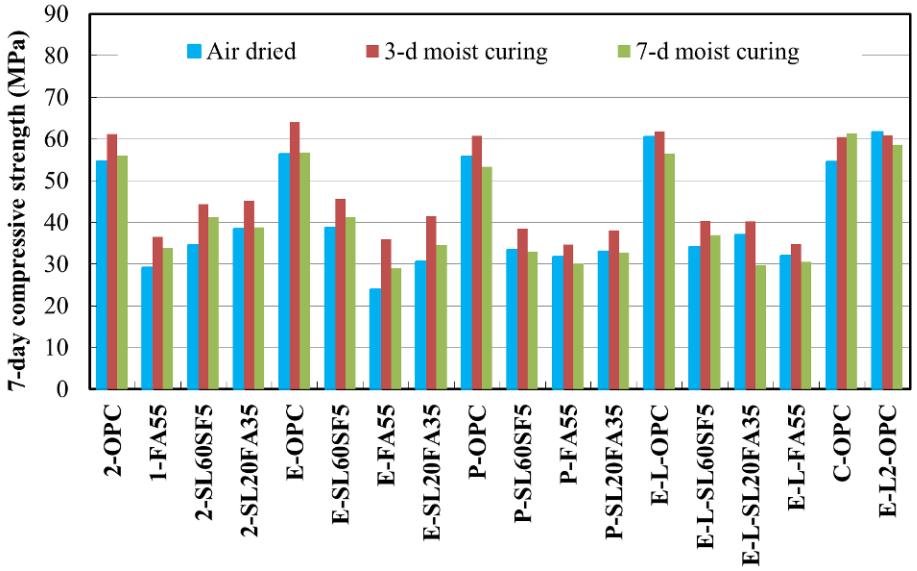

(a) 7-day (Note: 1 MPa = 145.04 psi)

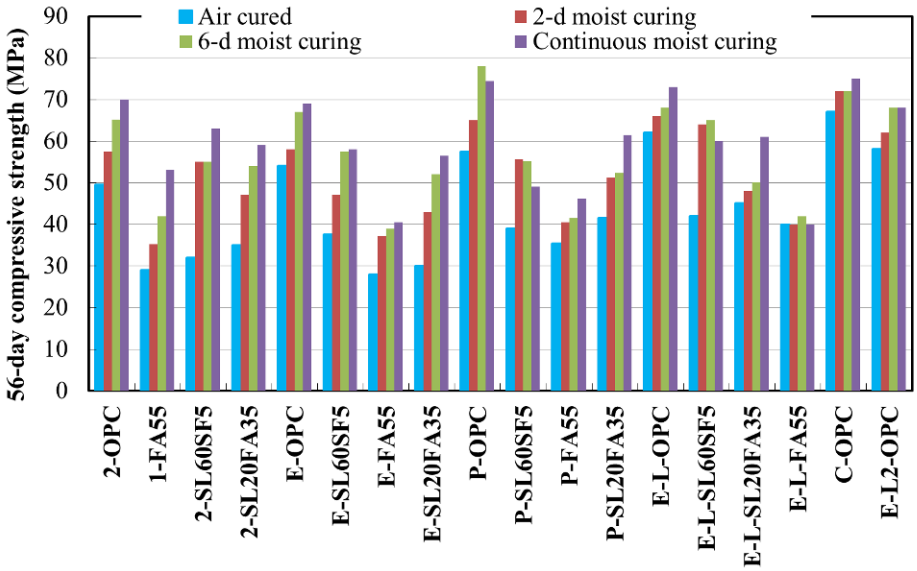

(b) 56-day (1 MPa = 145.04 psi)

Figure 4-20- Variations in compressive strength for mortars made with various binder compositions and shrinkage mitigating materials

4.3.3. Autogenous shrinkage

The variations in autogenous shrinkage of mortars made with different shrinkage mitigating materials and binder compositions are shown in Figure 4-21. As outlined in ASTM C1698, time

zero or starting point for autogenous shrinkage measurement was set at the final set of the investigated mixtures. All mixtures made with shrinkage mitigating materials exhibited lower autogenous shrinkage compared to –350 µstrain for control mixture after 150 days.

Regardless of the binder composition, the incorporation of expansive agent led to a significant expansion, especially in the case of the CaO-based EX system. The expansion provided by EX was more pronounced for mixtures containing high volume SCMs. This can be due to the lower resistance of such mixtures to expansion, resulting in larger free movement. The highest expansion of 1780 µstrain was observed for the mixture made with 55% FA replacement and 7.5% CaO-based EX. The magnitude, rate, and duration of expansion were influenced by the EX type, as shown in Figure 4-21. Mixtures incorporating 7.5% CaO-based EX exhibited substantially higher magnitude and rate of expansion for a longer duration compared to the 5% MgO-based EX. The use of CRA was shown to be effective in reducing the autogenous shrinkage. The incorporation of 2% CRA concentration resulted in an autogenous shrinkage of 230 µstrain compared to –350 µstrain for control mixture after 150 days.

The synergistic effect between EX with LWS resulted in lower autogenous shrinkage or higher expansion magnitudes for a longer duration. The highest expansion of 1980 µstrain was found for the E-L-SL60SF5 mixture with binary system of shrinkage mitigating materials including 7.5% CaO-based EX and 25% LWS replacement. This is attributed to the couple effect of lower self-desiccation and larger expansion resulting from the use of LWS along with EX systems. The internal relatively humidity (RH) of the prismatic samples was measured under sealed conditions using cast-in sensors. The sequence of casting and measurement procedure consists of casting the CEM in a prism measuring 75 × 75 × 285 mm (2.95 × 2.95 × 11.22 in.) followed by inserting two hollow PVC tubes with diameters of 20 mm and embedment depth of 40 mm into the fresh

mixture. Following final set, the sensors are embedded at the bottom of PVC tubes in contact with the CEM surface. The RH is measured by inserting a probe into the PVC tube after contact with the embedded sensors. The specimen was wrapped using two layers of adhesive aluminum sheet to prevent any moisture loss due to external drying. Figure 4-22 shows the effect of using LWS replacement on RH of CEMs. The mixture made with 25% LWS replacement had 18% higher RH after 10 days compared to the control mixture. The higher degree of saturation extends the wet curing period, which can reduce the capillary stresses induced by self-desiccation. Therefore, the higher degree of saturation of cement resulting from the use of LWS can enhance the magnitude and duration of expansion provided by the use of EX.

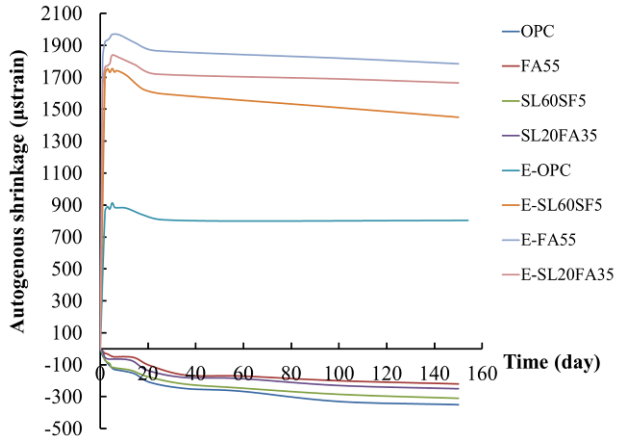

(a) Effect of CaO-based EX

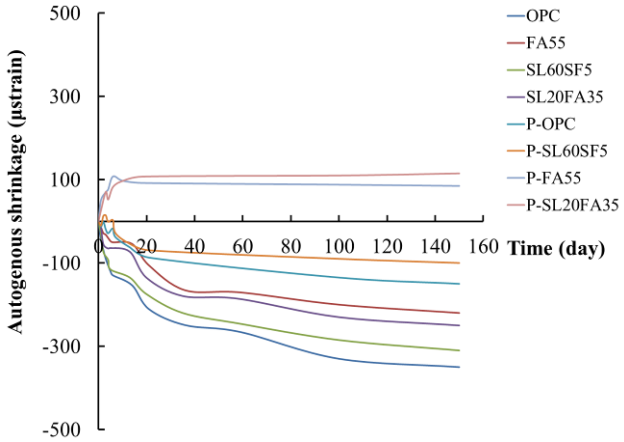

(b) Effect of MgO-based EX

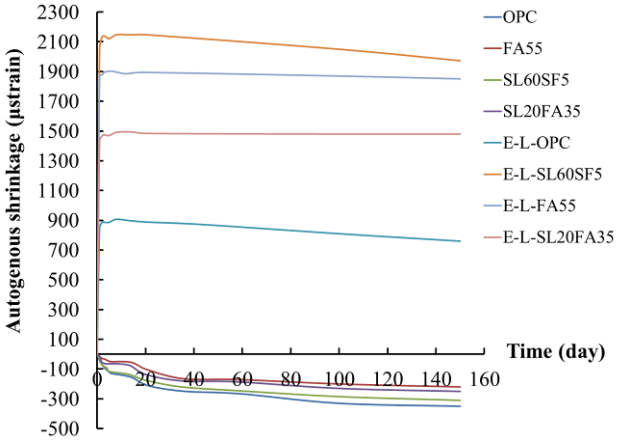

(c) Combined effect of CaO-based EX and LWS-1

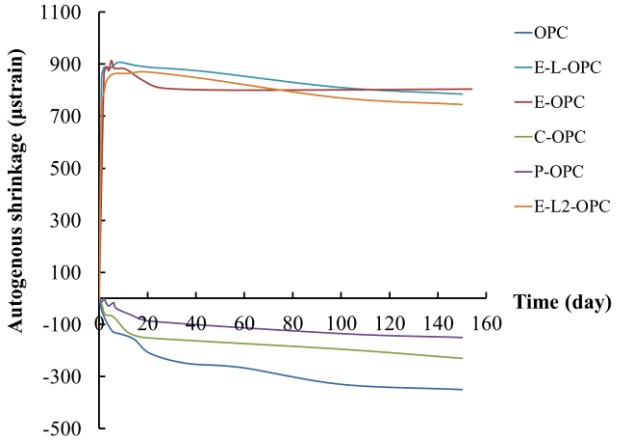

(d) Effect of LWS types and CRA

Figure 4-21- Autogenous shrinkage of mortars made with various binder compositions and shrinkage mitigating materials

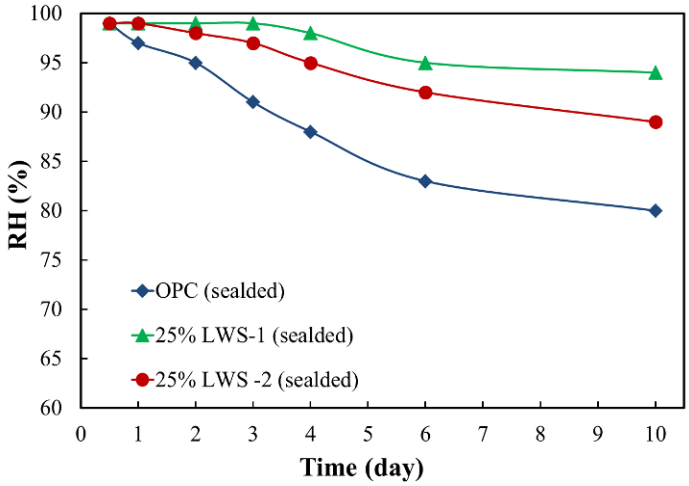

Figure 4-22- Effect of using LWS on RH of mortars over time

4.3.4. Drying shrinkage

Figure 4-23 shows the drying shrinkage of mortars made with different shrinkage mitigating materials and initial moist curing durations. Regardless of initial moist curing period, all mixtures containing shrinkage mitigating materials exhibited lower drying shrinkage than control mixture made with 100% OPC. For a given IMCP, mixtures proportioned with CaO-based EX exhibited larger expansion values compared to the similar mixtures made with 5% MgO-based EX. It is important to note that effectiveness of incorporating shrinkage mitigating materials to control shrinkage was shown to be significantly affected by the IMCP, especially for EX systems. As shown in Figure 4-23 (b) and (c), in the absence of IMCP, mixtures made with 7.5% EX or 5% MgO-based EX systems resulted no expansion. However, in the presence of 6 days of IMCP, the EX1 mixture resulted in an expansion of 450 μstrain after 6 days followed by a shrinkage of –460 μstrain after 360 days compared to –865 μstrain for a similar mixture when no IMCP was applied. Therefore, for EX systems, an initial moist curing should be applied to develop its potential expansion and consequently lower drying shrinkage.

As in the case of autogenous shrinkage, the incorporation of EX for a mixture made with a SCM replacement resulted in larger expansion and lower drying shrinkage compared to the similar mixture containing 100% OPC. In other words, for a given IMCP, mixtures made with SCM replacement resulted in higher expansion when combined with EX. For example, in the case of 6 days of IMCP, the E-SL20FA35 mixture exhibited an expansion of 670 μstrain compared to the 450 μstrain for similar mixture containing OPC and 7.5% CaO-based EX.

The duration of initial moist curing period was shown to have higher impact on shrinkage reduction than LWS replacement. In other words, moist-cured mixtures exhibit lower drying shrinkage compared to the use of 25% LWS without moist-curing. Unlike the autogenous

shrinkage trend, the combined use of EX and LWS resulted in lower expansion magnitude along with shorter expansion duration. Comparison between the investigated two different LWSs in Figure 4-23 (e) indicates that the use of LWS-1 is more efficient to reduce the drying shrinkage. This is attributed to the larger desorption capacity of this aggregate which can provide more internal water, thus resulting in lower shrinkage.

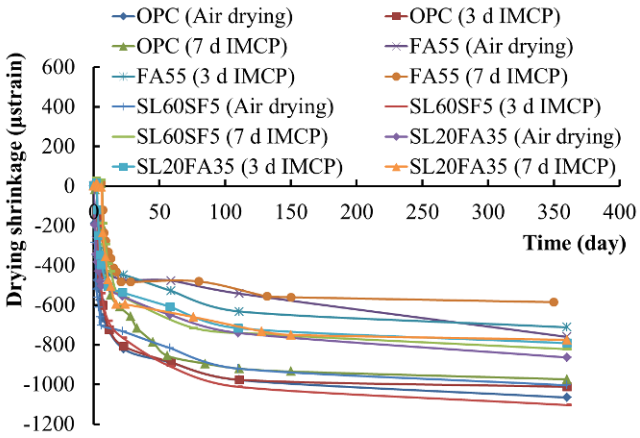

(a) Effect of binder compositions

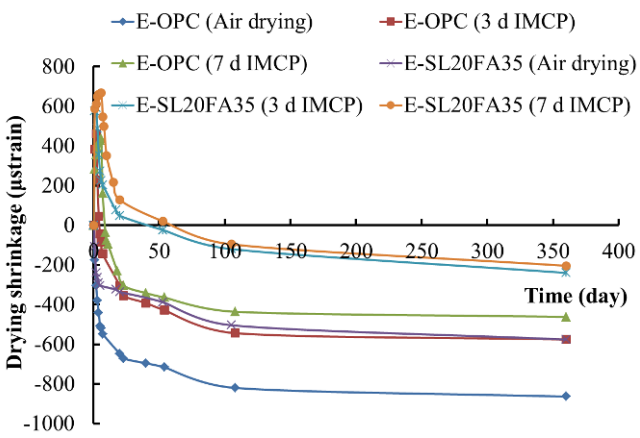

(b) Effect of CaO-based EX

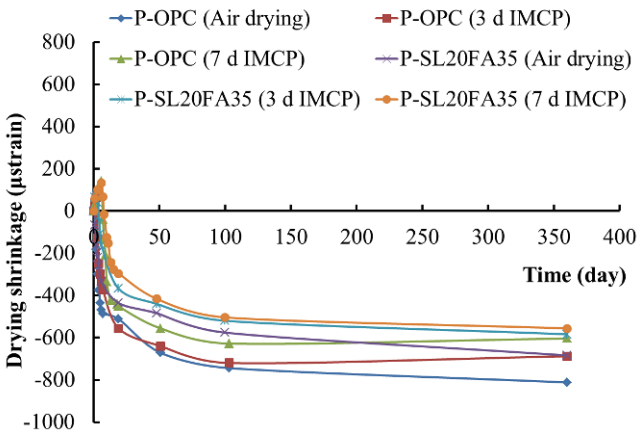

(c) Effect of MgO-based EX

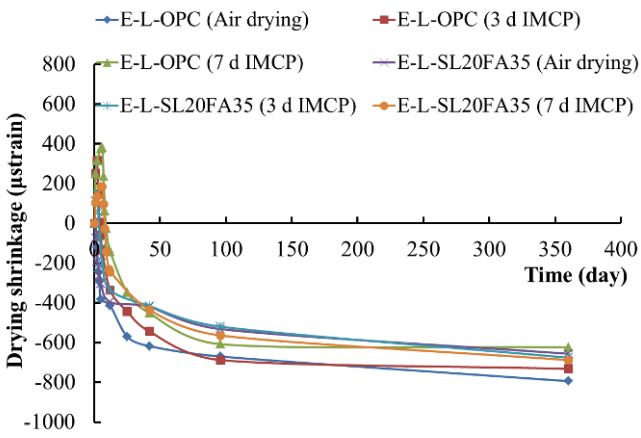

(d) Combined effect of CaO-based EX and LWS-1

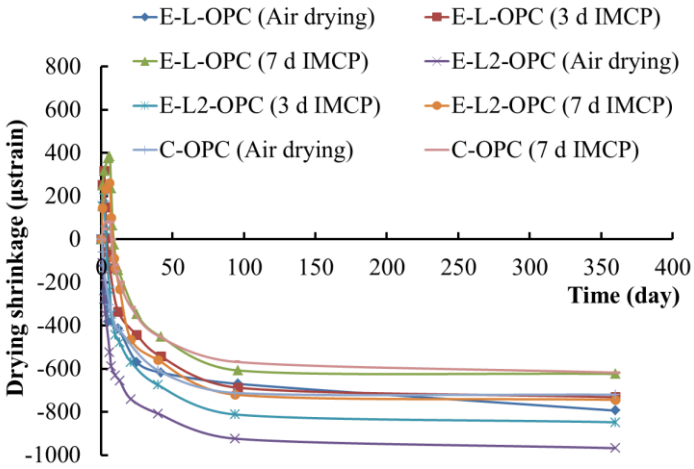

(e) Effect of LWS types and CRA

Figure 4-23- Drying shrinkage of mortars made with various binder compositions and shrinkage mitigating materials as a function of IMCP

4.4. Development of Eco and crack-free HPC

This subtask was undertaken to optimize the mix design and evaluate the performance of Eco and crack-free HPC. Based on the obtained results from Subtask 2-1, 2-2, and 2-3, the effect of different binder compositions, aggregate characteristics, and shrinkage mitigating materials were incorporated to design Eco- and crack-free HPC with different targeted applications (Eco-Pave-Crete and Eco-Bridge-Crete). The investigated mix design parameters are summarized in

Table 4-13 presents the mixture proportions of the investigated Eco- and crack-free mixtures. The binder contents varied between 320 (540 lb/yd^3) and 350 kg/m^3 (590 lb/yd^3) for pavement and transportation infrastructure applications, respectively. The OPC reference mixture was made with 100% cement and binder content of 350 kg/m^3 (590 lb/yd^3). The investigated mix design parameters included four different binder compositions, two types of fibers, and two various shrinkage mitigating materials. Depending on the targeted application, the HRWR dosage was adjusted to secure the slump consistencies varying between 50 mm and 200 mm (2 – 8 in.). The AEA concentration was also adjusted to ensure the fresh air volume of 5% ± 2% for all mixtures. The w/cm was fixed at 0.4 for all mixtures. The investigated test properties included workability, shrinkage, mechanical properties, and durability.

Table 4-12.

Table 4-13 presents the mixture proportions of the investigated Eco- and crack-free mixtures. The binder contents varied between 320 (540 lb/yd^3) and 350 kg/m^3 (590 lb/yd^3) for pavement and transportation infrastructure applications, respectively. The OPC reference mixture was made with 100% cement and binder content of 350 kg/m^3 (590 lb/yd^3). The investigated mix design parameters included four different binder compositions, two types of fibers, and two various shrinkage mitigating materials. Depending on the targeted application, the HRWR dosage was adjusted to secure the slump consistencies varying between 50 mm and 200 mm (2 – 8 in.). The AEA concentration was also adjusted to ensure the fresh air volume of 5% ± 2% for all mixtures. The w/cm was fixed at 0.4 for all mixtures. The investigated test properties included workability, shrinkage, mechanical properties, and durability.

Table 4-12- Investigated mix design parameters in Subtask 2-4

Codification	Description	Binder content		Binder type				Fiber type and content			Shrinkage mitigating strategy	
		320 (kg/m^3)	350 (kg/m^3)	100% OPC	60% OPC + 40% Class C FA	45% OPC + 20% SL + 35% Class C FA	35% OPC + 60% SL + 5% SF	TUF strand fiber (0.35%)	STRUX® 90/40 synthetic fiber (0.35%)	Recycled steel fiber from tire (0.35%)	25% LWS	7.5% CaO-based EX
350-OPC	Reference mixture		x	x								
320-20SL-35FA	Effect of binder type	x				x						
350-20SL-35FA			x			x						

320-40FA		x			x							
350-60SL-5SF			x				x					
350-20SL-35FA-25LWS	Effect of LWS		x			x					x	
320-40FA-25LWS		x			x						x	
350-60SL-5SF-25LWS			x				x				x	
350-20SL-35FA-0.35FT	Effect of fiber type		x			x		x				
350-20SL-35FA-0.35FG			x			x			x			
350-20SL-35FA-0.35FRW			x			x				x		
350-20SL-35FA-7.5EX	Effect of EX		x			x						x
350-20SL-35FA-7.5EX-0.35FT	Combined effect of fiber and EX		x			x		x				x
350-20SL-35FA-7.5EX-0.35FRW			x			x				x		x

OPC: Ordinary portland cement, SL: Blast furnace slag, CFA: Class C fly ash, and SF: silica fume, EX: expansive agent, LWS: lightweight sand

Codification: 350-20SL-35FA-7.5EX-0.35FRW: Binder content of 350 kg/m^3 containing 20% SL, 35% FA and 7.5% CaO-based EX and 35% recycled steel fibers

1 kg/m^3 = 1.685 lb/yd^3

Table 4-13- Mixture proportions of investigated Eco and crack-free HPC mixtures

	350-OPC	320-20SL-35FA	350-20SL-35FA	320-40FA	350-60SL-5SF	320-40FA-25LWS	350-20SL-35FA-25LWS	350-60SL-5SF-25LWS	350-20SL-35FA-0.35FT	350-20SL-35FA-0.35FG	350-20SL-35FA-0.35FRW	350-20SL-35FA-7.5EX	350-20SL-35FA-7.5EX-0.35FT	350-20SL-35FA-7.5EX-0.35FRW
Cement (kg/m^3)	350	144	158	192	158	192	158	158	158	158	158	145	158	158
Fly ash (kg/m^3)	—	97	106	111	—	111	106	—	106	106	106	98	106	106
Slag (kg/m^3)	—	60	64	—	192	—	64	192	64	64	64	60	64	64
Silica fume (kg/m^3)	—	—	—	—	13	—	—	13	—	—	—	—	—	—
Water (kg/m^3)	140	128	140	128	140	128	140	140	140	140	140	140	140	140
Sand (kg/m^3)	744	761	744	761	744	570	560	560	744	744	744	560	744	744
Agg. 3/8" (kg/m^3)	465	475	465	475	465	476	465	465	555	555	650	465	555	650
Agg. 1" (kg/m^3)	650	666	650	666	650	666	650	650	565	565	480	650	565	480
LWS (kg/m^3)	—	—	—	—	—	190	186	186	—	—	—	—	—	—
CaO-based EX (kg/m^3)	—	—	—	—	—	—	—	—	—	—	—	23	23	23
Fiber, by volume (type)	—	—	—	—	—	—	—	—	0.35 (synthetic)	0.35 (synthetic)	0.35 (steel fibers)	—	0.35 (synthetic)	0.35 (steel fibers)
	—	—	—	—	—	—	—	—				—		
HRWRA (l/kg^3)	1.12	0.45	0.89	0.9	1.05	1.1	1.05	1.25	1.05	1.2	1.2	0.9	1.1	1.4
AEA (ml/kg^3)	28	26	28	16	17	17	14	17	20	20	14	15	15	15

1 kg/m^3 = 1.685 lb/yd^3

The results of HRWR demand and slump consistency of the investigated HPC mixtures are shown in Figure 4-24. For a given slump consistency, HPC mixtures prepared with binary and ternary of SCMs required lower HRWRA demand to achieve required slump consistency compared to the control mixture made with 100% cement. This can be due to the lower water demand and higher packing density of SCMs binders. All mixtures exhibited no surface bleeding which is usually measured by collecting the excess surface solution as a function of time after placement (ASTM C232). As expected, mixtures containing fibers exhibited higher HRWR demand compared to similar mixtures made without any fiber.

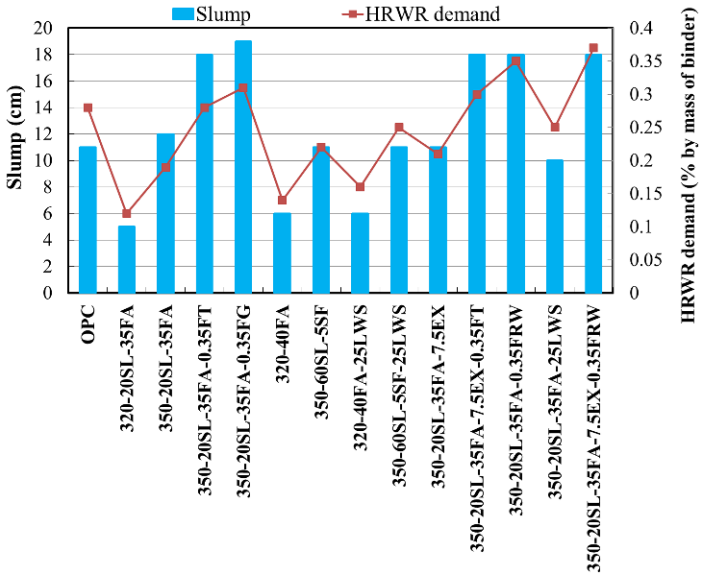

Figure 4-24- Slump consistency and HRWR demand of HPC mixtures

Mechanical properties

The results of mechanical properties development of the investigated concrete mixtures are compared in Figure 4-25. As expected, the mixture made with 100% cement developed higher early-age compressive strength. On the other hand, the majority of the investigated mixtures

resulted in approximately similar compressive strength value of 50 MPa (7252 psi) as that of the control mixture made with 100% OPC. The incorporation of fibers in concrete containing high volume of SCMs was shown to have 0 to 35% higher splitting tensile and flexural strengths than the control mixture made with 100% cement. The highest splitting tensile and flexural strength was obtained for the mixture made with 35% recycled steel fibers containing 20% SL and 35% FA. This mixture also exhibited similar compressive strength to the control mixture. For a given binder type and content, mixtures incorporating steel fibers recycled from scrap tires resulted in higher mechanical properties compared to the synthetic fibers for a given fiber content. All mixtures met the compressive strength requirements.

Shrinkage

The autogenous and drying shrinkage of the reference and Eco-HPC mixtures are presented in Figure 4-26. Mixture made with 100% cement exhibited the highest autogenous and drying shrinkages of 180 and 550 μstrain after 120 and 300 days of drying, respectively, compared to other Eco-HPCs made with SCMs and fibers. The incorporation of 7.5% CaO-based EX resulted in significant early-age expansion in autogenous and drying shrinkage. The 350-SL20FA35 mixture containing 7.5% CaO- based EX exhibited 180 μstrain expansion after three days of moist curing followed by 250 μstrain shrinkage after 300 days of drying.

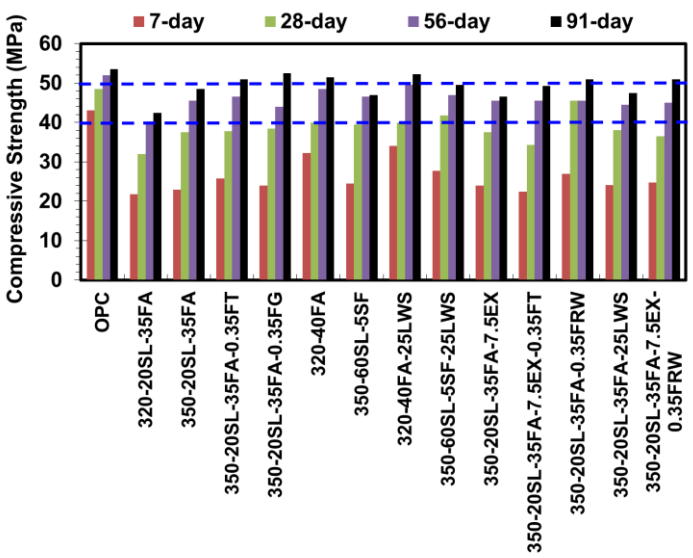

(a) Compressive strength

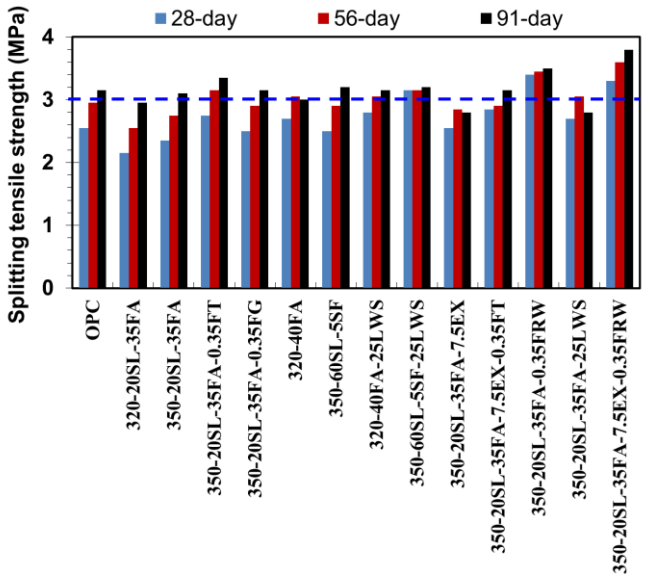

(b) Slitting tesnile strength

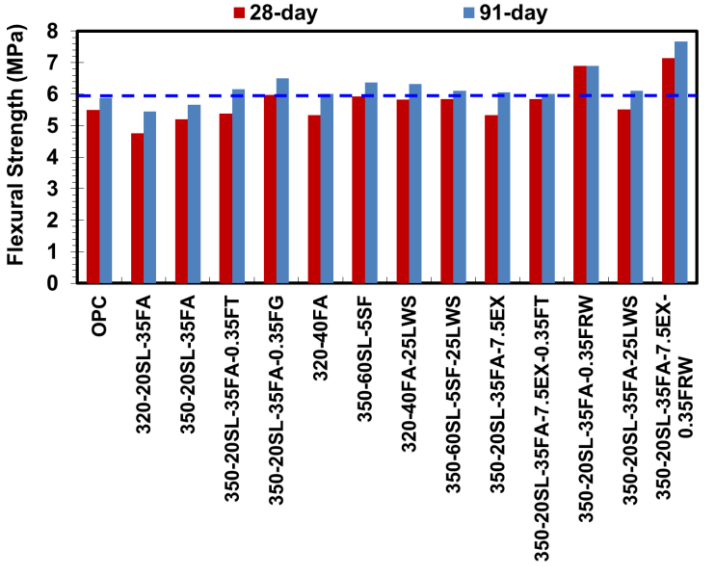

(c) Flexural strength

Figure 4-25- Mechanical properties of HPC mixtures

(Note: 1 MPa = 145.04 psi)

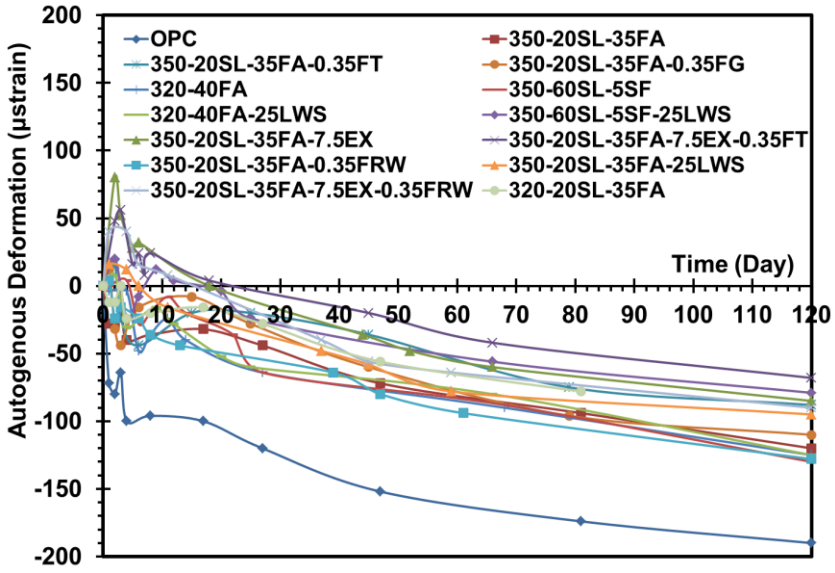

(a) Autogenous shrinkage

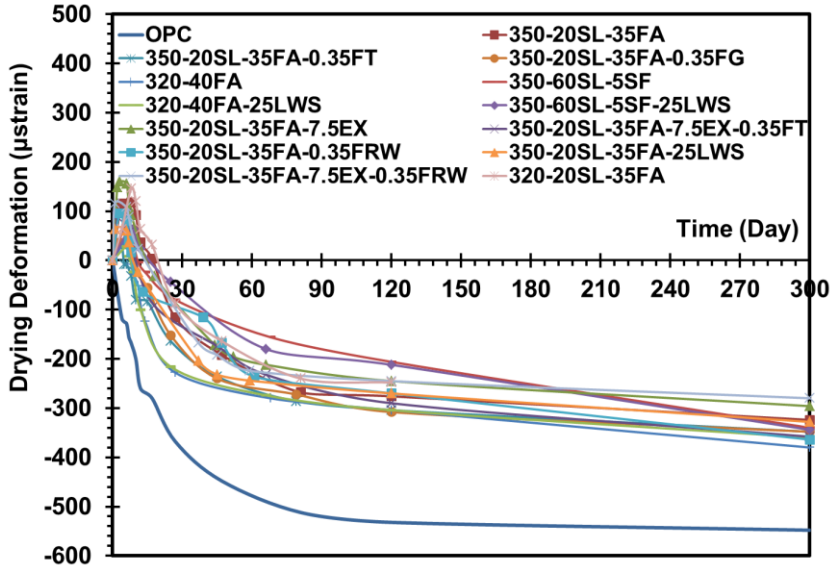

(b) Drying shrinkage

Figure 4-26- Shrinkage of HPC mixtures

Durability

Figure 4-27 compares the electrical resistivity results of the investigated concrete mixtures. The lowest electrical resistivity (10 kΩ.cm) was observed for the reference mixture. Ternary blends of 60% SL and 5% SF exhibited the highest electrical resistivity of 80 kΩ.cm among the

mixtures. According to the proposed relationship between surface resistivity and rapid chloride ion permeability by Chini et al. (2003), mixtures containing 60% SL replacement can be considered to exhibit low chloride ion permeability, regardless of shrinkage reducing materials.

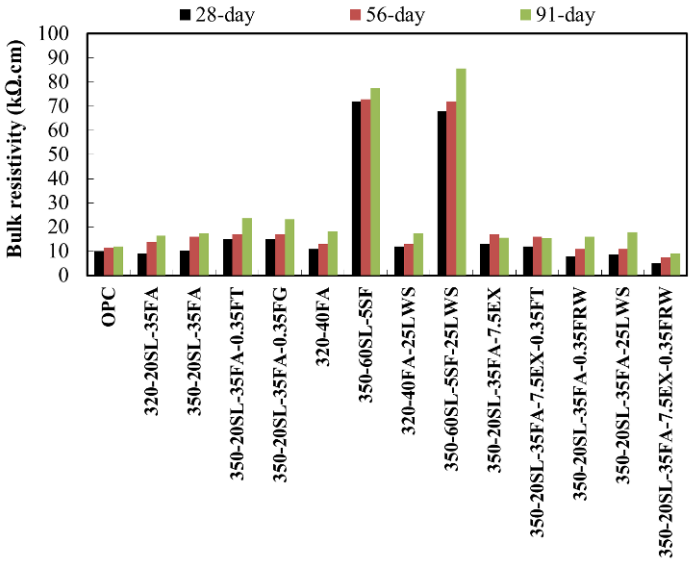

Figure 4-27- Electrical resisivity of HPC mixtures

The results of deicing salt scaling rating and cumulative mass of scaling residue of the investigated mixtures are presented in Table 4-14 and Figure 4-28, respectively. For a given w/cm, the partial substitution of cement by SCMs was shown to increase the mass of scaling residue compared to the reference mixture made with 100% OPC. Relatively high scaling values were obtained for binder compositions made with high volume SCM replacements of more than 50%. As presented in Table 4-14, all Eco-HPC mixtures exhibited the mass scaling rating lower than 4 after 50 freeze-thaw cycles. In the case of using high volume SCMs, the reduction of w/cm and stability of air void system would be beneficial in enhancing the resistance to de-icing salt scaling.

Table 4-14- Deicing salt scaling rating of HPC mixtures

Mixture	Number of freeze-thaw cycles						
	7	14	21	28	35	42	50
OPC	0	0	0	0	1	2	3
320-20SL-35FA	0	1	1	2	3	3	4
350-20SL-35FA	0	0	1	1	2	3	3
320-40FA	0	1	1	2	2	3	4
350-60SL-5SF	0	1	1	2	3	3	4
320-40FA-25LWS	0	1	1	2	2	3	3
350-60SL-5SF-25LWS	0	1	1	2	2	3	3
350-20SL-35FA-7.5EX	0	1	1	1	2	3	3
350-20SL-35FA-7.5EX-0.35FT	0	0	1	2	3	3	3
350-20SL-35FA-0.35FRW	0	1	1	2	3	3	4
350-20SL-35FA-25LWS	0	1	1	2	3	4	3
350-20SL-35FA-7.5EX-0.35FRW	0	0	1	1	2	2	3

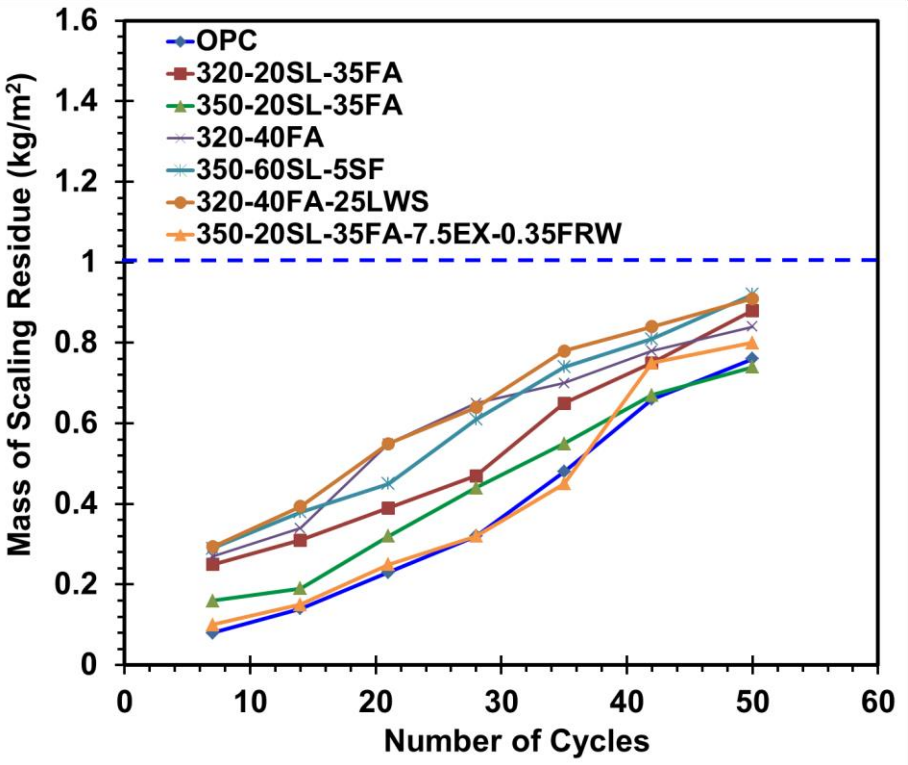

Figure 4-28- Mass of scaling residue of HPC mixtures with frezze-thaw cycles

4.5. Key engineering properties and durability

This subtask was aimed to further evaluate key engineering properties and durability of the optimal mixtures selected in the Subtask 2-4. Based on the obtained results from Subtask 2-4, four optimal concrete mixtures (with and without fibers) were selected for targeted applications, as listed in Table 4-15. Various tests were carried out to assess the workability, shrinkage, restrained shrinkage and cracking resistance, as well as mechanical properties and durability.

Table 4-15- Selected mixtures used in Subtask 2-5

Concrete type	Mixture	Binder content		Binder type				Fiber type and content		Shrinkage mitigating materials	
		320 (kg/m^3)	350 (kg/m^3)	100% OPC	60% OPC + 40% Class C FA	45% OPC + 20% SL + 35% Class C FA	35% OPC + 60% SL + 5% SF	TUF strand fiber (0.35%)	Recycled steel fiber from tire (0.35%)	25% LWS	7.5% Type G EX
Eco-Pave-Crete	320-40FA-25LWS	x			x					x	
	320-20SL-35FA-7.5EX-0.35FT	x				x		x			x
Eco-Bridge-Crete	350-60SL-5SF-25LWS		x				x			x	
	350-20SL-35FA-7.5EX-0.35FRW		x			x			x		x

Mechanical properties

The development of mechanical properties of the selected Eco-HPCs is presented in Figure 4-29. The mixture made with 0.35% recycled fibers and containing 20% slag and 35% fly ash replacements developed approximately similar compressive strength as that of the control mixture made with 100% cement. The incorporation of fibers in concrete made with high volume

of SCMs is shown to have 30% higher splitting tensile strength than that of the control mixture made with 100% cement. The mixture made with 0.35% recycled steel fibers developed the greater area under load-deflection curve compared to other mixtures proportioned with synthetic fiber. The reference mixture developed the lowest ductility behavior and residual strength among all mixtures. The 56-day flexural toughness (area under the load-deflection curve) results of mixtures made with fibers are compared in Figure 4-29 (e). It is interesting to note that for a given fiber content, the use of steel fibers recovered from waste tires had two times higher flexural toughness compared to the similar mixture made with synthetic fibers. In addition, the incorporation of expansive agent in combination with fibers (especially steel fibers) would enhance the reinforcing mechanism provided by fibers. This may be due to the induced compressive stress provided by expansive cements which can lead to forming of internal pre-stressed condition in concrete. Internal pre-stressed concrete may result in higher residual strength and flexural toughness. Bentz and Jensen (2004) also reported that as long as proper restraint is provided, the expansion of self-stressing materials can pre-stress concrete and improve its tensile capacity.

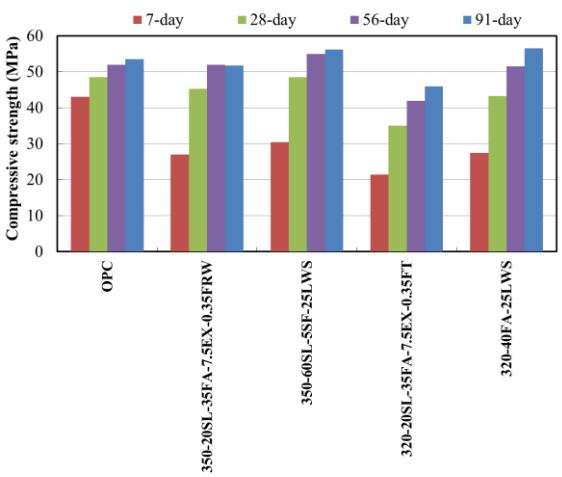

(a) Compressive strength

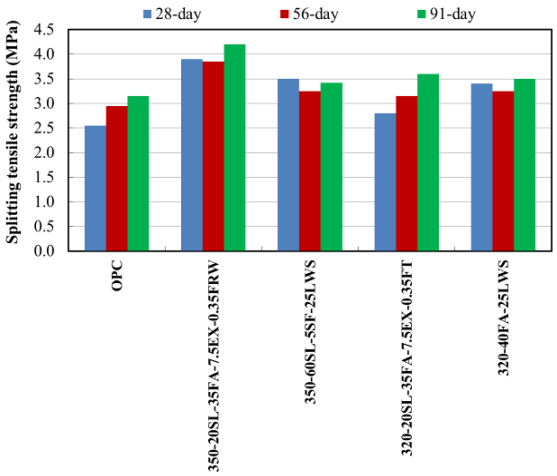

(b) Splitting tesnile strength

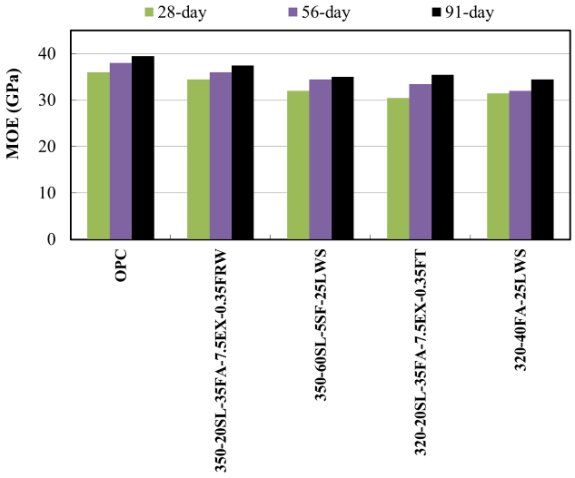

(c) Modulus of elasticity

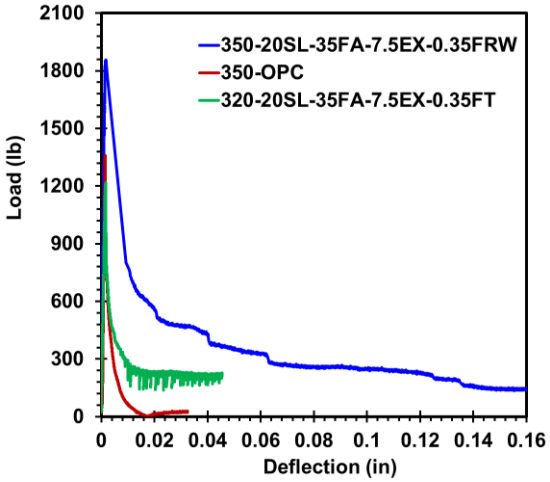

(d) Load-deflection response at 56 days

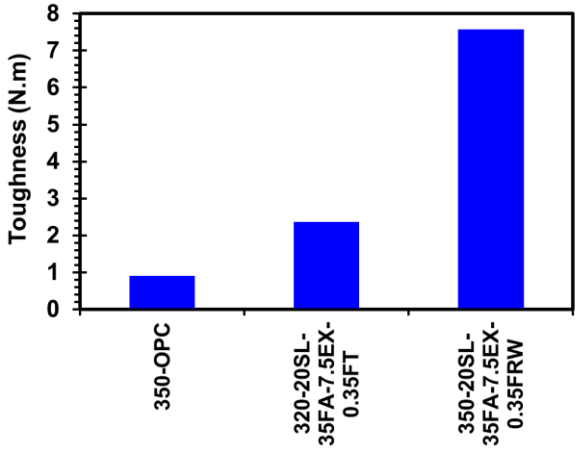

(e) Toughness of selected mixtures at 56 days

Figure 4-29- Mechanical properties of selected HPC mixtures

(Note: 1 MPa = 145.04 psi)

Shrinkage

The results of drying and restrained shrinkage of the selected mixtures are shown in Figure 4-30. Restrained shrinkage and cracking potential of mixtures were evaluated using ASTM C1581 ring test. Mixture made with 100% cement exhibited the highest drying shrinkages of 550 μstrain after 250 days of drying. The optimized Eco-HPC mixtures had lower drying shrinkage of 300 μstrain after 250 days of drying. The incorporation of 7.5% Type G expansive agent resulted in a significant early-age expansion of 100 μstrain. It is interesting to point out that no restrained shrinkage cracking was observed for the optimized concrete mixtures after 55 days of testing. However, the control mixture made with 100% cement exhibited elapsed time to cracking after 22 days. For mixtures containing EX, the tensile stress induced by restrained shrinkage was compensated by expansion induced by using EX, thus reflecting no cracking after 55 days. Average stress rate and cracking potential classification of investigated mixtures are summarized in Table 4-16. In accordance with ASTM C1581, the stress rate development induced by restrained shrinkage at the age of cracking can be calculated as follows:

$$q = \frac{G\left|\alpha_{avg}\right|}{2\sqrt{t_r}} \qquad \textbf{(4-7)}$$

where q is the stress rate in each test specimen, MPa/day (psi/day), G is a constant based on the ring dimension 72.2 GPa (10.5×10^6 psi), and t_r is the elapsed time to cracking or elapsed time when the test is terminated for each test specimen. $|\alpha_{avg}|$ is the absolute value of the average strain rate factor for each test specimen, (μstrain/day$^{1/2}$) which is determined as a slope of a fitted line between steel strain and square root of elapsed time. Mixtures made with EX had positive strain rate factor due to the expansion of such mixtures. In accordance with ASTM C1581, the reference mixture made with 100% cement was considered to exhibit moderate shrinkage cracking potential. On the other hand, mixtures proportioned with shrinkage reducing materials

have low cracking potential with compressive stress rate ranging between -6.9 to 1.7 MPa/day (-1000–247 psi/day).

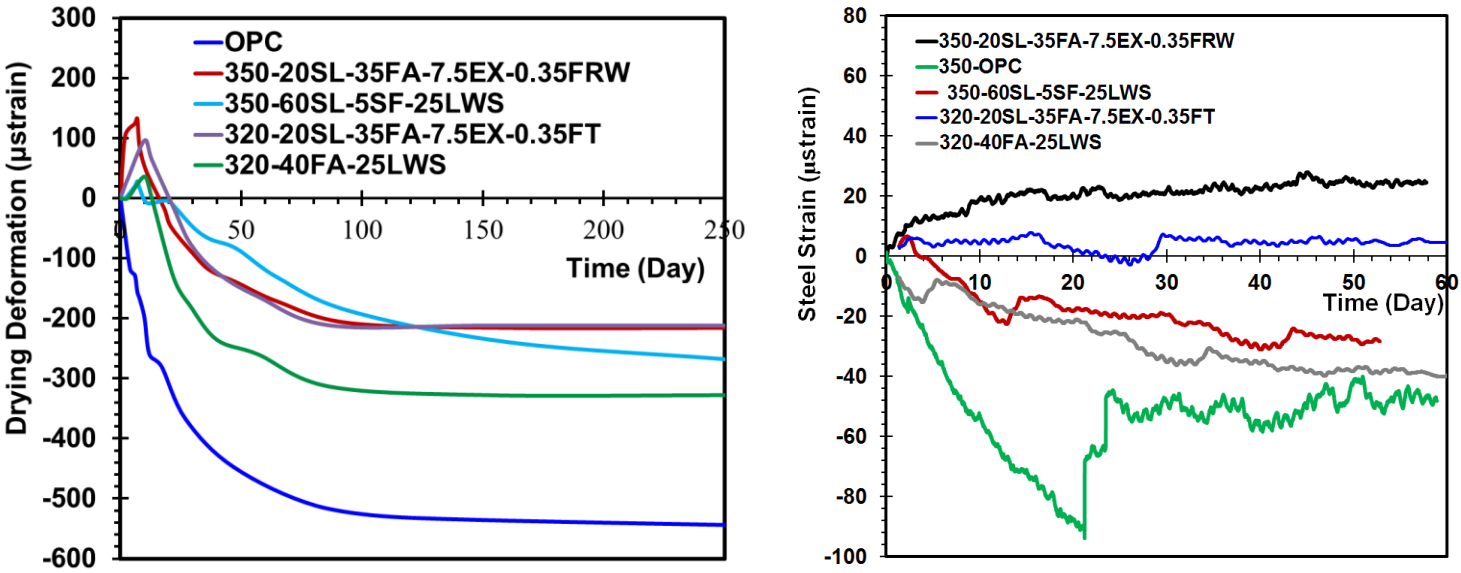

(a) Drying shrinkage **(b) Restrained shrinkage**

Figure 4-30- Shrinkage of selected HPC mixtures

Table 4-16- Cracking potential classification of HPC mixtures

Mixture	Time to cracking (day)	Average strain rate factor (µstrain/day$^{1/2}$)	Average stress rate (MPa/day)	Potential of cracking (ASTM C 1581)
350-OPC	22	-23.6	-26.4 (tension)	Moderate
350-20SL-35FA-7.5EX-0.35FRW	—	2.4	1.7 (compression)	Low
350-60SL-5SF-25LWS	—	-4.9	-3.5 (tension)	Low
320-20SL-35FA-7.5EX-0.35FT	—	1.3	1 (compression)	Low
320-40FA-25LWS	—	-9.7	-6.9 (tension)	Low

Note: 1 MPa = 145.04 psi

Durability

The performance of the selected Eco-HPCs for different durability aspects is presented in Figure 4-31. All selected Eco-HPC mixtures developed approximately similar performance as that of the control mixture made with 100% OPC. All Eco-HPCs developed frost durability factor

values higher than 80% after 300 freeze-thaw cycles, except for ternary blends of 60% SL and 5% SF with durability factor of 70%.

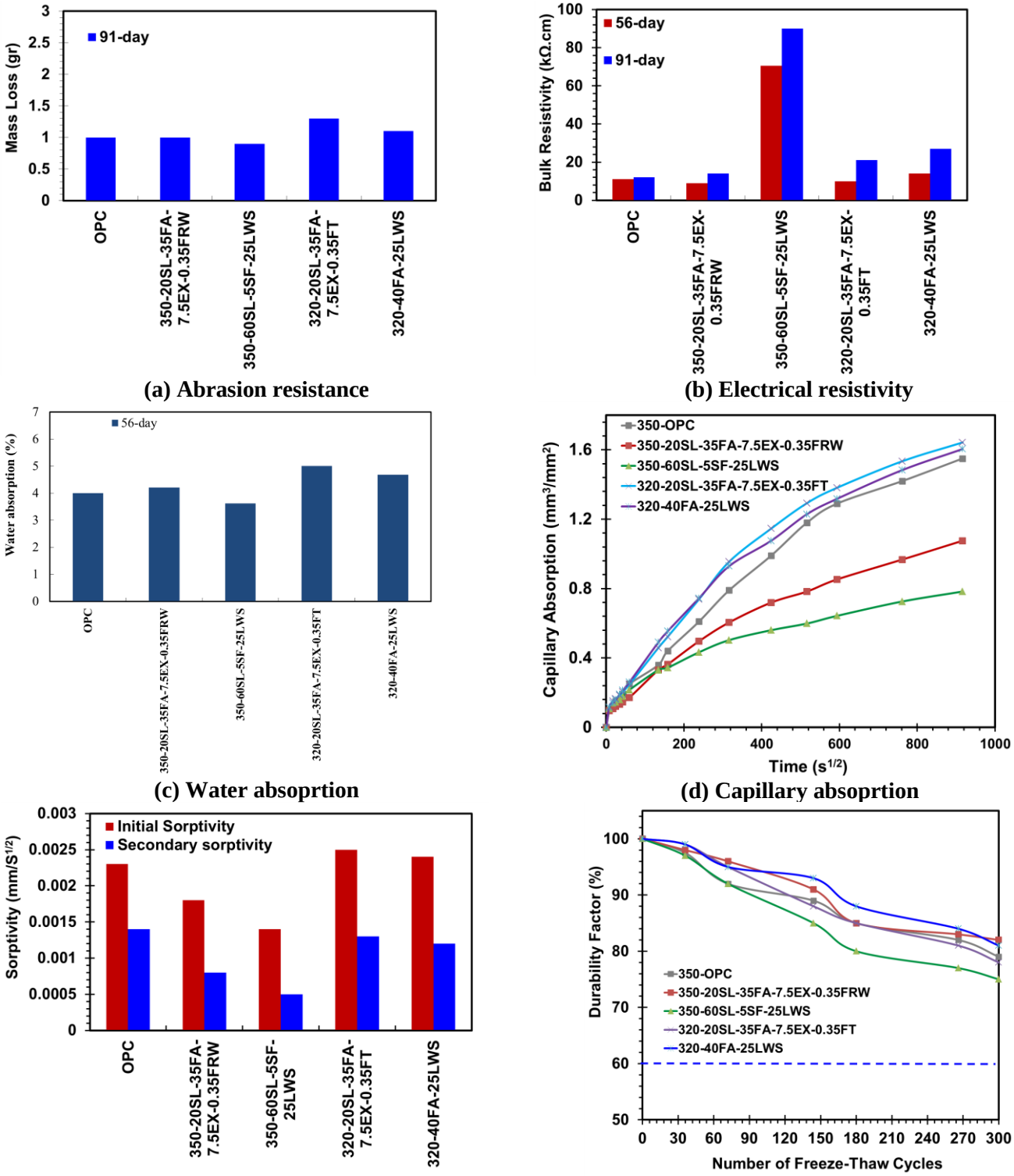

(a) Abrasion resistance **(b) Electrical resistivity**

(c) Water absoprtion **(d) Capillary absoprtion**

(e) Sorptivity index **(f) Frost durability factor**

Figure 4-31- Durability performance of selected HPC mixtures

5. SHRINKAGE AND STRUCTURAL PERFORMANCE OF LARGE-SCALE ELEMENTS

This chapter describes a summary of the performance of optimized Eco-HPCs used for large-scale elements. The aim of this task was to evaluate the shrinkage deformation of slab sections and flexural strength of reinforced concrete beams made with optimized Eco-Pave-Crete and Eco-Bridge-Crete. Large-scale specimens, including slab and beam elements, were constructed. This task consists of two subtasks as follows:

5.1. Shrinkage deformation of concrete slab section

The aim of this subtask was to evaluate the shrinkage deformation of concrete slabs made with selected concrete mixtures from Task II. As shown in Figure 5-1, three slabs measuring 1.8 × 1.8 m (6 × 6 ft) and 150 mm (6 in.) in depth were constructed to evaluate shrinkage deformation of different concrete mixtures. The investigated mixture parameters include the incorporation of fiber, lightweight sand, expansive agent, and high volume SCMs and the results were compared with that of the MoDOT reference mixture. The mix design parameters of selected concrete mixtures for slab sections are presented in Table 5-1.

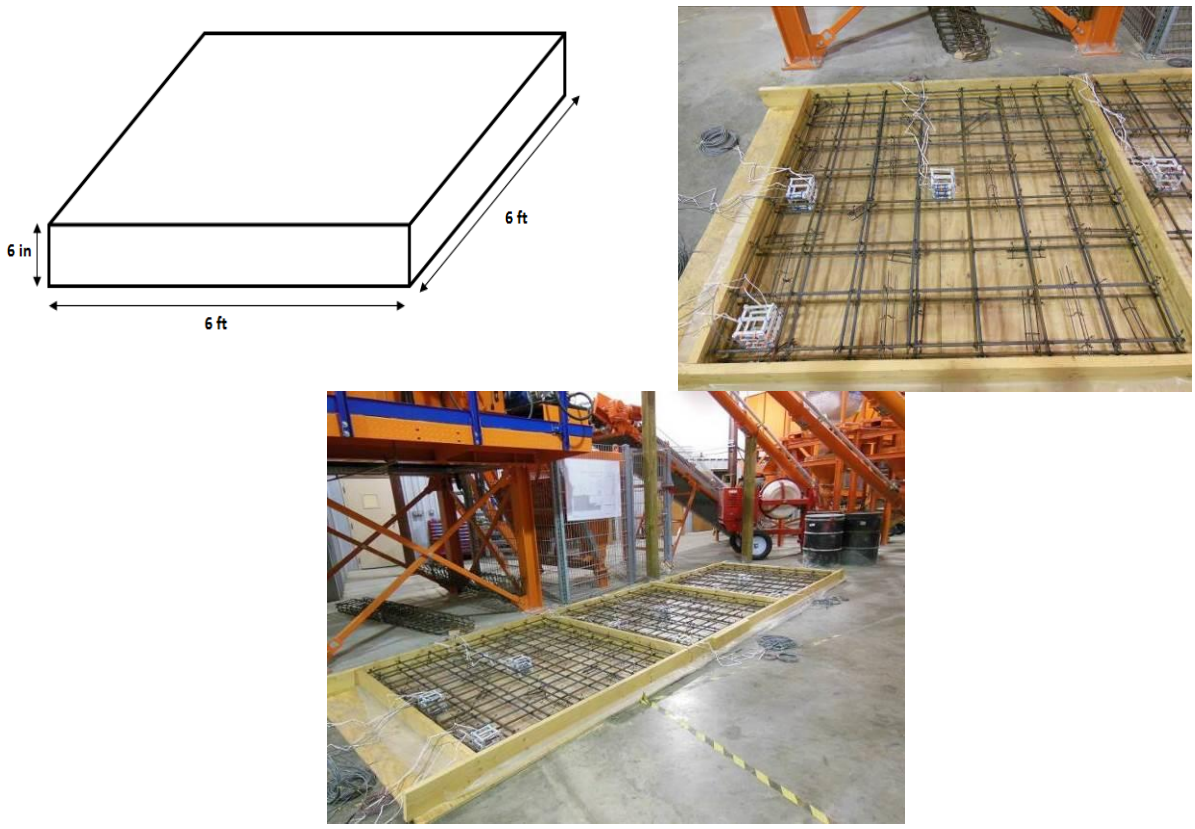

Figure 5-1- Slab section used for shrinkage deformation evaluation

Table 5-1- Selected concrete mixtures for slab sections

Concrete type	Codification	Reinforcement	w/cm	Binder content		Binder type		Fiber type and content		Shrinkage mitigating materials	
			0.40	350 kg/m^3 (590 lb/yd^3)	375 kg/m^3 (630 lb/yd^3)	75% OPC + 25% Class C FA	45% OPC + 20% SL + 35% Class C FA	TUF strand fibers (0.35%)	Steel fibers from tire (0.35%)	25% LWS	7.5% Type G EX
MoDOT reference mixture	FA25	x	x		x	x					
Optimized Eco-Bridge-Crete	SL20FA35-25LWS	x		x			x			x	
	SL20FA35-7.5EX-0.35FRW	x		x			x		x		x

The investigated slabs were fully instrumented by utilizing strain gauges, relative humidity sensors, and thermocouples to monitor the deformation caused by concrete shrinkage, humidity and temperature variations over time. A detailed description of the instrumentation used in this investigation is provided below:

Embedded strain gauges

In this study, the embedment type of strain gauges was used to monitor the shrinkage deformation of concrete, as shown in Figure 5-2. The sensor has the outer body of 120 mm (4.8 in.) sensing grid with an effective gauge length of 75 mm (3 in.). The gauge is waterproof and is designed to be placed in fresh concrete to directly measure the shrinkage deformation associated with concrete. The sensor consists of a 75 mm (3 in.) 120 ohm (Ω) foil strain gage (nickelchromium alloy on polymide backing). The surface of the gauge is designed to have a honeycomb pattern that enables adequate bond to concrete.

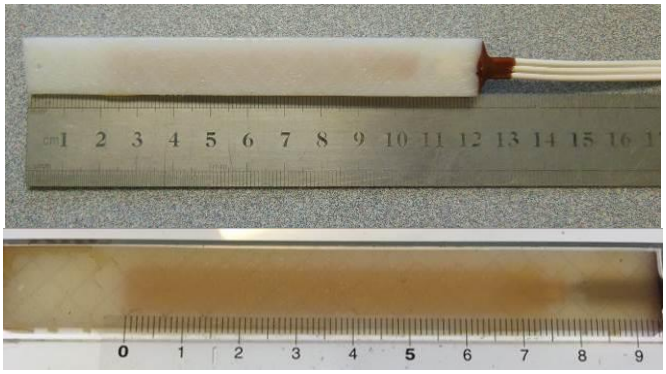

Figure 5-2- Embedded strain gauge for monitoring shrinkage deformation

Thermocouples

The thermocouple wire used in the instrumentation was a Type T 20 gage wire. These thermocouples consist of copper and constantan wires, and are functional between -250 to 250°

C. The ends of the solid thermocouple wires were twisted and then soldered to ensure an adequate electrical connection, as shown in Figure 5-3.

Figure 5-3- Thermocouple used for concrete temperature measurement

Relative humidity sensors

The small (6 × 20 mm) capacitive relative humidity sensor was used to measure the relative humidity inside concrete, as shown in Figure 5-4. The accuracy of the sensors is reported by the manufacturer to be ±2% RH between 10% and 90% RH, and range up to ±4% at 100% RH. In order to embed the RH sensor in concrete, the RH sensor was placed inside the 1/2" PVC tube and the end of the tube was covered by Gore-Tex to allow moisture transmission, while preventing the penetration of liquid water and solid particles that may lead to an error in measurement. The encapsulated RH sensor before embedding in concrete is shown in Figure 5-5.

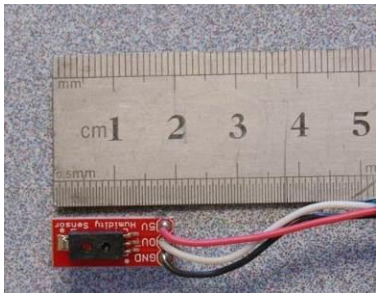

Figure 5-4- Relative humidity sensor used for RH measurement

Figure 5-5- Encapsulated relative humidity sensor before embedment in concrete

Figure 5-6 shows the instrumentation layout, including embedded concrete strain gauge, relative humidity sensor, and thermocouple for monitoring the shrinkage deformation of concrete used for slab sections. As indicated in Figure 5-7, each slab was instrumented at three different locations to monitor the concrete shrinkage behavior at the center, edge, and corner of the slab, corresponding to points A, B, and C, respectively. Station A located at the center of slab has three embedded strain gauges in the longitudinal direction, three thermocouples, and three relative humidity sensors placed along the height of the slab. Stations B and C located at the edge and corner of the slab have similar instrumentation layout, including four embedded strain gauges (two in the longitudinal as well as two in the transverse direction), two thermocouples, and two relative humidity sensors, as presented in Figure 5-6. Sensors were placed at different thicknesses of slab to monitor strain, temperature and relative humidity along the height of slabs as shown in as presented in Figure 5-6. The summary of instrumentation plan and designation of sensors utilized for each slab are listed in Table 5-2 and Table 5-3, respectively.

Both the strain and the temperature data was recorded using Campbell Scientific data acquisition hardware and software. Lead wires from the strain gages were routed through AM16-32 multiplexer, using a separate completion module for each gage on the multiplexer. The data logger used was a Campbell Scientific CR1000. The thermocouple wires were routed through an AM25T multiplexer, which has an internal RTD (resistance temperature detector) to measure the

cold junction temperature required to compute the temperature at the soldered end of the thermocouple. The multiplexer was controlled by the CR1000 data logger. In addition to the strain and temperature instrumentation, relative humidity sensors were collected.

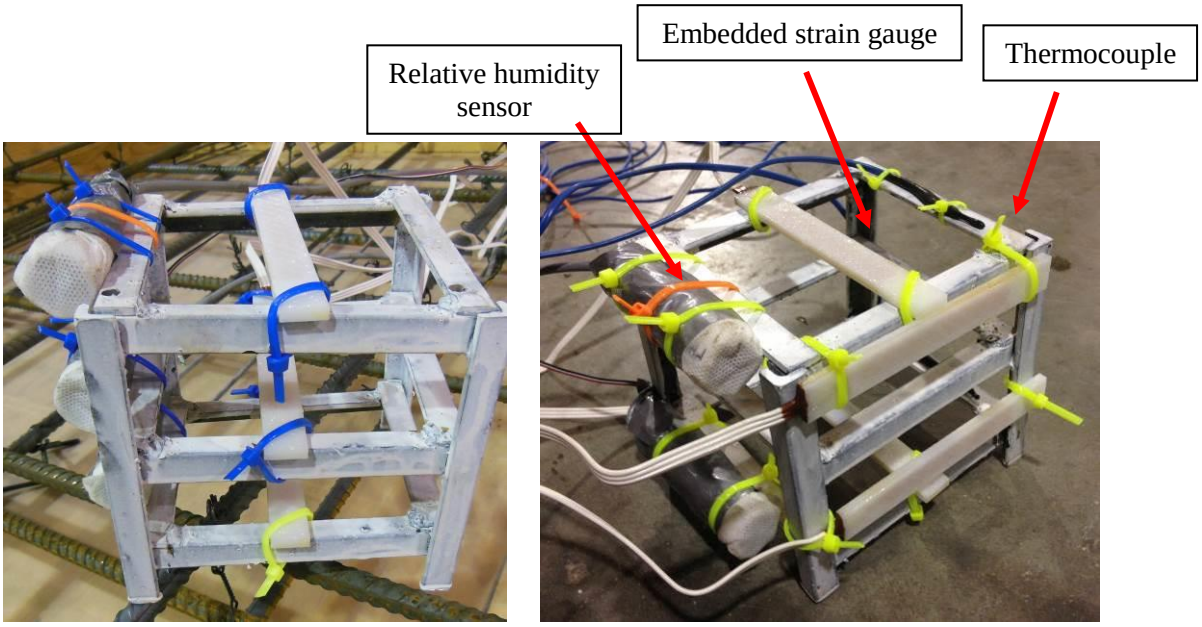

(a) **(b)**

Figure 5-6- Instrumentation layouts

(a) Layout A: 3 embedded strain gauges in longitudinal direction, 3 thermocouples and 3 relative humidity sensors

(b) Layout B: 4 embedded strain gauges (two longitudinal and two transverse directions), 2 thermocouples and 2 relative humidity sensors

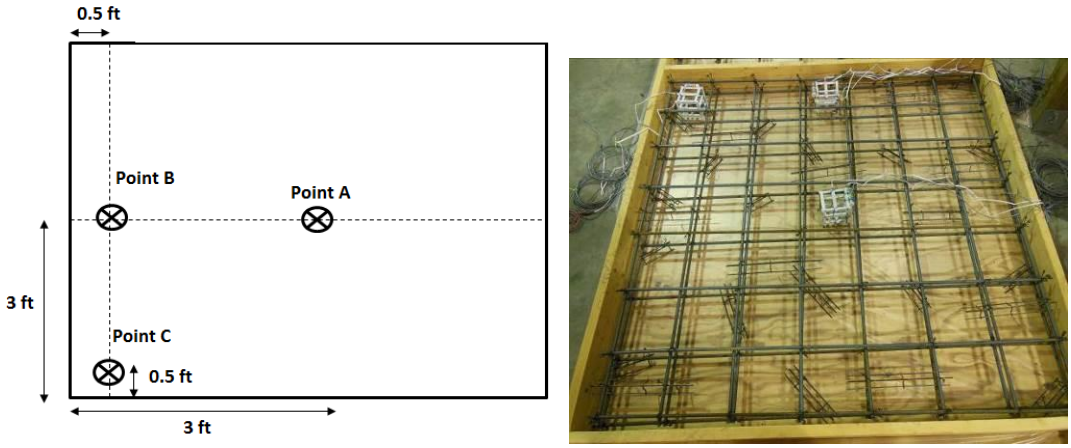

Figure 5-7- Instrumentation location plan for each slab

Table 5-2- Summary of instrumentation plan used for each slab

Point	# Embedded strain gauge	# Relative humidity sensor	# Thermocouple
A	3 (longitudinal direction)	3	3
B	4 (two longitudinal and two transverse directions)	2	2
C	4 (two longitudinal and two transverse directions)	2	2
Sum	11	7	7

Table 5-3- Codifications of sensors used for slab instrumentation

Slab #1 made with 25% FA (FA25)			
Strain sensors	Humidity sensors	Temperature sensors	Codifications
1-M-SL-1	1-M-H-1	1-M-T-1	• 1 refers to slab made with FA25 mixture (MoDOT reference mixture). • M, S, and C refer to center, side and corner points of slab. • S, H, and T refer to strain, humidity and temperature sensors. • SL and ST refer to strain gauges in longitudinal and transvers directions. • 1, 2, and 3 represents bottom, middle, and top parts along height of concrete slab. • Similar designations are used for other slabs, except that slabs made with SL20FA35-25LWS and SL20FA35-7.5EX-0.35FRW mixtures are designated as 2 and 3, respectively.
1-M-SL-2	1-M-H-2	1-M-T-2	
1-M-SL-3	1-M-H-3	1-M-T-3	
1-S-SL-1	1-S-H-1	1-S-T-1	
1-S-ST-1	1-S-H-3	1-S-T-3	
1-S-SL-3	1-C-H-1	1-C-T-1	
1-S-ST-3	1-C-H-3	1-C-T-3	
1-C-SL-1			
1-C-ST-1			
1-C-SL-3			
1-C-ST-3			

All slabs were reinforced with two reinforcement mats of longitudinal #4 bars spaced at 250 mm (10 in.) which were placed at the top and bottom parts of slabs, as shown in Figure 5-7. The top and bottom rebar mats were located 25 mm (1 in.) and 50 mm (2 in.) from the top and bottom of

the concrete, respectively. All concrete mixtures were made in local concrete batching plant to confirm the ability of proposed concrete mixtures to apply under actual field conditions. The HRWR dosage was adjusted to secure the slump consistencies varying between 150 mm and 200 mm (6 – 8 in.). The AEA concentration was also adjusted to ensure the fresh air volume of 5% ± 2% for all mixtures. The w/cm was fixed at 0.4 for all mixtures. In total three concrete slabs were constructed including two optimized Eco- and crack-free HPC and a control concrete slab using MoDOT reference mixture targeted for bridge deck, as given in Table 5-1.

After casting, the top surface of the beams was covered with wet burlap and plastic sheeting, and a wet surface was maintained for seven days to retain moisture for a proper initial moist curing. The burlaps and plastic sheets were removed, and the slabs were exposed to air drying in the lab environment. Shrinkage of the investigated concrete mixtures is not affected by humidity and temperature variations caused by seasonal changes. Therefore, the shrinkage results of the investigated concrete mixtures can be isolated from warping and curling deformations caused by seasonal variations. The slab construction procedures, including concrete arrival using mixing truck, placement, consolidating, finishing, and curing, are presented in Figure 5-8.

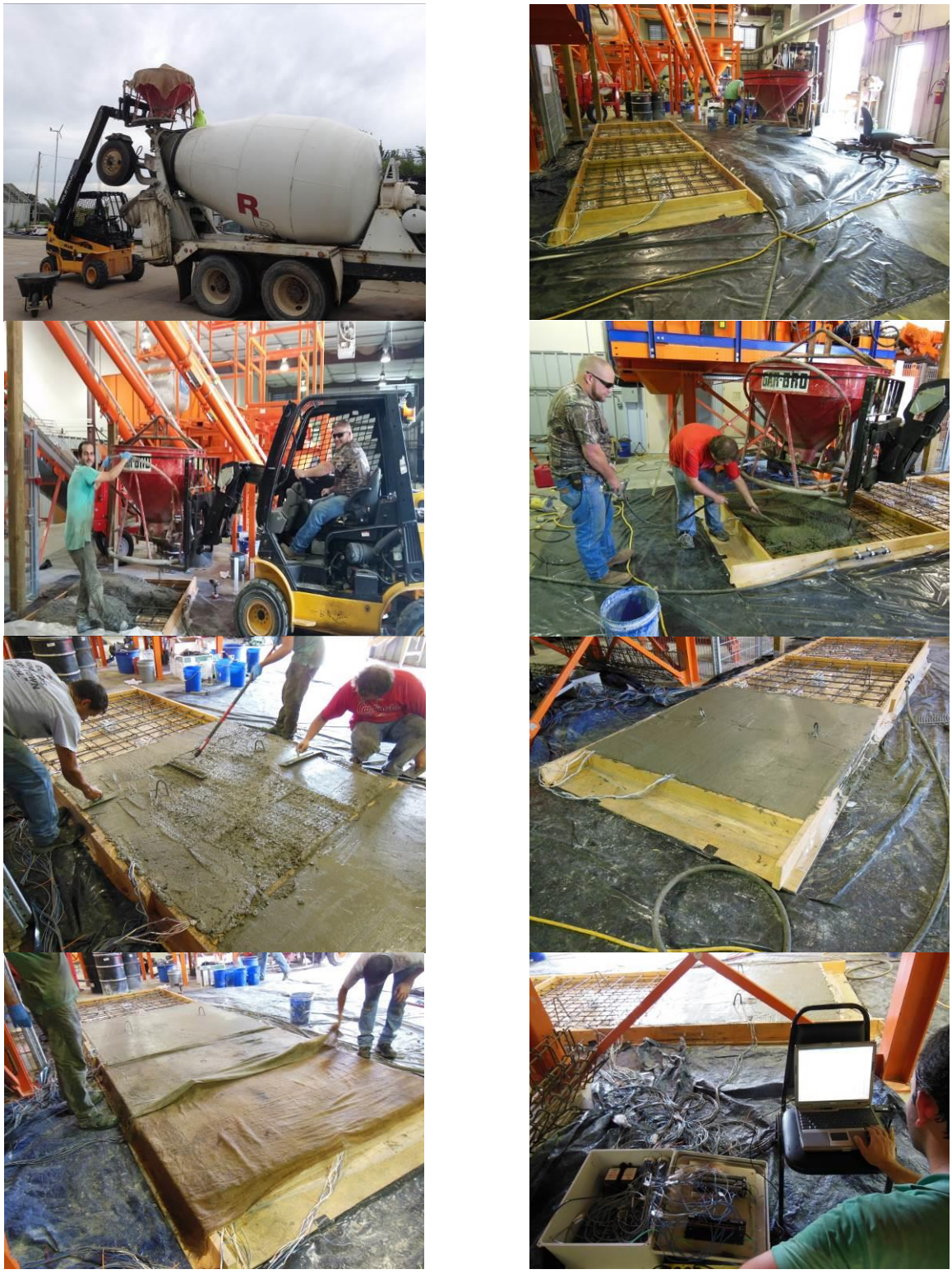

Figure 5-8- Concrete slab construction procedures

Shrinkage deformation and relative humidity measurement

Figure 5-9 present the results of shrinkage deformation along the height at different stations of the investigated slabs. In this figure, negative and positive signs correspond to shrinkage and expansion, respectively. As mentioned earlier, all slabs were subjected to wet curing using wet burlap and plastic sheet for seven days before exposure to air drying condition. The results of shrinkage deformation were shown to be a function of concrete mix design, location, and depth of slab. Expectedly, slab made with 25% FA replacement exhibited higher magnitude and rate of shrinkage deformation compared to the optimized Eco-Bridge-Crete. This difference became more dominant for the top surface of concrete slab. For instance, cluster A (i.e., station A in Figure 5-7) of the control slab had an expansion of 100 μstrain after 7 days of wet curing followed by 100 μstrain shrinkage after 30 of drying (see sensor 1-M-SL-3 in Figure 5-9). However, no shrinkage deformation was observed for other slabs prepared with optimized Eco-Bridge-Crete, as shown in Figure 5-9.

Regardless of the concrete composition, the top part of slab underwent larger shrinkage deformation compared to the mid-height and bottom part of slab thickness. This is attributed to faster evaporation rate of top surface of concrete, as indicated in Figure 5-10. Given the expansion induced stresses, the SL20FA35-7.5EX-0.35FRW mixture containing 7.5% CaO-based EX exhibited significant expansion. The magnitude of expansion was shown to vary along the height of slab. Strain gauges located at the top part of concrete slab experienced larger extent of expansion compared to the middle and bottom parts of slab. For example, top surface of concrete exhibited 600-800 μstrain expansion compared to 350-400 μstrain expansion recorded for sensors located at the middle and bottom parts of slab. This is on account of higher exposure of top surface to the moist curing provided by wet burlap during the first seven days. As explained earlier, the effectiveness of EX to generate expansion is significantly affected by the

initial moist curing. The penetration of water into concrete slab at early-age can provide more water to facilitate the hydration of CaO-based EX, thus indicating larger magnitude of expansion. The incorporation of 25% LWS was shown to be fully effective at reducing shrinkage rate and magnitude. No shrinkage was obtained for slab made with 20% SL and 35% FA containing 25% LWS. This confirms that the combined use of SCM replacement and LWS can be fully beneficial at reducing shrinkage rate and magnitude. As presented in Figure 5-10, slab containing 25% LWS exhibited higher relative humidity after 30 days of drying. This enhanced relative humidity of paste matrix is attributed to the internal curing provided by LWS which can maintain larger relative humidity within the paste matrix for a longer duration.

It can be noticed from Figure 5-9 that shrinkage deformations recorded for side and corner (stations B and C in Figure 5-7) points of slab were larger than that of the sensors located at the center (station A) of slab. This is due to faster rate of evaporation of concrete surface, as confirmed in Figure 5-10. This was consistent with results of humidity sensors placed at the side and corner parts of slab, where exhibited larger drop in relative humidity compared to that of the middle sensor, irrespective of concrete composition. Interestingly, this effect was less dominant for slab made with 25% LWS. The lowest relative humidity values observed for the FA25, SL20FA35-25LWS, and SL20FA35-7.5EX-0.35FRW mixtures were 82%, 96%, and 90%, respectively, which were recorded by RH sensors located at the top-corner part of slab. The shrinkage deformation values corresponding to such RH sensors were 80 μstrain (shrinkage), 40 μstrain (expansion), and 400 μstrain (expansion) for the FA25, SL20FA35-25LWS, and SL20FA35-7.5EX-0.35FRW mixtures, respectively, after 30 days of drying. Such shrinkage values corresponded to the largest deformation registered by sensors (the most critical point) after 30 day of drying. Trends of shrinkage deformation recorded by the transverse strain sensors

are similar to those of the longitudinal sensors. This phase is currently underway to achieve the stabilized shrinkage deformation.

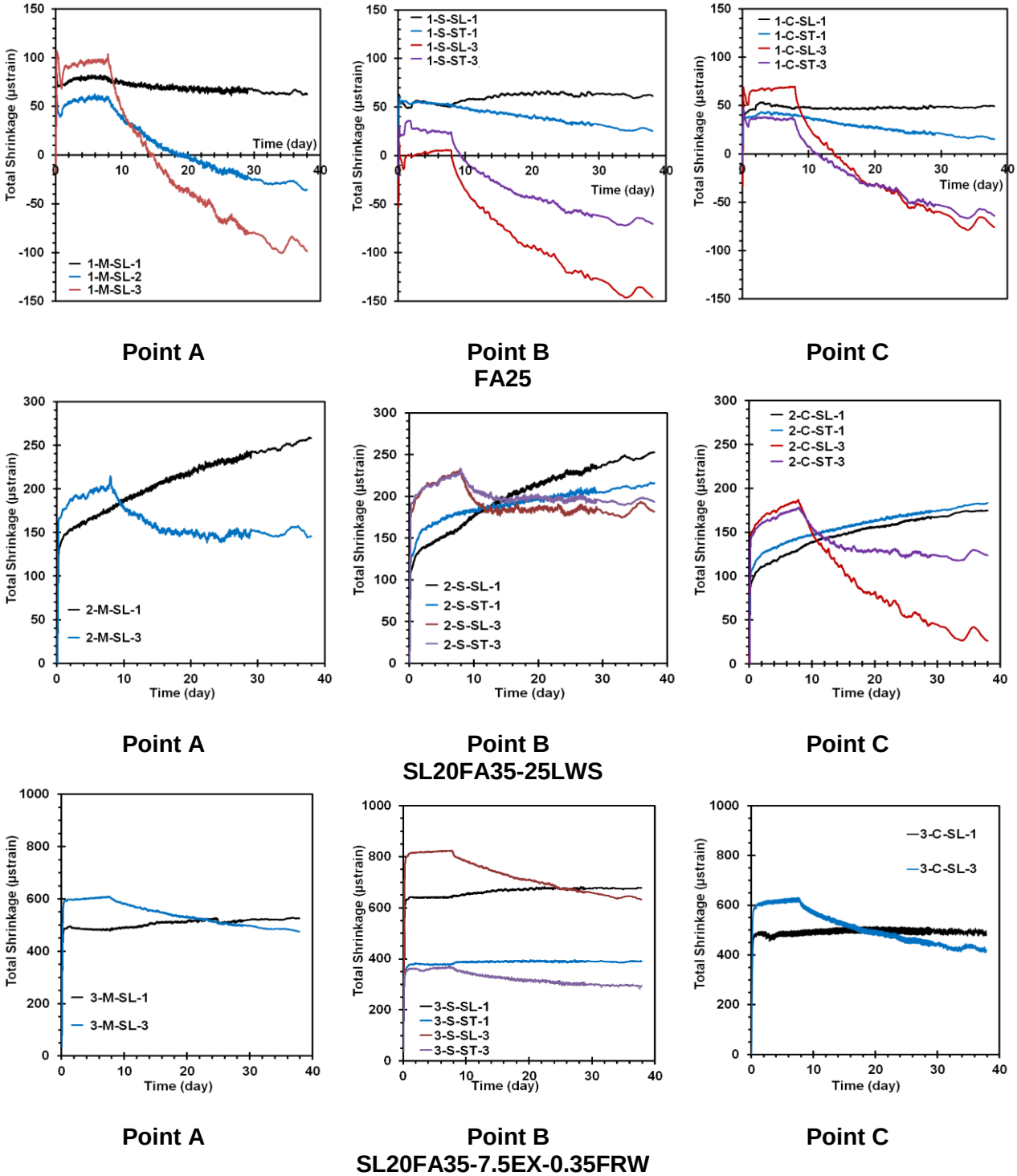

Figure 5-9- Shrinkage deformation along height of slabs at different stations (All slabs were moist cured for seven days before exposure to air drying.)

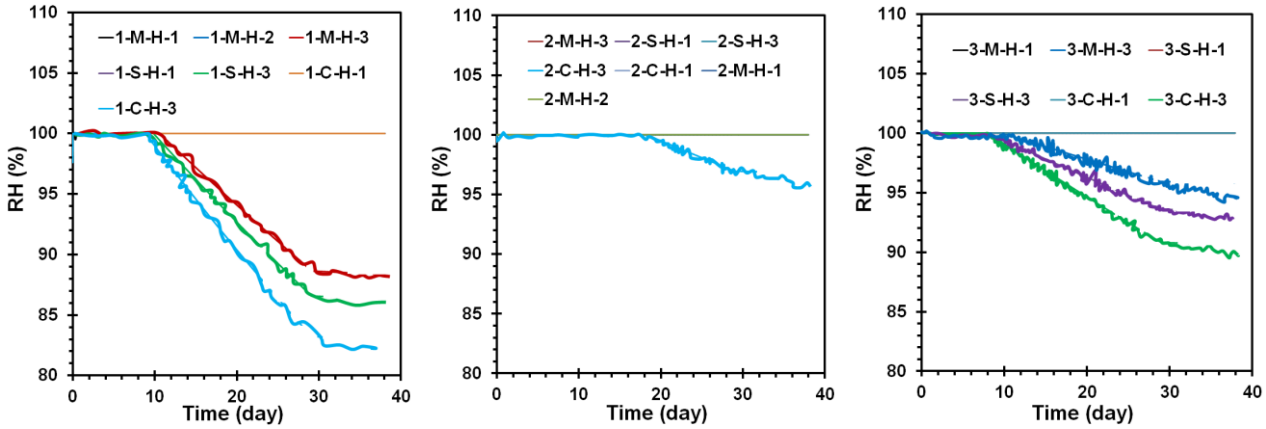

FA25 **SL20FA35-25LWS** **SL20FA35-7.5EX-0.35FRW**

Figure 5-10- Relative humidity variations along height of slabs at different stations

(All slabs were moist cured for seven days before exposure to air drying)

Temperature measurement

Figure 5-11 shows the temperature variations at different locations along the height of the investigated slabs. It is interesting to note that the slab FA25 made with higher binder content and lower OPC replacement (i.e., only 25% FA substitution) developed higher temperature rise (due to the hydration evolution of binder after concrete placement) compared to other slabs made relatively high volume SCMs. The maximum temperature recorded for slabs made with FA25, SL20FA35-25LWS, and SL20FA35-7.5EX-0.35FRW mixtures were 46°C, 38°C, and 42°C, respectively. The lowest temperature rise registered by embedded thermocouples was obtained for slab prepared with 25% LWS. This mixture also exhibited lower rate of heat transfer compared to the faster heat reduction observed for other mixtures.

As shown in Figure 5-11, the embedded thermocouples located at three depths within the deck depth captured similar temperature variation throughout the section. This is due to placement of slabs in lab environment which had consistent daily temperature. Regardless of the concrete mix

design, all slabs had similar temperature of 25°C after 30 days of drying which was consistent with ambient temperature registered for lab condition.

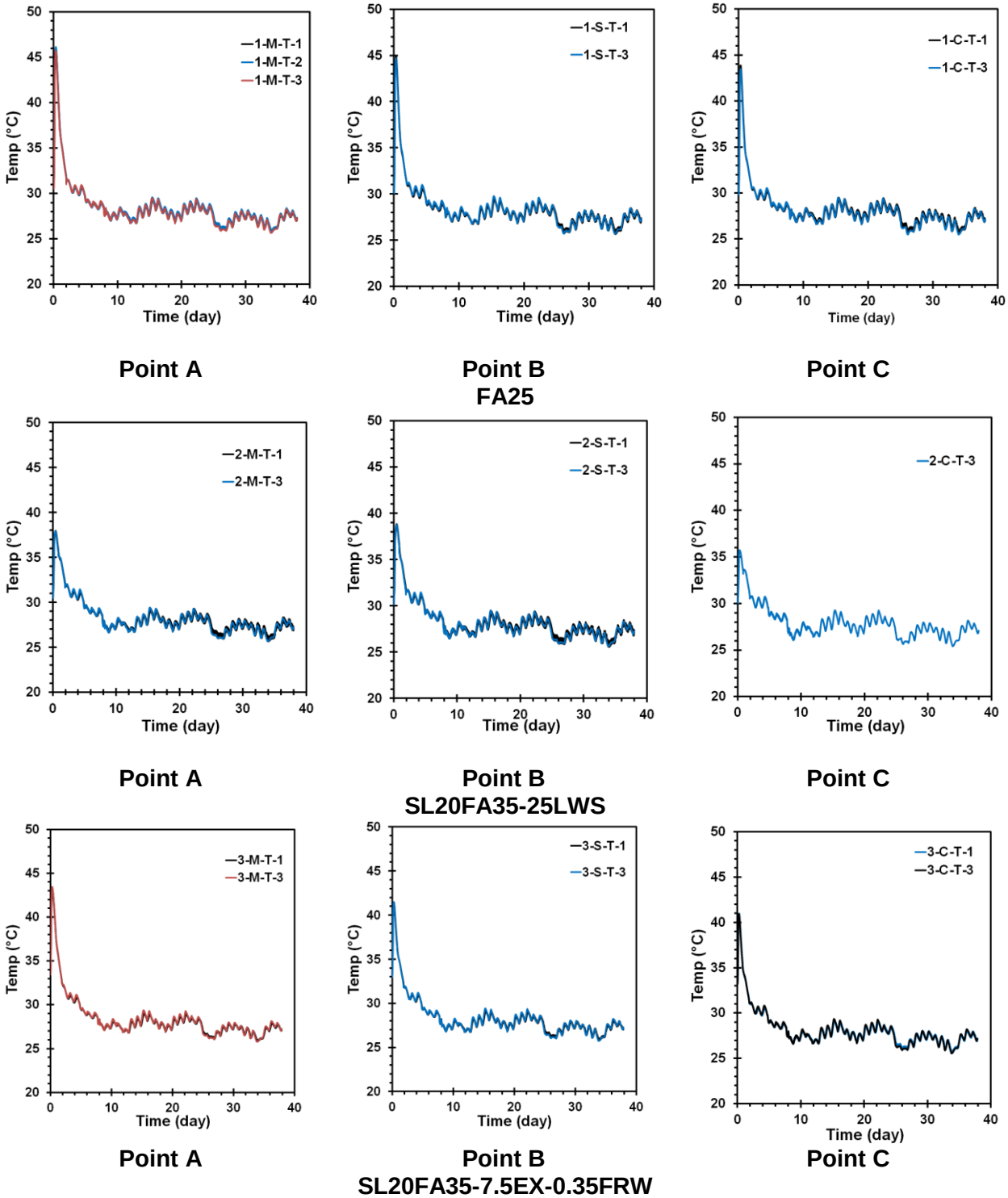

Figure 5-11- Temperature variations along height of slabs at different stations (All slabs were moist cured for seven days before exposure to air drying)

5.2. Structural performance of reinforced concrete beams

The aim of this subtask was to evaluate the flexural strength of reinforced concrete beams made with selected Eco-Bridge-Crete mixtures that were optimized in Task II. The results were compared with those obtained from beams made with the MoDOT reference mixture. The detail of the selected concrete mixtures used for reinforced concrete beams is given in Table 5-4.

Table 5-4- Selected concrete mixtures for reinforced concrete beams

Concrete type	w/cm	Binder content		Binder type			Fiber type and content		Shrinkage reducing/compensating materials	
	0.4	350 kg/m^3 (590 lb/yd^3)	375 kg/m^3 (630 lb/yd^3)	75% OPC + 25% Class C FA	45% OPC + 20% SL + 35% Class C FA	35% OPC + 60% SL + 5% SF	TUF strand fibers (0.35%)	Steel fibers from tire (0.35%)	25% LWS	7.5% Type G EX
MoDOT reference mixture	x		x	x						
Eco-Bridge-Crete	x	x			x				x	
	x	x			x					
	x	x			x		x			x
	x	x			x			x		x
	x	x				x			x	
	x	x				x		x		x

The beam dimensions, reinforcement layout, and position of strain gauges are depicted in Figure 5-12. All beams had identical reinforcement layout, as shown in Figure 5-12. The beams were reinforced with three longitudinal #4 bars for tension, two longitudinal #3 bars for compression,

and steel stirrups of #3. The side and vertical clear covers were kept constant at 25 mm (1 in.) for all the beams. Each beam measured 2.40 m (8 ft.) in length with a cross section of 200 × 300 mm (8 ×12 in.). All of the beams had #3 stirrups spaced at 4 in. within the bearing area to prevent premature failure, as well as #3 stirrups spaced at 5 in. within the middle region to prevent shear failure.

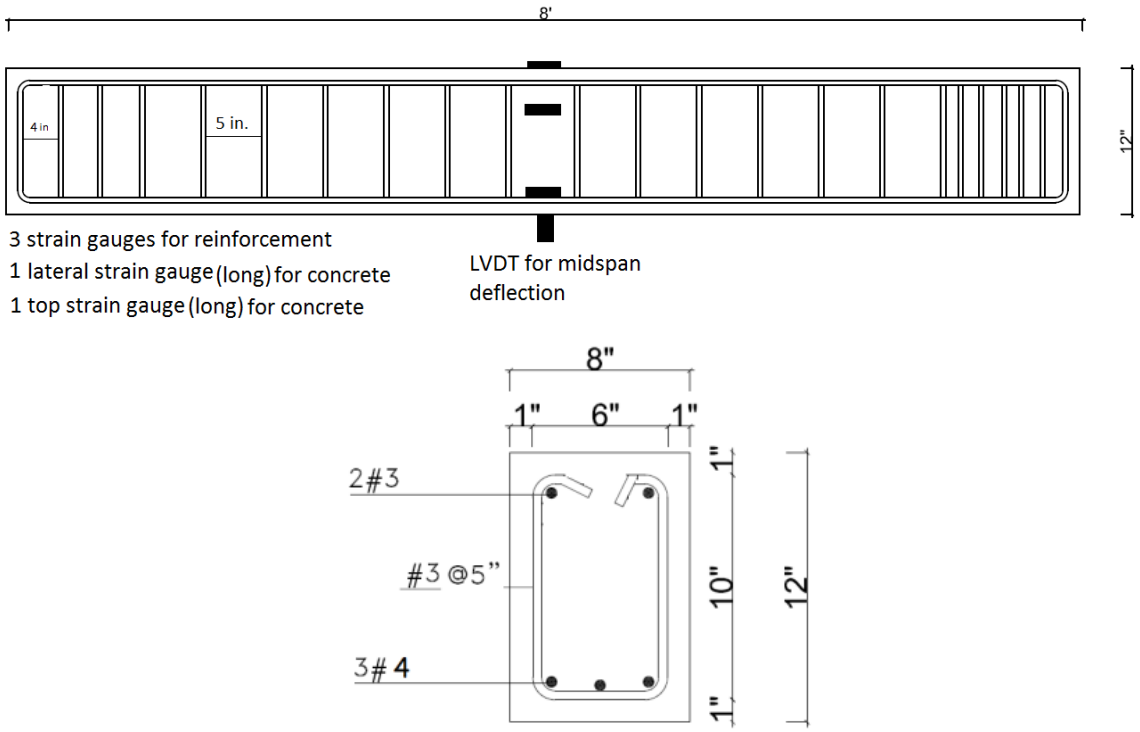

Figure 5-12- Reinforcement layout and locations of strain gauges for test beams

Figure 5-13 shows the fabrication and instrumentation of reinforcing cages. After assembling of reinforcement cages, the beam specimens were instrumented with different types of measurement devices in order to monitor global and local deformations and strains. The load is directly measured from the load cell of the actuators. All devices are connected to a data acquisition system capable of reading up to 120 channels. Two types of electrical resistance gauges were used to monitor local strains in the longitudinal reinforcing bars and concrete of the

test beams. The strain gauges consisted of constantan foil with 120 ohm resistance and had a linear pattern (uniaxial) with various gauge lengths of 6 and 70 mm (0.25 and 3 in.). All beams were instrumented using three small strain gauges bonded on longitudinal reinforcing bars located at the bottom (see Figure 5-13) as well as two long strain gauges placed on top and lateral side of concrete surface at the mid-span. In addition to strain gauges, a linear variable displacement transducer (LVDT) was used to monitor vertical deflection of the test beam under flexural testing.

Figure 5-13- Fabrication and instrumentation of reinforcing cages

A loading system with hydraulic jacks and a load cell of 500 kN (maximum capacity) closed-loop MTS actuator was used to test beams under four-point bending, as demonstrated in Figure 5-14 . A displacement controlled mode at a rate of 1.2 mm/min (0.05 in./min) was selected for applying the load. The actuator was supported by a steel frame and the load was transferred from the actuator to the tested beam through a steel spreader I-beam applied on the full width of the beam. A roller support was obtained by placement a steel cylinder between two steel flat plates.

A pin support was obtained by using specially adapted steel I-beam. The upper plate of the I-beam had a spherical groove and the plate was supported on the web plate which had a spherical end to house the plate and allow rotation. At each end of the tested beam, the roller and pin support were rested on steel I-beam, which was secured on the rigid floor of the lab. The combination of the two point loads and the two supports resulted in the desired four-point loading system. During loading, the crack pattern on the sides of the beams was marked and recorded. The applied load, deflection, and strain readings were electronically recorded during the test using data acquisition system monitored by a computer.

Figure 5-14- Beam flexural test setup

The beam was supported at two points 150 mm (6 in.) from the both ends and was loaded in the middle using two point loads separated by 300 mm (12 in.), as shown in Figure 5-15. The applied load was measured by the internal load cell on the actuator and the beams were instrumented with LVDT and strain gauges for steel reinforcement and concrete, as shown in Figure 5-16. The loading was stopped when the first crack appeared. The first crack appearance

was manually monitored and the width of the major crack was measured using a hand-held microscope. The visual observation of crack development was followed up throughout the loading operation. The crack network distribution on the lateral surface of the beams was marked.

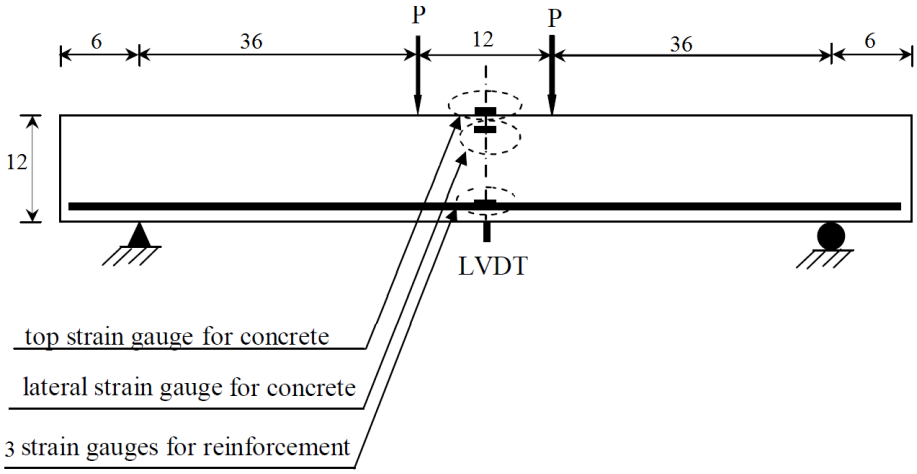

Figure 5-15- Loading and strain-control systems (dimensions expressed in in.)

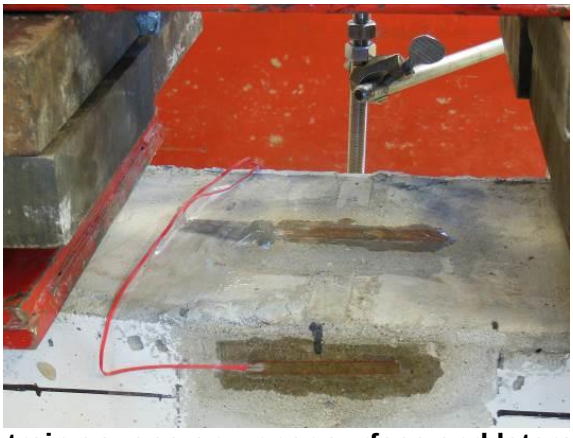

strain gauges on upper surface and lateral side of beam mid-span

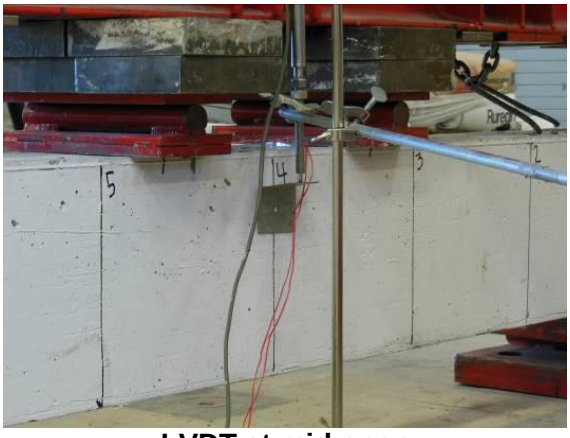

LVDT at mid-span

Figure 5-16- Installation of LVDT and strain gauges on surface of concrete beam

All concrete mixtures were made in local concrete batching plant to confirm the ability of proposed concrete mixtures to apply under actual field conditions. The beam construction

procedure is shown in Figure 5-17. Due to the incorporating high-volume SCMs in proportioning of Eco-HPC mixtures, the beams were cured between 35-56 days (Table 5-5) using wet burlap and plastic sheet before testing.

Figure 5-17- Concrete beam construction procedures

Concrete cylinders measuring 100 × 200 mm (4 × 8 in.) were prepared to evaluate the compressive strength of concrete mixtures used for beams. All samples were subjected to similar environmental condition to those of the concrete beams to simulate match curing condition. The

compressive strength results of concrete mixtures are present in Table 5-5. Regardless of binder composition and fiber inclusion, all mixtures achieved target range of 40 to 50 MPa (5800-7300 psi) at the age of testing.

Table 5-5- Compressive strength results of concrete mixtures used for beams

Mixture no.	Codification	Testing age (day)	Compressive strength (MPa)
B1	SL20FA35	56	47
B2	SL20FA35-7.5EX-0.35FT	50	53
B3	SL60SF5-25LWS	45	55
B4	SL60SF5-7.5EX-0.35FRW	45	50
B5	FA25 (MoDOT reference mixture)	40	50
B6	SL20FA35-25LWS	40	47
B7	SL20FA35-7.5EX-0.35FRW	40	45

(Note: 1 MPa = 145.04 psi)

Load-deflection response

The load-deflection responses of the investigated reinforced concrete beams are shown in Figure 5-18. The load-deflection relationship is tri-linear for all beams. The initial part up to flexural cracking was similar for all beams, which represents the behavior of the uncracked beam that depends on the gross moment of inertia of the concrete cross-section. The second part, corresponding to post-cracking up to steel yielding, represents the cracked beam with reduced moment of inertia. The third part, corresponding to steel yielding up to failure, shows degradation in the stiffness of the beams due to yielding of the reinforcing steel. Regardless of the binder composition, all concrete beams made with relatively high volume SCMs exhibited approximately comparable ultimate load to that of the FA25 (MoDOT reference mixture), as shown in Figure 5-18. It is noticed that the incorporation of either 0.35% structural synthetic

fibers or 0.35% recycled steel fibers led to higher ductility compared to the concrete beams made without any fibers. In other words, the use of fibers substantially improved the post-cracking behavior and enhanced energy absorption. This is attributed to the fact that the addition of fibers acts as an additional reinforcement for concrete to the rebar, where the fibers delayed yielding of steel bars compared to case of concrete made without any fibers. The maximum load carrying capacity was attained for beams containing fibers, especially for the case of 0.35% recycled steel fibers combined with 7.5% CaO-based expansive agent (EX). This can be attributed to the wavy form of recycled steel fibers which can provide better bond to the paste matrix as well as higher tensile strength compared to the synthetic fibers. This made steel fibers effective in contributing to the tensile strength of the concrete beam. This tensile strength is added to that contributed by the reinforcing bars to obtain the ultimate capacity of the beam.

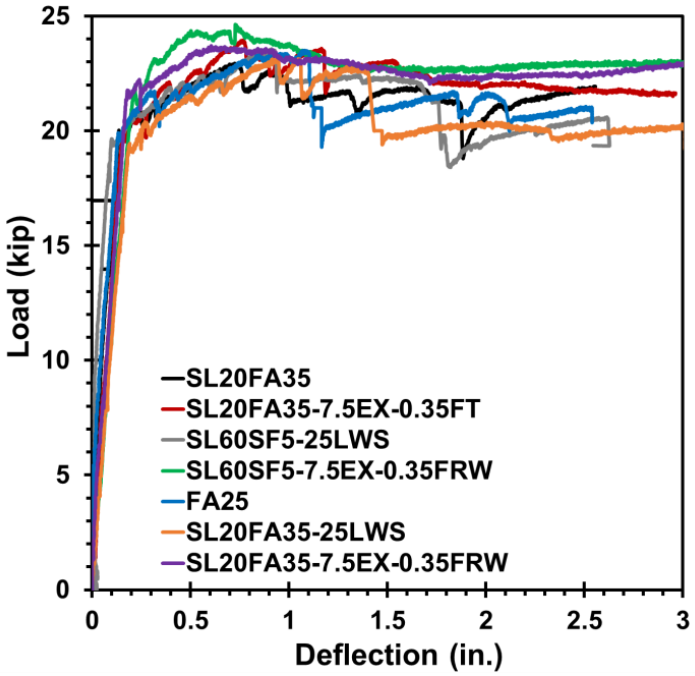

Figure 5-18- Load-deflection responses of tested beams

The results of ultimate load of the tested beams are presented in Figure 5-19. It is interesting to note that all beams made with optimized concrete mixtures containing more than 50% SCM replacements exhibited comparable ultimate load as that of the control beam made with MoDOT reference mixture (F25). All beams made with fibers exhibited slightly higher ultimate flexural strength compared to the similar beams without any fibers. However, given the relatively low volume fraction, the contribution of fibers to enhance ultimate flexural strength is not quite significant.

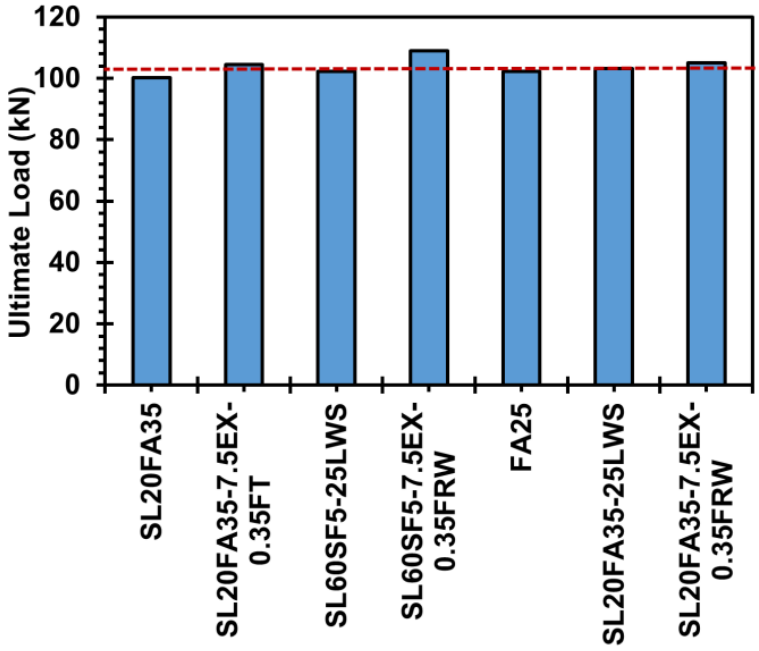

Figure 5-19- Ultimate load of tested beams

(Note: 1 kN = 0.245 kip)

Cracking behavior and strains

Figure 5-20 shows the crack patterns at failure of tested beams. Similar characteristics of the crack and failure patterns were observed for all beams. Crack formation was initiated in the flexural span between the two concentrated loads where the flexural stress is highest and shear stress is zero. The cracks were generally perpendicular to the direction of the maximum principal

tensile stress induced by pure bending. As load increased, additional flexural cracks opened within the shear span. However, because of the dominance of the shear stresses, the cracks became progressively more inclined and propagated towards the load point. As the load reached the yielding capacity of the beams, the crack opening rate increased, and the beams failed due to crushing of the concrete in the constant moment zone. In all beams, the longitudinal tensile steel bars initially yielded followed by the concrete crushing, which is a ductile failure mode, called tension failure. It is important to note that for fibrous beams, tightly spaced cracks formed perpendicular to flexural tensile stresses on the lower face of the beam. These results indicated that the use of recycled steel fibers can redistribute stresses and undergo multiple cracking before fiber pullout failure. However, non-fibrous beams underwent wider cracks and more crushing in their compression zones. The deflection-crack width propagation (major crack) of the tested beams is depicted in Figure 5-21. The crack width development of tested beam was found to vary with fiber addition and lightweight sand. For a given beam deflection, the use of recycled steel fibers significantly reduced the crack width in relation to that of the non-fibrous beams. Furthermore, the inclusion of lightweight sand was shown to improve the post-cracking response and decrease the crack width (given higher distribution of cracks). Such beams indicated smaller crack width and more distributed crack pattern in comparison with the control beam containing 25% FA replacement.

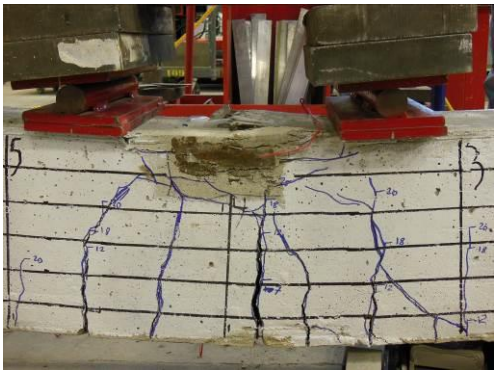

SL20FA35

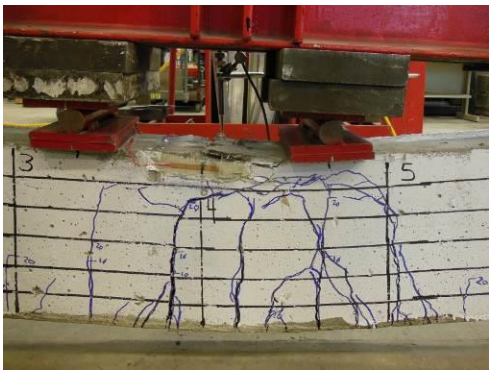

SL20FA35-7.5EX-0.35FT

SL60SF5-25LWS

SL60SF5-7.5EX-0.35FRW

SL20FA35-25LWS

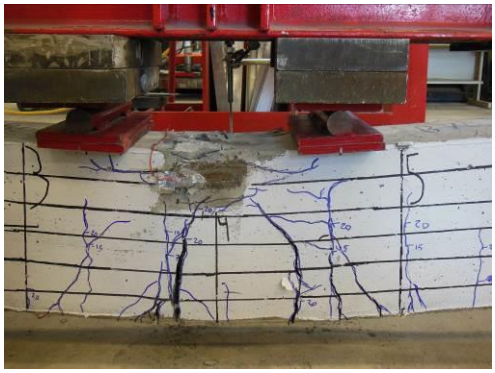

SL20FA35-7.5EX-0.35FRW

FA25

Figure 5-20- Crack patterns of tested beams at failure

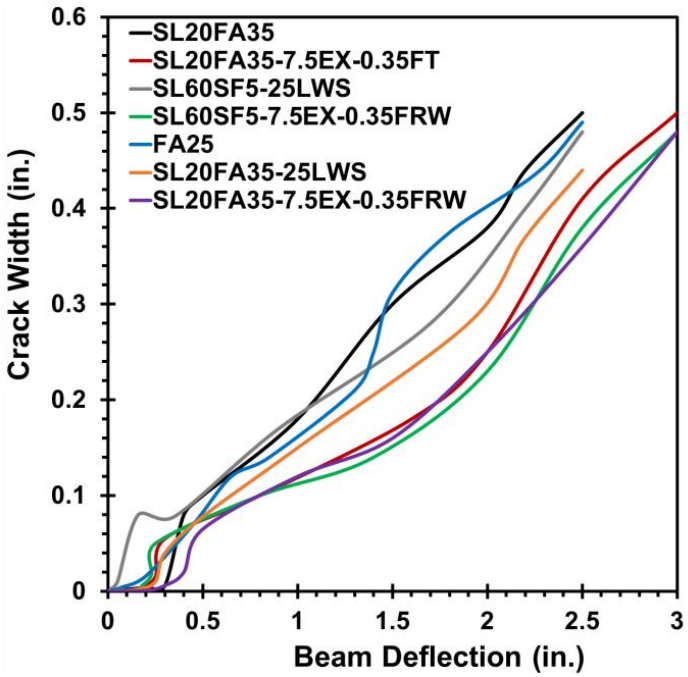

Figure 5-21- Deflection-crack width relationship of tested beams

The load-strain traces of steel reinforcement and concrete of the tested beams are shown in Figure 5-22. As expected, the top surface of concrete developed more strain values compared to the lateral side of concrete surface, regardless of concrete composition. The strains were proportional to the mid-span deflections and consistent with crack widths indicated in Figure 5-20 and Figure 5-21. It can be noticed from Figure 5-22 that the use of fibers, especially recycled steel fibers, can delay yielding point of rebars and enhance the capacity of concrete before subjected to crushing in the compression zones. This is attributed to the inclusion of fibers which restrict the opining of cracks under loading.

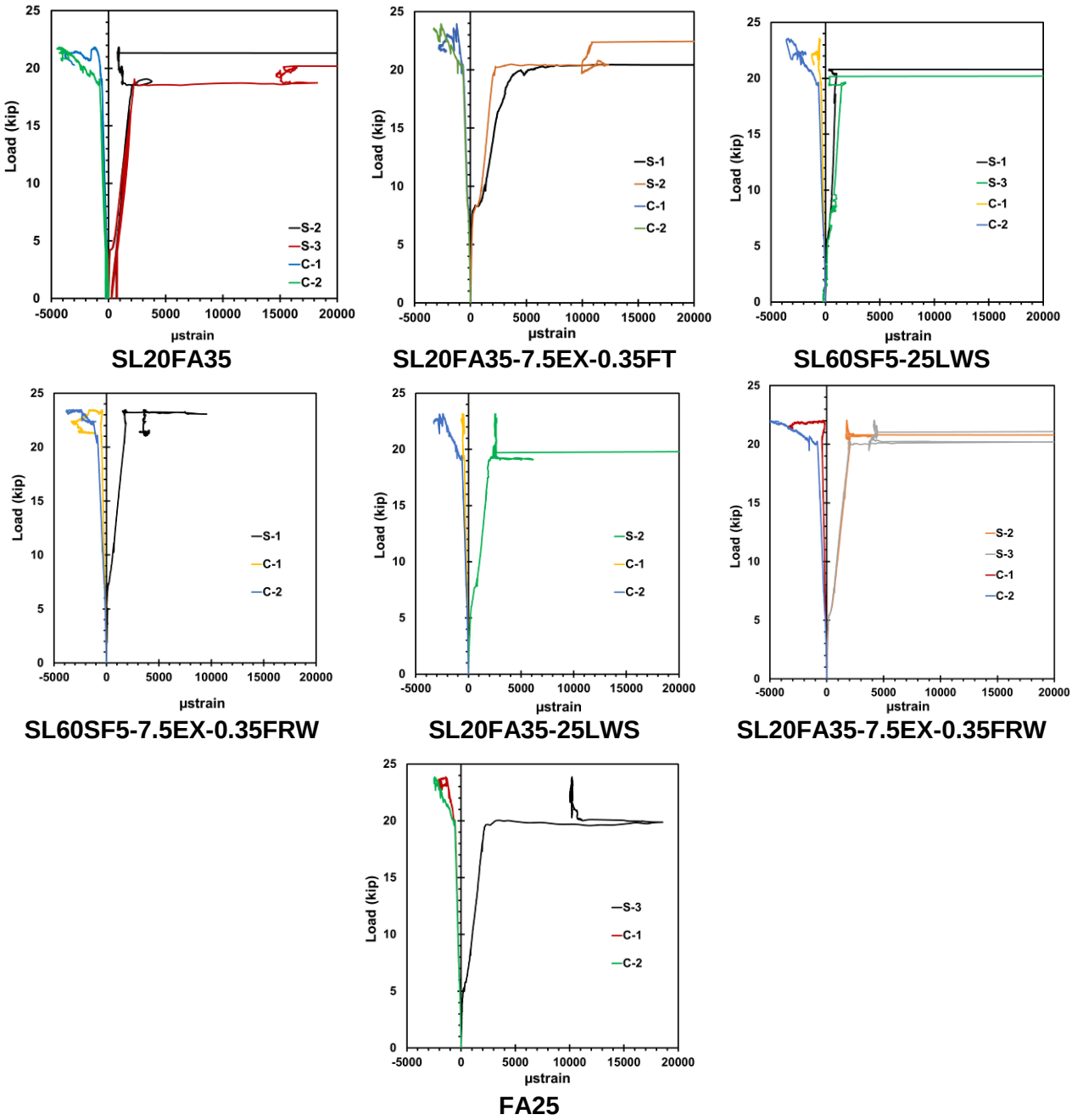

Figure 5-22- Load-strains of steel reinforcement and concrete response of tested beams

Toughness

Figure 5-23 compares the toughness results up to the failure of the tested beams. The toughness was obtained by calculation of the surface area under the curve of load-deflection of the beam. The inclusion of either structural synthetic fibers or recycled steel fibers was shown to

substantially enhance the toughness of beam. For example, beams made with SL20FA35-7.5EX-0.35FT, SL60SF5-7.5EX-0.35FRW, and SL20FA35-7.5EX-0.35FRW concrete mixtures developed 120%, 135%, and 130% higher flexural toughness, respectively, compared to the control beam prepared with MoDOT reference mixture. The highest load carrying capacity of 64500 lb.in was obtained for concrete beam made with 60% slag and 5% SF replacements and having 0.35% recycled steel fibers. In the absence of fibers, all concrete beams made with 350 kg/m^3 (590 lb/yd^3) more than 50% OPC replacement exhibited comparable flexural toughness to that of the control beam prepared with 375 kg/m^3 (630 lb/yd^3) containing 25% FA replacement. Therefore, in spite of incorporating high volume SCM replacements (more than 50% OPC replacement), the use of fibers was shown to be have good bond with matrix, thus attaining load carrying capacity. This tensile strength is added to that contributed by the reinforcing bars to obtain the ultimate capacity of the beam.

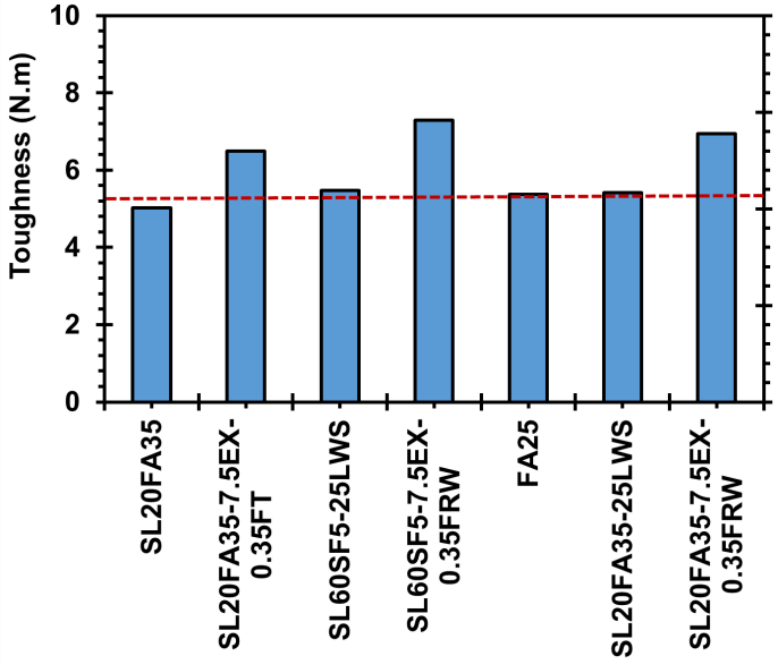

Figure 5-23- Toughness of tested beams

(Note: 1 N.m = 8.85 lb.in)

6. SUMMARY AND CONCLUSIONS

This research project was undertaken to develop a new class of environmentally friendly, cost-effective, and crack-free high-performance concrete (HPC) for use in pavement (Eco-Pave-Crete) and bridge infrastructure (Eco-Bridge-Crete) applications. The binder content of these novel materials were limited to 320 kg/m^3 (540 lb/yd^3) and 350 kg/m^3 (590 lb/yd^3), respectively, in order to reduce paste content, cost, CO_2 emissions, and shrinkage cracking. The rheological properties of the Eco-HPCs were adjusted to facilitate placement technique and structural element characteristics. Both Eco-HPC types were optimized to develop high resistance to restrained shrinkage cracking as well as to secure high durability. A number of parameters affecting material characteristics of these novel materials were investigated, including binder type and content, aggregate type and proportions, fiber type, and shrinkage mitigating materials. Based on the test results from research presented in this investigation, the following conclusions can be drawn:

Optimization of binder composition

This phase was conducted using concrete equivalent mortar (CEM) formulated from environmentally friendly Eco-HPC mix design proportioned with various binder contents of 320 kg/m^3 (540 lb/yd^3) and 350 kg/m^3 (590 lb/yd^3) which was targeted for Eco-Pave-Crete and Eco-Bridge-Crete, respectively.

- Proper substitution of cement by SCMs can ensure greater packing density of solid particles, reduce water/admixture demand, and improve rheological and hardened properties of cement-based materials.

- The packing characteristics of the combined cement and SCMs are an important factor that can reduce water demand, thus leading to decreased cement content, which is essential in the design of Eco-Crete. The greatest packing density of 0.796 was observed for the ternary binder composition containing 60% SL and 5% SF compared to 0.73 for mixture made with 100% OPC.
- The highest retention of rheological properties of concrete equivalent mortars made with w/cm of 0.40 (lowest variations in results between 10 and 70 min of age) was observed for the binary mixture containing 40% FA. This corresponds to the fact that the proper substitution of cement by SCMs can lead to longer retention of rheological properties and lower fluidity loss with respect to the mixture with 100% cement.
- Regardless of the binder content, all CEMs made with binary and ternary blends of SCMs (targeted for Eco-Pave-Crete and Eco-bridge-Crete) resulted in lower drying shrinkage compared to that of the control mixture made with 100% OPC. As expected, the increase in the binder content resulted in higher drying shrinkage, regardless of the binder compositions. The control OPC mixtures with binder contents of 320 kg/m^3 (540 lb/yd^3) and 350 kg/m^3 (590 lb/yd^3) and w/c of 0.40 exhibited the highest drying shrinkage of 840 and 940 μstrain, respectively, after 150 days of drying among the investigated binder compositions.

Optimization of aggregate characteristics

In total, 17 different aggregate samples with different shapes, textures, and PSDs from various aggregate quarries were evaluated to study the effect of aggregate characteristics on packing density of aggregate skeleton.

- The packing densities of aggregates are shown to vary with size, shape, surface texture, and angularity of aggregate. The packing densities of the investigated fine, intermediate, and coarse aggregates varied between 0.58-0.73, 0.6-0.73, and 0.57-0.61, respectively.
- The proportion of blended aggregate has substantial influence on the packing density of concrete. Based on the obtained results, the packing density of various aggregate proportions varied from 0.65 to 0.815 and 0.65 to 0.80 for rounded and crushed aggregates, respectively. The difference between the packing density of poorly-graded aggregate and well-graded aggregate was about 0.15, which significantly affects the required paste volume to fill the voids between solid particles. This can have considerable effect of material cost, CO_2 emission, and shrinkage.
- There exists an optimum sand-to-aggregate ratio (S/A) corresponding to the maximum achievable dry density, which is affected by the type and proportion of blended aggregate.
- A proposed statistical mixture design method was shown to be an effective in optimizing the proportioning of the blended aggregate to achieve the maximum possible packing density as well as to predict the packing density of the blended aggregates.
- The selected aggregate blend for the investigated concrete mixtures had a packing density of 0.81. The PSD of such aggregate was close to modified Andreasen and Andersen model with a q value of 0.275.

Comparison of shrinkage mitigating strategies

The effect of different shrinkage mitigating materials on autogenous and drying shrinkage, and compressive strength development of CEM mixtures was evaluated. Depending on the binder composition, the effectiveness of incorporating shrinkage mitigating materials can be different.

Therefore, in this phase the effect of shrinkage mitigating materials on shrinkage properties of mortars proportioned with optimized binder compositions from phase 1 of this investigation was examined. The investigated materials included expansive agents (CaO-based and MgO-based), crack reducing admixture (CRA), and lightweight sand (LWS). In total, 20 mortars made with different binder compositions and shrinkage mitigating materials were evaluated.

- The use of shrinkage mitigating materials containing LWS and CaO-based EX were shown to be effective in securing low shrinkage concrete.
- The magnitude, rate, and duration of expansion provided by the EX was significantly influenced by the initial moist curing duration. Prolonged wet curing extends the duration of expansion caused by a given dosage of EX.
- Greater expansion was obtained when using CaO-based Ex compared to MgO-based EX. Mixtures incorporating 7.5% CaO-based EX exhibited substantially higher magnitude and rate of expansion for a longer duration compared to the 5% MgO-based EX for the OPC mortar made with w/c of 0.40.
- The expansion provided by EX was significantly higher for mixtures containing high volume SCMs, such as 55% fly ash (FA). The highest expansion of 1780 μstrain was observed for mortar mixture made with 55% FA replacement and 7.5% CaO-based EX.
- The synergistic effect between EX with LWS resulted in lower autogenous shrinkage or higher expansion magnitudes for a longer duration. The highest expansion of 1980 μstrain was found for the E-L-SL60SF5 mortar mixture with a binary system of shrinkage mitigating materials, including 7.5% CaO-based EX and 25% LWS replacements. This is attributed to the coupled effect of lower self-desiccation and larger expansion resulting from the use of LWS along with EX systems.

- The strength gain resulting from initial moist curing period (IMCP) was found to be more critical for mixtures containing high volume SCMs, which caused the highest spread in compressive strength. The use of 25% LWS replacement was shown to compensate for the drop in compressive strength resulting from the absence of IMCP.

Development of crack-free Eco-HPC

Based on the obtained results from previous phases, the effect of different binder compositions, aggregate characteristics, and shrinkage mitigating materials were evaluated and the results were analyzed to design Eco- and crack-free HPC for different targeted applications (Eco-Pave-Crete and Eco-Bridge-Crete).

- The synergetic effect of the combination of shrinkage reducing materials, including LWS and EX coupled with fibers (synthetic fibers or recycled steel fibers) is quite effective to design low cracking potential concrete. The internal curing provided by the LWS can reduce the shrinkage and risk of early-age shrinkage cracking, especially for mixtures subjected to air drying without using any initial moist-curing.
- Given higher packing density and lower water demand of the optimized SCMs, the Eco-Crete mixtures prepared with binary and ternary of binders necessitated 10% to 40% lower HRWR demand to achieve the required fluidity compared to the control mixture made with 100% cement.
- Eco-HPC mixtures made with SCMs exhibited lower autogenous and drying shrinkage compared to the reference mixture made with 100% cement. Mixture containing 50% slag had autogenous and drying shrinkage values of 45 and 215 μstrain, respectively, compared to 210 and 360 μstrain for similar mixture made without any SCMs.

- The incorporation of fibers (synthetic fibers and recycled steel fibers) in concrete containing a high volume of SCMs was shown to have 0 to 35% higher splitting tensile and flexural strengths than the control mixture made with 100% cement. The highest splitting tensile and flexural strengths were obtained for the mixture made with 35% recycled steel fibers containing 20% SL and 35% FA. This mixture also exhibited similar compressive strength to that of the control mixture.
- For a given fiber content, the use of steel fibers recovered from waste tires had two times higher flexural toughness compared to the similar mixture made with synthetic fibers. The reference mixture (100% OPC) made without any fibers developed the lowest ductility behavior and residual strength among all mixtures.
- The optimized Eco-HPC mixtures had lower drying shrinkage of 300 μstrain after 250 days of drying compared to 550 μstrain for the control mixture with 100% OPC. The incorporation of 7.5% Type G EX resulted in a significant early-age expansion of 100 μstrain followed by shrinkage of 200 μstrain after 250 days of drying.
- The reference mixture made with 100% cement exhibited elapsed time to cracking of 22 days, that was tested under restrained shrinkage condition. In case of mixtures made with shrinkage reducing materials no cracking was observed until 55 days of testing. Regardless of the binder type, concrete mixtures made with 7.5% CaO-based EX exhibited an expansion of 20 μstrain compared to the 60 μstrain of shrinkage for the reference mixture under restrained shrinkage.
- Eco-HPC mixtures made with proper combination of SCMs coupled with shrinkage mitigating materials can lead to crack-free properties (limited crack width of 0.1 mm (0.004")) with high resistance to shrinkage cracking. Based on the obtained results from

this study, the use of 25% LWS or 7.5% CaO-based EX is quite effective in developing Eco-HPC with low risk of cracking.

Deformation and structural evaluation

The aim of this task was to evaluate the shrinkage deformation of slab sections and flexural strength of reinforced concrete beams made with optimized Eco-Bridge-Crete. Three slabs measuring 1.8 × 1.8 m (6 × 6 ft) and 150 mm (6 in.) in depth were constructed to evaluate shrinkage deformation of different concrete mixtures. The investigated mixture parameters include the incorporation of fibers, lightweight sand, expansive agent, and high volume SCMs and the results were compared with that of the MoDOT reference mixture targeted for bridge decks. In addition, eight reinforced concrete beams were constructed to evaluate the flexural strength of reinforced concrete beams made with selected Eco-Bridge-Crete mixtures that were optimized in Task II. The results were compared with that of the control beam made with MoDOT reference mixture.

- The control slab made with 25% FA replacement exhibited higher magnitude and rate of shrinkage deformation compared to the optimized Eco-Bridge-Crete mixtures. This difference became more dominant for the top surface of concrete slab. Cluster A located at the center of the control slab recorded an expansion of 100 μstrain after 7 days of wet curing followed by 100 μstrain shrinkage after 30 of drying. However, no shrinkage deformation was observed for other slabs prepared with optimized Eco-Bridge-Crete.
- Given the expansion induced stresses, the SL20FA35-7.5EX-0.35FRW mixture containing 7.5% CaO-based EX exhibited significant expansion. The magnitude of expansion was shown to vary along the height of slab. Strain gauges located at the top part of concrete slab experienced larger extent of expansion compared to the middle and

bottom parts of slab. Top surface of concrete exhibited 600-800 μstrain expansion compared to 350-400 μstrain expansion recorded for sensors located at the middle and bottom parts of slab.

- The incorporation of 25% LWS was shown to be fully effective at reducing shrinkage rate and magnitude. No shrinkage was obtained for slab made with 20% SL and 35% FA containing 25% LWS. This slab exhibited higher relative humidity after 30 days of drying compared to the other slabs made without any LWS. The lowest relative humidity values observed for the FA25, SL20FA35-25LWS, and SL20FA35-7.5EX-0.35FRW mixtures were 82%, 96%, and 90%, respectively. This confirms that the combined use of SCM replacement and LWS can be fully beneficial at reducing shrinkage rate and magnitude.
- Shrinkage deformations recorded for side and corner (stations B and C in Figure 5-7) points of slab were larger than that of the sensors located at the center (station A) of slab. This was consistent with results of humidity sensors placed at the side and corner parts of slab, where exhibited larger drop in relative humidity compared to that of the middle sensor.
- The shrinkage deformation values corresponding to such RH sensors were 80 μstrain (shrinkage), 40 μstrain (expansion), and 400 μstrain (expansion) for the FA25, SL20FA35-25LWS, and SL20FA35-7.5EX-0.35FRW mixtures, respectively, after 30 days of drying. Such shrinkage values corresponded to the largest deformation registered by sensors (the most critical point) after 30 day of drying.
- The slab FA25 made with higher binder content and lower OPC replacement (i.e., only 25% FA substitution) developed higher temperature rise (due to the hydration evolution

of binder after concrete placement) compared to other slabs made relatively high volume SCMs. The maximum temperature recorded for slabs made with FA25, SL20FA35-25LWS, and SL20FA35-7.5EX-0.35FRW mixtures were 46°C, 38°C, and 42°C, respectively. The lowest temperature rise registered by embedded thermocouples was obtained for slab prepared with 25% LWS. This mixture also exhibited lower rate of heat transfer compared to the faster heat reduction observed for other mixtures.

- All beams made with optimized concrete mixtures containing more than 50% SCM replacements exhibited equivalent or even higher ultimate flexural load than of the control beam made with MoDOT reference mixture (FA25).
- The use of recycled steel fibers can redistribute stresses and undergo multiple cracking before fiber pullout failure. However, non-fibrous beams underwent wider cracks and more crushing in their compression zones.
- The inclusion of either structural synthetic fibers or recycled steel fibers was shown to substantially enhance the toughness of beam. The SL20FA35-7.5EX-0.35FT, SL60SF5-7.5EX-0.35FRW, and SL20FA35-7.5EX-0.35FRW concrete beams developed 120%, 135%, and 130% higher flexural toughness, respectively, compared to the control beam prepared with MoDOT reference mixture. The highest load carrying capacity of 64500 lb.in was obtained for concrete beam made with 60% slag and 5% SF replacements having 0.35% recycled steel fibers.

Future work

Test results presented and discussed in this investigation confirm the effectiveness of utilizing packing density approach for developing Eco-Crete materials. Further research is required to study the effectiveness of theoretical packing models and determining the proper packing parameters for HPC mixtures with low binder content to improve particle packing and reduce the lubricant volume. Investigation of large-scale elements, including slab and beam members is recommended to examine the shrinkage deformation, cracking resistance, and structural performance of Eco-Crete. In addition, field study to implement and validate the performance of such concrete for use in pavement and bridges is required. Monitoring cracking resistance, mechanical properties, durability, and in-situ deformation are important to validate the behavior of Eco-Crete compared to conventional reference concrete.

As a follow-up project, the research team will investigate and validate the performance of Eco-HPC mixtures under actual field conditions. The main goal is to validate findings of the previous research project in the field implementation and to develop guidelines for the use of Eco-HPC for sustainable pavement and transportation infrastructure construction. The proposed project will employ two classes of Eco-HPCs: Eco-Pave-Crete for pavement construction and Eco-Bridge-Crete for transportation infrastructure construction. Eco-Bridge-Crete can be used in girders, piers and piles, sidewalk, and/or other bridge elements. The performance improvement of such advanced materials will be compared with performance of MoDOT reference mixtures designated for bridge deck and pavement construction.

REFERENCES

AASHTO TP 95, Standard Method of Test for Surface Resistivity Indication of Concrete's Ability to Resist Chloride Ion Penetration, 2011.

ACI Committee 234, "234R-96: Guide for the Use of Silica Fume in Concrete," Manual of Concrete Practice, American Concrete Institute, Farmington Hills, MI, 1996.

Ahari, R. S., Erdem, T. K., & Ramyar, K. (2015). Effect of various supplementary cementitious materials on rheological properties of self-consolidating concrete. Construction and Building Materials, 75, 89-98.

Aïssoun, B. M., Hwang, S. D., & Khayat, K. H. Influence of aggregate characteristics on workability of superworkable concrete. Materials and Structures, 1-13.

Ali EE, Al-Tersawy SH. Recycled glass as a partial replacement for fine aggregate in self compacting concrete. Constr Build Mater 2012;35:785–91.

Amini, K., Mehdipour, I., Hwang, S. D., & Shekarchi, M. (2016). Effect of binder composition on time-dependent stability and robustness characteristics of self-consolidating mortar subjected to prolonged agitation.Construction and Building Materials, 112, 654-665.

Andreasen, A.H.M., Anderson, J., The Relation of Grading to Interstitial Voids in Loosely Granular Products (With Some Experiments). Kolloid-Z., 49, 1929, 217-228.

Assaad, J., & Khayat, K. H. (2004). Assessment of Thixotropy of Self-Consolidating Concrete and Concrete-Equivalent-Mortar? Effect of Binder Composition and Content. ACI Materials Journal, 101(5).

ASTM C109, Standard Test Method for Compressive Strength of Hydraulic Cement Mortars (using 2-in. or [50-mm] Cube Specimens), 1999.

ASTM C1581, Standard Test Method for Determining Age at Cracking and Induced Tensile Stress Characteristics of Mortar and Concrete under Restrained Shrinkage, 2009.

ASTM C1698, Standard Test Method for Autogenous Strain of Cement Paste and Mortar, 2010.

ASTM C1760, Standard Test Method for Bulk Electrical Conductivity of Hardened Concrete, 2012.

ASTM C232, Standard Test Methods for Bleeding of Concrete, 2012.

ASTM C39, Standard Test Method for Compressive Strength of Cylindrical Concrete Specimens, 2005.

ASTM C403, Standard Test Method for Time of Setting of Concrete Mixtures by Penetration Resistance, 2008.

ASTM C496, Standard Test Method for Splitting Tensile Strength of Cylindrical Concrete Specimens, 2011.

ASTM C596, Standard Test Method for Drying Shrinkage of Mortar Containing Hydraulic Cement, 2001.

ASTM C642, Standard Test Method for Density, Absorption, and Voids in Hardened Concrete, 2006.

ASTM C666/C666M, Standard Test Method for Resistance of Concrete to Rapid Freezing and Thawing, 2008.

ASTM C939, Standard Test Method for Flow of Grout for Preplaced-Aggregate Concrete (Flow Cone Method).

ASTM C157/C157M, Standard Test Method for Length Change of Hardened Hydraulic-Cement Mortar and Concrete, 2008.

ASTM C1585. Standard Test Method for Measurement of Rate of Absorption of Water by Hydraulic-Cement Concretes. West Conshohocken, PA: American Society for Testing and Materials; 2004.

ASTM C1609/C1609M, Standard Test Method for Flexural Performance of Fiber-Reinforced Concrete (Using Beam With Third-Point Loading), 2012.

ASTM C1610/C1610M, Standard Test Method for Static Segregation of Self-Consolidating Concrete Using Column Technique, 2010.

ASTM C672 / C672M, (2012), Standard Test Method for Scaling Resistance of Concrete Surfaces Exposed to Deicing Chemicals.

ASTM C944/C944 M-99 (2005). “Standard Practice for Abrasion Resistance of Concrete

Barrett, T. J., Sun, H., Weiss, W. J. (2013). Performance of portland limestone cements: Cements designed to be more sustainable that include up to 15% limestone addition.

Bentz, D. P., Lura, P., & Roberts, J. W. (2005). Mixture proportioning for internal curing. Concrete International, 27(2), 35-40.

Bentz, D. P., Sant, G., & Weiss, J. (2008). Early-age properties of cement-based materials. I: Influence of cement fineness. Journal of Materials in Civil Engineering, 20(7), 502-508.

Bentz, D.P., Jensen, O., Mitigation Strategies for Autogenous Shrinkage Cracking. Cement and Concrete Composites, 26(6), 2004, 677-685.

Bentz, D.P., Snyder, K.A., Protected Paste Volume in Concrete: Extension to Internal Curing Using Saturated Lightweight Fine Aggregate. Cement and Concrete Research, 29(11), 1999, 1863-1867.

Beretka, J., Marroccoli, M., Sherman, N., Valenti, G.L., Influence of C4A3S Content and W/S Ratio on the Performance of Calcium Sulfoaluminate-Based Cements." Cement and Concrete Research 26 (11), 1996, 1673-1681.

Bonavetti, V.; Donza, H.; Menéndez, G.; Cabrera, O.; and Irassar, E. F., "Limestone Filler Cement in Low w/c Concrete: A Rational Use of Energy," Cement and Concrete Research, Vol. 33, 2003, pages 865 to 871.

Brooks, J.J., Megat Johari, M.A., Mazloom, M., Effect Of Admixtures on the Setting Times of High-Strength Concrete. Cement and Concrete Composites, 22, 2000, 293-301.

Brouwers, H.J.H., Radix, H.J., Self Compacting Concrete: Theoretical and Experimental Study, Cem. Concr. Res. 35, 2005, 2116–2136.

Brouwers, H.J.H., Particle-Size Distribution and Packing Fraction of Geometric Random Packings. Phys. Rev. E 74, 2006.

Brown, M., Sellers, G., Folliard, K., Fowler, D., Restrained Shrinkage Cracking of Concrete Bridge Decks: State-of-the-art Review. Texas Department of Transportation, 2001.

Bucher, B.; Radlinska, A.; and Weiss, J., Preliminary Comments on Shrinkage and Shrinkage Cracking Behavior of Cement Systems that Contain Limestone, SN3051, Portland Cement Association, Skokie, Illinois, USA, 2008, 9 pages. Reprinted from Concrete Technology Forum, National Ready Mixed Concrete Association, Silver Spring, Maryland, USA, 2008.

Caufin, B., & Papo, A. (1986). The influence of the hydration process on the rheology of cement pastes. ZKG international, 39(7), 389-391.

Chaunsali, P., & Mondal, P. (2014). Influence of Mineral Admixtures on Early-Age Behavior of Calcium Sulfoaluminate Cement. ACI Materials Journal, 111(1-6).

Chen CH, Wu JK, Yang CC. Waste E-glass particles used in cementitious mixtures. Cem Concr Res 2006;36(3):449–56.

Chen, I. A., Hargis, C. W., & Juenger, M. C. (2012). Understanding expansion in calcium sulfoaluminate–belite cements. Cement and Concrete Research, 42(1), 51-60.

Chini, A.R., Muszynski, L.C., Hicks, J., Determination Of Acceptance Permeability Characteristics For Performance-Related Specifications for Portland Cement Concrete, final report submitted to Florida Department of Transportation, 2003, 116-118.

Chouicha, K., The Fractal Dimension and the Granular Range as Parameters of Identification of Granular Mixes; Materials and Structures 39, 2006, 665-681.

Corinaldesi V, Gnappi G, Moriconi G, Montenero A. Reuse of ground waste glass as aggregate for mortars. Waste Manage 2005;25(2):197–201.

Cortas, R., Rozière, E., Staquet, S., Hamami, A., Loukili, A., Delplancke-Ogletree, M.P., Effect of the Water Saturation of Aggregates on the Shrinkage Induced Cracking Risk of Concrete at Early Age. Cement and Concrete Composites, 50, 2014, 1-9.

Courard, L., Darimont, A., Schouterden, M., Ferauche, F., Willem, X., Degeimbre, R., Durability of Mortars Modified with Metakaolin, CemConcr Res., 33, 2003.

Crowl, D., and M. Sutak. A Survey of High Performance Concrete Bridge Decks. Volume IV. Ohio Department of Transportation, District 12, 2002.

D.P. Bentz, C.F. Ferraris, M.A.Galler, A.S.Hansen, J.M. Guynn, Influence of particle size distributions on yield stress and viscosity of cement–fly ash pastes, Cem. Concr. Res. 42 (2012) 404–409.

Darwin,D., J. Browning, W. Lindquist, H. McLeod, J. Yuan, M. Toledo, and D. Reynolds. Low Cracking, High-Performance Concrete Bridge Decks. Transportation Research Record: Journal of the Transportation Research Board, Vol. 2202, 2010.

De la Varga, I., Castro, J., Bentz, D., & Weiss, J., Application of Internal Curing for Mixtures Containing High Volumes of Fly Ash. Cement and Concrete Composites, 34(9), 2012, 1001-1008.

De Larrard, F., Buil, M., Particle Size and Compactness in Civil Engineering Materials; Materials and Structures, 20, 1987, 117-126.

De Larrard, F., Structures Granulaires Et Formulation Des Bétons. 414, 1999.

Delatte, N., and D. Crowl. Case Studies of Internal Curing of Bridge Decks in the Greater Cleveland Area. Fall 2012 American Concrete Institute Convention in Toronto, ON, Canada, Vol. SP290-06, 2012.

Delatte, N., E. Mack, and J. Cleary. Evaluation of High Absorptive Materials to Improve Internal Curing of Low Permeability Concrete. 2007.

Deshpande, S., D. Darwin, and J. Browning. 2007. "Evaluating Free Shrinkage of Concrete for Control of Cracking in Bridge Decks." SM Report No. 89. University of Kansas. Lawrence. Kansas.

Du Hongjan, Tan Kiang Hwee. Concrete with recycled glass as fine aggregates. ACI Mater J 2014;111–M05 January–February:47–58.

Du, C. (2005). A review of magnesium oxide in concrete. Concrete international, 27(12), 45-50.

Du, H., & Tan, K. H. (2014). Transport properties of concrete with glass powder as supplementary cementitious material. ACI Materials Journal.

El-Chabib, H., & Syed, A. (2012). Properties of self-consolidating concrete made with high volumes of supplementary cementitious materials. Journal of materials in civil engineering, 25(11), 1579-1586.

Eren, O., Brooks, J.J., and Celik, T., Setting Times of Fly Ash and Slag-Cement Concretes as Affected by Curing Temperature. Cement, Concrete, and Aggregates, 17(1), 1995, 11-17.

Ezziane, K.; Kadri, E. H.; Hallal, A.; and Duval, R., "Effect of Mineral Additives on the Setting of Blended Cement by the Maturity Method," Materials and Structures, Vol. 43, 2010, pages 393 to 401.

Feys, D., Khayat, K. H., Perez-Schell, A., & Khatib, R. (2015). Prediction of pumping pressure by means of new tribometer for highly-workable concrete.Cement and Concrete Composites, 57, 102-115.

Folliard, K., C. Smith, G. Sellers, M. Brown, and J. E. Breen. 2003 (Oct.). "Evaluation of Alternative Materials to Control Drying-Shrinkage Cracking in Concrete Bridge Decks." Texas DOT Report No. FHWA/TX-04/04098-4.

Folliard, K.J., Berke, N.S., Properties of High-Performance Concrete Containing Shrinkage-Reducing Additives, Cement and Concrete Research, 24(3), 1997, 424–432.

Fuller, W.B., Thompson, S.E., The Laws of Proportioning Concrete, Trans. Am. Soc. Civ. Eng. 33, 1907, 222–298.

Fung, W.W.S., Kwan, A.K.H., Wong, H.H.C., Wet Packing of Crushed Rock Fine Aggregate. Materials and structures, 42(5), 2009, 631-643.

Funk, J.E., Dinger, D.R., Predictive Process Control of Crowded Particulate Suspensions, Applied to Ceramic Manufacturing, Kluwer Academic Publishers, Boston, the United States, 1994.

Germann Instruments Inc. ICAR Rheometer Manual. Evanston, Illinois, USA; 2007.

Ghezal, A., & Khayat, K. H. (2002). Optimizing self-consolidating concrete with limestone filler by using statistical factorial design methods. ACI Materials Journal, 99(3).

Golias, M., Castro, J., Weiss, J., The Influence of the Initial Moisture Content of Lightweight Aggregate on Internal Curing. Construction and Building Materials, 35, 52-62, 2012.

Goltermann, P., Johansen, V., Palbøl, L. (1997). Packing of aggregates: an alternative tool to determine the optimal aggregate mix. ACI Materials Journal, 94(5).

Grzybowski, M., Shah, S.P., Shrinkage Cracking of Fiber Reinforced Concrete. ACI Materials Journal, 87 (2), 1990, 138-148.

Güneyisi, E., Gesoğlu, M., & Özbay, E. (2010). Strength and drying shrinkage properties of self-compacting concretes incorporating multi-system blended mineral admixtures. Construction and Building Materials, 24(10), 1878-1887.

Habert, G., Roussel, N., Study of Two Concrete Mix-Design Strategies to Reach Carbon Mitigation Objectives. CemConcr Compos, 31, 2009, 397–402.

Hammer, T.A., Bjontegaard, O., Sellevold, E.G., Internal Curing—Role of Absorbed Water in Aggregates. High-Performance Structural Lightweight Concrete, SP-218, J. Ries and T. Holm, eds., American Concrete Institute, Farmington Hills, MI, 2004, 131-142.

Henkensiefken, R., Bentz, D., Nantung, T., Weiss, J., Volume Change and Cracking in Internally Cured Mixtures Made with Saturated Lightweight Aggregate under Sealed And Unsealed Conditions. Cement and Concrete Composites, 31(7), 2009, 427-437.

Holland, J.A. Mixture Optimization. Concrete International, 12(10), 1990.

Koehler, E.P. Aggregates in Self-Consolidating Concrete. ProQuest, 2007.

Yu, R., Spiesz, P., Brouwers, H.J.H., Mix Design and Properties Assessment of Ultra-High Performance Fibre Reinforced Concrete (UHPFRC). Cement and Concrete Research, 56, 2014, 29-39.

Hooton, R. D.; Nokken, M.; and Thomas, M.D.A.T, Portland-Limestone Cement: State-of-the-Art Report and Gap Analysis for CSA A 3000, SN3053, Cement Association of Canada, Toronto, Ontario, Canada, 2007, 60 pages.

Hooton, R.D., Canadian Use of Ground Granulated Blast-Furnace Slag as a Supplementary Cementing Material for Enhanced Performance of Concrete. Canadian Journal of Civil Engineering, 27(4), 2000, 754–760.

Hu, J., & Wang, K. (2011). Effect of coarse aggregate characteristics on concrete rheology. Construction and Building Materials, 25(3), 1196-1204.

Hunger, M., An Integral Design Concept for Ecological Self-Compacting Concrete. PhD thesis Eindhoven University of Technology, Eindhoven, the Netherlands, 2010.

Hunger, M., Brouwers, H.J.H., Development of Self-Compacting Eco-Concrete, in: H.B. Fischer, F.A. Finger (Eds.), Proceedings 16th Ibausil, International Conference on Building Materials (Internationale Baustofftagung),Weimar, F.A. Finger-Institut für Baustoffkunde, Weimar, Germany, 2006, 2-0189–2-0198.

Hüsken, G., Amultifunctional design approach for sustainable concrete with application to concrete mass products. PhD thesis Eindhoven University of Technology, Eindhoven, the Netherlands, 2010.

Hüsken, G., Brouwers, H.J.H., A New Mix Design Concept For Earth-Moist Concrete: A Theoretical And Experimental Study. Cement and Concrete Research, 38(10), 2008, 1246-1259.

Hwang, S. D., & Khayat, K. H. (2010). Effect of mix design on restrained shrinkage of self-consolidating concrete. Materials and structures, 43(3), 367-380.

Hwang, S. D., Khayat, K. H., & Youssef, D. (2013). Effect of moist curing and use of lightweight sand on characteristics of high-performance concrete. Materials and structures, 46(1-2), 35-46.

Hwang, S.D., Khayat, K.H., Durability Characteristics of Self-Consolidating Concrete Designated for Repair Applications. Materials and Structures, 42(1), 2009, 1-14.

Hwang, S.D., Khayat, K.H., Effect of Mix Design on Restrained Shrinkage of Self-Consolidating Concrete. Materials and structures, 43(3), 2010, 367-380.

Hwang, S.D., Khayat, K.H., Effect of Mixture Composition on Restrained Shrinkage Cracking of Self-Consolidating Concrete Used In Repair. ACI Materials journal, 105(5) 2008.

Hwang, S-D., Khayat, K.H., Effect of Various Admixture-Binder Combinations on Workability of Ready-Mix Self-Consolidating Concrete. ACI Special Publication 233 2006.

Jaturapitakkul, C., Kiattikomol, K., Sata, V., & Leekeeratikul, T. (2004). Use of ground coarse fly ash as a replacement of condensed silica fume in producing high-strength concrete. Cement and Concrete Research, 34(4), 549-555.

Jones, M. R., Zheng, L., & Newlands, M. D. (2002). Comparison of particle packing models for proportioning concrete constitutents for minimum voids ratio. Materials and structures, 35(5), 301-309.

Kassimi, F., Khayat, K.H., Effect of Fiber and Admixture Types on Restrained Shrinkage Cracking of Self Consolidating Concrete. Fifth North American Conference on the Design and Use of Self-Consolidating Concrete, Chicago, Illinois, USA, 2013.

Khayat KH, Libre NA. Roller compacted concrete: field evaluation and mixture optimization. No. NUTC R363, 2014.

Khayat KH, Mehdipour I. Design and performance of crack-free environmentally friendly concrete “Crack-Free Eco-Crete”. No. NUTC R322, 2014.

Khayat, K. H., Yahia, A., & Sayed, M. (2008). Effect of supplementary cementitious materials on rheological properties, bleeding, and strength of structural grout. ACI Materials Journal, 105(6), 585-593.

Khayat, K.H., Kassimi, F., Ghoddousi, P., Mixture Design and Testing of Fiber-Reinforced Self-Consolidating Concrete. ACI Materials Journal,111(2), 2014.

Khayat, K.H., Mehdipour, I., Optimization of Binder Compositions to Design Ecological Concrete; Wet Packing Density Approach. ECO-CRETE, International Symposium on Sustainability, Icelend, 2014.

Khayat, K.H., Yahia, A., Sayed, M., Effect of Supplementary Cementitious Materials on Rheological Properties, Bleeding, and Strength of Structural Grout. ACI Materials Journal, 105(6) 2008.

Khayat. K.H., Hu, C., Laye, J.M., Influence of Aggregate Grain-Size Distribution on Workability of Self-Consolidating Concrete. International Symposium on High Performance Concrete 1, 2000, 641-658.

Knop, Y., Peled, A., & Cohen, R. (2014). Influences of limestone particle size distributions and contents on blended cement properties. Construction and Building Materials, 71, 26-34.

Koehler, E.P. Aggregates in Self-Consolidating Concrete. ProQuest, 2007.

Kosmatka, S.H., Panarese, W.C. Design and control of concrete mixtures. 2002.

Kuder, K., Lehman, D., Berman, J., Hannesson, G., & Shogren, R. (2012). Mechanical properties of self consolidating concrete blended with high volumes of fly ash and slag. Construction and Building Materials, 34, 285-295.

Kwan, A. K. H., & Wong, H. H. C. (2008). Packing density of cementitious materials: part 2—packing and flow of OPC+ PFA+ CSF. Materials and structures, 41(4), 773-784.

Kwan, A.K.H., Chen, J.J., Adding Fly Ash Microsphere to Improve Packing Density, Flowability and Strength of Cement Paste. Powder Technology, 234, 2013, 19-25.

Kwan, A.K.H., Fung, W.W.S., Packing Density Measurement and Modelling of Fine Aggregate and Mortar. Cement and Concrete Composites, 31(6), 2009, 349-357.

Kwan, A.K.H., Li, L.G., Combined Effects of Water Film Thickness and Paste Film Thickness on Rheology of Mortar. Mater. Struct., 45(9), 2012, 1359–74.

Kwan, A.K.H., Li, L.G., Fung, W.W.S., Wet Packing of Blended Fine and Coarse Aggregate. Materials and structures, 45(6), 2012, 817-828.

Kwan, A.K.H., Mora, C.F., Effects of Various Shape Parameters on Packing of Aggregate Particles. Magazine of Concrete Research, 53 (2), 2001, 91-100.

Kwan, A.K.H., Wong, H.H.C., Packing Density of Cementitious Materials: Part 2—Packing and Flow Of OPC+ PFA+ CSF. Materials and structures, 41(4), 2008, 773-784.

Lange, F., Mo¨rtel, H., Rudert, V., Dense Packing of Cement Pastes and Resulting Consequences on Mortar Properties. Cem.Concr Res., 27(10), 1997, 1481–1488.

Lawler, J.S., Connolly, J.D., Krauss, P.D., Tracy, S.L., Ankenman, B.E., Guidelines for Concrete Mixtures Containing Supplementary Cementitious Materials to Enhance Durability of Bridge Decks. Transportation Research Board, 566, 2007.

Lee Gerry, Poon Chi Sun, Wong Yuk Lung, Ling Tung Chai. Effects of recycled fine glass aggregates on the properties of dry-mixed concrete blocks. Constr Build Mater 2013;38:638–43.

Lee, K.M., Lee, H.K., et al., Autogenous Shrinkage of Concrete Containing Granulated Blast-Furnace Slag. Cement and Concrete Research, Vol.3, 2006, 1279-1285.

Lee, S. H., Kim, H. J., Sakai, E., & Daimon, M. (2003). Effect of particle size distribution of fly ash–cement system on the fluidity of cement pastes. Cement and Concrete Research, 33(5), 763-768.

Li LG, Kwan AKH. Concrete mix design based on water film thickness and paste film thickness. Cem Concr Compos 2013;39:33–42.

Li, J., Yao, Y., A Study on Creep and Drying Shrinkage of High Performance Concrete. Cement and Concrete Research, 31(8), 2001, 1203-1206.

Li, Y., Bao, J., Guo, Y., The Relationship between Autogenous Shrinkage and Pore Structure of Cement Paste with Mineral Admixtures. Construction and Building Materials, 24, 2010, 1855-1860.

Li, Z., Qi, M., Li, Z., Ma, B., Crack Width of High-Performance Concrete Due to Restrained Shrinkage. Journal of Materials in Civil Engineering, 11(3), 1999, 214–223.

Lindquist, W., Darwin, D., Browning, J., McLeod, H. A., Yuan, J., & Reynolds, D. (2015). Implementation of concrete aggregate optimization. Construction and Building Materials, 74, 49-56.

Ling Tung-Chai, Poon Chi-Sun. Properties of architectural mortar prepared with recycled glass with different particle sizes. Mater Des 2011;32:2675–84.

Lura, P., Pease, B., Mazzotta, G., Rajabipour, F., Weiss, J., Influence of Shrinkage Reducing Admixtures on the Development of Plastic Shrinkage Cracks. ACI Materials Journal. 104(2), 2007, 187-194.

Malik MIqbal, Bashir Muzafa, Ahmed Sajad, Tariq Tabish, Chowdhary Umar. Study of concrete involving use of waste glass as partial replacement of fine aggregates. IOSR J Eng (IOSRJEN) July 2013;3(7):8–13.

Manai, K., Evaluation of the Effect of Chemical and Mineral Admixtures on the Workability, Stability, and Performance of Self-Compacting Concrete. master's thesis, Université de Sherbrooke, Québec, Canada, 1995.

Meddah, M.S., Sato, R., Effect of Curing Methods on Autogenous Shrinkage and Self-Induced Stress of High-Performance Concrete. ACI Materials Journal, 107(1), 2010.

Meddah, M.S., Suzuki, M., Sato, R., Influence of a Combination of Expansive and Shrinkage-Reducing Admixture on Autogenous Deformation and Self-Stress of Silica Fume High-Performance Concrete. Construction and Building Materials, 25(1), 2011, 239-250.

Mehdipour, I., & Khayat, K. H. (2016). Effect of Supplementary Cementitious Material Content and Binder Dispersion on Packing Density and Compressive Strength of Sustainable Cement Paste. ACI Materials Journal,113(3).

Mehta, P.K., Greeningof the Concrete Industry for Sustainable Development. Concrete international, 23, 2002.

Mehta, P.K., Monteiro, P.J.M., Concrete: Microstructure, Properties, and Materials. 3rd Ed. McGraw Hill, New York, 2006.

Mounanga, P.; Khokhar, M.; I., A.; El Hachem, R.; and Loukili, A., Improvement of the Early-Age Reactivity of Fly Ash and Blast Furnace Slag Cementitious systems using Limestone Filler, Materials and Structures, on-line edition, June 30, 2010. DOI: 10.1617/s11527-010-9637-1.

Mueller, F.V., Wallevik, O.H., Khayat, K.H., Linking Solid Particle Packing of Eco-SCC to Material Performance. Cement and Concrete Composites, 2014.

Nanthagopalan, P., Santhanam, M., An Empirical Approach for the Optimisation Of Aggregate Combinations for Self-Compacting Concrete. Mater. Struct., 45, 2012, 1167-1179.

Nassif, H., K. Aktas, and H. Najm. Concrete Shrinkage Analysis for Bridge Deck Concrete. No. FHWA NJ-2007-007. New Jersey Department of Transportation, Trenton, NJ, 2007.

Nmai, C. K., Vojko, D., Schaef, S., Attiogbe, E. K., & Bury, M. A. (2014). Crack-Reducing Admixture. Concrete international, 36(1), 53-57.

Okamura H., Ouchi, M., Self-Compacting Concrete. J. Adv. Concr. Technol., 1(1), 2003 5–15.

Park, C.K., Noh, M.H., Park, T.H., Rheological Properties of Cementitious Materials Containing Mineral Admixtures. Cem.Concr. Res., 35(5), 2005, 842–849.

Passuello, A., Moriconi, G., Shah, S.P., Cracking Behavior of Concrete with Shrinkage Reducing Admixtures and PVA Fibers. Cement and Concrete Composites, 31(10), 2009, 699-704.

Pera, J., Boumaza, R., Ambroise, J., Development of Pozzolanic Pigment from Red Mud. CemConcr Res., 27, 1997, 1513–22.

Quiroga, P.N., Fowler, D.W., The Effects of Aggregates Characteristics on The Performance of Portland Cement Concrete (No. ICAR 104-1F,). International Center for Aggregates Research, University of Texas at Austin, 2004.

Radlinska, A., Rajabipour, F., Bucher, B., Henkensiefken, R., Sant, G., Weiss, J., Shrinkage Mitigation Stategies in Cementitious Systems: A Closer Look at Differences in Sealed and Unsealed Behavior. Transportation Research Record. 2070. 2008, 59-67.

Rajabipour, F., Sant, G., Weiss, J., Interactions between Shrinkage Reducing Admixtures and Cement Paste's Pore Solution. Cement and Concrete Research, 38 (5), 2008, 606-615.

Rajabipour, F., Wright, J., Laman, J., Radlińska, A., Morian, D., Jahangirnejad, S., & Cartwright, C. (2012). Longitudinal Cracking in Concrete at Bridge Deck Dams on Structural Rehabilitation Projects (No. FHWA-PA-2012-006-100303).

Ramseyer, C.C., Kiamanesh, R., Optimizing Concrete Mix Designs to Produce Cost Effective Paving Mixes (No. FHWA-OK-08-11). Civil Engineering and Environmental Science, University of Oklahoma, 2009.

Rashad, A. M. (2014). Recycled waste glass as fine aggregate replacement in cementitious materials based on Portland cement. Construction and Building Materials, 72, 340-357.

Ray, I., Gong, Z., Davalos, J. F., & Kar, A. (2012). Shrinkage and cracking studies of high performance concrete for bridge decks. Construction and Building Materials, 28(1), 244-254.

Şahmaran, M., Lachemi, M., Hossain, K., Li, V.C., Internal Curing of Engineered Cementitious Composites for Prevention of Early Age Autogenous Shrinkage Cracking. Cement and Concrete Research, 39(10), 2009, 893-901.

Şahmaran, M., Yaman, İ. Ö., Tokyay, M., Transport and Mechanical Properties of Self Consolidating Concrete with High Volume Fly Ash. Cement and concrete composites, 31(2), 2009, 99-106.

Sata, V., Jaturapitakkul, C., Kiattakomol, K., Influence of Pozzolan from Various Byproduct Materials on Mechanical Properties of High-Strength Concrete. ConstrBuild Mater, 21, 2007,1589–98.

Schmitt, T. R. and Darwin, D. (1999). "Effect of Material Properties on Cracking in Bridge Decks," Journal of Bridge Engineering, ASCE, Vol. 4, No. 1, February, pp. 8-13.

Schneider, M., Romer, M., Tschudin, M., & Bolio, H. (2011). Sustainable cement production—present and future. Cement and Concrete Research, 41(7), 642-650.

Shah, S.P.; Karaguler, M.E., Sarigaphuti, M., Effects of Shrinkage Reducing Admixtures on Restrained Shrinkage Cracking of Concrete. ACI Materials Journal, 89(3), 1992, 291-295.

Shayan, A., Xu, A., Value-Added Utilisation of Waste Glass in Concrete. CemConcrRes., 34, 2004, 81–9.

Shi Y, Matsui I, Feng N. Effect of compound mineral powders on workability and rheological property of HPC. Cem Concr Res 2002;32(1):71–8.

Shilstone, J. M. Sr., Concrete Mixture Optimization, Concrete International: Design and Construction. 12(6), 1990.

Shing, P. B., and N. Abu-Hejleh. 1999 (Aug.).“Cracking in Bridge Decks: Causes and Mitigation” Report No. CDOT-DTD-R-99-8. Colorado Department of Transportation.

Sobolev, K., & Arikan, M. (2002). High volume mineral additive for eco-cement. American Ceramic Society Bulletin, 81(1), 39-43.

Sobolev, K., Turker, P., Soboleva, S., & Iscioglu, G. (2007). Utilization of waste glass in ECO-cement: Strength properties and microstructural observations. Waste Management, 27, 971-976

Soliman, A.M., Nehdi, M.L., Effects of Shrinkage Reducing Admixture and Wollastonite Microfiber on Early-Age Behavior of Ultra-High Performance Concrete. Cement and Concrete Composites, 46, 2014, 81-89.

Sounthararajan, V.M., Sivakumar, A., Drying Shrinkage Properties of Accelerated Fly Ash Cement Concrete Reinforced with Hooked Steel Fiber. ARPN Journal of Engineering and Applied Sciences, 8 (1), 2013.

Spiesz, P., Yu, Q.L., Brouwers, H.J.H., Development of Cement-Based Lightweight Composites—Part 2: Durability Related Properties, Cem. Concr. Comput. 44, 2013, 30–40.

Sprung, V. S., and E. Siebel, E., “Assessment of the Suitability of Limestone for Producing Portland Limestone Cement,” ZKG International, Vol. 1, 1991, pages 1 to 11. (In German. English text in No. 3, 1991, pages 43 to 48.)

Subramaniam, K., and A. K. Agrawal. 2009 (Jan.). “Concrete Deck Material Properties.” Final Report. SPR Project C-02-03. New York State Department of Transportation.

Taha Bashar, Nounu Ghassan. Utilizing waste recycled glass as sand/cement replacement in concrete. J Mater Civil Eng, ASCE 2009;December:709–21.

Tangtermsirikul, S., Class C Fly Ash as a Shrinkage Reducer for Cement Paste. ASTM Special Publication, American Society for Testing and Materials, 153, 1995.

Tangtermsirikul, S., Class C Fly Ash as a Shrinkage Reducer for Cement Paste. ASTM Special Publication, American Society for Testing and Materials, 153, 1995.

Temiz, H., Kantarcı, F., & İnceer, M. E. (2015). Influence of blast-furnace slag on behaviour of dolomite used as a raw material of MgO-type expansive agent. Construction and Building Materials, 94, 528-535.

Tennis, P. D., Thomas, M. D. A., & Weiss, W. J. (2011). State-of-the-Art Report on Use of Limestone in Cements at Levels of up to 15%. Portland Cem Assoc, 10-20.

Tritsch, N., Darwin, D., Browning, J., Evaluating Shrinkage and Cracking Behavior of Concrete Using Restrained Ring and Free Shrinkage Tests. The Transportation Pooled Fund Program Project No. TPF-5(051), Structural Engineering and Engineering Materials SM Report No.77, The University of Kansas Center for Research, Inc. at Kansas, 2005.

Tsivilis, S.; Batis, G.; Chaniotakis, E.; Grigoriadis, Gr.; and Theodossis, D., "Properties and Behavior of Limestone Cement Concrete and Mortar," Cement and Concrete Research, Vol. 30, 2000, pages 1679 to 1683.

Tsivilis, S.; Chaniotakis, E.; Badogiannis, E.; Pahoulas, G.; and Ilias, A., "A Study on the Parameters Affecting the Properties of Portland Limestone Cements," Cement and Concrete Composites, Vol. 21, 1999a, pages 107 to 116.

U.S. Environmental Protection Agency, Office of Resource Conservation and Recovery, Municipal Solid Waste Generation, Recycling, and Disposal in the United States Tables and Figures for 2010, 2011, pp. 58.

Uysal, M., Akyuncu, V., Durability Performance of Concrete Incorporating Class F and Class C Fly Ashes. Construction and Building Materials, 34, 2012, 170-178.

Uysal, M., Yilmaz, K., & Ipek, M. (2012). The effect of mineral admixtures on mechanical properties, chloride ion permeability and impermeability of self-compacting concrete. Construction and Building Materials, 27(1), 263-270.

Vance, K., Kumar, A., Sant, G., & Neithalath, N. (2013). The rheological properties of ternary binders containing Portland cement, limestone, and metakaolin or fly ash. Cement and Concrete Research, 52, 196-207.

Voglis, N.; Kakali, G.; Chaniotakis, E.; and Tsivilis, S., "Portland-Limestone Cements. Their Properties and Hydration Compared to those of Other Composite Cements," Cement and Concrete Composites, Vol. 27, 2005, pages 191 to 196.

Voigt, T., Bui, V.K., Shah, S.P., Drying Shrinkage of Concrete Reinforced with Fibers and Welded-Wire Fabric. ACI Materials Journal, 101(3), 2004.

Vu, D.D., Stroeven, P., Bui, V.B., Strength and Durability Aspects of Calcinedkaolin Blended Portland Cement Mortar and Concrete. CemConcr Compos, 23, 2001, 471–8.

Vuk, T.; Tinta, V.; Gabrovšek, R.; and Kauĉiĉ, V., "The Effects of Limestone Addition, Clinker Type and Fineness on Properties of Portland Cement," Cement and Concrete Research, Vol. 31, No. 1, 2001, pages 135 to 139.

Walker, W.J., Persistence of Granular Structure During Compaction Processes. KONA, 21, 2003,133-142.

Wallevik, O.H., Mueller, F.V., Hjartarson, B., and Kubens, S., The Green Alternative of Self-Compacting Concrete, Eco-SCC, 35th conference on our world in concrete and structures, Singapore, 2010.

Wang, H. Y., Zeng, H. H., & Wu, J. Y. (2014). A study on the macro and micro properties of concrete with LCD glass. Construction and Building Materials, 50, 664-670.

Wang, X. (2014). Proportioning and performance evaluation of self-consolidating concrete (Doctoral dissertation, Iowa State University).

Wang, X., Wang, K., Taylor, P., & Morcous, G. (2014). Assessing particle packing based self-consolidating concrete mix design method. Construction and Building Materials, 70, 439-452.

Weiss, J., Yang, W., Shah, P., Shrinkage Cracking of Restrained Concrete Slabs. Journal of Engineering Mechanics, 124(7), 1998, 765-774.

Weiss, W. J., & Shah, S. P. (2002). Restrained shrinkage cracking: the role of shrinkage reducing admixtures and specimen geometry. Materials and Structures, 35(2), 85-91.

Weiss, W.J., Berke, N.S., Admixtures for Reduction of Shrinkage and cracking. Early Age Cracking In Cementitious Systems, Chapter 7.5, RILEM Report 25, A. Bentur, ed., Bagneux, France, 2003, 323-338.

Weiss, W.J., Shah, S.P., Restrained Shrinkage Cracking: The Role of Shrinkage Reducing Admixtures and Specimen Geometry. Materials and Structures, 35(246) 2012, 85-91.

Westerholm, M., Lagerblad, B., Silfwerbrand, J., & Forssberg, E. (2008). Influence of fine aggregate characteristics on the rheological properties of mortars. Cement and Concrete Composites, 30(4), 274-282.

Wong, H.H.C., Kwan, A.K.H., Packing density of Cementitious Materials: Part 1– Measurement Using a Wet Packing Method. Mater Struct., 41(4), 2008, 689–701.

Yu, Q.L., Spiesz, P., Brouwers, H.J.H., Development of Cement-Based Lightweight Composites—Part 1: Mix Design Methodology and Hardened Properties. Cem Concr Compos. 44, 2013, 17–29.

Yu, R., Spiesz, P., Brouwers, H.J.H., Mix Design and Properties Assessment of Ultra-High Performance Fibre Reinforced Concrete (UHPFRC). Cement and Concrete Research, 56, 2014, 29-39.

Yuan, J., Darwin, D., and Browning, J. (2011). "Development and Construction of Low-Cracking High-Performance Concrete Bridge Decks: Free Shrinkage Tests, Restrained Shrinkage Tests, Construction Experience, and Crack Survey Results," SM Report No. 103, University of Kansas Center for Research, Lawrence, KS, 505 pp.

Yurdakul, E., Taylor, P. C., Ceylan, H., Bektas, F., Effect of water-to-binder ratio, air content, and type of cementitious materials on fresh and hardened properties of binary and ternary blended concrete. Journal of Materials in Civil Engineering, 2013.

Zhang TS, Yu QJ, Wei JX, Zhang PP. Effects of size fraction on composition and fundamental properties of Portland cement. Constr Build Mater 2011;25(7):3038–43.

Zhang, T., Yu, Q., Wei, J., & Zhang, P. (2012). Efficient utilization of cementitious materials to produce sustainable blended cement. Cement and Concrete Composites, 34 (5), 692-699.

Zheng, J., Johnson, P.F. Reed, J.S., Improved Equation of the Continuous Particle Size Distribution for Dense Packing. Journal of the American Ceramic Society, 73 (5), 1990, 1392-1398.

Zheng, L., Xuehua, C., & Mingshu, T. (1992). Hydration and setting time of MgO-type expansive cement. Cement and concrete research, 22(1), 1-5.